



HAL
open science

Two phase flow at small scale - Application to the cooling of a Proton Exchange Membrane Fuel Cell (PEMFC)

Ulrich Soupremanien

► **To cite this version:**

Ulrich Soupremanien. Two phase flow at small scale - Application to the cooling of a Proton Exchange Membrane Fuel Cell (PEMFC). Fluids mechanics [physics.class-ph]. Institut Polytechnique de Grenoble, 2010. English. NNT: . tel-03591952

HAL Id: tel-03591952

<https://hal.science/tel-03591952v1>

Submitted on 3 Mar 2022

HAL is a multi-disciplinary open access archive for the deposit and dissemination of scientific research documents, whether they are published or not. The documents may come from teaching and research institutions in France or abroad, or from public or private research centers.

L'archive ouverte pluridisciplinaire **HAL**, est destinée au dépôt et à la diffusion de documents scientifiques de niveau recherche, publiés ou non, émanant des établissements d'enseignement et de recherche français ou étrangers, des laboratoires publics ou privés.

GRENOBLE INP - INSTITUT POLYTECHNIQUE DE GRENOBLE

N° attribué par la bibliothèque

--	--	--	--	--	--	--	--	--	--

PhD THESIS :

in order to obtain the doctoral degree from

Grenoble INP - L'Institut polytechnique de Grenoble

Specialty : « *Fluid mechanics, Energy and Processes engineering* »

prepared at the Laboratoire des Écoulements Géophysiques et Industriels
inside the **École Doctorale** : « *Ingénierie - Matériaux, Mécanique, Environnement,
Énergétique, Procédés, Production* »

presented in public

by

Ulrich SOUPREMANIEN

in July 21th 2010

Two phase flow at small scale - Application to the cooling of a Proton Exchange Membrane Fuel Cell (PEMFC)

Thesis directors : **Yann BULTEL** and **Stéphane LE PERSON**

Thesis committee :

Mrs. Catherine COLIN	INP-Toulouse - IMFT	« Rapporteur »
Mr. Benoît STUTZ	Université de Savoie - LOCIE	« Rapporteur »
Mr. Jean-Pierre FRANC	CNRS - LEGI	Examinator
Mr. Yann BULTEL	G-INP - LEPMI	Thesis director
Mr. Stéphane LE PERSON	Université Joseph Fourier - LEGI	Thesis co-director
Mr. Michel FAVRE-MARINET	G-INP - LEGI	Invited
Mr. Olivier VERDU	HELION	Examinator

Acknowledgments

December 30th 2021

I have decided to translate my French PhD thesis manuscript in English, at first, just for my pleasure (like a personal challenge). Then, I thought that it could be interesting to make it public. This is the reason why I have submitted this translated work on the HAL platform. Why to not share it if it may be « useful » for someone ;-)?

I have chosen to keep (deliberately) all the Figures in French, I think most of them will be quite easy to understand with the comments in the text. *In advance, all my apologies if some English sentences look unclear or contain mistakes in the writing.* If some part of the content of this manuscript needs discussion please feel free to contact me through my professional address : ulrich.soupremanien@cea.fr.

Somewhere around July 21st 2010

This thesis work is the result of a collaboration between the « Laboratoire des Écoulements Géophysiques et Industriels (LEGI) » and the « Laboratoire d'Électrochimie et de Physicochimie des Matériaux et des Interfaces (LEPMI) » .

I would like to thank Alain Cartellier (Head of the LEGI lab when I started my PhD) and then Christophe Baudet (his successor) for having made this PhD work to be possible during all my 4 years at LEGI.

My next thanks go for the people that gave me their trust during this work :

▷ **Yann Bultel**, who despite all his responsibilities (teaching, in charge of one specialty at the doctoral school, supervision of other PhD students, etc...), has very much contributed to the promotion of the results of this work. He always pushes me to value these results through the participation in congresses and in the writing of publications.

▷ **Stéphane Le Person**, who first proposes me to work on the subject of this PhD, subject for which my interest became stronger and stronger up to the end of this study. The quality of his follow-up of my work, despite of the context, counted very much regarding the achieved success.

▷ **Michel Favre-Marinet**, for whom I express **all my gratitude** for his very efficient guidance. His availability and his outstanding responsiveness allow for long debates on various scientific aspects related to this work. The added value resulting from such a collaboration has been very significant from my point of view.

I would like to thank very much **Jean-Pierre Franc** for reading with great care my manuscript with this very high speed and for accepting to be the president of my thesis committee. I thank

Acknowledgments

also **Olivier Verdu** for his interest regarding my work. His numerous questions during my defense have opened new perspectives. Finally, I express all my gratitude to **Benoît Stutz** and **Catherine Colin**, « rapporteurs » of this work. All their remarks and comments have allowed for the improvement of my manuscript quality.

During these four years, I had the chance to work closely with bachelor and master students that, at the end, became familiar with my experimental test loop and they had the opportunity to bring new and relevant ideas to this work :

▷ **Simon Valdenaire**, for the countless hours that we spent on the Labview program. The creation of this program would have been much more complicated without his contribution.

▷ **Florent Longa**, whose talent, diligence and very strong creativity regarding the home-made MATLAB code (data image processing), have sometimes surprised me. It is obvious that this complex but important part of this work still requires hours of analyzes because the duration of an internship is clearly not sufficient. However, the numerical basis that have been laid are solid and promising.

▷ **Quentin Lancereau**, who was very autonomous on the formulation of the CFD problem regarding my test section using the softwares Gambit and Fluent. His autonomy associated with his high efficiency allowed for the rapid progresses on several numerical studies related to my PhD work.

▷ **Déborah Fannière**, for her rigor and her very important motivation, that allowed for the determination of a more relevant range of parameters for my experiments in single phase flow but also in convective boiling conditions. Thank to her support we determined a range of values for which the uncertainties were the lower ones.

Your contribution to all four have been very significant and have enriched the data that are given in this manuscript. I would like to give you my warm thanks and hope that you will succeed in your next projects.

I would like to thank other people that often work behind the scenes but whose role has been important for the success of this project :

Joseph Virone, who was very frequently called by me in the corridors of the LEGI in order that he made a last minute hydraulic assembly on my experimental test bench, or for the manufacturing of a part (fortunately it was not always like this, isn't it Joseph?). Pierre Carrechio, who contributed very much to my electronics montages. His availability and his talent help me to save many hours of work. I do not forget the other members of the « pool technique » because they all know my experimental bench : Milé Kusulja, Stéphane Mercier, Vincent Govart. I also greet the staff from the « service instrumentation », for all the loan I was able to do : Laure Vignal and Muriel Lagauzère, who also helped me for the development of the code for the data

acquisitions. I would like also to express all my gratitude to François Bonnel whose availability helped me a lot regarding all the visualization techniques. A big thank to Gabriel Moreau and Olivier De-Marchi for their very good management of the IT network of the LEGI.

I would like to thank Pierre Kern from the « Laboratoire d’Astrophysique de l’Observatoire de Grenoble (LAOG) » whose allow me to use the black body of the lab in order to calibrate my pyrometer regarding my test section and more specifically regarding the visualization window. I also thanks Hébert Sallée who devote me a lot of time for the test that we made on the micro-calorimeter of the « Centre Scientifique et Technique du Bâtiment (CSTB) ». Thanks also to Yannick Molmeret for all the tests that we made on the rheometer of the « Laboratoire de Rhéologie » and for his help regarding the viscosimeter of the LEPMI.

I thank the administrative service, in particular, Nicole Bourhy who helped me regarding all the buying procedures for the experimental bench. Of course, I greet Sylvie Champavier who followed closely all the files regarding my missions.

To conclude with my professional sphere, I would like to greet Stéphane Montésino, my first office colleague and Meera Mohan, the last one, for whom I want to give a special thanks because she allowed me to really improve my english. I would like to thank Céline Berni, whose significantly contribute to the improvement of the lessons I gave to the bachelor student of ENSE3. Thanks to Marcelo Andreotti for his great and quasi-permanent great mood (and also for having gave me the announce for the « Boiling Conference » de Florianopolis ;-)). I do not forget the other colleagues who contribute to the very cool atmosphere along during my PhD work at LEGI in particular : Michael, Johannes, Corinne, Clélia, Sylvain, Hélène and Nicolas.

I would like to thank my family who also push me during all my studies. Finaly, my last thanks go to Laura who, in between, became my wife. Only her knows what it means to be at my side all the days and specifically during a PhD work. You always encouraged me during these four years despite my limited availability and for that I am very grateful to you D’dou.

Ulrich Soupremanien

Nomenclature

Latin letter

a	channel width	m
A	cross section	m^2
b	channel height	m
c	adjustment parameter	
c_p	specific heat at constant pressure	$J.kg^{-1}.K^{-1}$
C	Chisholm et Laird (1958) parameter	
d	diameter	m
f	friction coefficient	
g	acceleration due to gravity	$m.s^{-2}$
G	mass flow	$kg.m^{-2}.s^{-1}$
h	heat transfer coefficient	$W.m^{-2}.K^{-1}$
h	enthalpy	$J.kg^{-1}$
h_w	latent heat of vaporization	$J.kg^{-1}$
I	current	A
j	superficial velocity	$m.s^{-1}$
K	Hagenbach factor	
L	channel length	m
\dot{m}	mass flow rate	$kg.s^{-1}$
M	molar mass	$kg.mole^{-1}$
p	perimeter	m
P	pressure	Pa
q''	heat flux	$W.m^{-2}$
Ra	mean roughness	m
S	heat exchange surface	m^2
t	time	s
T	temperature	K
u	flow velocity	$m.s^{-1}$
\dot{v}	flow rate	$m^3.s^{-1}$
V	voltage	V
x	vapor quality	
x, y, z	space variables	

Nomenclature

Greek letters

α	void fraction	
γ	aspect ratio	
Δ	variation of ...	
ϵ	media permittivity	$A.s.V^{-1}.m^{-1}$
η	efficiency	
θ	contact angle	$^{\circ}$ or <i>rad</i>
κ	dielectric constant	
λ	thermal conductivity	$W.m^{-1}.K^{-1}$
μ	dynamic viscosity	$Pa.s$
ν	kinematic viscosity	$m^2.s^{-1}$
ρ	mass density	$kg.m^{-3}$
σ	surface tension	$N.m^{-1}$
τ	stress	Pa
Φ	two-phase multiplier	
Φ	thermal power	W
χ	Lockhart et Martinelli (1949) parameter	

Subscripts, exponents and acronyms

<i>acc</i>	acceleration	<i>crit</i>	critical
<i>CHF</i>	Critical heat flux	<i>cv</i>	convective evaporation
<i>det</i>	detachment	<i>diph</i>	two-phase
<i>fr</i>	friction	<i>elec</i>	electric
<i>h</i>	hydraulic	<i>hom</i>	homogeneous
<i>l</i>	liquid	<i>AME</i>	absolute mean error
<i>mel</i>	mixture	<i>nb</i>	nucleate boiling
<i>o</i>	one phase only	<i>ONB</i>	onset of nucleate boiling
<i>PE</i>	full scale	<i>r</i>	reduced
<i>sat</i>	saturation	<i>SR</i>	subcooling
<i>v</i>	vapor		

Non-dimensional numbers

$$Bo = \frac{q''}{Gh_{lv}} \quad \text{boiling number}$$

C_o	$= \sqrt{\frac{\sigma}{g(\rho_l - \rho_v)} \frac{1}{d_h}}$	confinement number
Co	$= \left(\frac{\rho_v}{\rho_l}\right)^{0,5} \left(\frac{1-x}{x}\right)^{0,8}$	convection number
f	$= \frac{\Delta P D_h}{2\rho_l u^2 L}$	friction coefficient
Fr	$= \frac{G^2}{\rho^2 g d_h}$	liquid Froude number
l_c	$= \sqrt{\sigma / (g(\rho_l - \rho_v))}$	capillary length
M	$= \frac{\lambda_p}{\rho_l c_{pl}} \frac{e_p}{uL} \frac{1}{b}$	number defined by Maranzana <i>et al.</i> (2004)
Nu	$= \frac{h d_h}{\lambda}$	Nusselt number
Pr	$= \mu C_p / \lambda$	Prandtl number
Po	$= f Re$	Poiseuille number
Re	$= \frac{G d_h}{\mu}$	Reynolds number
Re_{io}	$= \frac{G d_h}{\mu_{io}}$	Reynolds number of the phase i that flowed alone in the duct
Re_i	$= \frac{G d_h}{\mu_i}$	Reynolds number of the phase i
We	$= \frac{G^2 d_h}{\sigma \rho}$	Weber number
Φ_k^2	$= \left[\frac{(dP/dz)_{fr}}{(dP/dz)_{fr,i}} \right]$	two-phase multipliers of the phase i
χ	$= \sqrt{\frac{(dP/dz)_{fr}}{(dP/dz)_{fr,i}}}$	Lockhart et Martinelli (1949) parameter

Table des matières

Preface	1
Current context of fuel cell application	1
Thermal issues related to proton exchange membrane fuel cell	2
Issues related to the cooling at small scale	3
Outline of the manuscript	4

PARTIE I STATE OF THE ART

1 Compendium on single-phase flows in mini-channels	7
1.1 Flows in laminar regime	9
1.1.1 Pressure drops in rectangular channels.	9
a) Fully developed region	10
b) Flow regimes for the entry region	11
1.1.2 Heat transfer coefficients in channels.	12
a) Fully developed regime	12
b) Flow regime in the entry region	13
1.2 Flows for turbulent regime	15
1.2.1 Pressure drop in rectangular channels	15
1.2.2 Heat transfer coefficients in channels.	16
1.3 Effect of the axial conduction in the mini-channels	17
1.4 Some experimental results	18
1.4.1 Summary of the main experiments that were made at LEGI	18
1.4.2 Experiments regarding pressure drops evolutions.	20
1.4.3 Experiments regarding heat transfer coefficients evolution	21
1.5 Chapter 1 Conclusions	23

2	Literature review on the boiling in mini-channels	25
2.1	Fundamental definitions in two-phase flows	27
2.1.1	Parameters of reference	27
2.1.2	Definition of main non-dimensional numbers	29
2.1.3	Other numbers and definition of some important notions	31
2.2	From the conventional scales to the smaller ones	33
2.2.1	Introduction	33
2.2.2	Flow classification	33
a)	Regarding the geometry	33
b)	Classification regarding physical phenomena	34
2.2.3	Flow regime for convective boiling	36
2.2.4	Heat transfer mechanisms during boiling	37
a)	Without inertial effect : pool boiling	37
b)	With inertial effects : internal convective boiling	40
2.3	Parameters that have an influence on the boiling nature	46
2.3.1	Working fluid selection	46
a)	Pressure drop evolution	46
b)	Heat exchange coefficient evolution	50
2.3.2	Wettability properties of the fluid with the wall	56
2.3.3	Working conditions	59
2.3.4	Flow cross section	67
2.4	Prediction of the pressure drops evolution	73
2.4.1	Presentation of theoretical data	73
2.4.2	Pressure drops for two-phase flow	73
a)	Homogeneous model	74
b)	Separated flow model	75
2.4.3	Void fraction evolution	84
a)	Homogeneous model	84
b)	Separated flow models	84
2.5	Prediction of the heat transfer coefficients evolution	88
2.5.1	Presentation of the theoretical data	88
2.5.2	Correlations taken from literature	90
a)	Superposition model	90
b)	Asymptotic model	91
c)	Intensification model	92
2.6	Chapter 2 conclusions	98

PARTIE II EXPERIMENTAL TECHNIQUES

3	Description of the experimental approach	103
3.1	Goal of the study and experimental approach	105
3.2	Working fluid selection	106
3.3	Preliminary cautions for studying a boiling flow	111
3.4	Working fluid selection	111
3.4.1	General description of the fluid	112
3.4.2	Thermophysical properties of Forane 365 HX	112
3.5	Chapter 3 conclusions	115
4	Experimental set-up description	117
4.1	Hydraulic test loop presentation	119
4.1.1	General description	119
4.1.2	Degassing system	121
4.1.3	Preheating method	124
4.1.4	Test section description	124
4.1.5	Mini-channels sizing	126
4.2	Data acquisition of the experimental measurements	127
4.3	Cameras acquisition system description	128
4.4	Presentation of the list of made experimental tests	130

PARTIE III EXPERIMENTAL RESULTS

5	Single-phase flow in mini-channels	135
5.1	Study of the friction coefficients in mini-channel	137
5.1.1	Methodology and study description	137
5.1.2	Experimental determination of the friction coefficients	137
5.1.3	Experimental uncertainties	138
5.1.4	Measurements and results	140
5.2	Study of the heat transfer coefficients in mini-channel	148
5.2.1	Methodology and study description	148
5.2.2	Determination of the heat transfer coefficients	148
5.2.3	Experimental uncertainties	150

5.2.4	Measurements and results	152
5.3	Conjugated (heat/flow) numerical analysis	165
5.3.1	Numerical results	165
5.3.2	Correction of the experimental data	171
5.4	Chapitre 5 conclusions	174

6 Boiling flows in mini-channels 177

6.1	Fundamental estimations in convective boiling conditions	178
6.1.1	Experimental determination of the transferred heat flux	178
6.1.2	Reference fluid temperature determination	180
6.1.3	Measurement uncertainties	181
6.2	Study of the ONB in the mini-channels	183
6.2.1	Study description and methodology	183
6.2.2	Measurements and results	183
6.3	Flow regime visualization in mini-channels	194
6.4	Evolution of boiling curves with wall heat flux	206
6.4.1	Boiling curves presentation	207
6.4.2	Pressure drop evolution	212
6.4.3	Evolution of the heat transfer coefficients	227
6.4.4	Conditions that lead to wall dryout	238
6.5	Chapter 6 conclusions	244

PARTIE IV TRANSPOSITIONS TO THE APPLICATION

7 Application to proton exchange membrane fuel cell cooling 247

7.1	Short presentation of the working principle	249
7.1.1	General system presentation.	249
7.1.2	Thermal regulation of a fuel cell	251
7.2	Comparison of the energy efficiency	256
7.3	Sizing of the cooling channels	260
7.4	Chapter 7 conclusions	261

General Conclusions and Prospects 263

Appendices	xiii
A Forane 365 HX properties	xv
A.1 Forane 365 HX thermophysical properties	xv
A.2 Chemical compatibility tables for forane 365 HX with other materials	xvi
B Visualization window	xvii
C How the experiments were made...	xix
C.1 How to determine friction coefficients?	xix
C.2 How to determine heat exchange coefficients?	xx
C.3 How to identify the onset of nucleate boiling?	xx
C.4 How to obtain the boiling curves?	xxi
D Other results coming from this study	xxiii
D.1 Results for the evolution of the single phase flow data	xxiii
D.2 Results for the evolution of boiling data	xxvi
E Presentation of the modeling	xxvii
F Void fraction determination via image processing	xxxiii
F.1 Why to go through image processing to analyze the results?	xxxiii
F.1.1 Bubbly flow regime	xxxiv
F.1.2 Plug flow regime	xxxiv
F.1.3 Slug flow regime	xxxv
F.2 Image processing using Matlab	xxxv
F.2.1 Block diagram for the threshold program	xxxvii

Preface

The discovery of the « fuel cell effect » was associated with the works of Sir Humphry Davy on electrolysis of distilled water in 1806. By imposing an electrical current to a volume of distilled water, Sir Humphry Davy succeed in having hydrogen and oxygen. About thirty years later, it was Christian Friedrich Schoenbein who observe the first, in 1838, that when shutting down the electrical field, the resulting gases produced an electrical current in an opposite direction regarding the former one. The principle of fuel cell working was born in 1839. After an interview with Schoenbein in a congress in Birmingham, William Robert Grove worked on these experimental data and presented, the same year, his famous experience with a fuel cell working with a liquid electrolyte.

Current context of fuel cell application

Nowadays, development of fuel cell is motivated by three main goals :

▷ **Environmental motivation : greenhouse gases (GHG) reduction**

Since about thirty years, the environmental motivation became one of the first worldwide interest. The inherent pollution due to human activities (industry, transports, etc...) are responsible of the emission of pollutants of short lifetime (carbon monoxide, nitrogen monoxide and nitrogen dioxide - NO_x - not burned hydrocarbons and also particles) but also pollutants of longer lifetime (greenhouse gases (GHG) and gases responsible of ozone depletion) whose regulation became necessary. In particular, the emission in atmosphere of GHG (carbon dioxide, CO_2 , represent 53% of the GHG¹) related to our activities contribute to global warming² and have to be limited.

Generation of electricity when using an electrochemical converter will have a lower environmental impact. Indeed, the electrochemical reaction, generated at the fuel cell core, which results from the combination of hydrogen and oxygen, lead only to electricity generation and to the release of heat and pure water.

▷ **Use of an unique and spread energy carrier**

The best candidate for this spread is electricity. Indeed, this energy is easily convertible into other energies. Moreover its use is simple and this energy is easily transportable using existing infrastructures. The main constraint to its use comes from the issue related to its storage.

1. According to <http://www.afh2.org> - Pourquoi l'Hydrogène? Version 4.4 10/2006.

2. Report of the Intergovernmental Panel On Climate Change (IPCC) 2001 - Chapter 12

Thermal issues related to proton exchange membrane fuel cell

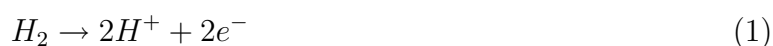
▷ Rapid reduction of primary energies

The experts admit that the fossil energy resources are reducing and that these resources should have disappeared at the end of this century. Moreover, the projections showed that the numerous fluctuation, in terms of cost, of these energies will become more significant as they will become rare. At the moment, it should have in reserve forty years (or so) of conventional fossil energy at current cost³. However, other large primary fossil energy, having a lower cost in production (coal, schist, oil sands, lignite, natural gas) are still available in larger quantity. Nonetheless, these last primary energies have the drawback of generating large amount of CO_2 . Taking into account this drawback our economy must be redirected toward other sources of energy as the renewable energies⁴.

Thermal issues related to proton exchange membrane fuel cell

Electric energy generation through electrochemical generator, as proton exchange membrane fuel cell, always produce heat as the global oxido-reduction reaction between hydrogen and oxygen is exothermic.

At the anode, hydrogen is oxidized and the reaction could be written as :



To start the reaction, a specific energy must be given for the dissociation of the hydrogen molecule in ions H^+ . When the temperature is of $25^\circ C$, this activation energy is about $432 kJ.mol^{-1}$.

From cathode side, the reduction reaction of oxygen follows :



The activation of this reaction needs $247 kJ.mol^{-1}$ at $25^\circ C$, but the generation of a water molecule leads to the release of $916 kJ.mol^{-1}$ (the reaction is globally exothermic).

It is admitted that when a proton exchange membrane fuel cell product $1 kW$ of electric energy, it releases at the same time about $1 kW$ of thermal energy. This very strong thermal dissipation is a significant drawback when looking at the thermal requirements inside the proton exchange membrane fuel cell⁵. Moreover, the constraint related to compactness leads to the

3. <http://www.x-environnement.org> - L'Hydrogène vecteur énergétique de l'avenir ? 09/2004.

4. www.eia.doe.gov/oiaf/ieo/index.html

5. In the middle of the sixteenth, General Electric (GE) invent a new technology of fuel cell which use a solid electrolyte allowing for scale reduction.

analysis of the thermal cooling issues. For increasing the lifetime of the different components the thermal gradients through the fuel cell should be lowered as much as possible.

Issues related to the cooling at small scale

Since about forty years, a new scientific field had emerged with the development of the miniaturization processes (related to the improvement of the microelectronics techniques applied to silicon semi-conductors substrates). Miniaturization find a number of applications, from electronics, through biology, chemistry, and fundamental physics. The benefit of these processes lead to : volume reduction, improvement of the electrical performances, reduction of the response times, and reduction of the fluid volume (for the specific cases of systems using fluids).

The advantages of using such miniaturization principles in proton exchange fuel cell are clear as the confinement inside this device may be important. Moreover the need for a homogeneous wall temperature is a strong constraint for these electrochemical generators (PEMFC work at low temperature). It is in this context that the convective boiling flows inside channels of smaller dimensions may be interesting. The phase change leads at the same time to an increase of the heat transfer, for same vapor flow rate, and to a better wall temperature homogenization (when comparing to the single phase flow case) as the phase change from liquid state to vapor state occurred at constant temperature (fpr a constant pressure)

Thus, the question that needs to be answered is :

▷ Are the defined two-phase flows' laws and correlations still valid for cooling channels having hydraulic diameters lower than 1.5 mm ?

Outline of the manuscript

This manuscript is separated in four parts :

▷ PART I

An analysis regarding the data from literature has been done regarding two complementary aspects. For the first aspect ([Chapter 1](#)), the different phenomena occurring in single phase flow in tube have been analyzed. For the second point ([Chapter 2](#)), the different phenomena that influenced the boiling flow have been presented. The literature survey had been discussed for understanding the experimental conditions that impacted the pressure losses and heat transfer in mini-channels. Moreover, the more often predictive tools are given and a summary of the parameters that influenced the correlations are described.

▷ PART II

After this literature survey, the second part of this manuscript was dedicated to the description of the experimental approach. We discussed the sizing of the test section and helped in the selection of the geometrical parameter also. The working fluid has been selected consistently regarding the cooling of a fuel cell application ([Chapter 3](#)). Then, the full experimental test bench has been presented in [Chapter 4](#). An original method for the degassing process has been detailed in this chapter.

▷ PART III

In a first step, the data were collected from single phase flows experiments. The obtained results were compared to the correlations from literature. For studying more specifically these experimental data, a numerical model was built. The results coming from this model have been reported in [Chapter 5](#). After this work, the impact of the geometrical parameters on convective boiling inside the mini-channel are given in [Chapter 6](#). Comparisons of the experiments with literature correlations were done and more suitable ones are proposed.

▷ PART IV

Finally, a transposition of the results for the cooling of a proton exchange membrane fuel cell has been done considering simplifying assumptions ([Chapter 7](#)).

Following this last section, the conclusions and prospects issued from this thesis work have been given.

Première partie

STATE OF THE ART

Compendium on single-phase flows in mini-channels

1.1	Flows in laminar regime	9
1.1.1	Pressure drops in rectangular channels	9
1.1.2	Heat transfer coefficients in channels	12
1.2	Flows for turbulent regime	15
1.2.1	Pressure drop in rectangular channels	15
1.2.2	Heat transfer coefficients in channels	16
1.3	Effect of the axial conduction in the mini-channels	17
1.4	Some experimental results	18
1.4.1	Summary of the main experiments that were made at LEGI	18
1.4.2	Experiments regarding pressure drops evolutions	20
1.4.3	Experiments regarding heat transfer coefficients evolution	21
1.5	Chapter 1 Conclusions	23

Summary :

WHEN studying an experimental boiling flow, the first questions are related to the validity of the pressure drop and heat transfer values for single-phase flow, for which well known correlations exist. The aim of this chapter, far to be exhaustive, was to give a summary of the main theoretical analysis for laminar and turbulent flows for tubes having smooth surfaces. Then, we report some of the up to date results for the single-phase flow.

The recent results from the literature agreed between them and showed that for channels of small hydraulic diameters¹ (Judy *et al.* (2002), Bavière (2005), Lee et Mudawar (2005b), Steinke et Kandlikar (2006), McPhail (2007)), the experimental data for single phase flow did not present any deviations with respect to the Navier-Stokes' theoretical analysis. For these flow conditions, numerous correlative laws have been established and allow for the prediction of pressure drops and heat exchange coefficients in rectangular channels. These laws are dependent of various parameters such as : flow regime (laminar or turbulent), geometry of the cross section, surface roughness and the fluid type.

1.1 Flows in laminar regime

1.1.1 Pressure drops in rectangular channels

For the laminar regime, two sub-regimes that depend on the development of the flow boundary layers can be observed. These layers have been represented on Figure 1.1 for a flow in a tube having an uniform velocity profile at the inlet.

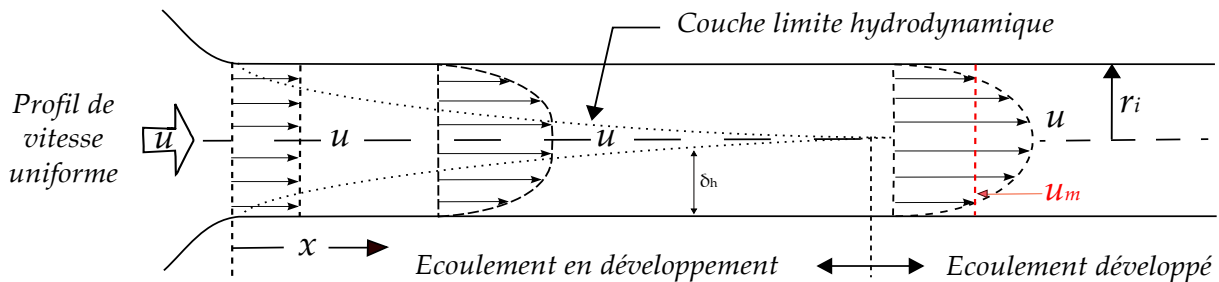


FIGURE 1.1 – Development of the hydraulic boundary layers according to Shah et Sékulić (2003)

It can be distinguished :

- the entrance length region,
- the fully developed flow region.

When considering the entrance effects, the velocity profile depends on position but not on time, whereas for fully developed flow it does not depend neither on time nor position. The fully developed regime took place generally far from the entrance. Regarding these two sub-regimes, the correlations for determining the pressure drops are different and are influenced by entrance effects². It should be point out that the evolution of the predictives correlations which are valid for entry region needs the knowledge of the fully developed conditions. Therefore, it is necessary

1. A classification which depends on hydraulic diameter is given on **Chapter 2**, equation (2.18).
2. The entrance profile can modify the position z from which the flow is fully developed.

to discuss the results for these fully developed conditions before the conditions for the entry region.

a) Fully developed region

In this configuration, Shah et London (1978) have determined the flow velocity profile regarding the width (a) and the height (b) of a channel (Figure 1.2).

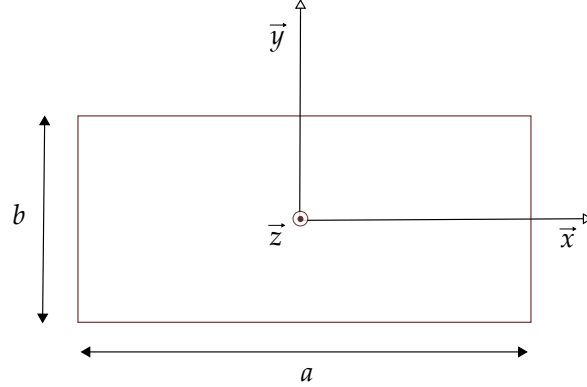


FIGURE 1.2 – Duct rectangular cross section

with γ representing the aspect ratio³ defined as :

$$\gamma = \frac{b}{a} \quad (1.1)$$

The velocity profile in the duct follows :

$$u(x, y) = -\frac{4a^2}{\pi^3\mu_l} \left(-\frac{dP}{dz}\right) \sum_{n=1,3,\dots}^{\infty} \frac{1}{n^3} (-1)^{(n-1)/2} \left[1 - \frac{\cosh(n\pi y/a)}{\cosh(n\pi b/a)}\right] \cos\left(\frac{n\pi x}{a}\right) \quad (1.2)$$

with μ_l which is the dynamic viscosity and $\frac{dP}{dz}$ the pressure drop.

The mean velocity on a flow cross section is given by :

$$u_m = -\frac{a^2}{12\mu_l} \left(-\frac{dP}{dz}\right) \left[1 - \frac{192}{\gamma\pi^5} \sum_{n=1,3,\dots}^{\infty} \frac{1}{n^5} \tanh\left(\frac{n\pi\gamma}{2}\right)\right] \quad (1.3)$$

The channel wall imposes a tangential stress on the fluid which hinder its motion⁴. The mean wall friction coefficient (f) can be determined using :

$$f = \frac{d_h}{2\rho_l u_m^2} \left(-\frac{dP}{dz}\right) \quad \text{with} \quad d_h = \frac{4A}{p} = \frac{4ab}{2(a+b)} \quad (1.4)$$

3. No clear consensus exist for the definition of the aspect ratio which is defined as $\gamma = a/b$ also.

4. Viscosity effect led to a velocity equalled to zero at the wall.

where ρ_l is the fluid density, u_m the mean velocity, d_h the hydraulic diameter, S the cross section and P the wetted perimeter.

Using the Poiseuille number ($f \times Re$) which relate the pressure drop evolution, we obtain :

$$fRe = - \left(- \frac{dP}{dz} \right) \frac{2a^2b^2}{u_m(a+b)^2\mu_l} \quad (1.5)$$

with Re which is the Reynolds number.

This expression can be rewritten using equation (1.3) and by expressing u_m , leading to :

$$fRe = \frac{24}{\left(1 + \frac{1}{\gamma}\right)^2 \left(1 - \frac{192}{\gamma\pi^5} \sum_{n=1,3,\dots}^{\infty} \frac{1}{n^5} \tanh\left(\frac{n\pi\gamma}{2}\right)\right)} \quad (1.6)$$

As showed by Shah et London (1978), equation (1.6) can be approximated by the following 5th order polynomial expression :

$$fRe = 24(1 - 1.3553\gamma + 1.9467\gamma^2 - 1.7012\gamma^3 + 0.9564\gamma^4 - 0.2537\gamma^5) \quad (1.7)$$

b) Flow regimes for the entry region

Literature results (Hrnjak et Tu (2006), Lee et Garimella (2006), Steinke et Kandlikar (2006), *among others*) have showed that the friction coefficients for the flows in the entry region are higher compared to the fully developed conditions. For expressing their evolution, it was interesting to introduce L^+ , which is a non-dimensional channel length, that characterizes (regarding the entrance conditions) the evolution of the length from which the flow became fully developed.

$$L^+ = \frac{L}{Red_h} \quad (1.8)$$

where L is the duct length.

Shah et London (1978) have defined a correlation based on the results of the boundray layers development for infinite plates for fully developed flows in circular and non-circular ducts :

$$f_{app}Re = 3.44(L^+)^{-0.5} + \frac{K(\infty)/(4L^+) + fRe - 3.44(L^+)^{-0.5}}{1 + C'(L^+)^{-0.2}} \quad (1.9)$$

$K(\infty)$ is the Hagenbach factor⁵ and C' are tabulated numbers deducted from numerical studies. Here, f_{app} is named apparent friction coefficient. Values of these constants are given for some aspect ratios in Table 1.1.

5. Value at infinity of $K(x)$ that characterizes the pressure drop due to entrance effects of geometrical type, Rohsenow *et al.* (1998) (the velocity profile is supposed to be uniform in any cases).

γ	$K(\infty)$	C'
1	1.43	0.00029
0.5	1.28	0.00021
0.2	0.931	0.000079
0.0	0.674	0.000029

TABLE 1.1 – $K(\infty)$ and C' values for different aspect ratio (for a rectangular channel)

More recently, Steinke et Kandlikar (2006) have determined an evolution of the $K(\infty)$ factor with respect to the aspect ratio⁶ using a numerical model :

$$K(\infty) = 0.6796 + 1.2197\gamma + 3.3089\gamma^2 - 9.5921\gamma^3 + 8.9089\gamma^4 - 2.9959\gamma^5 \quad (1.10)$$

These last authors did not determined the dependence of C' with respect to the aspect ratio γ .

1.1.2 Heat transfer coefficients in channels

a) Fully developed regime

When heat transfer between the fluid and a solid surface occurred, the thermal gradient is more pronounced in a region very close to the wall when considering a region near the channel entrance. The evolution of the thermal boundary layers has been reported on Figure 1.3 for laminar internal flows. When considering the entry region, the heat transfer between the wall and the fluid is controlled by the development of these thermal boundary layers.

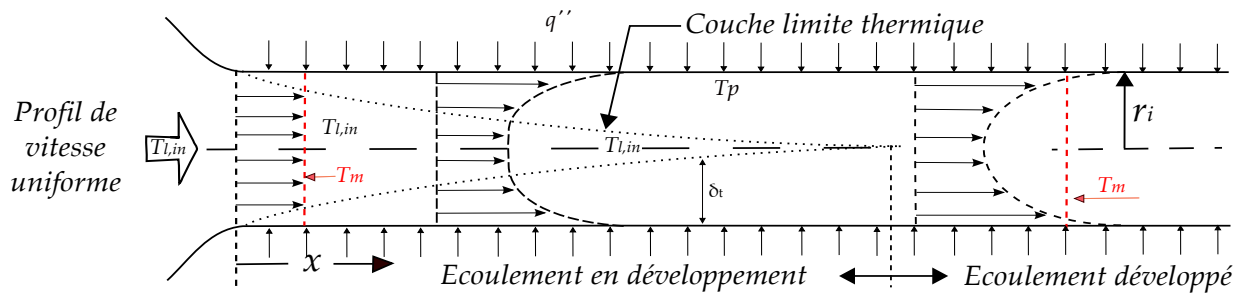


FIGURE 1.3 – Thermal boundary layers as represented by Shah et Sékulić (2003)

Rohsenow *et al.* (1998) showed that the main important parameters that allow the characterization of the heat transfer for a flow in a duct are : liquid temperature T_l , and heat transfer coefficient h .

6. We pointed out that their results are slightly different compared to the ones calculated by Shah et London (1978).

For a fully developed flow, the mean fluid temperature ($T_{l,m}$), can be defined as :

$$T_{l,m} = \frac{1}{Su_m} \int_S uT_l dS \quad (1.11)$$

with S which is the flow cross section.

For a homogeneous heat flux (q''), the heat exchange coefficient is defined as :

$$h(z) = \frac{q''}{T_{p,m}(z) - T_{l,m}(z)} \quad (1.12)$$

where $T_{p,m}$ is the mean wall temperature on the perimeter of the channel.

In this configuration, the heat transfer coefficient $h(z)$ is constant throughout the duct and it is possible to determine the mean Nusselt number that characterizes the heat transfer rate between the wall and the fluid by :

$$Nu_m = \frac{h_m d_h}{\lambda_l} \quad (1.13)$$

Shah et London (1978) have determined a 5th order polynomial function that allow for the calculation of a rough Nusselt number for a uniform channel wall heat flux :

$$Nu = 8.235(1 - 2.042\gamma + 3.085\gamma^2 - 2.476\gamma^3 + 1.058\gamma^4 - 0.186\gamma^5) \quad (1.14)$$

b) Flow regime in the entry region

Similarly to the hydrodynamic conditions, it was necessary to introduce a non-dimensional number z^* that characterized the evolution of the length where the flow reach the fully developed conditions in a thermal point of view.

$$z^* = \frac{1}{RePr} \frac{z}{d_h} \quad (1.15)$$

where Pr is the Prandtl number.

Chapitre 1. Compendium on single-phase flows in mini-channels

Shen *et al.* (2006) showed that the results of Shah et London (1978), which allow for the calculation of Nusselt number, can be correlated on three different domains regarding z^* , the aspect ratio and the Prandtl number values.

$$\begin{cases} Nu = (\text{value given by 1.14}) & , \text{ if } z^* \geq 0.1 \\ Nu = 3.35z^{*-0.13}\gamma^{-0.12}Pr^{-0.38} & , \text{ if } 0.013 \leq z^* < 0.1 \\ Nu = 1.87z^{*-0.3}\gamma^{-0.056}Pr^{-0.036} & , \text{ if } 0.005 \leq z^* < 0.013 \end{cases} \quad (1.16)$$

More recently, Lee et Garimella (2006) have numerically demonstrated that the Nusselt number evolution could be written in a more straightforward way following :

$$Nu = \frac{1}{C_1(z^*)^{C_2} + C_3} + C_4, \text{ for } 0.1 \leq \gamma \leq 1, z^* \leq z_{num}^* \quad (1.17)$$

C_1, C_2, C_3, C_4 and z_{num}^* , are parameters that were numerically defined by these authors. z_{num}^* was the length, from which the flow is thermally fully developed.

Following their model this length can be expressed as :

$$\begin{aligned} z_{num}^* = & -1.275 \times 10^{-6}\gamma^{-6} + 4.709 \times 10^{-5}\gamma^{-5} - 6.902 \times 10^{-4}\gamma^{-4} \\ & + 5.014 \times 10^{-3}\gamma^{-3} - 1.769 \times 10^{-2}\gamma^{-2} + 1.845 \times 10^{-2}\gamma^{-1} + 5.691 \times 10^{-2} \end{aligned} \quad (1.18)$$

One can notice that by reducing the aspect ration the length for reaching the fully developed conditions is reduced also (Figure 1.4).

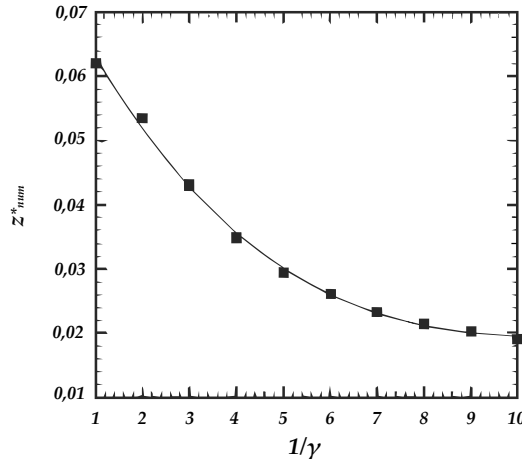


FIGURE 1.4 – Length to reach fully developed conditions in function of the aspect ratio following Lee et Garimella (2006)

The constants which are given in the equation (1.17) can be expressed using :

$$\begin{cases} C_1 = -3.122 \times 10^{-3}\gamma^{-3} + 2.435 \times 10^{-2}\gamma^{-2} + 2.143 \times 10^{-1}\gamma^{-1} + 7.325 \\ C_2 = 6.412 \times 10^{-1} \\ C_3 = 1.589 \times 10^{-4}\gamma^{-2} + 2.603 \times 10^{-3}\gamma^{-1} + 2.444 \times 10^{-2} \\ C_4 = 7.148 - 1.328 \times 10^1\gamma + 1.515 \times 10^1\gamma^2 - 5.936\gamma^3 \end{cases} \quad (1.19)$$

📌 **Summary on the theoretical data for laminar conditions**

The evolution of the friction coefficients and of the heat exchange coefficients are dependent on the flow conditions that took place into the duct for the laminar regime. When considering the entry length, these coefficients are dependent of the aspect ratio and of Reynolds and Prandtl numbers (for the thermal cases). For fully developed conditions, it is interesting to observe that the values of these coefficients are only aspect ratio dependent as demonstrated by Shah et London (1978).

1.2 Flows for turbulent regime

1.2.1 Pressure drop in rectangular channels

In turbulent regime, the friction coefficients are Reynolds and wall roughness dependent. There are several correlations that took into account the evolution of these friction coefficients. Nonetheless, the analysis of all these correlations go beyond the context of this study. Therefore, the analysis will be restricted to two representative correlations⁷ :

$$\begin{aligned} - \text{Blasius (1913)} \quad & f = 0.079Re^{-1/4} \quad 4000 < Re < 10^5 \\ - \text{Colebrook (1939)} \quad & 4f = 0.25 \left[\log \left(\frac{e/d_h}{3.7} + \frac{2.51}{Re\sqrt{4f}} \right) \right]^{-2} \quad 10^4 < Re < 10^7 \end{aligned} \quad (1.20)$$

where e is the mean roughness height.

The Colebrook (1939) correlation is related to the Prandtl (1944) and Von Karmàn (1934) equations. This correlation is implicit and show the impact of the relative roughness (e/d_h). From this correlation, it is possible to draw the Moody (1944) diagram which is often used for the friction factors determination in ducts used for industrial applications. The method of

⁷. An important number of predictive correlation for the determination of the pressure drops can be found in Rohsenow *et al.* (1998) (Table 5.8).

Blasius (1913) is more direct and took into account the turbulent regime in a smooth tube. However this law allow for the calculation of friction coefficients on a smaller range of Reynolds numbers.

1.2.2 Heat transfer coefficients in channels

In turbulent regime, the evolution of the Nusselt number is influenced by the flow velocity, the fluid thermal properties, the duct hydraulic diameter and, regarding some of the correlations by the friction coefficients. In the context of this study, the analysis was restricted to the correlations that are most often used for the prediction of Nusselt number evolution :

$$\begin{aligned}
 & \text{- Dittus et Boelter (1930)} \quad Nu = 0.023 \left(\frac{\lambda_l}{d_h} \right) Re^{0.8} Pr^{0.4} \\
 & \text{- Petukhov et Popov (1963)} \quad Nu = \frac{(c_f/2)RePr}{C + 12.7(c_f/2)^{1/2}(Pr^{2/3} - 1)} \\
 & \quad \text{with } C = 1.07 + \frac{900}{Re} - \frac{0.63}{1 + 10Pr} \\
 & \text{- Gnielinski (1976)} \quad Nu = \frac{(c_f/2)RePr}{1 + 12.7(c_f/2)^{1/2}(Pr^{2/3} - 1)}
 \end{aligned} \tag{1.21}$$

where λ_l ($W.m^{-1}.K^{-1}$) is the fluid thermal conductivity, d_h (m) the duct hydraulic diameter and c_f the friction coefficient given by :

$$c_f = (1.82 \times \log(Re) - 1.64)^{-2} \quad \text{with } c_f \approx 4f \tag{1.22}$$

f is given in equation (1.20). c_f is similar to $4f$ at $\pm 4\%$ on the range of Reynolds number between 4000 and 10000. Note that the Petukhov et Popov (1963) correlation took better into account the heat transfer dependence regarding the Prandtl number for the determination of the heat transfer coefficient (Carey (2008)).

Summary on the theoretical data for turbulent regime

In turbulent regime, several correlations exist, but have not been presented in this part. In the context of this Phd study, the use of the Blasius (1913) correlation will be the most relevant for the comparison with our experiments. The comparison with Gnielinski (1976) correlation will be done also. This last correlation is often used in the literature as a predictive tool for the heat transfer coefficients determination for channels of small dimensions. Note that a large part of the realized studies related to flows at small scale has been made for laminar conditions.

1.3 Effect of the axial conduction in the mini-channels

The results from the literature showed that the importance of the coupling between the conduction and the convection effects, increased when the cross section dimensions decreased. In a mini-channel, the thickness of the wall is generally of the same order of magnitude (often larger) than the hydraulic diameter. Unlike the studies that were made in tube of large hydraulic diameter, the conductive heat flux through the duct walls, particularly the longitudinal ones, may become very significant compared to the heat flux convected by the flow in mini-channels. Indeed, the heat flux streamlines, tended to be driven toward the cooler parts of the flow (Clausius principle (1850)). This phenomenon intensified with the increase of the distance between the fluid and the heat source (increase of the wall thickness) or with the reduction of the mass flow. This heat flux streamlines distortion may lead to a non-linear repartition of the temperature along the channel wall in the most unfavourable conditions. Using a numerical study, Maranzana *et al.* (2004) have introduced a non-dimensional number (M) which allow for the consideration of the relative importance of the conductive heat flux, Φ_{cond} , compared to the convective heat flux, Φ_{conv} . Therefore, for a 2D channel having a height of b , a length of L , with wall thickness of e_p and a thermal conductivity λ_p , M can be written as :

$$M = \frac{\Phi_{cond}}{\Phi_{conv}} = \frac{\lambda_p}{\rho_l c_{pl} u L} \frac{e_p}{b} \quad (1.23)$$

where ρ_l is the liquid density, c_{pl} the liquid specific heat and u the flow velocity in the duct. More recently, Bigot (2005) showed that the results of Maranzana *et al.* (2004) were not applicable to the mini-channels of small width. Indeed, these last authors considered in their model that the channel width (b) and the heated plate width (l_p) were infinite compared to the channel thickness, what can be reduced to a 2D modelling. The occurrence of a transverse confinement for the case of the mini-channels having a relatively small width (a) led to a 3D study of the heat transfer study (Figure 1.5).

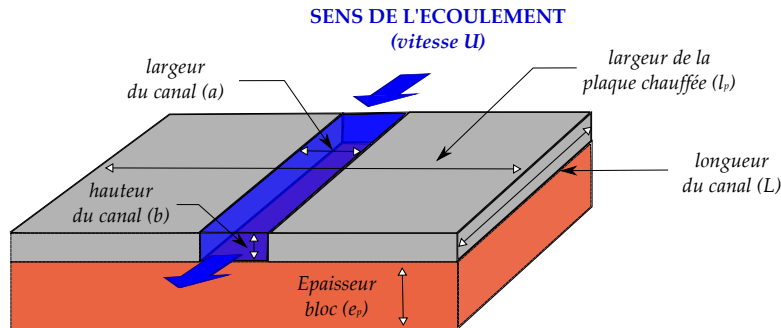


FIGURE 1.5 – Representation of the geometrical parameters

Therefore, Bigot (2005) proposed another definition of the Maranzana *et al.* (2004) parameter for these cases :

$$M' = \frac{\lambda_p}{\rho_l c_{pl} u L} \frac{e_p \times l_p}{a \times b} \quad (1.24)$$

with l_p which is the heated plate width.

For our experimental study the repartition of the heat flux has been evaluated using this number. Following that, we have realized a numerical study to better understand the results that were obtained experimentally (§ 5.3).

1.4 Some experimental results

For the last decade, a large part of the studies has be directed toward the researches aiming at identifying if new physical phenomenon occurred when the flow characteristic dimensions were reduced⁸. The numerous literature results, which have been obtained recently in the context of single-phase flows in mini-channels, have demonstrated the validity of the classical Navier-Stokes approach for the mini-channels¹ (even for the micro-channels). This result has been confirmed in the team into which my work took place for this PhD study. The heat transfer in fluids flowing at small scale has been studied for more than a decade in the LEGI team. Therefore, we will present in a first part, a short summary of the results that have been obtained at LEGI⁹. We will then give some literature results regarding the evolution of the pressure drop and heat transfer coefficients in the related mini-channels.

1.4.1 Summary of the main experiments that were made at LEGI⁹

The experimental bench of Gao *et al.* (2002) that was built at the Laboratoire des Écoulements Géophysiques et Industriels (LEGI) allowed for the study of heat transfer and pressure drop in mini-channels of small aspect ratio (large width compared to channel height). The test section was fabricated with two brass blocks where a hollowed-out aluminum plate (of variable thicknesses ($100 \mu m < b < 1 mm$)) was put in between. Four heating cartridges were inserted inside the upper and the lower blocks, parallely to the flow, allow for the heating of the fluid.

8. This analysis is related to the classification given by ? for gases, where, from a specific dimension (evaluated using the Knudsen number) there is a break of the hypothesis of continuum mechanics.

9. We will focus our attention strictly on the experimental test sections that have been used by Gao *et al.* (2002), Bavière (2005) and Gamrat (2007). We can note that other test sections exist and have been made in collaboration with the « Groupement pour la Recherche sur les Échangeurs Thermiques (GRETh) », which was localized on the scientific polygon of Grenoble.

The heating was supposed to be uniform. A representation of the test section is given in Figure 1.6.

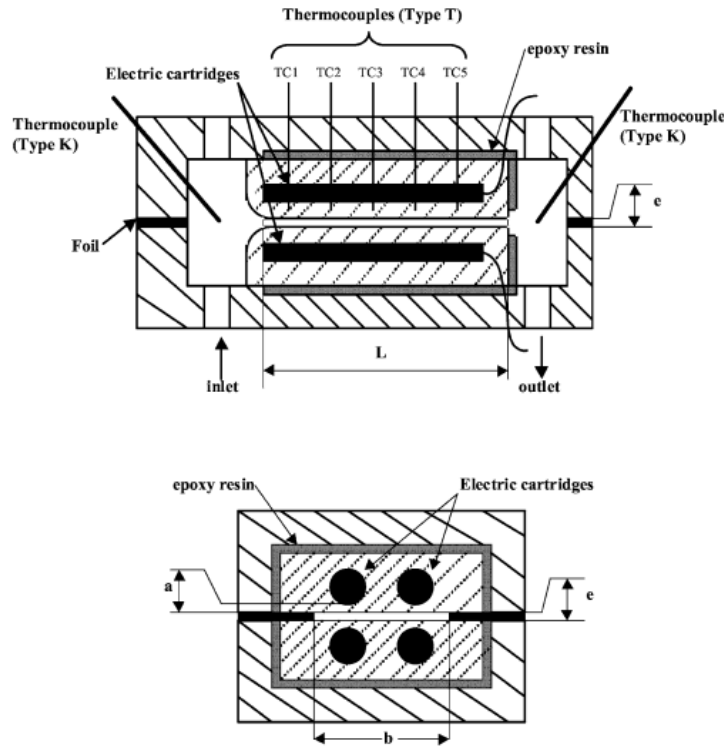


FIGURE 1.6 – Test section designed by Gao *et al.* (2002)

Gao *et al.* (2002) found a very good agreement between their experimental data and the theoretical data for the evolution of the friction coefficients. Nonetheless, for the evolution of the heat transfer coefficients, they noted that the heat transfer coefficients decreased as soon as the channel thickness became lower than 0.5 mm . The reduction of the hydraulic diameter could even lead to a drastic drop of almost 60% of the heat exchange coefficients for the plate having a thickness of 0.1 mm . Gao *et al.* (2002) did not arrived to explain what were the reasons of such a discrepancy with the theoretical data and for a moment they had suspected the appearance of scale effect. Some time later, Bavière (2005) pursued the work initiated by Gao *et al.* (2002) and has improved the test section by modifying the heating system, assuming that the appearance of some thermal effect which was not considered by Gao *et al.* (2002). As presented in § 1.3, the effects of axial conduction were not negligible when compared to the transverse conduction as soon as the geometrical dimensions were reduced. Therefore, for limiting this effect, Bavière (2005) inserted the heating cartridges perpendicularly to the flow and added insulated compartments. A more detailed description of this test section will be given in § 4.1.1.

The author demonstrated that the difference observed by Gao *et al.* (2002) was certainly due to a wall temperature measurement bias. By considering the influence of this bias, Bavière (2005)

showed that its results and those of Gao *et al.* (2002) were in agreement with the classical theoretical data regarding heat transfer variations (Figure 1.7).

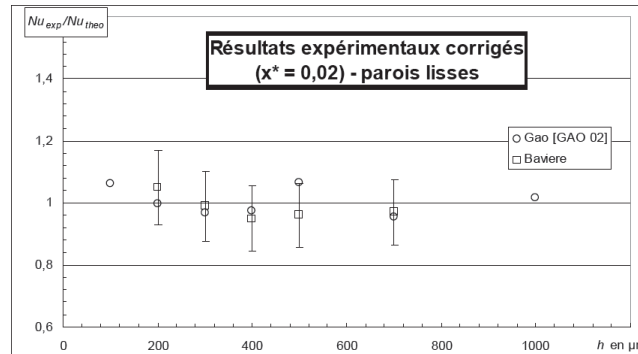


FIGURE 1.7 – Comparison of the experimental data of Bavière (2005) with theoretical data

Bavière *et al.* (2006) have then characterized the influence of the surface roughness on the friction and heat transfer coefficients. They showed that the roughness slightly increased the amplitude of the heat transfer. The obtained results showed that the usual hydrodynamic and thermal correlations were still valid for the entire set of studied channels.

Gamrat (2007) continued the work made by Bavière (2005) by realizing numerical and experimental analysis. During this work, Gamrat (2007) has developed a 2D model for determining the influence of the wall roughness on the friction and heat transfer coefficients (this roughness has been distributed in a controlled manner on the surface). The obtained results have showed, that no new phenomena were expected to occur at the studied scales (channel of $100 \mu m$ height), but roughness, could become an important parameter in the micro-channel and played a significant role in the flow pressure drops and heat transfer rate.

1.4.2 Experiments regarding pressure drops evolutions

Three papers (among various other) will be presented in the following paragraph. These three publications have been selected because they represent a recent summary of the literature results on the pressure drop evolution. The first paper gave a review on the pressure drop evolution in mini-channel for independent works. A interesting technique for measuring the local pressure drop is given in the second one. The third one was selected because it analyzes the evolution of the pressure drop for three different working fluids in the same test section.

Steinke et Kandlikar (2006) have analysed more than 150 publications and 40 in a more detailed way. They wrote that the results that present deviations regarding usual correlations for the pressure drops did not considered, for most of them :

- the existence of singularities at the entrance or the outlet of the test section,

- the entry region for the development of the hydrodynamic boundary layers.

Thus the authors showed that no deviations occurred regarding the classical correlations used for determining the pressure drops (for hydraulic diameters ranged from $8 \mu m$ to $990 \mu m$ and for Reynolds numbers lower than 5000).

Within the most complete researches, the experimental study made by Kohl *et al.* (2005) allow for the determination of the local pressure drop variation for water (formerly degassed). The authors have realized five different test sections that were made with channels of different hydraulic diameters (25, 41, 61, 93 et $100 \mu m$). The pressure drop was determined locally using 10 pressure sensor along the micro-channel (Figure 1.8). According to their results, the friction coefficient could be precisely determined from the defined correlation for channel having large hydraulic diameters.

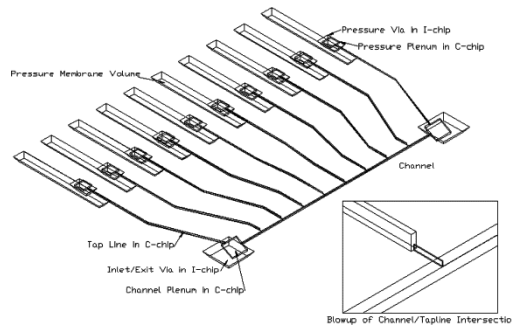


FIGURE 1.8 – Measurement of the static pressure in a micro-channel, Kohl *et al.* (2005)

Judy *et al.* (2002) have realized different experimental campaigns using three working fluids (distilled water, methanol, isopropanol), in ducts having different cross sections (square, circular) of hydraulic diameters ranged from 15 to $150 \mu m$ and for Reynolds number ranged from 8 to 2300. The author did not noticed any deviations from the usual Navier-Stokes laws for these experiments.

1.4.3 Experiments regarding heat transfer coefficients evolution

Similarly to the pressure drop analysis, many results have been obtained for the evolution of the transfer coefficients in the literature. Therefore, we introduced in the next paragraphs, two papers (among many) which summarized the recent convergence of the experimental results related to the heat transfer in mini-channels.

Qu et Mudawar (2001) have experimentally studied the flow of deionized water in a network of 21 parallel channels of hydraulic diameter of $349 \mu m$. The test section was fabricated in a copper block and was closed using a polycarbonate cover. In order to limit the effects of longitudinal conduction, the heating elements were inserted in thermally insulated compartments. The

Chapitre 1. Compendium on single-phase flows in mini-channels

range of studied Reynolds numbers was varied between 139 and 1672 for two different wall heat fluxes of 100 W cm^{-2} and 200 W cm^{-2} . In parallel, the authors realized a 3D numerical model (which took into account hydrodynamics and thermal behaviors) that was in good agreement with their experimental results.

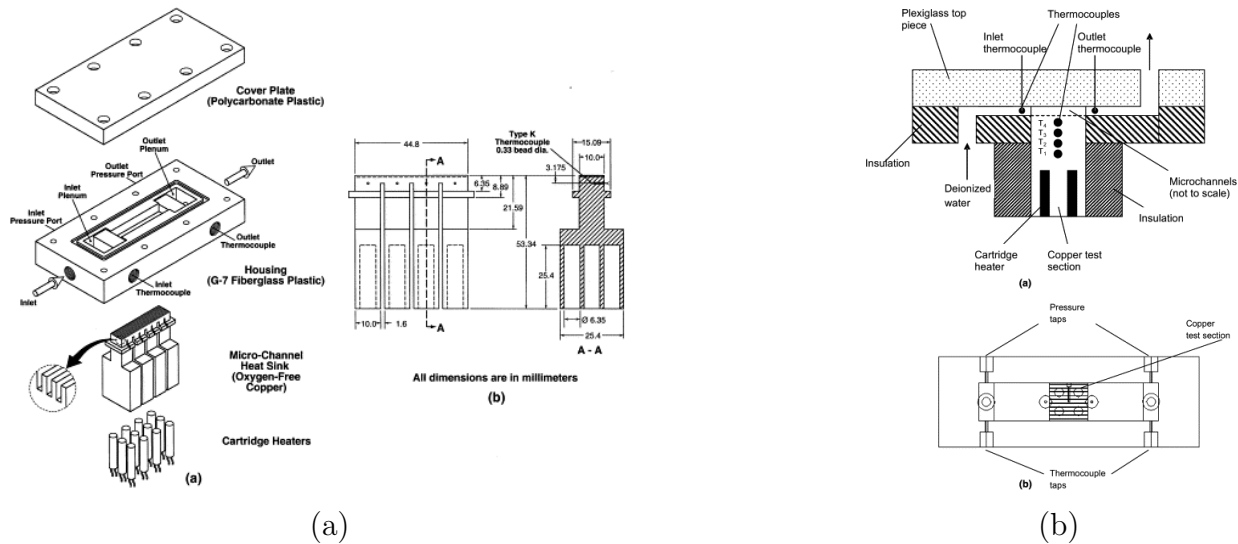


FIGURE 1.9 – Test section developed by : (a) Qu et Mudawar (2001) (b) by Lee et Mudawar (2005b)

Lee et Mudawar (2005b) studied the heat transfer for 5 different test sections whose hydraulic diameter was varied between $318 \mu\text{m}$ and $903 \mu\text{m}$. Each test section consisted of 10 parallel micro-channels. The Reynolds number was comprised in between 300 and 3500. The working fluid was deionized water. The test section was fabricated in a copper block with a PMMA (Poly(methyl methacrylate)) cover sit on its top, which was thermally insulated using an epoxy resin in the lower part, and surrounded by glass fibers. Drilled holes that were realized in the lower part of the test section, allowed for the insertion of four heating cartridges which can give a combined and maximal power of 800 W . Four thermocouples were axially distributed under the channel and were spaced by 6.15 mm . The first thermocouple was placed at 3.18 mm from the solid/liquid interface.

The authors were interested in the fully developed laminar regime and in the transition regimes. Their results showed that the heat transfer coefficients increased with the decrease of the hydraulic diameter. A 3D numerical simulation, which took into account the conjugated effects due to hydrodynamics and thermal conditions, has been realized and showed a good agreement between experimental and numerical data. The authors explained that if the entrance conditions and the boundary conditions were well defined, it was then possible to describe correctly the flow evolution using the conventional analysis made by Navier-Stokes.

1.5 Chapter 1 Conclusions

The whole set of recent results showed that the evolution of the friction and heat transfer coefficients remained consistent with the theory for the ducts of very small dimensions. The differences that have been observed in the literature were certainly due to, incorrect considerations of the geometry (entrance effects for example), not well defined experimental conditions, and/or to unadapted sensors regarding the test sections.

In single-phase flow and for high heat flux (or high confinement), the wall temperature variations can be very large between the inlet and the outlet of the test section. These conditions can bring penalties for the cooling efficiency. Moreover, when the dimensions become smaller, the pressure drops increase very rapidly with the flow rate. As a consequence, for the cooling of systems of small dimensions, it could be mandatory to increase the pumping power as soon as the cross section is decreased. The study of internal boiling flow should take into account some of these issues as for an equivalent pressure drop, the heat transfer has usually a higher amplitude. The analysis of hydrodynamics and heat transfer at smaller scales is the focus of the present study. Therefore, we have to highlight the most important points which impact the hydrodynamics and heat transfer rate evolutions for an internal convective boiling flow in channels of small dimensions. We will analyze these points in **Chapter 2**.

Literature review on the boiling in mini-channels

2.1	Fundamental definitions in two-phase flows	27
2.1.1	Parameters of reference	27
2.1.2	Definition of main non-dimensional numbers	29
2.1.3	Other numbers and definition of some important notions	31
2.2	From the conventional scales to the smaller ones	33
2.2.1	Introduction	33
2.2.2	Flow classification	33
2.2.3	Flow regime for convective boiling	36
2.2.4	Heat transfer mechanisms during boiling	37
2.3	Parameters that have an influence on the boiling nature	46
2.3.1	Working fluid selection	46
2.3.2	Wettability properties of the fluid with the wall	56
2.3.3	Working conditions	59
2.3.4	Flow cross section	67
2.4	Prediction of the pressure drops evolution	73
2.4.1	Presentation of theoretical data	73
2.4.2	Pressure drops for two-phase flow	73
2.4.3	Void fraction evolution	84
2.5	Prediction of the heat transfer coefficients evolution	88
2.5.1	Presentation of the theoretical data	88
2.5.2	Correlations taken from literature	90
2.6	Chapter 2 conclusions	98

Summary :

THE objective of this chapter is to give a summary of the main mechanisms of convective boiling in mini-channels. We will present in a first step the

Chapitre 2. Literature review on the boiling in mini-channels

parameters which will be used throughout this manuscript. Then from the current literature, the parameters which impacted the hydrodynamics and heat transfer rate of a boiling flow will be detailed. This paragraph will specify the influence of the geometry on the evolution of the heat transfer coefficients. In a last paragraph, we will give the main predictive correlation that allow for the calculation of the pressure drops and heat transfer rate.

2.1 Fundamental definitions in two-phase flows ¹

We introduce in this paragraph the fundamental definitions that will be used in the manuscripts, as well as the simple relations that can relate them.

2.1.1 Parameters of reference

📖 *Vapor quality*

Vapor quality (x) is an important variable which expresses the vapor proportion into an internal two-phase flow. It is defined as the ratio between the vapor mass flow and the total mass flow. For an adiabatic flow it is given as :

$$x = \frac{\dot{m}_v}{\dot{m}_l + \dot{m}_v} \quad (2.1)$$

with \dot{m}_v and \dot{m}_l which are the vapor and liquid mass flow rates respectively. The calculation of the vapor quality needs the measurement of the mass flow of the two different phase (liquid and vapor) as showed by equation (2.1). its value can be defined on the whole duct length as soon as the entrance conditions are known for an adiabatic flow. When phase change occur, this value cannot be determined using equation (2.1) and it become particularly difficult to determine its value with accuracy. This is due to the existence of a thermal non equilibrium between the liquid and the vapor phase. Therefore, a fictive vapor quality, that is called thermodynamic vapor quality can be calculated using :

$$x = \frac{h_m(z) - h_l}{h_{lv}} \quad (2.2)$$

where h_l is the liquid enthalpy for saturated conditions, h_{lv} the latent heat of vaporization. $h_m(z)$ is the mean enthalpy value on the cross section which is located at the position z of the duct, which is calculated following :

$$h_m(z) = h_{amont} + \frac{1}{\dot{m}} \int_{amont}^z \dot{q}''(z) dz \quad (2.3)$$

with h_{amont} that is the enthalpy at the duct entrance, \dot{m} , the total mass flow rate and $\dot{q}''(z)$, the heat flux density.

1. Numerous notions that have been given in this section can be found in Agostini (2008).

Void fraction

The void fraction (α) is a fundamental parameter in two-phase flow, that is often difficult to characterize experimentally. It defines (in the case where the void fraction is measured on the cross section) the ratio between the area occupied by vapor (A_v) and the total area ($A_{tot} = A_v + A_l$, where A_l is the area occupied by the liquid) :

$$\alpha = \frac{A_v}{A_l + A_v} \quad (2.4)$$

Mass flux

The mass flux (G) is a parameter which is often used for internal two-phase flow that occurred in duct of different cross section (A). Indeed, it allows for the consideration of the impact of this cross section on the total mass flow rate (\dot{m}) and is given using :

$$G = \frac{\dot{m}}{A} \quad (2.5)$$

Liquid and vapor velocities

The true velocities are very important values, but often very difficult to obtain. Indeed, the calculation of these velocities needs the knowledge of the thermodynamic vapor quality and at the same time of void fraction. The calculation of the liquid (u_l) and vapor (u_v) velocities is made following the relations :

$$u_l = \frac{G(1 - x)}{\rho_l(1 - \alpha)} \quad (2.6a)$$

$$u_v = \frac{Gx}{\rho_v\alpha} \quad (2.6b)$$

where ρ_l is the liquid density and ρ_v the vapor one.

Liquid and vapor superficial velocities

In an experimental way, it is more easy to obtain the thermodynamic vapor quality instead of the void fraction. Therefore, in order to draw flow maps that give the transition between the different flow regimes, the liquid (j_l) and vapor (j_v) superficial velocities are generally used. There are defined as :

$$j_l = \frac{G(1 - x)}{\rho_l} \quad (2.7a)$$

$$j_v = \frac{Gx}{\rho_v} \quad (2.7b)$$

2.1.2 Definition of main non-dimensional numbers

👁️ Reynolds number

The Reynolds number (Re) is a key parameter in fluids mechanics. It represents the ratio between the inertia forces to the viscous ones and it is often used to characterize the transition from a laminar flow to a turbulent one. In the case of a single-phase flow, it is expressed following :

$$Re = \frac{\rho_l u_l d_h}{\mu_l} \quad (2.8)$$

with μ_l which is the dynamic liquid viscosity and d_h the hydraulic diameter. This parameter (d_h) represent the ratio between the channel cross section (A) and the wetted perimeter (p_l) :

$$d_h = \frac{4A}{p_l} \quad (2.9)$$

By considering the two-phase flow as a juxtaposition of two 1D flow and by using the true velocities [equations (2.6a) and (2.6b)], it is possible to express the Reynolds numbers for the liquid and vapor phases as :

$$Re_l = \frac{G(1-x)d_h}{(1-\alpha)\mu_l} \quad (2.10a)$$

$$Re_v = \frac{Gxd_h}{\alpha\mu_v} \quad (2.10b)$$

👁️ Nusselt number

The Nusselt number (Nu) gives the ratio between the convective and conductive heat effect. For an internal flow, the reference length is the duct hydraulic diameter. This non-dimensional number is expressed following :

$$Nu = \frac{hd_h}{\lambda_l} \quad (2.11)$$

where h is the heat transfer coefficient and λ_l , the liquid thermal conductivity.

Prandtl number

The Prandtl number (Pr) is the ratio between the viscous diffusivity and the thermal diffusivity effects. It can be expressed regarding the liquid or vapor phase as :

$$Pr_l = \frac{c_{p,l}\mu_l}{\lambda_l} \quad (2.12a)$$

$$Pr_v = \frac{c_{p,v}\mu_v}{\lambda_v} \quad (2.12b)$$

where $c_{p,l}$ and $c_{p,v}$ are the liquid and vapor specific heat at constant pressure. μ_v and λ_v are the dynamic viscosity and the thermal conductivity of the vapor phase.

Weber number

The Weber number (We) gives the ratio between inertia and surface tension forces. Similarly to the Nusselt number, the reference length is the duct hydraulic diameter. This number is expressed as :

$$We = \frac{\rho_l u_l^2 d_h}{\sigma} \quad (2.13)$$

where σ is the liquid surface tension.

Boiling number

The boiling number (Bo) defines the ratio between the vapor velocity for a domain place far from the surface to the velocity located alongside to the heated surface. It allows for the characterization of the impact of the nucleate boiling regime on the heat exchange during the convective boiling and is expressed following :

$$Bo = \frac{q''}{Gh_{lv}} \quad (2.14)$$

Convection number

The convection number (Co) is a number that was considered for replacing the Lockhart et Martinelli (1949) parameter. It is wise to use it when the viscosity ratio between the vapor and the liquid is close to unity. This number represents the ratio between the liquid and vapor pressure drops. Generally it allows for the characterization of the convective contribution and is expressed following :

$$Co = \left(\frac{x}{1-x} \right)^{0.8} \left(\frac{\rho_v}{\rho_l} \right)^{0.5} \quad (2.15)$$

2.1.3 Other numbers and definition of some important notions

☞ Capillary length

This characteristic number gives the length from which the capillary forces are equivalent to the gravity forces. This length can become relevant when one looks to a way to define a transition for the flow in conventional channels compared to the ones for the channels of small dimensions. It is given using :

$$l_c = \sqrt{\frac{\sigma}{g(\rho_l - \rho_v)}} \quad (2.16)$$

where g is the gravity acceleration.

☞ Critical and reduced thermophysical properties

The critical point is a singular point from which the transition between the liquid and vapor phases do not exist any more. The phase diagram (Figure 2.1) gives the frontiers from which a phase change occurs. At the critical point, the liquid boiling mechanism and the vapor condensation occurred at same time and can not be observed experimentally. Moreover above this value, the fluid thermophysical properties are generally not well known².

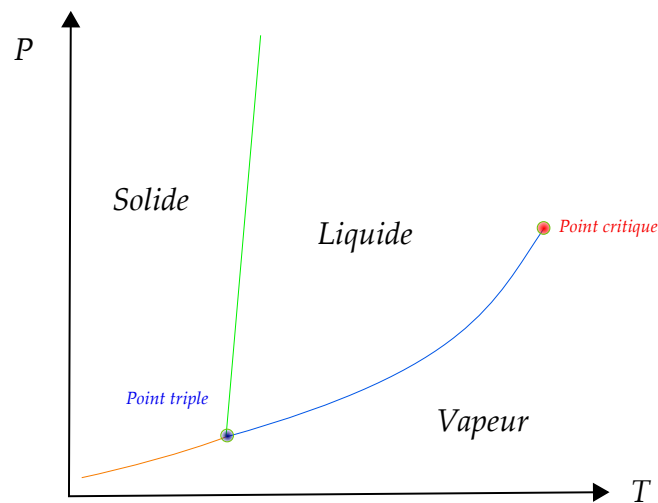


FIGURE 2.1 – Phase diagram (triple point and critical point are given)

2. We can take as an example the surface tension of the liquid which become close to zero. In this configuration the mass transfer at the interfaces is very strong.

Chapitre 2. Literature review on the boiling in mini-channels

It is important, when doing a study related to phase-change, to know the temperature, pressure and density values that allow for the obtaining of the critical conditions. On Table 2.1 some temperatures, pressures and densities values have been reported for several fluids that have been used in literature (in the context of boiling flows).

Fluides	T_{crit} ($^{\circ}C$)	P_{crit} (bar)	ρ_{crit} (kg/m^3)
Eau	374.1	220	322
CO ₂	30.1	73.7	467.6
Ammoniaque	132.2	113	225
Propane	96.6	42.4	218.5
Propanol	235.1	47.6	270
HCFC 141b	206.8	44.6	460
HFC 134a	101.1	40.5	511.9
Forane 365 HX	189	29.8	N/A
HFE 7100	195.3	22.3	555
FC 72	175.8	18.3	N/A

TABLE 2.1 – Critical properties for several fluids that have been used for cooling in boiling flow conditions - N/A is related to a non available data

The reduced temperature, pressure and density are values which allow for the determination of the working condition more or less close to the critical point. Indeed, specific process that take place in a boiling flow (as the for the conditions leading to the critical heat flux) may depend on the reduced properties. These properties can be expressed as :

$$T_r = \frac{T}{T_{crit}} \quad (2.17a)$$

$$P_r = \frac{P}{P_{crit}} \quad (2.17b)$$

$$\rho_r = \frac{\rho}{\rho_{crit}} \quad (2.17c)$$

2.2 From the conventional scales to the smaller ones

2.2.1 Introduction

Since the first analysis of Tuckermann et Pease (1981), a very important work has been done in the context of heat and mass transfer at small scale. The miniaturization of the heat exchangers led to a significant reduction of the volume to surface ratio, what allow for the increase of the heat and mass transfer. Nowadays there is many different technologies that have been considered for the cooling of small scale systems. Agostini *et al.* (2007) have identified 4 different technologies for the cooling of duct subjected to very high heat fluxes :

- ① single-phase flows with channels of small dimensions,
- ② flows in porous media,
- ③ cooling using impacting jets,
- ④ two-phase flow in channels of small dimensions.

The authors have showed that boiling in channels of small dimensions allow for the obtaining of the best performances (i.e. small pumping power and high heat transfer coefficients). Nonetheless, when the channels dimensions are reduced, deviations from the usual correlation may exist. Then, it become necessary to establish, the domain of validity of these laws, in order to draw laws that could be more adapted to these scales.

2.2.2 Flow classification

a) Regarding the geometry

Up to date, the most part of the internal two-phase flows takes place in circular tubes of relatively large hydraulic diameter. At these scales, numerous laws and correlations have been made for describing the observed flow in the Petroleum and Nuclear Engineering fields. A smaller scale, the flow cross section may be reduced in a important fashion and have very different shapes compared to the one of a circular tubes. Indeed, the photo-lithographic techniques that have been used for the fabrication of reduced geometry allow for the realization of non-circular cross sections (namely, rectangular, triangular or trapezoidal among other). In this context, the use of the hydraulic diameter as a parameter of reference became more and more relevant in the literature. This parameter allow for the direct comparisons between the various results that have been obtained for a flow in a circular tube and a flow inside these different cross sections.

The literature results (Bergles *et al.* (2003), Dupont et Thome (2005), Saitoh *et al.* (2005), Harirchian et Garimella (2009) among other) showed that some deviations regarding the existing law for bigger scale for the two-phase flows, may occur when the flow cross section is reduced. These deviations are related to friction coefficient, flow regime repartition (vapor and liquid

phases) and heat transfer rate evolutions. In order to define a threshold for the use of the laws used at larger scale, several authors (Mehendale et Jacobi (2000), Kandlikar (2002) among others) have drawn classifications that depend on hydraulic diameter (d_h). These classification allow for the establishment of a confidence level for the use of the correlation that have been constructed for tube of larger dimensions. The Kandlikar (2002) classification, which is largely used refers to the different categories of dimensions that can be encountered in industry :

$$\left\{ \begin{array}{ll} d_h > 3\text{mm} & \text{(conventional channels)} \quad (a) \\ 200\mu\text{m} < d_h \leq 3\text{mm} & \text{(mini-channels)} \quad (b) \\ 10\mu\text{m} < d_h \leq 200\mu\text{m} & \text{(micro-channels)} \quad (c) \end{array} \right. \quad (2.18)$$

One can note that Agostini (2002) assesses that the expression of the hydraulic diameter is not a strong marker of the confinement effect in a rectangular channel and the transition from macroscale to microscale flow should be defined regarding the smaller dimension of the cross section which play the most important role compare to the other one. He suggests in his work to define a confinement parameter following this smallest dimension.

Thome (2004) underlined that these classifications did not take into account any physical phenomena occurrence inside the two-phase flow and suggest that these classifications should be used with caution.

b) Classification regarding physical phenomena

Thome (2004) explained that it should be more relevant to refer to the bubble diameter detachment from the wall for defining a confinement parameter. Thus, when the bubble detachment is larger than the hydraulic diameter, the flow may be defined as a microfluidic one. Numerous correlations for estimating this detachment diameter have been obtained in pool boiling studies. The author suggest to refer in a first step to the Fritz (1935) correlation for determining this diameter ³ :

$$d_{det} = 0.0208\theta \left[\frac{\sigma}{g(\rho_l - \rho_v)} \right]^{1/2} \quad (2.19)$$

θ is the contact angle between the fluid and the surface wall, σ the liquid surface tension, g the acceleration due to gravity, ρ_l et ρ_v , the liquid and vapor densities.

The Kew et Cornwell (1997) parameter (C_0), compared the buoyancy to the gravity forces.

3. Other correlation may be found in Kutateladze (1961) or more recently in Phan *et al.* (2009).

It has been established to take into account the physical effects that may take place for a two-phase flow :

$$C_0 = \sqrt{\left(\frac{\sigma}{g(\rho_l - \rho_v)}\right)} \left(\frac{1}{d_h}\right) \quad (2.20)$$

The results that have been obtained by these authors have demonstrated that the laws that have been defined for larger scales are respected as soon as $C_0 < 0.5$. Other authors (Cheng *et al.* (2007), Ullman et Brauner (2006)⁴) have nonetheless proposed different values for the confinement number to establish this transition toward the microfluidic flows. This discrepancy in the confinement number analysis proved that this parameter did not bring to an agreement for determining the transition from macro-scale flows to the micro-scale ones. Recently, Chen *et al.* (2009) have suggested that the transition from the large scale flow and the micro-scale flows may be controlled by the competition between the inertial and surface tension forces. Contrary to Kew et Cornwell (1997), the authors assumed that the buoyancy forces are negligible compared to the inertia forces when the flow cross section is reduced. From this assumption they obtained an analytical expression of the transition hydraulic diameter (d_{tran}) from which the two-phase flow should be confined :

$$d_{tran} = \frac{160}{9} \frac{(\sigma\rho_l - 3\mu_l G)}{G^2} \quad (2.21)$$

where μ_l is the liquid dynamic viscosity and G the flow mass flux. One can note that this parameter has not been tested at large scale in the literature to be confirmed yet, but it seems to be promising.

It is interesting to note that the value of this transition diameter depend on the flow rate. Notwithstanding all tentatives, a relevant physical parameter has not been determined yet for characterizing a transition from macro-scale flows to micro-scale one. In the framework of the results given in this manuscript, the studied dimension will refer to the mini-channel flows regarding the classification given by Kandlikar (2002).

4. These references have been extracted from Agostini *et al.* (2008).

2.2.3 Flow regime for convective boiling

During the study of boiling, it is essential to identify the different flow regimes that will be established in the duct. These regimes are strongly dependent of the working conditions such as the pressure, flow rate and wall heat flux, thermophysical characteristics of the working fluid as well as surface roughness also. The identification step of the flow regime is important for the understanding the physical phenomena that characterize the evolution of the friction and heat transfer coefficients. On Figure 2.2 the flow regime that have been encountered in the study of Fu *et al.* (2007) have been given for a tube of 1.931 mm and an upward flow of liquid nitrogen.

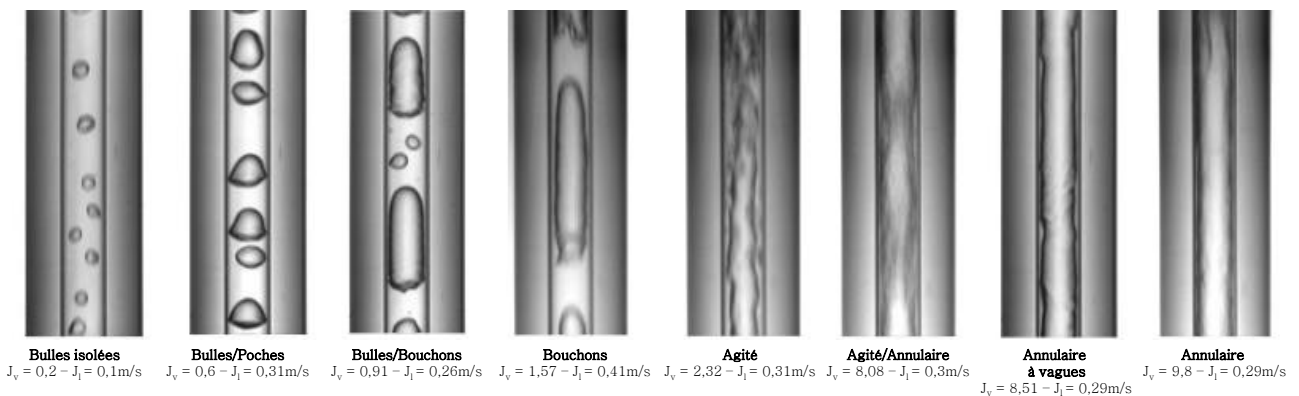


FIGURE 2.2 – Flow regime and transition that occurred in a upward vertical flow of liquid nitrogen in a tube of 1.931 mm regarding Fu *et al.* (2007)

For horizontal flows, the flow configurations are more numerous than for the vertical flows for duct of large hydraulic diameters. Indeed, the gravity force brake the flow symmetry and a stratified flow may take place. When the dimensions are reduced, the surface tension effect play a most important role and the stratified flow, which could be visible for large tubes, may completely vanished. In this case the flow direction and orientation may have a smaller importance.

At small scales, there is nowadays numerous results. Nonetheless, there is no universal definition for the flow regime description that occur inside mini-channels. It can be noticed that numerous analysis have been made for adiabatic conditions. Nevertheless, Carey (2008) specified that the flows subjected to heat flux had similar flow regimes transitions compared to adiabatic flow as soon as the unstable phenomena related to flow reversal did not take place.

Kew et Cornwell (1997) have studied R141b flows in tubes of hydraulic diameters ranged between 1.39 – 3.69 mm and three flow configurations have been observed : isolated bubble regimes, confined bubble regime, alternating of annular and vapor slugs regime. A flow that consisted of a mixing of water / air in the duct of circular and triangular cross section ranged

between 1.1 – 1.5 mm have been studied by Triplett *et al.* (1999). The authors have counted up to five regimes for the analysed configurations. Fu *et al.* (2007) have analysed a liquid nitrogen flow in a tube of 1.931 mm, and observed four regimes in their configuration. Saisorn et Wongwise (2010) counted the same number of flow regime for a mix between water / air in three tubes of hydraulic diameter of 0.53 mm, 0.22 mm and 0.15 mm, but they were different to those observed by Fu *et al.* (2007). The numerous discrepancies between these data were due to the still subjective character of the observations that have been realized in the literature. These discrepancies were mainly due to different considerations between the transitions between the flow regime.

When the identification of the flow regimes has been made, maps that are velocity-dependent (real or superficial) regarding the liquid or the vapor can be built. These maps allow for the realization of experiments where the appearance of a specific regime can be favoured regarding the targeted application. Some of the well-known maps can be found in Baker (1954), Mandhane *et al.* (1974), Taitel et Dukler (1976).

2.2.4 Heat transfer mechanisms during boiling

a) Without inertial effect : pool boiling

For addressing the description of the heat transfer mechanisms that appear during convective boiling, it is necessary to consider, in a first step, a simple configuration without taking into account the inertial effects : pool boiling. Physical phenomena related to heat transfer between a wall and a boiling fluid have been studied for this configuration (see Nukiyama (1934)).

The influence of the heat flux on the evolution of wall superheat is given on the Figure 2.3. This figure is often called boiling curve.

The evolution of the boiling curve can be described as followed :

- (1) From point A to point C (or C' if the heat flux is the parameter of control), the surface is surrounded by the liquid and the heat transfer is made by natural convection. The heat transfer coefficient, which is associated with the natural convection, is relatively small and the heat flux q'' increases slightly with the temperature difference between wall temperature and saturation temperature ($T_p - T_{sat}$).
- (2) When wall superheated become sufficiently important (point C/C'), small vapor bubbles incipience occur on specific locations of the surface, which are called nucleation sites. This step is currently called onset of nucleate boiling (ONB)⁵. This is the nucleate boiling regime with isolated bubbles (C/C'-E). Two different situations may occur if :

5. In the remaining part of the manuscript, we will employ this term for defining this conditions.

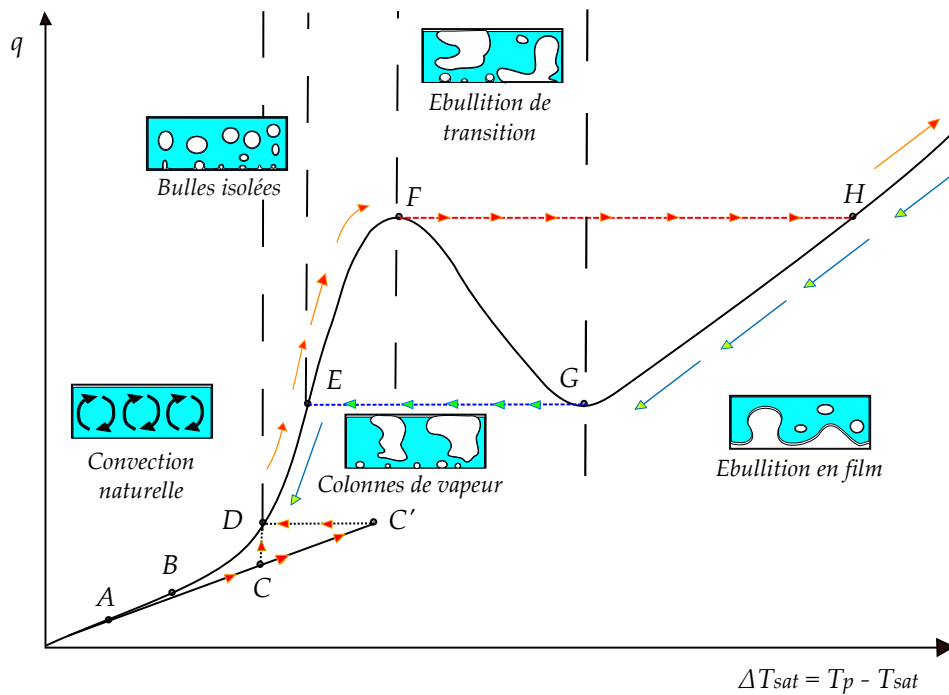


FIGURE 2.3 – Evolution of the boiling curve in function of the heating or the cooling

- a - The wall temperature is kept constant : the vapor bubbles occurrence lead to a heat flux increase. The system goes from point C to point D on a vertical branch,
 - b - the heat flux is kept constant : the apparition of the vapor bubbles lead to a reduction of the wall temperature. The system goes from point C' to point D on a horizontal branch.
- (3) When boiling has started, an increase of the wall superheat (or heat flux) activates more sites and the bubbles are produced with higher frequency. The vapor quantity increases with the increase of the parameter of control (q'' or $T_p - T_{sat}$). The bubbles coalesce, forming gas slugs and gas columns that rise up into the liquid (which is static) (E-F). At point F, the vapor volume production is so high that the liquid cannot reach the heated surface to cool it down. This surface is partially covered with vapor slugs that trap liquid. This liquid evaporates what lead to a surface local dry out. Two different situations can take place. If :
- a - the temperature is kept constant : the dry surface spots, which are covered with vapor, will transfer less heat than the spots that are wetted by the liquid. This lead to a decrease of the heat transfer convected by the liquid (from point F to G),
 - b - the heat flux is kept constant : above a threshold value (at point F), a very strong increase of the heated surface temperature can take place and in specific cases can

« damaged » strongly the cooling device. The system goes from point F to point H on a horizontal branch.

The maximal heat flux value (F) which is called Critical Heat Flux (CHF) correspond to boiling crisis.

- (4) Above the point G, the vapor thin film is stable. This is the thin film boiling regime, for which the heat flux increase in a monotonically way with the temperature. The conductive and convective heat transport is increased with the wall superheat. The radiative transport through the vapor layer may become important when considering very high temperature.

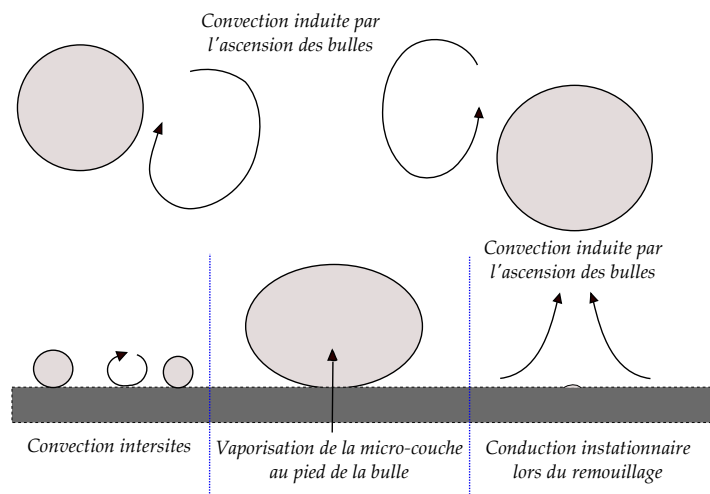


FIGURE 2.4 – Heat transfer mechanism in nucleate boiling regime

It should be noticed that for saturated nucleate boiling regime (between the points D and F), three main contributions related to heat exchange between the wall and the fluid may be identified (Figure 2.4) :

- ▷ the heat exchange by convection in between the nucleation sites and the heat exchange due to the convection which is induced by the rising of the bubbles that detached from the surface (liquid agitation that makes easier the convection transport near the surface),
- ▷ the liquid micro-layer vaporization at the bubble foot,
- ▷ the thermal exchange by non-stationary conduction during the wall re-wetting by a cooler liquid after the bubble departure.

When the mechanism is driven by the heat flux, the boiling curve present a hysteresis with depend on the heating or cooling (of the plate or the wires). During the heating, the boiling curve evolution goes through the succession of points given in the series ①, that is describe below. During the cooling (when the flow is in the film boiling regime), the boiling curve

evolution goes through the series ②. In these two following cases, it is possible to observed that the transition boiling regime does not exist if the mechanism is driven by the heat flux.

① $A \rightarrow C \rightarrow C' \rightarrow D \rightarrow E \rightarrow F \rightarrow H$.

② $H \rightarrow G \rightarrow E \rightarrow D \rightarrow B \rightarrow A$.

Numerous parameters may modified the evolution of the boiling curve (undercooling, pressure, surface roughness, fluid wettability, thermophysical properties of the fluid) but this aspect is beyond the analysis that has been made in this manuscript. More detailed analysis may be found in Collier et Thome (1994) or Carey (2008).

b) With inertial effects : internal convective boiling

The consideration of the heat transfer mechanism during convective boiling is more complex when compared to pool boiling. The addition of an inertial component can make appear new forces, that act on the flow and can in some cases drive the heat transfer from the wall to the liquid. From a thermodynamic point of view, phase change implies two mechanism during convective boiling :

▷ Nucleate boiling

This mechanism is driven by bubbles development on a heated wall. In this specific case, the pool boiling experiments showed that heat exchange coefficient is not affected by the flow rate or the thermodynamic vapor quality. In other hand, this heat exchange coefficient is fully driven by the wall heat flux (or the wall superheating). Numerous correlative laws exist for determining this heat transfer coefficient during this bubbles development mechanism. These correlations can be written in a general form as followed :

$$q'' = \eta [T_p - T_{sat}(P)]^m \quad (2.22)$$

η is a parameter that is dependent on surface and fluid thermophysical properties. T_{sat} is the saturation temperature that is determined in function of the system pressure P . The parameter m is a exponent that is comprised between 2 and 4.

▷ Convective evaporation

This mechanism correspond to the liquid vaporization at the liquid/vapor interfaces when there is a liquid flow. In this configuration, the correlations that have been established are often dependent of the flow rate or thermodynamic vapor quality variations. For this case, the heat flux does not have a significant impact on the heat transfer rate and it can be assumed that surface roughness impact is negligible.

Onset of nucleate boiling

An important parameter that should be considered for the study of the convective boiling is the determination of the position where the onset of nucleate boiling (which is related to the transition from a single-phase flow to a two-phase flow) occur. This parameter cover the phenomena of bubble incipience on the wall, its possible sliding on the wall, up to its detachment from this wall. From this point, the results that have been obtained in a experimental way start to deviate from the correlations that have been drawn for the single-phase flows. Therefore, the determination of the heat flux (or wall superheat) conditions leading the ONB incipience is key for the sizing of the heat exchangers.

Hsu (1962) seems to be the first author that has built a semi-empirical model for determining the criteria that lead to ONB. He has supposed that a vapor embryo was located on a nucleated site placed on the wall. The heating of the wall led to the development of the boundary layer near this site. Hsu (1962) showed that ONB may occur in function of a minimal wall superheat ($T_p - T_{sat}$). Its model allow for the determination of a range of nucleation site diameter that can be activated for pool boiling conditions.

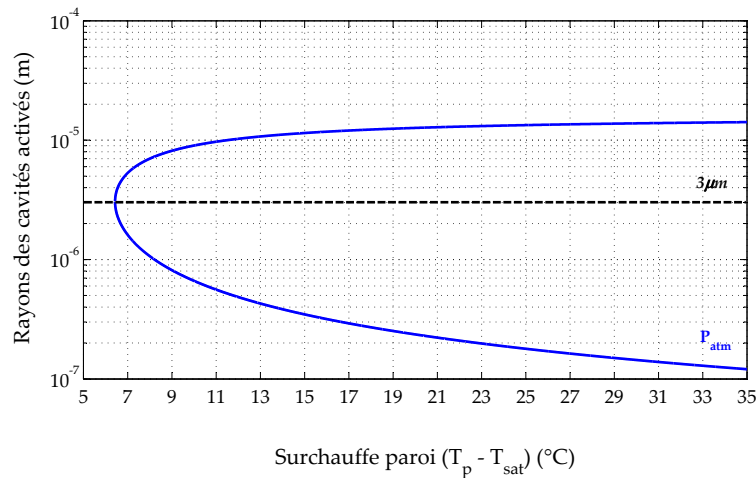


FIGURE 2.5 – Activable nucleation site regarding Hsu (1962) for Forane 365 HX

The Figure 2.5 gives the range of nucleation sites for Forane 365 HX by considering a heat transfer coefficient of $4000 \text{ W}\cdot\text{m}^{-2}\cdot\text{K}^{-1}$. The thermal boundary layer has a thickness of $32 \mu\text{m}$ where the first nucleation sites should have a radius of $3 \mu\text{m}$ for a minimal wall superheat of 6.4°C regarding the data given by Hsu (1962).

Using the large current database for convective boiling flows for water under saturated conditions, other authors (Bergles et Rohsenow (1964), Sato et Matsumura (1964), Davis et Anderson (1966)), have determined the minimal heat flux for reaching the ONB conditions.

Chapitre 2. Literature review on the boiling in mini-channels

Frost et Dzakowic (1967) have determined the heat flux necessary for the ONB for a very large set of fluid (including refrigerants) for saturated conditions ⁶ :

$$q''_{ONB} = \frac{\lambda_l h_{lv} \rho_v}{8\sigma T_{sat}} [(T_p - T_{sat})^2 Pr_l^{-2}] \quad (2.23)$$

where λ_l is the liquid thermal conductivity, h_{lv} the latent heat of vaporization, ρ_v the vapor density and Pr_l the liquid Prandtl number.

The knowledge of the heat flux or of the wall superheat, allow for the estimation of the position of the ONB, using a heat balance made on the mini-channel. For a single-phase flow that is fully developed and using an assumption of uniform heat flux, a constant cross section and with a inlet temperature equals to $T_{l,amont}$, this balance can be written (Figure 1.3) as :

$$\int_0^a \int_0^b \rho_l c_{p,l} (T_l(z) - T_{l,amont}) \vec{u}_l \cdot \vec{n} dS = - \int_0^{z_{ONB}} q'' p dz \quad (2.24)$$

where ρ_l is the liquid density, $c_{p,l}$ the liquid specific heat at constant pressure. By expressing u_l (fluid velocity) in function of G and the perimeter value (p) and the channel cross section (S) in function of the channel width (a) and height (b) we obtain :

$$q''_{ONB} = \frac{G c_{p,l} (T_l(z_{ONB}) - T_{l,amont})}{z_{ONB}} \left[\frac{ab}{2(a+b)} \right] \quad (2.25)$$

If the convective heat transfer coefficient (h_l) is constant along the channel wall with a homogeneous heat flux, then :

$$q'' = h_l [T_p(z) - T_l(z)] \quad (2.26)$$

By replacing $T_l(z_{ONB})$ expression from equations (2.25) and (2.26), the position where the ONB occur is given by :

$$z_{ONB} = G c_{p,l} \left[\frac{ab}{2(a+b)} \right] \left[\frac{(T_p(z_{ONB}) - T_{l,amont})}{q''_{ONB}} - \frac{1}{h_l} \right] \quad (2.27)$$

Practically, only the correlation can allow for the determination of the right position for the ONB occurrence, which is due to the combination of numerous mechanisms, what make its prediction complex. Several teams work currently on semi-analytical theories that take into account the physical phenomena which act on ONB of bubble detachment. This study is above the analysis given in this manuscript but the reader who get interest in this topic may rely on the work of Colin *et al.* (2009).

6. Numerous correlations can be found in Liu *et al.* (2005) (See Table 1).

Instabilities in confined spaces

Instabilities can occur when the duct hydraulic diameter is reduced. Indeed, for the flows in mini-channels, the bubbles detachment from the wall can induced coalescence and from vapor slugs, that tackle the liquid which is trapped very near the wall. This condition leads to an increase of the interfacial and wall frictions. A reduction of the mass flow rate that lead to a wall temperature increase can occurred in this case. From a specific duct threshold, the bubble growth can become so quick (and violent) that their axial growth can make appear cyclic instabilities conditions (Figure 2.6). Some situation where backflow (bubble growth toward the channel entrance)⁷ may be seen. This backflow is followed by a flow rate reduction which lead to an increase of the inlet pressure and lead to the draining of the bubble from the duct. After the bubble draining the phenomenon can be repeated with a new elongated bubble growth in the duct.

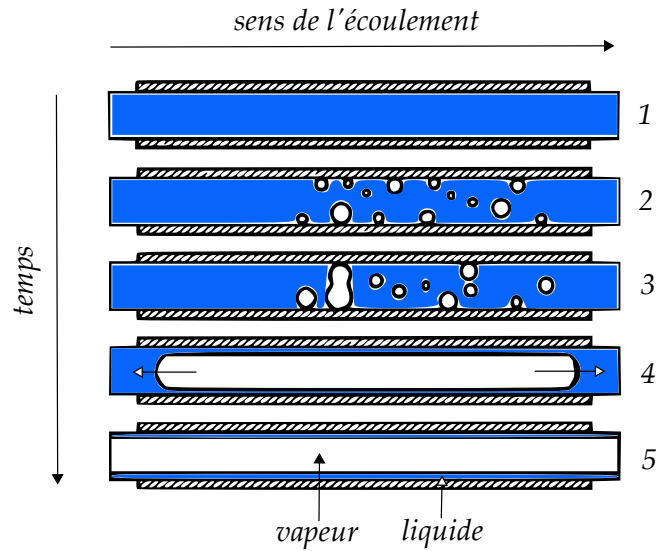


FIGURE 2.6 – Instabilities in small dimensions ducts Consolini (2008)

7. The interested reader may find more information on mini-channels instabilities in Wu et Cheng (2003), Kandlikar (2006), Huh *et al.* (2007), Wang *et al.* (2007), Consolini (2008).

Critical heat flux (CHF)

The conditions for CHF occurrence during convective boiling are of high importance. For heat fluxes values (see ①), or for heat exchanger that are not well sized⁸ (see ②), some mechanisms of wall dryout that can deteriorate the working of the heat exchanger may occur.

① The bubble generation frequency is very high. The bubble very close to each other tend to coalesce between them and formed vapor slug that insulated completely the mini-channel wall from the liquid that is in the center line. The increase of the wall temperature in these cases is very high and can damaged quickly the experimental device. the incipience of the phenomenon is called the dryout of first type or Departure from Nucleate Boiling (DNB).

② The convective boiling goes from a succession of flow regimes. During the annular regime, the vapor velocity at the duct center can become very high compared to the liquid velocity. For the conditions where the velocity difference or the difference between the liquid and vapor densities, the evaporation of the liquid thin film may lead to this dryout if the duct length is too long.

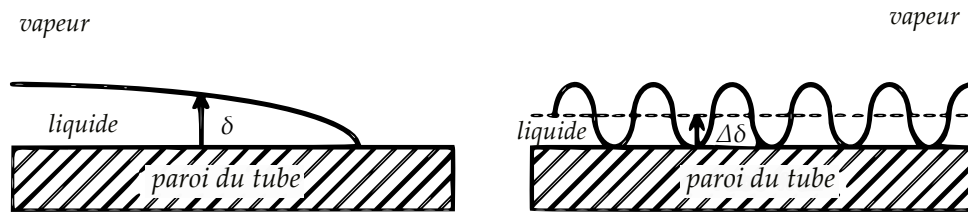


FIGURE 2.7 – Mechanism that lead to dryout respecting case ② according to Revellin *et al.* (2008)

For the conditions for which this velocity difference is large, significant interfacial shear stress may lead to interfacial instabilities of Kelvin-Helmholtz type (Figure 2.7). In function of the amplitude of these instabilities, dry spot region can appear. In this last case, the partial dryout conditions are fulfilled. The wall temperature increase for this case in less harsh compared to the previous one. This phenomena is called dryout of second type.

8. The working conditions are defined at §2.3.3, but also the working fluid nature can modify significantly the critical heat flux value

Summary on the mechanism that occur during convective boiling

Generally the addition of an inertial component, lead to the improvement of the heat exchange. Moreover, one can notice that for the ducts of small dimensions pool boiling does not seem to be adapted because the confinement should lead to a more rapid dryout of the wall ^a.

During the convective boiling study, it become necessary to determine for each mass flow condition, the values of heat transfer allowing for the boiling incipience and the conditions for the occurrence of dryout phenomenon. These two mechanisms are fundamental for the sizing of mini-channels, because their restrict their working range for boiling conditions. One can point out that instabilities related to mini-channels geometrical scale reduction may take place when the bubble dimension tend to become larger than the duct cross section. As a consequence, the bubble can grow only in the longitudinal direction. These data must be taken into account when the cross section of a boiling flow is reduced.

a. Geisler et Bar-Cohen (2009).

2.3 Parameters that have an influence on the boiling nature

In this paragraph, the impact of specific parameters : working fluid type, fluid wettability with channel wall, working conditions, mini-channel geometry, that have an impact on the heat exchange coefficient, the pressure drops or the transition between the flow regimes will be analyzed. It should be point out that the influence of all these parameters can affect significantly the ONB, the instabilities that can take place in the channel, the phenomena that suppress the nucleate boiling but also the CHF occurrence, nonetheless these analysis will not be detailed in this state of the art review.

2.3.1 Working fluid selection

It is useful to estimate the influence of the selected working fluid on the evolution of the pressure drops as well as the heat transfer rate for a boiling flow. This important task allow for the realization of preliminary choices for the working fluid selection. Nevertheless, the comparison between the data of the state of the art review are particularly difficult to do, because of different experimental conditions. The reasons of this difficulty are related to the different operating conditions (working pressure, inlet temperature, flow cross section, wall surface roughness) that can be encountered experimentally. Nevertheless, when studies are done for different working fluid on a same experimental bench, it is possible to do an objective comparison of the impact of the fluid thermophysical properties. We will give some results that proposed to compare the evolution of the pressure drops and heat transfer coefficients for different fluids on a same experimental device.

a) Pressure drop evolution

We have point out that the influence of the working fluid on the pressure drop is not much studied in the literature. In this paragraph, a summary of three interesting papers that allow for an evaluation of the impact of fluid type on the evolution of the pressure for duct of small dimensions is given. The determination of the thermophysical properties that have a very important impact on the pressure drops during convective boiling in mini-channels will be realized.

Revellin et Thome (2006) experimental results

Revellin et Thome (2006) used R134a and R245fa as working fluids. Their experimental test sections consisted of a stainless steel of hydraulic diameter of 0.509 mm . An evaporator that is located before the observation zone allow for the obtaining of the phase change. This evaporator had a length of 70.7 mm . The pressure drops study is made for adiabatic conditions⁹. The mass

9. An external system allow for the regulation of the temperature all around the visualization section

Section 2.3. Parameters that have an influence on the boiling nature

velocity is of $700 \text{ kg.m}^{-2}.s^{-1}$ and the undercooling at the tube inlet is comprised between 5 and 6°C . The thermophysical properties of the two fluids are reported in Table 2.2¹⁰ respecting the related operating conditions.

Fluid	T_{sat}	ρ_l	ρ_v	h_{lv}	c_{pl}	c_{pv}	μ_l	μ_v	λ_l	λ_v	Pr_l	Pr_v	σ
Units	$^\circ\text{C}$	kg/m^3	kg/m^3	kJ/kg	kJ/kg.K	kJ/kg.K	$\mu\text{kg/m.s}$	$\mu\text{kg/m.s}$	mW/m.K	mW/m.K	S.U	S.U	mN/m
R134a	35	1167	43.4	168.2	1.47	1.1	172	12.1	76.8	14.8	3.3	0.9	6.7
R245fa	35	1311	11.9	184.8	1.36	0.9	358	10.6	86.9	14.7	5.6	0.67	12.7

TABLE 2.2 – Thermophysical properties of R245fa at 213 kPa and of R134a at 887 kPa according to Revellin et Thome (2006)

The data given in the Figure 2.8 showed that for all of their results, the pressure drops expression is higher for the R245fa. The authors specified that $3\rho_v(\text{R245fa}) \cong \rho_v(\text{R134a})$, what lead to a higher vapor superficial velocity than for the R245fa for a same thermodynamic vapor quality.

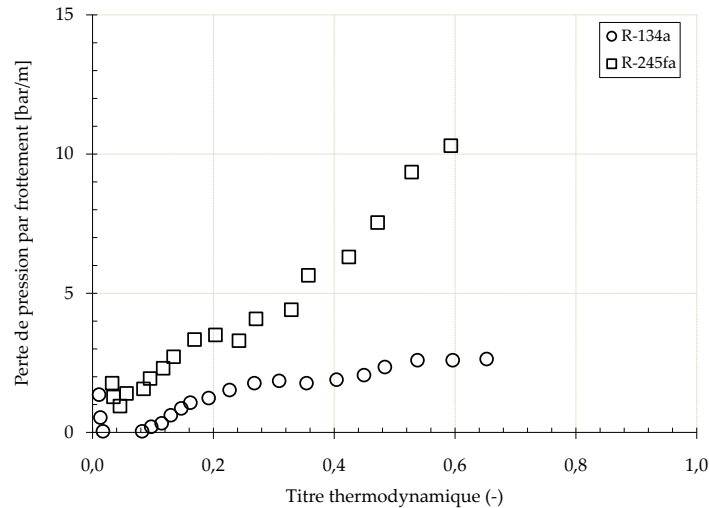


FIGURE 2.8 – Pressure drop evolution for R134a and R245fa for a mass velocity of $700 \text{ kg.m}^{-2}.s^{-1}$ according to Revellin et Thome (2006)

This mean that the interfacial shear stress is more important for this fluid. In addition, the liquid Reynolds number (based on the superficial velocity) is higher for R245fa what lead to parietal constraint that were more important. The collective influence of these two evolutions lead to a higher pressure drop for this fluid than for the R134a.

10. Some of the data reported in this Table comes from the paper of Revellin et Thome (2006), the other have been calculated using the Refprop 7 (2002) software or the data from the literature. We have calculated in a similar way the thermophysical properties that have been given in the next Tables, when those are not given in the cited publication also.

Chapitre 2. Literature review on the boiling in mini-channels

Jassim et Newell (2006) experimental results

Jassim et Newell (2006) based their analysis on the results given by Niño (2002) for the realization of flow map of probabilist type. The working fluid that have been used are R410a¹¹, R134a and a mixing between water/air that we will not be considered here. Some values of the thermophysical properties of the used fluids in their working conditions are given in Table 2.3.

Fluid	T_{sat}	ρ_l	ρ_v	h_{lv}	c_{pl}	c_{pv}	μ_l	μ_v	λ_l	λ_v	Pr_l	Pr_v	σ
Units	$^{\circ}C$	kg/m^3	kg/m^3	kJ/kg	$kJ/kg.K$	$kJ/kg.K$	$\mu kg/m.s$	$\mu kg/m.s$	$mW/m.K$	$mW/m.K$	S.U	S.U	mN/m
R410a	10	1132	42.5	206.8	1.53	0.78	145	12.2	94	12.8	2.4	0.74	7.2
R134a	10	1261	20.2	190.7	1.37	0.94	235	11.1	88	12.4	3.7	0.84	10.1

TABLE 2.3 – Thermophysical properties of R134a at 414 kPa and of R410a at 1088 kPa according to Jassim et Newell (2006)

Not much data are given regarding the test section dimensions. On can note that it consisted of 6 parallel channels (the four located in the center are rectangular and the two remaining ones that are located on the outer part are circular and all the channels have a hydraulic diameter which has been estimated at 1.54 mm). The test section has been made in extruded aluminum.

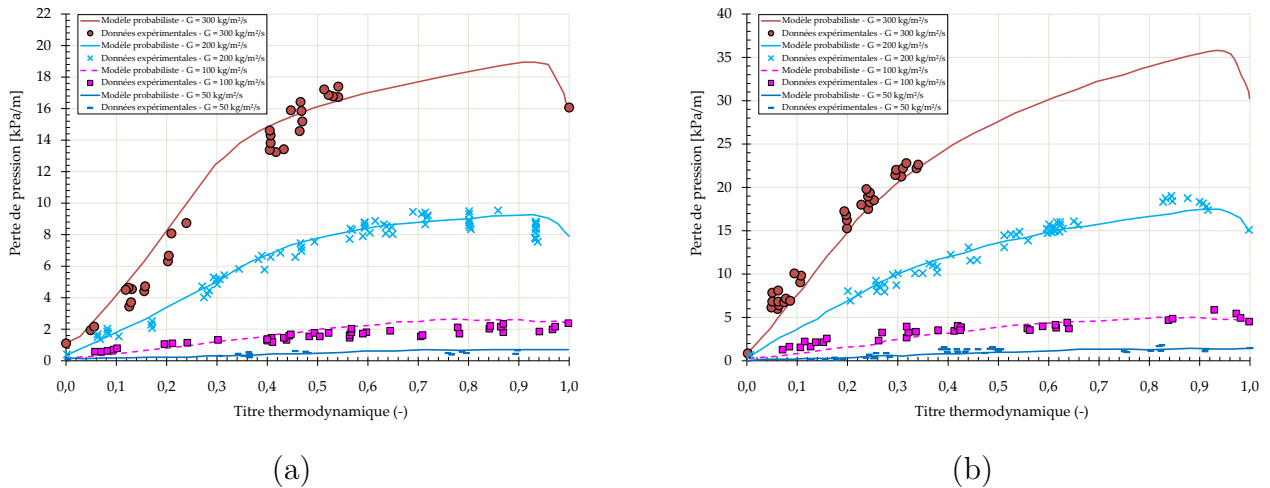


FIGURE 2.9 – Pressure drops evolution for the : (a) R410a (b) R134a according to Jassim et Newell (2006)

The experiments have been done for **adiabatic** conditions for mass velocities ranged between 50 and $300\text{ kg}\cdot\text{m}^{-2}\cdot\text{s}^{-1}$ and a saturated fluid. In figure 2.9 it can be observed that the pressure drops are more significant for R134a for the whole range of thermodynamic vapor quality for

11. The thermophysical data for this fluid have been obtained through the website <http://www.ineosfluor.com/>

Section 2.3. Parameters that have an influence on the boiling nature

all tested flow rate. One can note that $\rho_v(\text{R134a}) \cong 2\rho_v(\text{R410a})$. Moreover, this observation allow for the affirmation, that, for a same thermodynamic vapor quality, the superficial vapor velocity is approximately two time higher for the R134a than for the R410a. As a consequence, the two-phase flow pressure drop is, for this situation, mainly driven by the vapor velocity (at equivalent liquid superficial velocities), this pressure drop is then higher for R134a than for R410a.

☞ *Tran et al. (2000) experimental results*

Tran *et al.* (2000) studied the presure drop evolution for R12 and R134a. Their test section was fabricated in brass¹² using a tube of circular cross section of hydraulic diameter of 2.46 mm , for a length of 914 mm . The experiments have been realized for diabatic conditions and for a saturated fluid. Some thermophysical properties of the fluids that have been used are given in Table 2.4 for their operating conditions.

Fluide	T_{sat}	ρ_l	ρ_v	h_{lv}	c_{pl}	c_{pv}	μ_l	μ_v	λ_l	λ_v	Pr_l	Pr_v	σ
Unités	$^{\circ}C$	kg/m^3	kg/m^3	kJ/kg	$kJ/kg.K$	$kJ/kg.K$	$\mu kg/m.s$	$\mu kg/m.s$	$mW/m.K$	$mW/m.K$	S.U	S.U	mN/m
R12	34.4	1275	47.2	133.4	1.01	0.73	170	12	64	11	2.7	0.8	7.3
R134a	32.8	1176	40.8	170.4	1.46	1.08	177	12	78	14.6	3.3	0.89	7

TABLE 2.4 – Thermophysical properties of R134a and R22, at 835 kPa according to Tran *et al.* (2000)

On the whole range of heat fluxes (Figure 2.10), we can remark that the pressure drop is always smaller for R134a. The authors specified that for reaching the same value of transferred heat flux to the fluid, the mass flow rate must be higher for R12, which has a smaller latent heat than for R134a. This lead to a higher pressure drop for R12. The comparison of the thermophysical properties of the two fluids showed that neither the viscosity effect (which is close for the two fluids), nor the mass density (which are close for the liquid and vapor phases) can be suspected to play a role in this difference.

12. This material is particularly interesting regarding the small surface roughness.

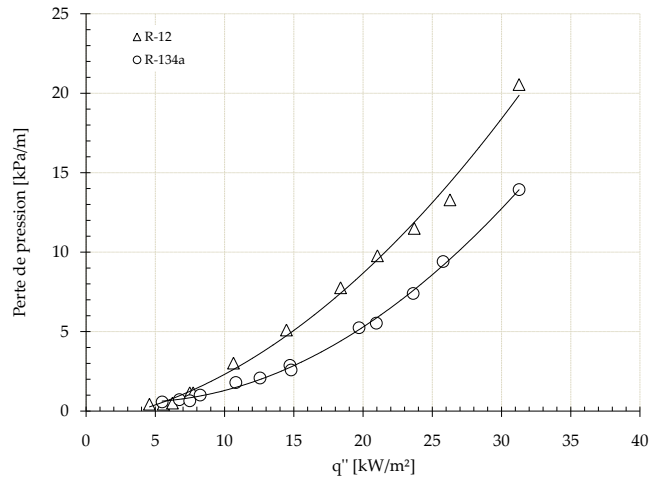


FIGURE 2.10 – Pressure drops evolutions for the R134a and the R12 according to Tran *et al.* (2000)

Summary : Influence of the fluid selection on the pressure drops

The fluid selection and particularly the selection of the couple ρ_l/ρ_v are of paramount importance for the evaluation of the pressure drop for internal convective boiling. Indeed, the data from the state of the art showed that if the difference between the liquid and vapor mass density is significant, the two-phase flow pressure drops will be important. Indeed, the increase of the difference between these two densities has a contribution to the intensification of interfacial shear stress which are generated by more intense slippage between the two phases. Consequently, when choosing a fluid, a specific attention must be paid to this couple of thermophysical properties.

b) Heat exchange coefficient evolution

Diaz et Schmidt (2007) experimental results

Diaz et Schmidt (2007) had compared the evolution of the heat transfer coefficients for water and ethanol at atmospheric pressure. Their test section, was fabricated using a Nickel alloy (Inconel 600), and consisted of a single rectangular channel. The channel height was of 0.3 mm, the width of 12.7 mm for a length of 200 mm ($d_h = 586 \mu m$). The thermophysical properties of their two fluids has been given in Table 2.5.

Section 2.3. Parameters that have an influence on the boiling nature

Fluide	T_{sat}	ρ_l	ρ_v	h_{lv}	c_{pl}	c_{pv}	μ_l	μ_v	λ_l	λ_v	Pr_l	Pr_v	σ
Unités	$^{\circ}C$	kg/m^3	kg/m^3	kJ/kg	$kJ/kg.K$	$kJ/kg.K$	$\mu kg/m.s$	$\mu kg/m.s$	$mW/m.K$	$mW/m.K$	S.U	S.U	mN/m
Eth.	78.3	757	1.435	963	3	1.8	428.7	10.4	154	20	8.37	0.96	17
Eau	100	958	0.597	2257	4.2	2	277.5	12.5	679	25	1.72	1.02	59

TABLE 2.5 – Thermophysical properties of water and ethanol at atmospheric pressure

The experimental data points that have been obtained for a mass velocity of $500 kg.m^{-2}.s^{-1}$ have been reported on the Figure 2.11.

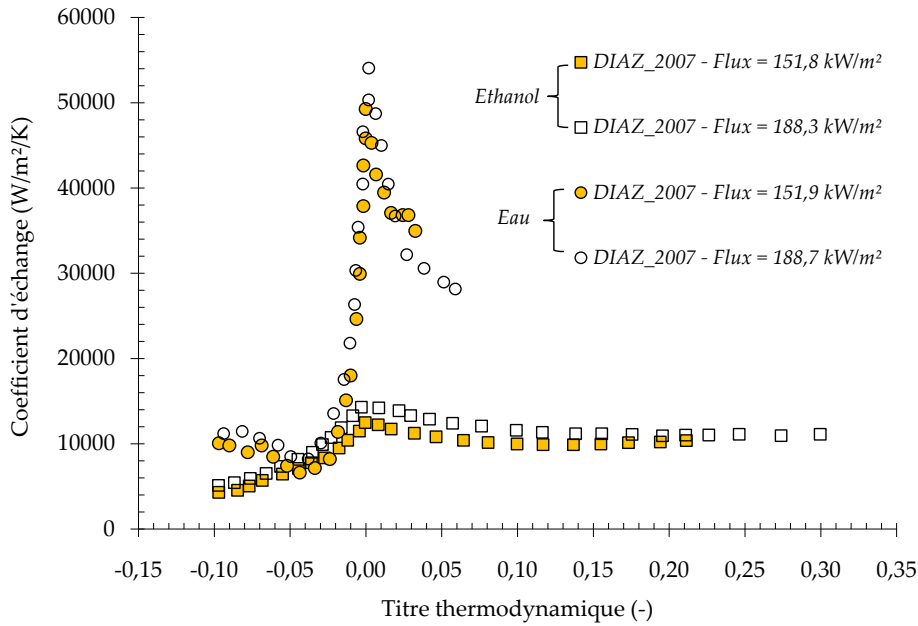


FIGURE 2.11 – Heat transfer coefficients comparison between water and ethanol according to Diaz et Schmidt (2007)

The given data showed that the heat transfer coefficients present a very huge dependence to the working fluid that had been used. Indeed, for a same thermodynamic vapor quality, the heat transfer coefficients that have been obtained for water are generally higher. This is due to the higher latent heat of the water, which for an equivalent vapor flow rate, led to the intensification of the heat transfer rates.

In addition, the appearance of a sharp peak during the transition from the subcooled conditions ($x < 0$) to the saturated conditions ($x \geq 0$) for water as a working fluid has not been observed for ethanol. According to our understanding, this behavior was due to the bubble

Chapitre 2. Literature review on the boiling in mini-channels

growth mechanism¹³, and to the flow confinement also, which varied regarding the used working fluid¹⁴.

Bertsch et al. (2009) experimental results

Bertsch *et al.* (2009) worked with R134a and R245fa as working fluids for the study of the heat transfer coefficient evolution. Their test section consisted of 33 rectangular copper channel (purified in oxygen content). The channels height was of 953 μm , the width of 381 μm , for a length of 9.53 mm . Some of the thermophysical fluids properties are reported in Table 2.6.

Fluid	T_{sat}	ρ_l	ρ_v	h_{lv}	c_{pl}	c_{pv}	μ_l	μ_v	λ_l	λ_v	Pr_l	Pr_v	σ
Units	$^{\circ}C$	kg/m^3	kg/m^3	kJ/kg	$kJ/kg.K$	$kJ/kg.K$	$\mu kg/m.s$	$\mu kg/m.s$	$mW/m.K$	$mW/m.K$	S.U	S.U	mN/m
R134a	18.7	1230	26.7	183.4	1.4	1	211	11.4	84	13.2	3.5	0.85	8.9
R245fa	20.3	1352	7.2	193.6	1.3	0.9	431	10	91.5	13.5	6.3	0.66	14.7

TABLE 2.6 – Thermophysical properties of R245fa at 125 kPa and of R134a at 550 kPa according to Bertsch *et al.* (2009)

The comparison of these data is particularly interesting because the numerous thermophysical properties of these two fluids are relatively similar; what allow for the estimation of the specific influence of some of them (ρ_v , μ_l , σ). The author explain that for the pool boiling conditions the heat transfer is inversely proportional to the surface tension (according to the equation of Bennet et Chen (1980)). The authors concluded by saying that their results were in agreement with the predicted evolution related to this equation, what lead to better heat transfer coefficient for the R134a (Figure 2.12).

This is a conclusion that can seemed surprising compared to the results given by Diaz et Schmidt (2007), where water had surface tension higher than ethanol but allowed for the reaching of better heat transfer coefficients. This result may be explained by the difference of the liquid viscosity (μ_l) which can have an impact of the heat transfer coefficient evolution as we may understand it¹⁵.

13. The water contact angle with Nickel is ranged between 60° and 70° according to Wang *et al.* (2002) and is, generally, much more smaller that the couple alcohols/metals. By doing an assumption and saying that this contact angle is about 10° for ethanol, the Phan *et al.* (2009) correlation predict, for a pool boiling condition, a bubble detachment diameter of 1.453 mm for water and of 0.728 mm for ethanol.

14. According to the Kew et Cornwell (1997) analysis, the flow confinement with water, should be more important($Co = 4.27$) than for ethanol ($Co = 2.63$) according to the Diaz et Schmidt (2007) study

15. One can note that the value of the couple ρ_l/ρ_v had mainly an influence on the pressure drops variation. The impact of the surface tension (σ) is generally significant on the flow regime transitions. Nonetheless, these transitions did not implied systematically (when the conditions are far from the dryout point), an improvement or a decrease of the heat transfer coefficient as it will be shown in the study of Ong et Thome (2009).

Section 2.3. Parameters that have an influence on the boiling nature

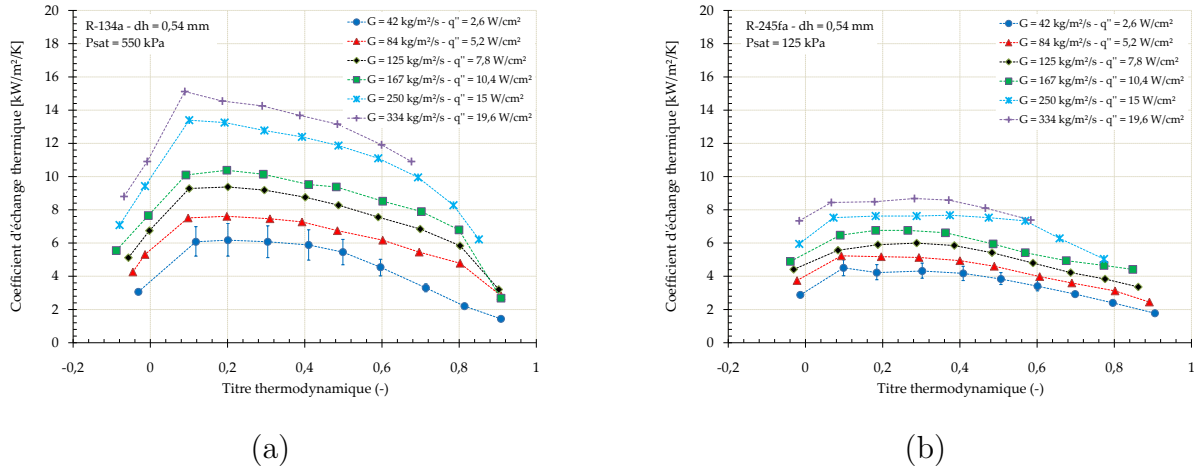


FIGURE 2.12 – Heat transfer coefficient evolution according to Bertsch *et al.* (2009) for the : (a) R134a (b) R245fa

The study of the liquids Prandtl numbers, allow the formulation of an assumption that explain the reasons for this evolution for the low to moderate thermodynamic vapor qualities. The evolution of this number specified that for the use of R134a, the phenomena of thermal diffusion will be quicker than the momentum diffusivity. As an improvement of the heat transfer rate can be observed for the R134a whereas the flow rates were the same (by comparing the results that have been obtained for R245fa), it can be concluded that the heat transfer rate is controlled by the wall heat flux¹⁶ for these thermodynamic vapor qualities. The analysis of this number should allow for the justification of the Diaz et Schmidt (2007) results.

🔍 Ong et Thome (2009) experimental results

Ong et Thome (2009) used three working fluids for studying the evolution of the heat transfer coefficients for a mini-tube. Some of the thermophysical properties of these three fluids can be found in Table 2.7.

Fluid	T_{sat}	ρ_l	ρ_v	h_{lv}	c_{pl}	c_{pv}	μ_l	μ_v	λ_l	λ_v	Pr_l	Pr_v	σ
Units	$^{\circ}C$	kg/m^3	kg/m^3	kJ/kg	$kJ/kg.K$	$kJ/kg.K$	$\mu kg/m.s$	$\mu kg/m.s$	$mW/m.K$	$mW/m.K$	S.U	S.U	mN/m
R134a	30.9	1184	38.6	170.2	1.45	1.07	181	11.9	78	14.4	3.3	0.88	7.29
R236fa	30.9	1339	22.2	142.4	1.28	0.9	265	11	71	13.3	4.8	0.75	9.36
R245fa	30.8	1323	10.4	187.4	1.35	0.92	377	10.4	88	14.3	5.8	0.67	13.3

TABLE 2.7 – Thermophysical properties of R245fa at 184 kPa, of R236fa at 331 kPa and of R134a at 792 kPa according to Ong et Thome (2009)

16. This results is confirmed for the related range of thermodynamic vapor qualities - $0.1 \leq x \leq 0.8$. For higher thermodynamic vapor qualities, the heat exchange coefficient can become better for R245fa.

Chapitre 2. Literature review on the boiling in mini-channels

The mini-tubie which was in stainless steel (AISI304), had a hydraulic diameter of 1.03 mm for a length of 180 mm . The results of this study were given in a very impacting way by the authors, because they allow for the understanding of the impact of thermophysical properties on the evolution of the heat transfer coefficients. The evolution of the flow transition regimes that were analysed with the variation of the heat transfer coefficients have been given in Figure 2.13.

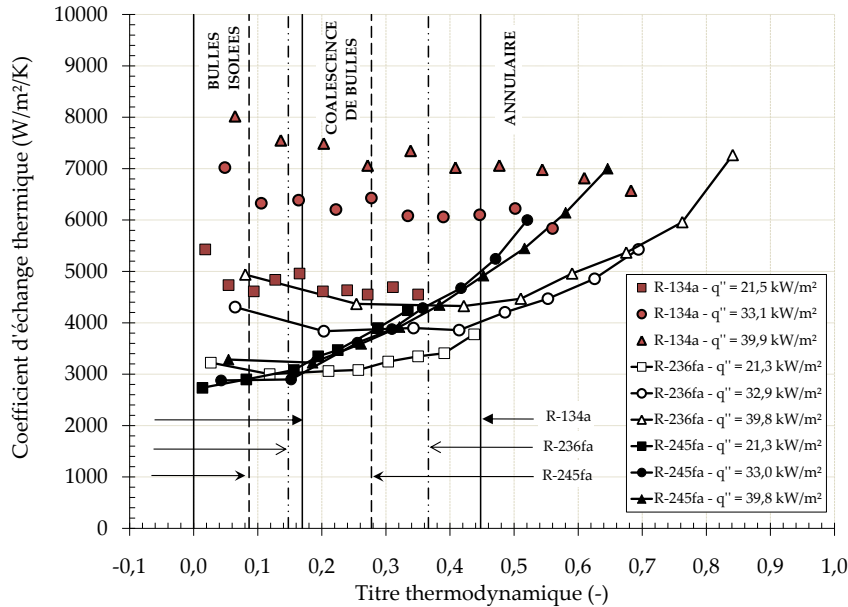


FIGURE 2.13 – Evolution of the heat transfer coefficient for R134a, R236fa and R245fa according to Ong et Thome (2009)

The results were obtained for a mass velocity of $200\text{ kg}\cdot\text{m}^{-2}\cdot\text{s}^{-1}$ and a subcooling of 4°C at tube inlet. The authors based their analysis on the confinement parameter defined by Kew et Cornwell (1997) [equation (2.20)] for confirm the flow regime transition chronology for the different working fluids¹⁷. One can notice that when the surface tension was high the flow regime transitions were quicker. Indeed, when the surface tension is small, the required energy to keep the interface stable is reduced, what explain the longer times for the flow regimes transitions for this situations. However, it is possible to note that the transitions between the flow regimes did not seemed to have a similar effect on the evolution of the heat transfer coefficients for these three fluids.

It can be pointed out that for this study, the heat transfer coefficients were higher for R134a when the thermodynamic vapor qualities were low to moderate. When its value was large, the heat transfer coefficients became higher for R236fa and R245fa. The decrease of the heat

17. The transitions between the regimes are more rapid when the following direction is considered : R245fa ($C_o = 0.98$) \rightarrow R236fa ($C_o = 0.82$) \rightarrow R134a ($C_o = 0.78$).

Section 2.3. Parameters that have an influence on the boiling nature

transfer coefficients for the R134a can be explained by the intensification of the partial dryout with the vapor quality. The authors said that this increase was due to the liquid film thickness reduction with the vapor quality, what lead to the intensification of the heat transfer rate (reduction of the thermal resistance of the thin liquid film for R236fa and R245fa).

✍ Summary : Impact of the fluid selection on the heat exchange coefficient

There is no clear agreement on the fluid thermophysical properties impact on the evolution of heat transfer rate in a mini-channel. Indeed, numerous properties seemed to play a role in the variation of the heat transfer rate. Therefore, we can cite : the latent heat, the specific heat, the thermal conductivities, the mass densities, the liquid and vapor viscosities as well as the surface tension. Nonetheless, we think that the evolution of the liquid Prandtl number may give a relevant indication related to the thermal behaviors that have been observed in convective boiling for low to moderate thermodynamic vapor qualities.

2.3.2 Wettability properties of the fluid with the wall

The influence of contact angle (θ) between the wall and the fluid on hydrodynamic or thermal behavior has been analysed in this paragraph. We remind that the contact angle is the angle between the liquid interface and the solid surface, and by convention, this angle is measured in the liquid phase. This angle depends on the fluid/material couple. With the help of our state of art review it can be noted that the impact of the contact angle has been little studied in the literature for convective boiling conditions, although this parameter plays an important role. In particular, it can significantly influence the boiling behavior and the mechanisms leading to dryout.

Li et al. (2004) experimental results

The numerical study that has been made by Li *et al.* (2004), took into account the influence of the contact angle regarding two different points of view. The authors showed that the needed energy for the occurrence of the boiling is reduced when this contact angle is increased (Figure 2.14).

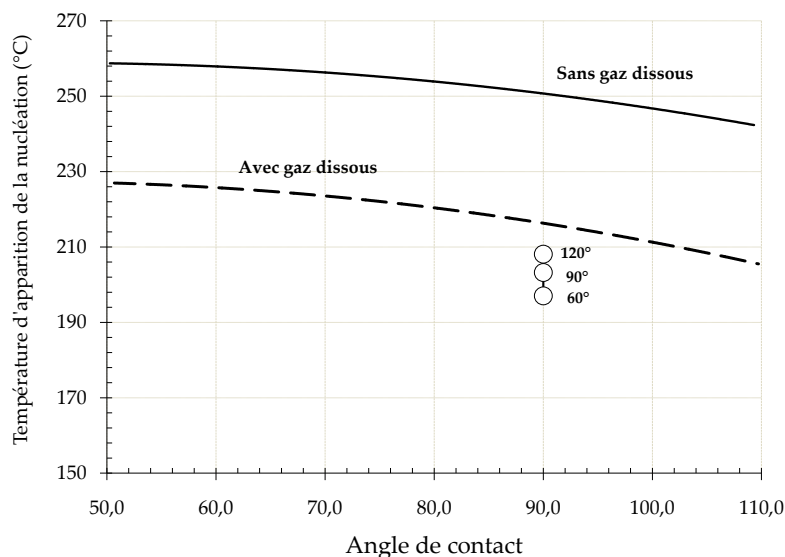


FIGURE 2.14 – Impact of the contact angle on the bubble incipience according to Li *et al.* (2004)

This results can be demonstrated using the simplified example of the behavior of two liquid droplets that flowed in a conical cavity with a constant open angle (Figure 2.15).

Using this drawing, the case of a advancing contact angle is considered. It can be specified that the value of this angle is higher than the static contact angle. Here the droplet ① has an advancing contact angle larger than the droplet ②. If it is assumed that the vapor that is

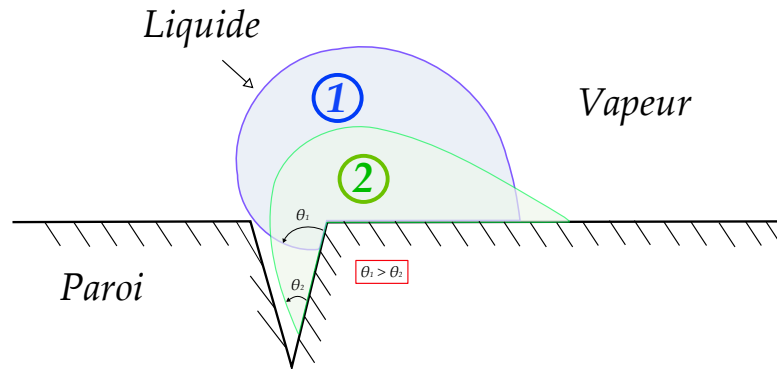


FIGURE 2.15 – Filling of a cavity by two droplets having different advancing contact angles

entrapped in the cavity did not dissolved itself in the liquid during the cavity filling, the droplet ① should be able to entrap more vapor than the droplet ②. However, this is the contact angle difference that will allow for the appearance of a more or less quick boiling and of a modification of the bubble diameter during the detachment (Stutz (2003)).

With this example, it can be highlighted the potential impact of the mini-channel corners. These corners may allow for the retention of different vapor volume with respect to the heated surface, regarding the opening angle. Thus for a same contact angle of 90° , Li *et al.* (2004) showed that the needed energy for the ONB is smaller when the opening angle of the corner is reduced (Figure 2.15).

👁 *Barajas et Paton (1993) and Lee et Lee (2008) experimental results*

On former paragraph, it has been shown that the contact angle may influenced significantly the ONB due the gas volume that can be trapped inside a cavity. This contact angle may have an impact on the convective boiling regime as showed by Barajas et Paton (1993). The working principle of the experimental tests can be explain as followed. The authors sent gases via a compressed air system in a set-up that contain water. The contact angle is modified using tubes that have been realized with different materials in which there was the fluid flow. These tubes have a same hydraulic diameter of 1.6 mm and a length of 300 mm . The authors showed that the contact angle can even allow for the modification of the flow regimes when its value is larger that 90° (non wettable liquid). According to the Figure 2.16, the flow regimes transitions which were more affected by this contact angle were the bubbles/plugs, annular/dispersed, plugs/multiple water rivulets¹⁸ and plugs/annular. The transition took place for lower liquid and vapor velocities.

More recently, Lee et Lee (2008) have confirmed the results that have been obtained by

18. Barajas et Paton (1993) observed that for this regime, water liquid jets flowed on the tube surface. These jets did not flowed respecting a straight line but flapped in the longitudinal tube direction.

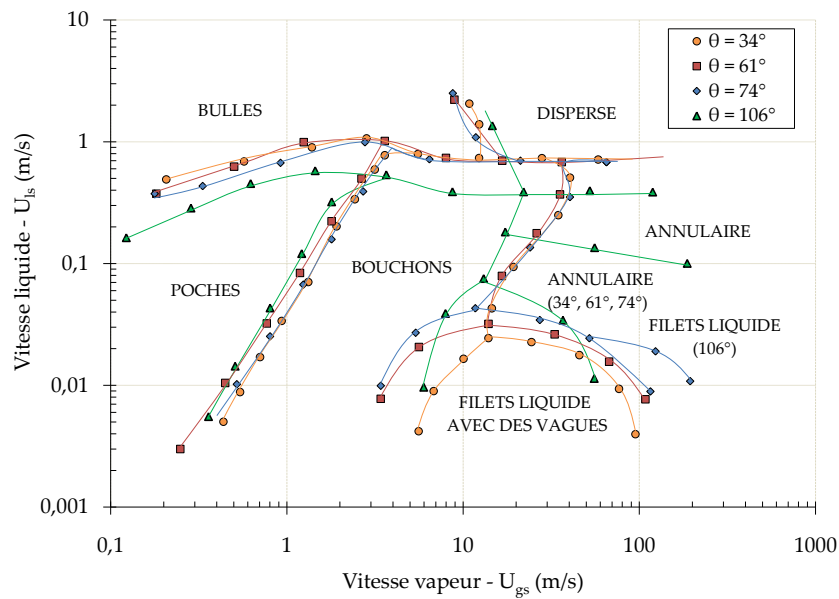


FIGURE 2.16 – Contact angle impact on the flow regimes transitions according to Barajas et Paton (1993)

Barajas et Paton (1993). The author used water as working fluid. Four tubes were studied in this work in order to varied the contact angle. The hydraulic duct diameters were comprised between 1.46 to 2mm and had a length of 650mm. The authors showed that when the wettability between the fluid and the wall is modified, the flow regimes transitions were different and were obtained for lower liquid and vapor velocities.

Summary : Impact of the fluid wettability properties

The impact of the fluid wettability with the wall (selection of the couple fluid/material) can be important for the two-phase flow behavior. It can be said that this parameter has not been studied much in the state of the art. However, the contact angle should have a significant influence of the ONB and the dryout phenomena. These two parameter are key for the sizing of a heat exchanger. For the study that have been made in this paragraph, it as been demonstrated that this parameter can allow for the modification of specific flow regime transition also. This situation usually took place when the fluid have a low wettability with the surface ($\theta > 90^\circ$).

2.3.3 Working conditions

A large number of studies that have been realized in the context of the convective boiling considered mainly the impact of one or several working conditions on the heat exchange or on the flow hydrodynamic aspect. The working conditions¹⁹ on which a particular analysis is nowadays focused in the literature are the :

- ▷ saturated pressure (or temperature)
- ▷ the liquid sub-cooling at the duct inlet
- ▷ mass flow rate
- ▷ heat flux

🔍 *The saturated pressure (or temperature)*

The influence of the working pressure on the evolution of the pressure drops in boiling conditions has been not much studied in the state of the art review that has been analysed in this study. Park et Hrnajk (2009) have studied the heat transfer rate and the pressure drops in a tube having a hydraulic diameter of 3.5 mm, a length of 150 mm made in copper.

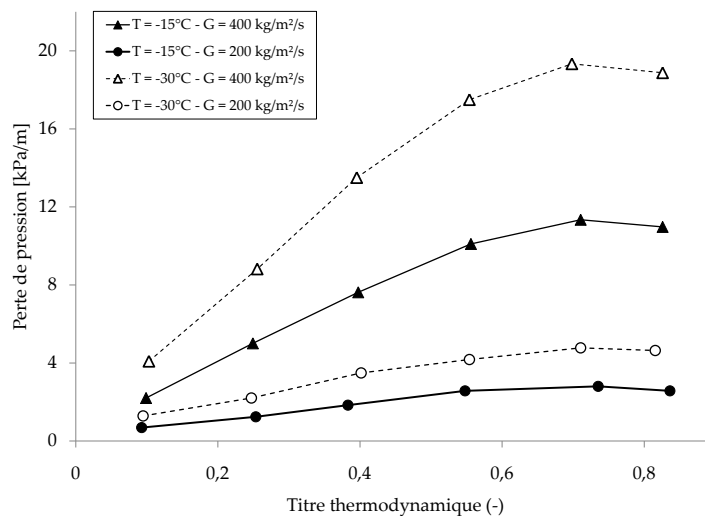


FIGURE 2.17 – Pressure drop variation with the system working pressure according to Park et Hrnajk (2009)

The results that have been obtained by these authors showed that the working pressure acted on the evolution of the pressure drop between the tube inlet and the tube outlet (Figure 2.17).

19. The orientation of the mini-channel, as showed by Kandlikar et Balasubramanian (2005), may have an influence on the heat transfer coefficients or on the pressure drops in mini-channels, but we will not be analysed this case in this manuscript.

Chapitre 2. Literature review on the boiling in mini-channels

This pressure drop is significantly reduced with the increase of the working pressure²⁰. The authors explained that the pressure increase led to a decrease of the liquid viscosity which lead to a reduction of the intensity of the wall shear stress. On same time, the vapor density increase with the working pressure and allow for the reduction of the superficial vapor velocity. The reduction of this velocity lead to a weakness of the interfacial shear stress and to a global reduction of the two-phase pressure drop for boiling conditions.

The influence of the working pressure on the evolution of the heat transfer coefficient is relatively well understood since several years for boiling conditions. Bertsch *et al.* (2009) have studied the evolution of the heat exchange coefficient for R134a in a tube of hydraulic diameter of 0.54 mm . The authors showed that the heat exchange coefficient increases with the working pressure for low thermodynamic vapor qualities (Figure 2.18(a)). Choi *et al.* (2009) underlined an increase of the heat transfer coefficient with the pressure on a larger range of vapor thermodynamic qualities (Figure 2.18(b)). These last authors used propane for two tubes of different hydraulic diameters (1.5 mm et 3 mm for a length of 1 and 2 m respectively), that was fabricated in stainless steel.

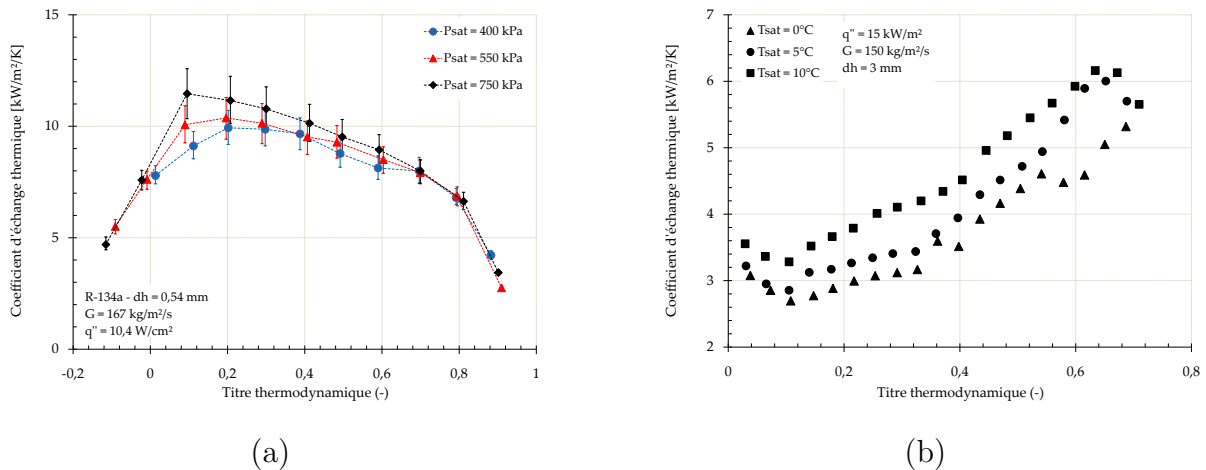


FIGURE 2.18 – Saturated pressure (or temperature) influence on the evolution of the heat transfer coefficient according to : (a) Bertsch *et al.* (2009). (b) Choi *et al.* (2009)

According to our analysis, this result may be explained by the influence of the surface tension that can have an important impact on the heat transfer rate intensity²¹.

As showed in Table 2.8, the fluid latent heat is reduced when the working pressure is increased ; this means that for a same vapor flow rate, the thermal power due to the phase change should be reduced, what is not the case for the made experiments. This result can be explained by the

20. One can note that the saturation temperature increases with the working pressure

21. Similarly to the data that have been given on § 2.3.1-b), the heat exchange rates are generally improved for the low to moderate thermodynamic vapor qualities whe the liquid Prandtl number is decreased.

Section 2.3. Parameters that have an influence on the boiling nature

P	T_{sat}	ρ_l	ρ_v	h_{lv}	c_{pl}	c_{pv}	μ_l	μ_v	λ_l	λ_v	Pr_l	Pr_v	σ
kPa	$^{\circ}C$	kg/m ³	kg/m ³	kJ/kg	kJ/kg.K	kJ/kg.K	μ kg/m.s	μ kg/m.s	mW/m.K	mW/m.K	S.U	S.U	mN/m
450	8.9	1265	19.5	191.6	1.36	0.94	238	11.1	88	12.3	3.7	0.84	10.2
550	18.7	1230	26.7	183.4	1.4	1	211	11.4	83.8	13.2	3.5	0.86	8.9
750	29.1	1191	36.5	174	1.44	1.05	185	11.8	79.3	14.2	3.3	0.88	7.3

TABLE 2.8 – Thermophysical properties of R134a at 450, 550 and 750 kPa according to Bertsch *et al.* (2009)

influence of the surface tension which is reduced with the pressure as shown by the data given in this last table. This behavior allow for the promotion of the nucleate boiling regime²² insofar the required energy that is necessary for the interface resistance become lower. Furthermore, the saturation temperature increase with the working pressure. Thus for reaching the same vapor thermodynamic quality, it is necessary to increase the heat flux density between the wall the boiling flow (by assuming a same inlet temperature). This increase led to a improvement of the heat transfer coefficients. In addition Saitoh *et al.* (2005) showed that the impact of this working pressure seemed to increase when the duct hydraulic diameter is decreased..

Summary : Influence of the saturation pressure

The increase of the saturation pressure allow generally for the intensification of the heat transfer rate in mini-channel by promoting the nucleate boiling regime. On same time, this increase lead to an augmentation of vapor density and a reduction of the liquid one what conduct to the pressure drops reduction. These two behaviours, allow for the deduction that the increase of this pressure allow for the improvement of performance of heat exchangers during boiling. Moreover, we noted that the influence of this pressure seemed to increase when the mini-channels hydraulic diameter is reduced (Saitoh *et al.* (2005))

22. The bubbles diameter is reduced for a same exchanged heat flux and the interaction between these bubbles are more numerous and improve the mixing

Liquid subcooling at the duct entrance

Among the read papers, only the data of Revellin et Thome (2006) took in consideration the impact of the subcooling on the pressure drops evolution. The results that have been obtained by these authors suggested that the subcooling at the mini-tube entrance has very low impact on the pressure drop regarding the thermodynamic vapor quality for the studied temperature range. We noted that the studied subcooling were very close and equalled $2^{\circ}C$, $3^{\circ}C$ and $5^{\circ}C$.

The interest for the study of the boiling condition for subcooled condition has grown with research related to the cooling of power electronics (electronic components that generated very high heat fluxes). Martin-Callizo *et al.* (2007) have studied the evolution of the heat transfer coefficients for three tubes of following hydraulic diameters 0.83 mm - 1.22 mm - 1.7 mm that were fabricated in stainless steel (AISI 316) and having a length of 310 mm . The working fluid that has been used in this study was R134a.

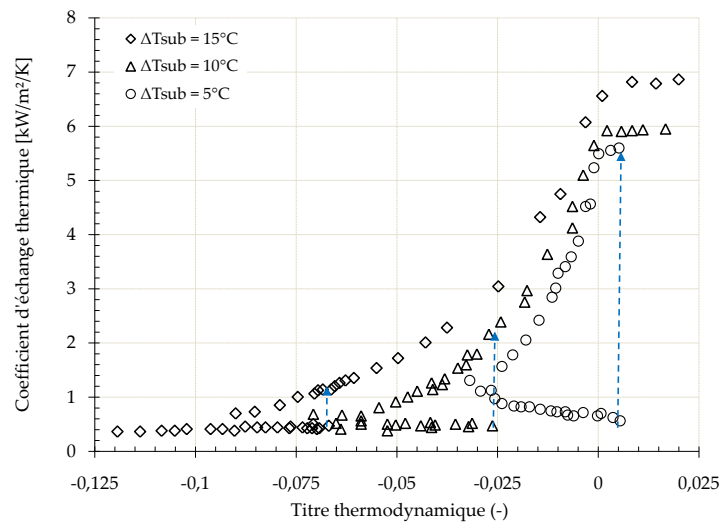


FIGURE 2.19 – Liquid subcooling influence on the heat exchange coefficient for R134a in a tube of 1.22 mm according to Martin-Callizo *et al.* (2007)

The data that have been given on Figure 2.19 showed that for a same thermodynamic vapor quality, the heat transfer coefficients were improved when the subcooling increased. Indeed, for subcooled conditions, the fluid which is close to the wall is at saturation temperature [or slightly superheated ($T_l > T_{sat}$)], whereas the fluid in the flow core is subcooled ($T_l < T_{sat}$). Martin-Callizo *et al.* (2007) showed that for reaching the same thermodynamic vapor quality when the inlet temperature is decreased (or when the subcooling is increased), it was necessary to impose a higher heat flux. In this case, the nucleation sites activity increased, what allow for the intensification of the heat exchange rate.

Summary : Liquid inlet subcooling impact

The increase of the liquid inlet subcooling impact allow for the intensification of the heat transfer rate for a same thermodynamic vapor quality. Indeed, it is necessary to increase the heat flux value between the wall and the flow when the inlet temperature decrease for obtaining a same thermodynamic vapor quality. This increase lead to the enhancement of the bubbles interactions for the mini-tubes what contribute to the improvement of the heat transfer. However, the subcooling impact on the pressure drop is not clear yet, but it seems that the evolution of these pressure drops regarding the thermodynamic vapor quality is not much sensitive regarding this parameter.

The mass flow rate

The results that have been studied in the literature, come to an agreement for saying that the pressure drop increase with the flow rate as showed in Figure 2.17.

Nowadays, the impact of the flow rate on the heat transfer is not fully understood yet when the dimensions are reduced. Some authors argued that the contribution of the nucleate boiling diminished for convective evaporation. The intensification of the heat transfer would be mainly due to the vaporization of a liquid film that is localized in between the mini-tube wall and the vapor flow. Contrarily other authors supported that the nucleate boiling that it is generated in the liquid film remained and this mechanism drove the heat transfer rate.

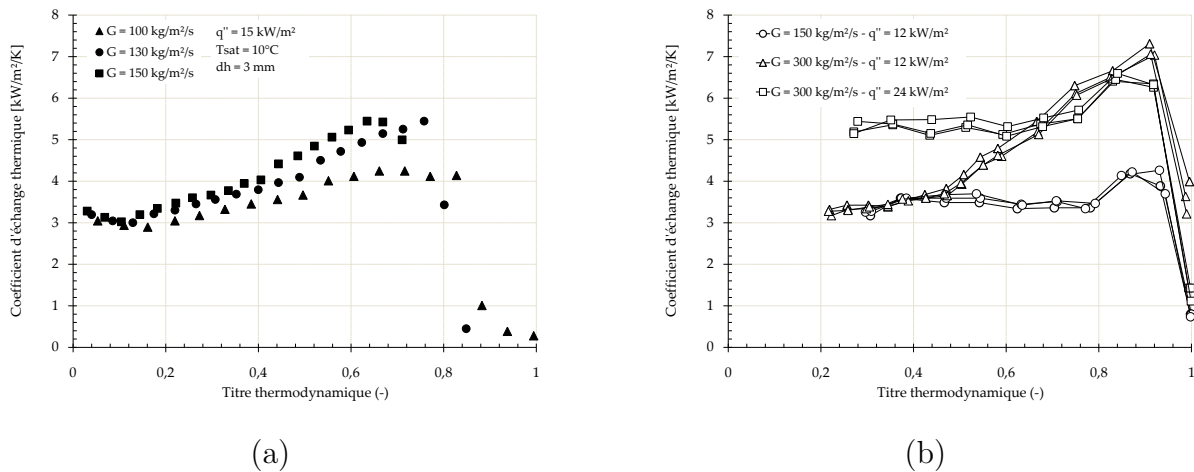


FIGURE 2.20 – Impact of the mass flow rate on the heat exchange coefficient according to : (a) Choi *et al.* (2009) (b) Saitoh *et al.* (2005)

Choi *et al.* (2009) and Saitoh *et al.* (2005) have studied the heat transfer coefficient evolution with the mass velocity. The last authors have studied the R134a flow in three tube of different

Chapitre 2. Literature review on the boiling in mini-channels

hydraulic diameters (0.51 - 1.12 and 3.1 mm having a length of 550 - 935 and 3235 mm respectively) that have been fabricated in stainless steel (SUS304). Figures 2.20(a) and 2.20(b) showed the results that have been obtained by these authors. It is particularly interesting to point out that for low thermodynamic vapor qualities [$x < 0.15$ for Figure 2.20(a) and $x < 0,4$ for Figure 2.20(b)], the heat exchange coefficient did not evolved either with the flow rate, nor the thermodynamic vapor quality. For $x > 0.15$ (or $x > 0.4$ regarding what these authors observed), the mass flow and thermodynamic vapor quality impacts on the heat transfer coefficients until the dryout appearance. Then it decreased drastically [$0.65 < x_{crit} < 0.85$ for Figure 2.20(a) and $0.85 < x_{crit} < 0.95$ for Figure 2.20(b)].

Dryout phenomena take place for lower thermodynamic vapor quality when the flow rate was increased according to Choi *et al.* (2009). For the study of boiling in smaller tubes, the mass flow impact become more difficult to characterize as the results of Kuo et Peles (2007) showed it (Figure 2.21).

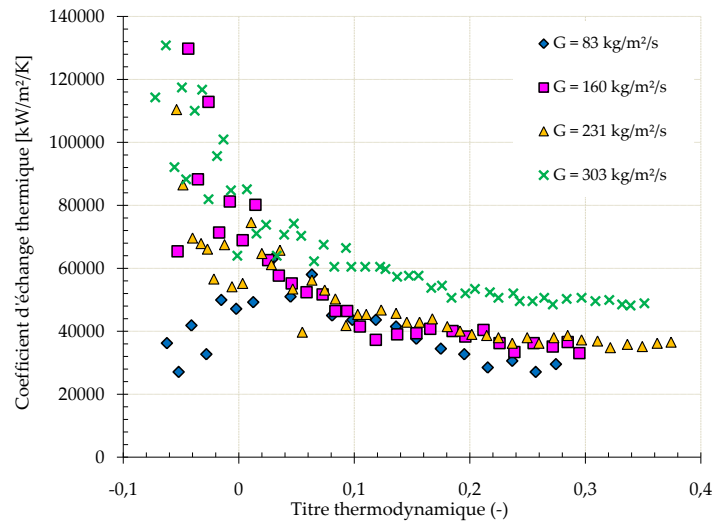


FIGURE 2.21 – Heat transfer coefficient evolution regarding the flow rate according to Kuo et Peles (2007)

When the thermodynamic vapor quality is higher to 0.05, the authors showed that the heat transfer coefficient evolved not much with the flow rate (when $G \leq 231 \text{ kg} \cdot \text{m}^{-2} \cdot \text{s}^{-1}$). They made the assumption that the convective evaporation is not the main mechanism of heat transfer for this configuration. For a mass velocity of $303 \text{ kg} \cdot \text{m}^{-2} \cdot \text{s}^{-1}$, the heat transfer coefficient increased significantly and for this case, the impact of the flow rate cannot be neglected. This results showed that the evolution of the heat transfer process on devices of small dimensions is much more complex than for the cases of conventional ones.

Wall heat flux

Similarly to the impact of the mass velocity, the heat flux impact is not well understood when the system dimensions are reduced. Moreover, the use of different working fluids can modify the impact of the heat flux on heat transfer rate. The experimental results of Ong et Thome (2009) showed how much this phenomenon is complex (Figure 2.13). For these results, the heat transfer coefficient increased with the heat flux on the full range of thermodynamic vapor quality, when using the R134a as working fluid. When R236fa was used, the heat transfer coefficient increased with the heat flux for $x < 0.4$. Above this value, the heat transfer coefficients was not much influenced by the heat flux. Besides, the heat transfer coefficient is not sensitive to the heat flux when R245fa has been used. If an attention is paid on the Choi *et al.* (2009) results, it can be point out a very close behavior compared to what Ong et Thome (2009) observed when R236fa is used as working fluid.

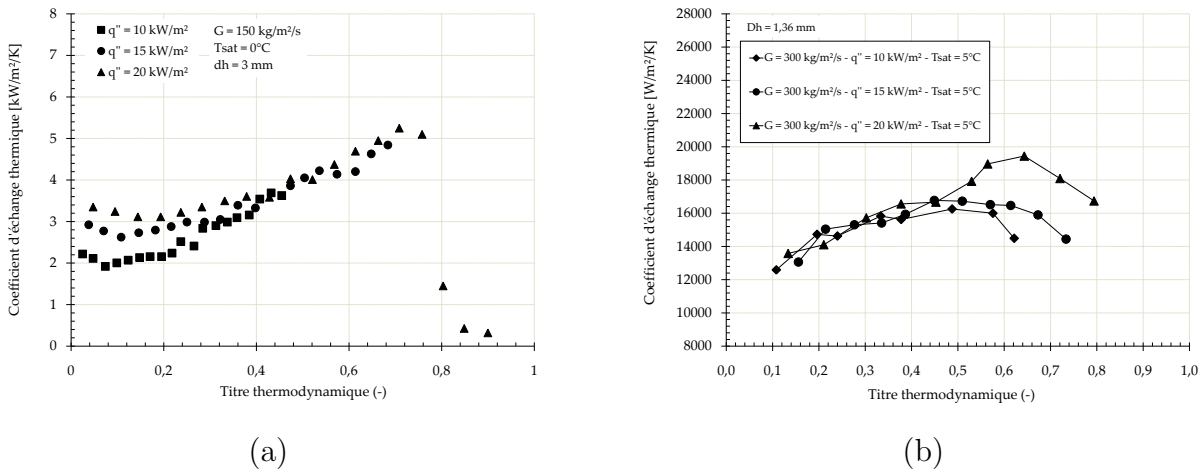


FIGURE 2.22 – Heat transfer coefficient evolution regarding the wall heat transfer according to : (a) Choi *et al.* (2009) (b) Yun *et al.* (2006)

Figure 2.22(a) showed that the heat transfer coefficient was not dependent on heat flux when $x < 0.45$. Beyond this value, the heat transfer coefficient seemed to be independent of the wall heat flux. Yun *et al.* (2006) studied the evolution of the heat transfer coefficient for R410a in two test sections that consisted in multi-channels of 1.36 mm and 1.44 mm of hydraulic diameter. The authors did not give the name of the material in which the test section was fabricated, but regarding the related application we can assumed that it was aluminum. Yun *et al.* (2006) noted that the heat transfer coefficient is not much sensitive to heat flux variation for small values of thermodynamic vapor qualities. Then for a thermodynamic vapor quality higher than 0.5, the heat exchange increased with heat flux. Yun *et al.* (2006) explained this surprising

phenomenon²³ by instabilities occurrences what create interaction between the channels for thermodynamic vapor qualities higher than 0.5. These interactions intensified when the heat flux is increased and led to the improvement of the heat transfer rate²⁴.

Summary of the flow rate and heat flux impact

We can classify, the impact of these parameters regarding two categories of duct :

① For **ducts of large hydraulic diameters**, the influence of the flow rate and of the heat flux on the evolution of the heat transfer rate are clear enough. For the small thermodynamic vapor qualities, the heat transfer coefficient is generally not dependent on the flow rate but is heat flux dependent. This behavior is characteristic of the mechanism of nucleate boiling for pool boiling conditions. Moreover, the visualizations that have been made in this situation often showed that this is the bubbles regime which prevail when the thermodynamic vapor quality is small. For the moderate to important thermodynamic vapor qualities, this coefficient can be increased with flow rate^a but stay generally not dependent on the flow rate. As a general rule, the maximal heat flux increased with the flow rate, but also with the wall heat flux. Moreover, the flow rate increase modified the thermodynamic vapor quality value (namely the critical one) for which the maximal heat flux is transmitted (thermodynamic vapor qualities are usually smaller for larger mass flows).

② For the **smaller duct hydraulic diameters**, the flow rate and heat flux influence are not fully understood. However, we can point out the the dryout take place generally for small thermodynamic vapor qualities and around this point the heat transfer coefficients are usually important. This maximal intensity increase with the flow rate or with the heat flux. Nowadays, there is no clear physical understanding which allow for the explanation of the very large diversity (and discrepancy) of the experimental results. Moreover, the experimental conditions may be largely influenced by the fluid selection which can make appear very different evolution for a same test section.

a. One can notice that there are results which showed a continuous decrease of the heat transfer coefficients for an increase of the thermodynamic vapor quality (Agostini (2002), Huo *et al.* (2004), among other).

23. The heat transfer coefficient dependence with the wall heat flux is related to the nucleate boiling mechanism that usually took place for small thermodynamic vapor quality for these dimensions.

24. This results showed the difficulty of the studies in mini-channels for boiling conditions. For this PhD study, we have chosen to limit our study to single mini-channels.

2.3.4 Flow cross section

As written previously, numerous parameters act on the heat transfer rate and on pressure drops evolutions for boiling flows. The impacts of some factors are currently very often studied (saturation pressure, subcooling and heat flux) and there are numerous data in the literature that are related to these results²⁵. The influence of other parameters, as the dimensions and especially the cross section geometries, is particularly difficult to characterize at the mini-channels scale.

The numerical study of Hasan *et al.* (2009) that has been realized for single-flow conditions, compare the hydraulic and thermal performances for counter flows in duct of same length (10 mm) but for which the cross section change for identical fluid volume (Table 2.9)

Geometry	Ducts dimensions
circular	$d_h = 100\mu m$
square	$a \times b = 100\mu m \times 100\mu m$
rectangular	$a \times b = 135\mu m \times 67.5\mu m$
isocel	small side = $122.7\mu m$, large side = $173.5\mu m$
trapezoidal	small side = $71.75\mu m$, large side = $143.5\mu m$, $b = 62.1\mu m$

TABLE 2.9 – Geometrical ducts dimensions. Numerical study of Hasan *et al.* (2009)

It is particularly interesting to note that this single geometrical modification can impact, in a significant way, the pressure drops and heat transfer evolutions. The authors showed that the thermal conductivities ratio (substrate on fluid ones) is a parameter that has an impact on the heat transfer rate evolutions and on the pressure drops²⁶ as showed in Figure 2.23.

25. These results are not all convergent, but the regular and new experimental and numerical results allow for the refinement of the global understanding of the thermal and hydrodynamic behaviours.

26. This observation showed clearly that the fluid and substrate selection is important.

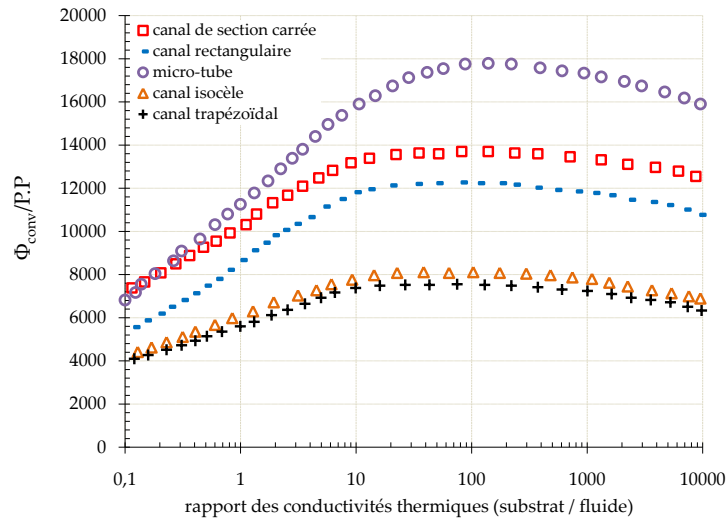


FIGURE 2.23 – Energy efficiency evolution regarding the used geometry and regarding the thermal conductivity ratio between the substrate and the fluid - Numerical study of Hasan *et al.* (2009)

The results that have been given in Figure 2.23 were obtained for a Reynolds number of 50. Φ_{conv} is the convected thermal power and $P.P$ is the pumping power. Thus, the y-axis is an expression representing the energy efficiency. According to our analysis, since the geometrical modification has an impact for single-phase flow, it may be possible that it has an impact for boiling flow conditions also.

Still nowadays, very few studies took into account this influence in the literature. Moreover, for the tubes of sufficiently large hydraulic diameter, the geometry did not seem to have an effect on heat transfer, pressure drop or flow regime transitions²⁷.

The results given by Tran *et al.* (1996) showed that there is no influence of the geometry on the heat transfer coefficient when comparing a tube of hydraulic diameter of 2.46 mm, with a channel having a height of 1.7 mm and a width of 4.06 mm ($d_h = 2.4$ mm). The two test sections have the same heated length which is of 0.9 m and have been fabricated in brass. By considering the Kew et Cornwell (1997) parameter, $C_o \cong 0.32$ for the Tran *et al.* (1996) study, the flow should not be considered as confined for the data that have been obtained by these authors what confirmed their analysis.

Hetsroni *et al.* (2006) specified that the boiling and its evolution is mainly controlled by the bubbles deformation and in particular of those located close to the channel walls which allow for intensification of the heat transfer of ducts of very small dimensions. Harirchian et Garimella (2009) have studied the FC-77 flow in twelve single ducts of hydraulic diameters

27. Carey (2008) (Chapter 10)

Section 2.3. Parameters that have an influence on the boiling nature

ranged between $100 \mu m$ and $748.8 \mu m$ and the authors showed that it exist a cross section from which ($S = 0.089 mm^2$) the thermal transfer became stronger. Choi *et al.* (2009) showed that the cross section reduction allow for the intensification of the heat exchange for small to moderate thermodynamic vapor qualities (Figure 2.24).

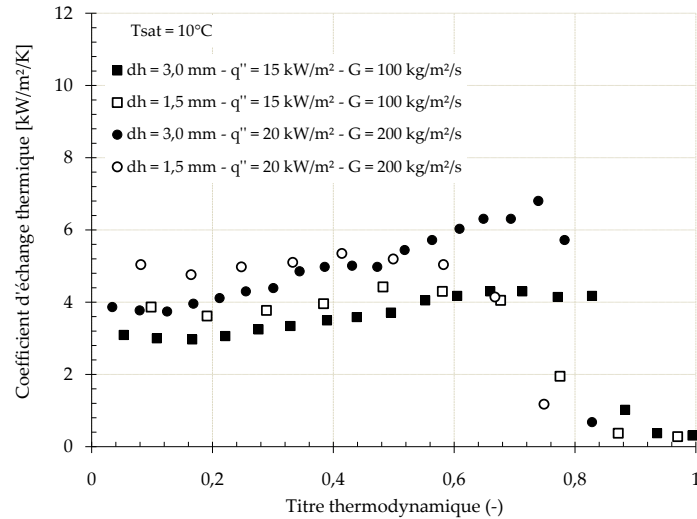


FIGURE 2.24 – Hydraulic diameter influence on the heat transfer coefficient according to Choi *et al.* (2009)

It can be highlighted that the dryout occur for smaller thermodynamic vapor quality when this hydraulic diameter was reduced. The heat transfer coefficients become better for the larger hydraulic diameter for larger thermodynamic vapor quality. Contrary to these results, the analysis of Dupont et Thome (2005), that have been made with R-123 as working fluid, showed that the mean heat transfer coefficient decreased when the duct hydraulic diameter (ranged between $0.5 mm$ and $2 mm$) is reduced. In addition, the authors found that the maximum heat flux was not sensitive to this hydraulic diameter. The results of Saitoh *et al.* (2005) suggest however that the maximum heat flux that can be transferred increased with the reduction of this hydraulic diameter. They found similarly to the study of Dupont et Thome (2005) that when this hydraulic diameter was reduced the dryout took place for lower thermodynamic vapor qualities, what is in accordance with the Choi *et al.* (2009) study.

Otherwise Harirchian et Garimella (2009) analyzed the influence of their rectangular mini-channels cross sections on pressure drop evolutions. Their showed that the flow cross section reduction generally leads to an increase of the pressure drop for convective boiling conditions. The results that have been obtained by Revellin et Thome (2006) and Choi *et al.* (2009) are in agreement with this former result as showed on Figure 2.25.

Chapitre 2. Literature review on the boiling in mini-channels

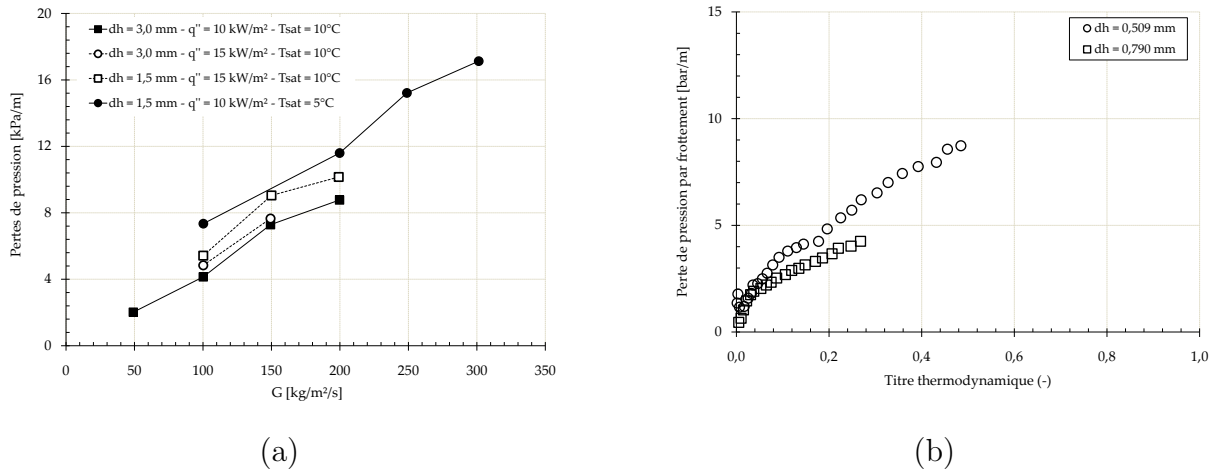


FIGURE 2.25 – Duct diameter influence of the two-phase flow pressure drop evolution according to : (a) Choi *et al.* (2009). (b) Revellin et Thome (2006)

The original study of Yen *et al.* (2006) dealt with the cross section impact on the evolution of the heat transfer coefficients evolution. This study is interesting because the authors have made visualization of their boiling flow. These visualizations allow for the understanding of the physical mechanisms that played a role when modifying the cross section. The working fluid was HCFC123 for the two ducts : a tube having a hydraulic diameter of $210\mu\text{m}$ and a squared channel with a hydraulic diameter of $214\mu\text{m}$. These two ducts were fabricated in pyrex and had been covered with a thin film made of ITO/Ag (Indium-Tin oxide/silver) to guarantee their heating using the Joule effect and the simultaneous flow visualization.

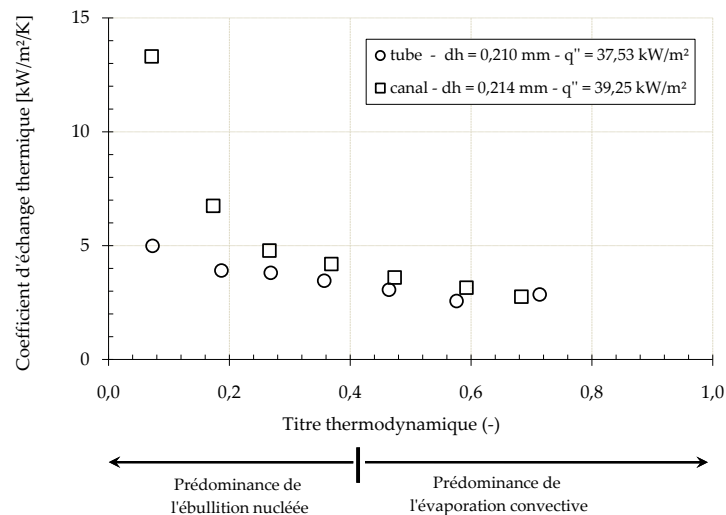


FIGURE 2.26 – Heat transfer coefficient for two ducts of different cross sections according to Yen *et al.* (2006)

Section 2.3. Parameters that have an influence on the boiling nature

The results that have been given in Figure 2.26 showed that when the flow is in the nucleated boiling regimes, the heat transfer coefficient is more important for the duct having a squared cross section compare to the circular one. This result showed that during boiling²⁸ the thermal performance increase more rapidly than for these mini-channels. The authors explained that this is due to the channel corners that act as nucleation sites (Figure 2.27). These corner favour the heat transfer in the nucleate boiling conditions. It is then followed by a shrinking of the thin liquid film (without it disappearance which would lead to dryout) in the corners for these conditions. This liquid film may continue to subsist even when the plug/slug or annular regimes took place. The appearance of these flow regimes for convective boiling regime for a tube lead generally to the suppression of nucleation on the wall²⁹ and does not favour the heat transfer in these conditions.

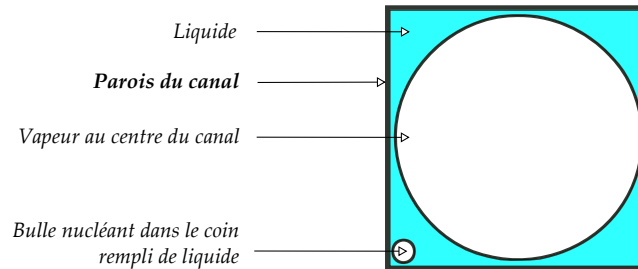


FIGURE 2.27 – Corners that act as nucleation sites according to Yen *et al.* (2006)

In addition, the authors suggested that the use of a duct of squared cross section delay the dryout effect compared to the case of test section of circular cross section. Similarly to the work done by Diaz et Schmidt (2007) or Kuo et Peles (2007), it is particularly interesting to note that the heat transfer coefficients depend on the evolution of the thermodynamic vapor quality for nucleate boiling conditions. This phenomena seems to be surprising compared to the studies that have been made for conventional ducts ($d_h > 3 \text{ mm}$) for which this coefficient is not dependent on the thermodynamic vapor quality during nucleate boiling regime.

Qu et Mudawar (2002) have studied the convective boiling of water in 21 parallel and rectangular channels of $231 \mu\text{m}$ of width and having a height of $713 \mu\text{m}$. They noted the appearance of bubbles in the channels corners for ONB. Moreover, Li *et al.* (2004) made a numerical study on the impact of the corner angle on the boiling that allow for the demonstration that the minimal energy needed for the generation of the bubbles in a corner decreased with the opening angle of these corner (Figure 2.14).

28. Hasan *et al.* (2009) have showed that in single-phase flow the performances were better for mini-tubes.

29. The temperature difference between the fluid and the wall become so low that the needed superheat for activation of the nucleation sites is not high enough.

Summary : Impact of the duct cross section

During the study of convective boiling, the influence of the cross section or of the mini-tube dimensions can play an important role on the intensity of the heat transfer, the evolution of the pressure drops and also on the flow regimes transitions. The reduction of the mini-duct hydraulic diameter seem to lead to the intensification of the heat transfer. However, in a same time, the reduction of the flow cross section lead to the increase of the pressure drop. Thus, for considering the energetic efficiency of a thermal exchanger it should be necessary to consider the ratio between the wall heat transfer and the pumping power.

Still nowadays, relatively few studies were focused on the analysis of these parameters on these two power values. According to the results of our literature survey, the use of the mini-channels seemed to enhance the heat transfer coefficients compared to the mini-tubes for low thermodynamic vapor qualities. Moreover, the dryout phenomena would be reached for higher heat fluxes values for the mini-channels compared to the mini-tubes of same hydraulic diameters. Besides, for the mini-channels case, the influence of the aspect ratio on the hydrodynamic and thermal behaviours is far to be understood. We can assumed that for the mini-channels for which one dimension of the cross section is lower to the bubble detachment diameter, this geometrical parameter (aspect ratio) should certainly play a significant role on the hydrodynamic or thermal behaviours.

2.4 Prediction of the pressure drops evolution

2.4.1 Presentation of theoretical data

The pressure drop prediction for a boiling flow is a data that is very important for the heat exchanger sizing and particularly for the determination of the pumping power. In this paragraph, we will make a theoretical recall regarding the construction of the laws and correlations that have been established for the pressure drops prediction for an internal two-phase flow.

From a general point of view, the expression of the total pressure drop for **two-phase** flow can be written as followed :

$$-\left(\frac{dP}{dz}\right)_{diph(tot)} = -\left(\frac{dP}{dz}\right)_{diph(fr)} + [(1 - \alpha)\rho_l + \alpha\rho_v] g \sin\beta + \frac{d}{dz} \left[\frac{G^2 x^2}{\rho_v \alpha} + \frac{G^2 (1 - x)^2}{\rho_l (1 - \alpha)} \right] \quad (2.28)$$

This total pressure drop is the contribution of three elements :

- ① the pressure drop due to the friction between the fluid and the channel wall $\left(\frac{dP}{dz}\right)_{diph(fr)}$,
- ② the pressure drop generated by the gravity forces that act on the fluid (*which are dependent on the channel/tube orientation (β) for a sufficiently large diameter*),
- ③ the pressure drop due to the flow acceleration (or flow deceleration) during phase change.

One of the most problematic term that has to be determined in the equation (2.28) is the one related to the pressure drops due to the parietal frictions. Indeed, in numerous two-phase flow configurations, it can be obtained only using an empirical method. The two other terms can be calculated using the void fraction α and thermodynamic vapor quality x evolutions. It is possible to relate these two parameters using the equation :

$$\alpha = \frac{A_v}{A} = \frac{1}{1 + \left(\frac{1 - x}{x}\right) \frac{\rho_v u_v}{\rho_l u_l}} \quad (2.29)$$

The knowledge of the void fraction and the thermodynamic vapor quality allow for the determination of the liquid and vapor velocities as showed by the equations (2.6a) et (2.6b). It can be highlighted that for horizontal flows, the term due to the hydrostatic pressure [second term on right side of the equation (2.28)] equalled zero.

2.4.2 Pressure drops for two-phase flow

In this section, the expression of different correlations or laws that characterize the pressure drops due to wall friction are reported.

a) Homogeneous model

The homogeneous model is a concept that allow for the simple representation of the evolution of the pressure drops for specific flow configurations. For these cases, the fluid mixture obeys to the same laws compared to the ones of a single phase flow by considering that the evolution of the thermophysical properties of the mixture are similar to a single specific fluid. For this configuration, the two phases are considered to flow a same velocity inside the duct ($u_v/u_l = 1$), what lead to the simplification of specific equations. The mixture mass density can be defined as followed :

$$\rho_{hom} = \rho_v \alpha + \rho_l (1 - \alpha) \quad (2.30)$$

ρ_{hom} can be written regarding the thermodynamic vapor quality and using equation (2.29) :

$$\rho_{hom} = \left(\frac{x}{\rho_v} + \frac{1-x}{\rho_l} \right)^{-1} \quad (2.31)$$

Therefore, the pressure drop term that is due to the two-phase flow acceleration (or deceleration) is given by :

$$\left(\frac{dP}{dz} \right)_{diph(acc)} = \frac{d}{dz} \left(\frac{G^2}{\rho_{hom}} \right) \quad (2.32)$$

For an horizontal flow, the hydrostatic term equals zero. Using the thermophysical properties of the mixture, it is possible to obtain the pressure drop expression for a homogeneous flow :

$$\left(\frac{dP}{dz} \right)_{diph(fr)} = \frac{2f_{hom}G^2}{d_h \rho_{hom}} \quad (2.33)$$

The friction coefficient, f_{hom} depends on the flow regime that is developed in the duct. Its expression followed the equation :

$$f_x = a Re_x^{-b} \quad (2.34)$$

with x , which is expressing either the vapor phase or the liquid one or the two-phase mixture. The constants, a and b , are dependent of the flow regime that is developed in the duct. In the case of a laminar flow (Re_l, Re_v ou $Re_{hom} < 2000$), the value of a is given by the equation (1.7) for the rectangular channel case and $b = 1$. For a turbulent flow (Re_l, Re_v ou $Re_{hom} > 2000$), $a = 0.079$ et $b = 0.25$. The Reynolds number expression for a homogeneous flow is given following :

$$Re_{hom} = \frac{Gd_h}{\mu_{hom}} \quad (2.35)$$

μ_{hom} is the mixture dynamic viscosity which is defined by Cicchitti *et al.* (1960) following³⁰ :

$$\mu_{hom} = x\mu_v + (1-x)\mu_l \quad (2.36)$$

30. Other definition of μ_{hom} can be found in Lee et Mudawar (2005a)

This is a model that is often used when bubble flow regime occurred with the phases that are close to saturation conditions, high mass velocities or a low density ratio between the liquid and vapor phases.

b) Separated flow model³¹

☞ *Lockhart et Martinelli (1949) correlation*

The results from the literature have showed that it was possible to correlate the experimental data by characterizing the friction pressure drops evolution for a two-phase flow in tube of large hydraulic diameters. Lockhart et Martinelli (1949) have used the concept of two-phase multipliers for correlating their experimental data using the wall friction that were obtained during a liquid or vapor single-phase flow. Thus the pressure drops due to the wall friction for a two-phase flow can be written as :

$$\left(\frac{dP}{dz}\right)_{diph(fr)} = \Phi_l^2 \left(\frac{dP}{dz}\right)_{l(fr)} = \Phi_v^2 \left(\frac{dP}{dz}\right)_{v(fr)} = \Phi_{lo}^2 \left(\frac{dP}{dz}\right)_{lo(fr)} \quad (2.37)$$

Where Φ_l , Φ_v and Φ_{lo} are the two-phase multipliers of the liquid, vapor and liquid (if it was flowing alone along the duct). By considering the liquid flow, the force balance on the domain when the flow is fully developed (for horizontal case, the hydrostatic pressure equals zero) may be given by³² :

$$\pi \frac{d_h^2}{4} \left[P(z) - \left(P(z) + \frac{dP}{dz} dz \right) \right] = \pi d_h \tau_p dz \quad (2.38)$$

The expression of the pressure drop due to the friction is as a consequence equaled to :

$$\left(\frac{dP}{dz}\right)_{l(fr)} = -\frac{4\tau_p}{d_h} \quad (2.39)$$

But, if the liquid phase flow is take into account, τ_p can be given as :

$$\tau_p = \frac{1}{2} f_l \rho_l [(1 - \alpha) u_l]^2 \quad (2.40)$$

f_l is the friction coefficient and u_l the liquid velocity. The expression of the liquid and vapor velocities are given using :

$$u_l = \frac{G(1 - x)}{\rho_l(1 - \alpha)} \quad (2.41a)$$

$$u_v = \frac{Gx}{\rho_v \alpha} \quad (2.41b)$$

31. Some of the analysis presented there have been presented in Thome (2006), chapitre 13

32. This demonstration can be done for a rectangular channel also

Chapitre 2. Literature review on the boiling in mini-channels

By substituting the equation (2.40) and (2.41a) into equation (2.39) it is possible to obtain :

$$\left(\frac{dP}{dz}\right)_{l(fr)} = -\frac{2f_l G^2 (1-x)^2}{\rho_l d_h} \quad (2.42a)$$

By using the same approach for the vapor we obtained :

$$\left(\frac{dP}{dz}\right)_{v(fr)} = -\frac{2f_v G^2 x^2}{\rho_v d_h} \quad (2.42b)$$

The equation (2.42a) represent the liquid wall friction with the duct. Finally, the equation (2.37) can be rewritten for the liquid as :

$$\left(\frac{dP}{dz}\right)_{diph(fr)} = -\Phi_l^2 \left(\frac{2f_l G^2 (1-x)^2}{\rho_l d_h}\right) \quad (2.43)$$

Chisholm et Laird (1958) have formalized the Lockhart et Martinelli (1949) approach and proposed to represent Φ_l by the expression :

$$\Phi_l = \left(1 + \frac{C}{\chi} + \frac{1}{\chi^2}\right)^{1/2} \quad (2.44)$$

C is a variable that depends on the flow regimes that are developed (viscous³³ or turbulent) for the liquid and vapor phases of the two-phase flow. The values that are taken by this constant are given in Table 2.10.

Liquid	Vapor	Designation subscript	C
Turbulent	Turbulent	tt	20
Viscous	Turbulent	vt	12
Turbulent	Viscous	tv	10
Viscous	Viscous	vv	5

TABLE 2.10 – Separated flows

χ is the Martinelli parameter that is defined by :

$$\chi = \left[\frac{(dP/dz)_l}{(dP/dz)_v}\right]^{1/2} \quad (2.45)$$

Using equations (2.42a) and (2.42b) we obtained :

$$\chi = \left(\frac{\rho_v}{\rho_l}\right)^{1/2} \left(\frac{f_l}{f_v}\right)^{1/2} \left(\frac{1-x}{x}\right) \quad (2.46)$$

33. The terminology of Chisholm (1973) will be kept, by recalling that for the cases of the laminar flows, the inertial forces are not necessarily negligible

Section 2.4. Prediction of the pressure drops evolution

The values of the coefficients f_l and f_v can be found using equation (2.34). Using the whole set of data, it is possible to determine the pressure variations that are due to the two-phase flow regarding the flow regime that is developed in the duct. Numerous studies (Mishima et Hibiki (1996)[1], Lee et Lee (2001a)[2], Qu et Mudawar (2003)[3], Lee et Mudawar (2005b)[4], Lee et Mudawar (2008)[5], Megahed et Hassan (2009)[6]) based their analysis on this demonstration for correlating their experimental results by modifying the value of C (Table 2.11).

Aut.	Fluide(s)	sect.	d_h (mm)	Orient.	C
[1]	water/air	circ.	1 - 4	Vert.	$C_{xx} = 21(1 - e^{-319d_h})$
[2]	water/air	rect.	0.8 - 6.7	Horiz.	$C_{vt} = 0.062Re_{lo}^{0.73}$
[3]	water	rect.	0.349	Horiz.	$C_{vv} = 21(1 - e^{-319d_h})(0.00418G + 0.0613)$
[5]	water	rect.	0.16 - 0.54	Horiz.	$C_{vv} = 2566G^{0.5466}d_h^{0.8819}(1 - e^{-319d_h})$
[4]	<i>R134a</i>	rect.	0.349	Horiz.	$C_{vv} = 2.16Re_{lo}^{0.047}We_{lo}^{0.6}$ $C_{vt} = 1.45Re_{lo}^{0.25}We_{lo}^{0.23}$
[6]	<i>FC72</i>	rect.	0.25	Horiz.	$C_{vv} = \frac{0.0053Re_{lo}^{0.934}}{C_0^{0.73}(X^2)^{0.175}}$ $C_{vt} = \frac{0.0002Re_{lo}^{1.7}}{C_0^{0.7}(X^2)^{1.24}}$

TABLE 2.11 – C value for different studies taken from literature

For Mishima et Hibiki (1996), the C parameter is a function that depends on the hydraulic diameter, whereas for Lee et Lee (2001a), Qu et Mudawar (2003) and Lee et Mudawar (2008), it is dependent of the mass velocity also. We can point out that for Lee et Mudawar (2005b) and Megahed et Hassan (2009), C is a more complex function which depends on hydraulic diameter, mass velocity, surface tension and gravity acceleration.

For finding the expression of the pressure variation for a two-phase flow, it is then necessary to integrate the following expression :

$$\Delta P_{diph(fr)} = \frac{L_{diph}}{x} \int_0^x \Phi_l^2 \left(\frac{2f_l G^2 (1-x)^2}{\rho_l d_h} \right) \quad (2.47)$$

It is considered that the Lockhart et Martinelli (1949) correlation is useful when $\mu_l/\mu_v > 1000$ et $G < 100 \text{ kg.m}^{-2}.\text{s}^{-1}$.

☞ *Chisholm (1973) correlation*

The correlation that have been given by Chisholm (1973) came from an empirical and extensive method (graphical method of Baroczy (1966)) which is applicable for experimental

Chapitre 2. Literature review on the boiling in mini-channels

conditions that are very often encountered. The pressure gradient related to friction is given by :

$$\left(\frac{dP}{dz}\right)_{diph(fr)} = \Phi_{ch}^2 \left(\frac{dP}{dz}\right)_{l(fr)} \quad (2.48)$$

Chisholm (1973) defined a parameter, Y , that was obtained from the ratio due to the friction pressure gradients that allow for the obtaining of the two-phase multiplier Φ_{ch} :

$$Y^2 = \frac{\left(\frac{dP}{dz}\right)_{vo}}{\left(\frac{dP}{dz}\right)_{lo}} \quad (2.49)$$

where the subscripts (vo and lo) represent vapor and liquid phase as flowing along in the duct.

The two-phase multiplier is correlated using the parameter according to :

$$\Phi_{ch}^2 = 1 + (Y^2 - 1) \left[(Bx(1-x))^{(2-b)/2} + x^{2-b} \right] \quad (2.50)$$

where b is the exponent that can be found in equation (2.34). The value of the constant B is given for different values of Y , which are reported in Table 2.12.

$0 < Y < 9,5$	$G \geq 1900$	$\rightarrow B = 55/G^{1/2}$
	$500 < G < 1900$	$\rightarrow B = 2400/G$
	$G < 500$	$\rightarrow B = 4.8$
$9,5 < Y < 28$	$G \geq 600$	$\rightarrow B = 520/(YG^{1/2})$
	$G < 600$	$\rightarrow B = 21/Y$
$Y > 28$	$\forall G$	$\rightarrow B = 15000/(Y^2G^{1/2})$

TABLE 2.12 – B values according to Chisholm (1973)

The Chisholm (1973) is used when $\mu_l/\mu_v > 1000$ and $G > 100 \text{ kg.m}^{-2}.\text{s}^{-1}$.

Tran et al. (2000) correlation

More recently, Tran *et al.* (2000) started from the Chisholm (1973) analysis for characterizing the friction pressure drop, by considering the confinement and surface tension effect on the evolution of the two-phase flow and they obtained :

$$\left(\frac{dP}{dz}\right)_{diph(fr)} = \Phi_{tran}^2 \left(\frac{dP}{dz}\right)_{l(fr)} \quad (2.51)$$

Section 2.4. Prediction of the pressure drops evolution

The authors defined the expression of their two-phase multiplier according to :

$$\Phi_{tran}^2 = 1 + (4.3Y^2 - 1)(C_o(x(1-x))^{0.875} + x^{1.75}) \quad (2.52)$$

with the confinement number C_o which can be expressed according to equation (2.20).

☞ *Friedel (1979) correlation*

Friedel (1979) used the same to-phase multipliers concept than Lockhart et Martinelli (1949) for determining the evolution of the pressure drop in the two-phase flow :

$$\left(\frac{dP}{dz}\right)_{diph(fr)} = \Phi_{fried}^2 \left(\frac{dP}{dz}\right)_{l(fr)} \quad (2.53)$$

His analysis was based on the study of more than 25000 experimental data points for tubes having a horizontal or a vertical orientation and for upward or downward flows. These flows took place in tubes having a circular cross section or rectangular channels. The evolution of the two-phase multiplier of Friedel (1979) is not dependent of the same parameters compared to the one defined by Lockhart et Martinelli (1949) :

$$\Phi_{fried}^2 = E + \frac{3.24FH}{Fr_l^{0.045}We_l^{0.035}} \quad (2.54)$$

The author defined the Froude (Fr) and Weber (We) numbers³⁴ :

$$Fr_l = \frac{G^2}{gd_h\rho_{hom}^2} \quad ; \quad We_l = \frac{G^2d_h}{\sigma\rho_{hom}} \quad (2.55)$$

The expression of ρ_{hom} can be found using the equation (2.31) and the expression of the constants E , F , H is given according to :

$$E = (1-x)^2 + x^2 \frac{\rho_l f_v}{\rho_v f_l} \quad ; \quad F = x^{0.78}(1-x)^{0.224} \quad ; \quad H = \left(\frac{\rho_l}{\rho_v}\right)^{0.91} \left(\frac{\mu_v}{\mu_l}\right)^{0.19} \left(1 - \frac{\mu_v}{\mu_l}\right)^{0.7} \quad (2.56)$$

The use of the Friedel (1979) correlation is recommended when the ratio $(\mu_l/\mu_v) < 1000$ and $G < 2000 \text{ kg m}^{-2} \text{ s}^{-1}$.

☞ *Grönnerud (1972) correlation*

Grönnerud (1972) had developed this correlation specifically for the use of refrigerants. The originality of this correlation came from the construction of a two-phase multiplier that

³⁴. We can note that these numbers are dependent of the medium mass density which was considered as uniformed.

depends on a pressure drop correlated with the Froude number and on the thermodynamic vapor quality :

$$\left(\frac{dP}{dz}\right)_{diph(fr)} = \Phi_{gd}^2 \left(\frac{dP}{dz}\right)_{l(fr)} \quad (2.57)$$

The two-phase multiplier that have been defined by the author follow the law :

$$\Phi_{gd} = 1 + \left(\frac{dP}{dz}\right)_{gd} \left[\frac{\left(\frac{\rho_l}{\rho_v}\right)}{\left(\frac{\mu_l}{\mu_v}\right)^{0.25}} - 1 \right] \quad (2.58)$$

Surprisingly, the pressure gradient that have been defined by Grönnerud (1972) is non-dimensional and depends on a friction coefficient, f_{gd} :

$$\left(\frac{dP}{dz}\right)_{gd} = f_{gd} [x + 4(x^{1.8} - x^{10} f_{gd}^{0.5})] \quad (2.59)$$

The friction coefficient value can depends on the Froude number variation :

$$\begin{cases} \text{Si } Fr_l \geq 1 \rightarrow f_{gd} = 1 \\ \text{Si } Fr_l < 1 \rightarrow f_{gd} = Fr_l^{0.3} + 0.0055 \left[\ln \left(\frac{1}{Fr_l} \right) \right]^2 \end{cases} \quad (2.60)$$

where the Froude number is equaled to :

$$Fr_l = \frac{G^2}{gd_h \rho_l^2} \quad (2.61)$$

Müller-Steinhagen et Heck (1986) correlation

Müller-Steinhagen et Heck (1986) proposed a correlation that represent the interpolation between the whole flow that was considered as fully liquid and the one fully vapor. The authors have determined this correlation using a set of a large database that cover the : water vapor/water, air/water, air/heavy oils and several refrigerants flow for a total of 9300 experimental data points and hydraulic diameters from 4 to 392 *mm*. It is very interesting to note that this correlation did not took into account the two-phase multiplier notion as defined in preceding paragraphs.

$$\left(\frac{dP}{dz}\right)_{diph(fr)} = G_{msh}(1-x)^{1/3} + A_2 x^3 \quad (2.62)$$

G_{msh} equalled :

$$G_{msh} = A_1 + 2(A_2 - A_1)x \quad (2.63)$$

A_1 and A_2 express the pressure drops in the case of a flow considered as fully liquid [equation (2.42a)] or fully vapor [equation (2.42b)] respectively.

✓ *Representation of the correlations that predict the two-phase pressure drop evolution*

The whole set of the correlations that were described in this paragraph have been represented on Figure 2.28 for a duct having a hydraulic diameter of 1.4mm , a mass velocity of $100\text{kgm}^{-2}\text{s}^{-1}$ with Forane 365 HX ($\mu_l/\mu_v \approx 42$) as working fluid for a relative working pressure of 70kPa . This figure will be considered as the one of reference during the study of the impact of the working conditions on the evolution of the pressure drops given in Figure 2.29.

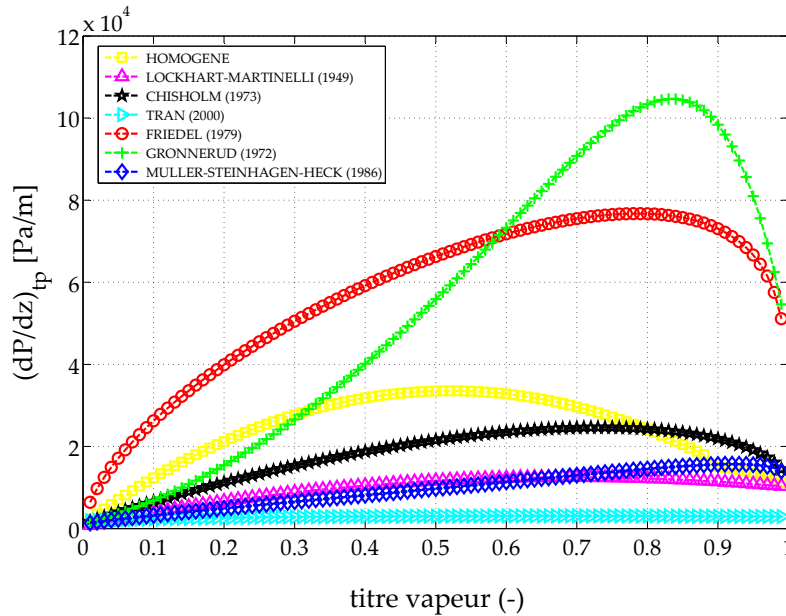


FIGURE 2.28 – Representation of the correlation for the evolution of the pressure drop for a duct having a hydraulic diameter of 1.4mm , a mass velocity of $100\text{kgm}^{-2}\text{s}^{-1}$ for forane 365 HX at 70kPa (relative pressure)

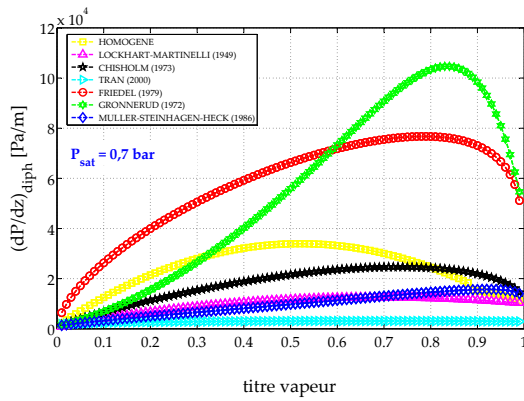
The results given in Figure 2.28 showed that some important differences exist between the correlations that have been given for describing the pressure drop evolution. Thus, it is possible to deduce that a clear understanding of the physical phenomenon that take place during the two-phase flow internal pressure is not conclusive for the moment. The difference can reached a ratio ranged between 1 and 10 (for the most unfavourable cases). The whole set of correlations

Chapitre 2. Literature review on the boiling in mini-channels

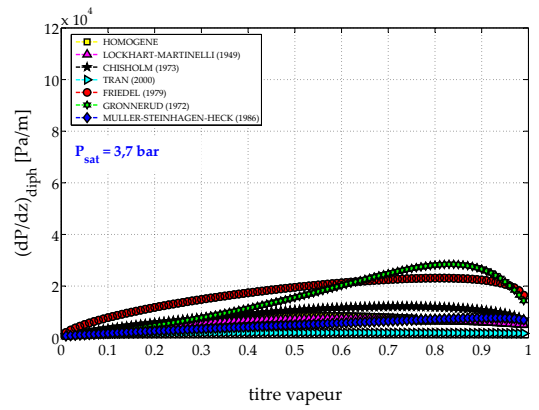
showed that the pressure drop caused by the friction during the two-phase flow is higher than the equivalent pressure drop for single phase flow. This was due to the mean velocity, which was raised to the power two in the pressure drop expression, which became higher for a two-phase flow and led to an increase of this term. It is possible to remark that the pressure drop increase than generally decrease for higher thermodynamic vapor qualities. This behavior can be explained because for large thermodynamic vapor qualities, the liquid wall thin film can completely disappear and lead to a suppression of the interfacial stresses what lead to a reduction of the wall friction.

Figure 2.29 showed that although all the important differences between these correlations, they all keep a relevant physical evolution regarding the experimental pressure drop (according to the data of the literature survey) with the operating conditions. Thus, when the saturation pressure is increased, these correlations predict a diminution of the pressure drop and they predicted an increase of this term when the mass flow rate is increased or when the hydraulic diameter is reduced.

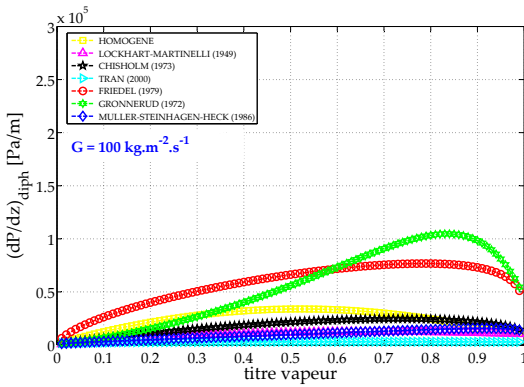
Section 2.4. Prediction of the pressure drops evolution



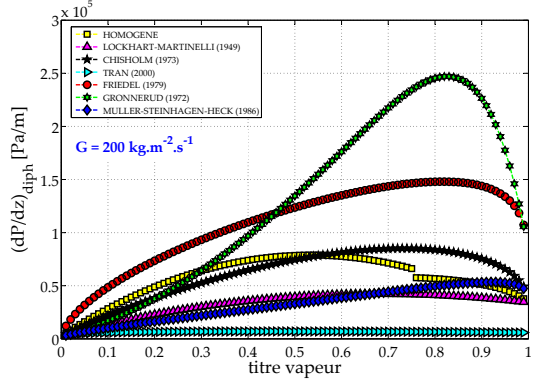
I - (a)



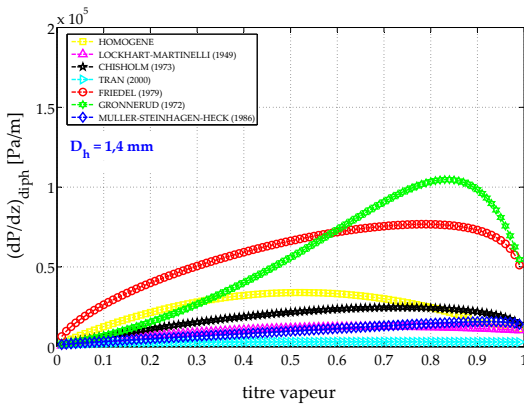
I - (b)



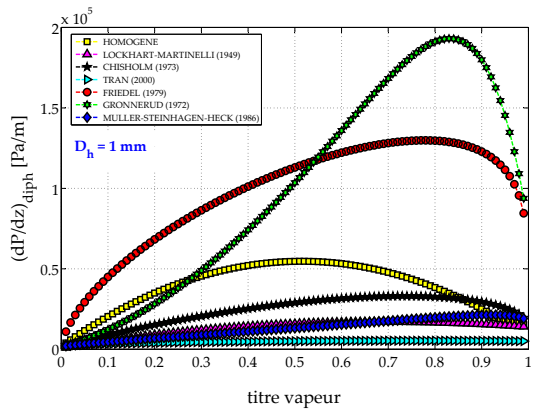
II - (a)



II - (b)



III - (a)



III - (b)

FIGURE 2.29 – Representation of the correlations for the pressure drops evolution for Forane 365 HX : **I** - that flow in a duct having a hydraulic diameter of 1.4 mm, a mass velocity of $100 \text{ kg m}^{-2} \text{ s}^{-1}$ and a saturation pressure at : (a) 70 kPa (b) 370 kPa, **II** - that flow in a duct of 1.4 mm, at a saturation pressure of 70 kPa and a mass velocity of : (a) $100 \text{ kg m}^{-2} \text{ s}^{-1}$ (b) $200 \text{ kg m}^{-2} \text{ s}^{-1}$, **III** - that flow at a saturation pressure of 70 kPa, a mass velocity of $100 \text{ kg m}^{-2} \text{ s}^{-1}$ in a duct having a hydraulic diameter of : (a) 1.4 mm (b) 1 mm

2.4.3 Void fraction evolution

It is often very difficult to obtain the evolution of the void fraction using direct physical measurements³⁵ at small scale. However this value is very important for characterizing the acceleration (or deceleration) due to pressure drop evolution of the two-phase flow³⁶. A solution, for avoiding this difficulty consisted to used the established correlations for the determination of the void fraction evolution with respect to the thermodynamic vapor quality (which is a value that is easier to determine). In this section, some of the models of reference that allow for the determination of the void fraction value have been presented.

a) Homogeneous model

By considering that liquid and vapor phases flowed at same velocity, we obtain $u_l/u_v = 1$. Thus, equation (2.29) is simplified and can be written as :

$$\alpha = \frac{1}{1 + \left(\frac{1-x}{x}\right) \frac{\rho_v}{\rho_l}} \quad (2.64)$$

b) Separated flow models

Zuber et Findlay (1965) correlation

Zuber et Findlay (1965) model (drift flux model) has been developed from the study of numerous flows in vertical tubes. For solving the momentum equation of the mixture, the authors defined a drift flux law that relate the vapor velocity, the liquid velocity and the void fraction ($f(u_v, u_l, \alpha) = 0$). According to them, a drift velocity between the vapor phase (that move faster near the centerline) and the liquid phase exist and its importance is controlled by the liquid and vapor density ratio (or the buoyancy forces). The authors thus defined a drift law that follow the equation :

$$u_{lv} = u_l - u_v = U_\infty(1 - \alpha)^{n-1} \quad (2.65)$$

with U_∞ the velocity that is called the terminal one (or drift one) of the flow and n is a parameter that can be adjusted regarding the flow regimes. In order to determine the void fraction expression, the authors expressed the gas velocity, only, and result in another form an the equation (2.65) :

$$U_v = D_0 J + U_\infty \quad (2.66)$$

35. A literature survey on the measurement techniques of the void fraction can be found in Desrats (2006) (Annexe 2)

36. This term may become very important in the case of phase change

Section 2.4. Prediction of the pressure drops evolution

J represent the superficial velocities sum and can be written as :

$$J = \frac{Gx}{\rho_v} + \frac{G(1-x)}{\rho_l} \quad (2.67)$$

D_o is a bubbles distribution parameter in the flow ($\rightarrow D_o \geq 1$). D_o and U_∞ are variables that are necessary to adjust regarding flow configuration (Table 2.13). Using the equation (2.41b), the void fraction can be expressed as :

$$\alpha = \frac{1}{D_o \left(1 + \frac{(1-x)\rho_v}{x\rho_l} \right) + \frac{\rho_v U_\infty}{Gx}} \quad (2.68)$$

Flow	D_o	U_∞
Bubbles	$1.4 - 0.4P_r$	$1.53 \left[\sigma \frac{g(\rho_l - \rho_v)}{\rho_l^2} \right]^{1/4}$
Slug	1.2	$0.35 \sqrt{\frac{gd_h(\rho_l - \rho_v)}{\rho_l}}$
Annular	1	$\frac{23\mu_l G(1-x)}{\rho_v d_h} \left(\frac{\rho_l - \rho_v}{\rho_l^2} \right)$

TABLE 2.13 – D_o and U_∞ values for a rectangular channel according to Zuber et Findlay (1965) regarding the flow configuration

with P_r representing the reduced pressure (see definition in §2.1.3).

☞ Premoli et al. (1971) correlation

Premoli *et al.* (1971) have defined a correlation which is based on the study of refrigerants flows. They defined a parameter (S) that represent the ratio between the liquid and vapor velocities.

$$\alpha = \frac{\rho_l x}{S\rho_v(1-x) + \rho_l x} \quad (2.69)$$

S can be calculated using :

$$S = 1 + E_1 \left(\frac{y}{1 + yE_2} - yE_2 \right)^{1/2} \quad (2.70)$$

with :

$$\left\{ \begin{array}{l} y = \frac{\beta}{1 - \beta} \quad ; \quad \beta = \frac{\dot{m}_v}{\dot{m}_v + \dot{m}_l} \\ E_1 = 1.578 Re_{lo}^{-0.19} \left(\frac{\rho_l}{\rho_v} \right)^{0.22} \quad ; \quad E_2 = 0.0273 W e_{lo} Re_{lo}^{-0.51} \left(\frac{\rho_l}{\rho_v} \right)^{-0.08} \end{array} \right. \quad (2.71)$$

Steiner (1993) correlation

Thome (2006) recommended the use of the Steiner (1993) correlation who used the drift flux flow concept. The expression of the void fraction is, for the case of horizontal flow, equalled to :

$$\alpha = \frac{x}{\rho_v} \left[(1 + 0.12(1 - x)) \left(\frac{x}{\rho_v} + \frac{1 - x}{\rho_l} \right) + \frac{1.18(1 - x) [g\sigma(\rho_l - \rho_v)]^{0.25}}{G^2 \rho_l^{0.5}} \right]^{-1} \quad (2.72)$$

General form for the writing of the void fraction evolution according to Butterworth (1975)

Butterworth (1975) have demonstrated that it was possible to established a general formula for several correlation/models that allow for the calculation of the void fraction :

$$\alpha = \left[1 + B_B \left(\frac{1 - x}{x} \right)^{n_1} \left(\frac{\rho_v}{\rho_l} \right)^{n_2} \left(\frac{\mu_l}{\mu_v} \right)^{n_3} \right]^{-1} \quad (2.73)$$

The values of the constants are reported in Table 2.14.

Correlation or model	B_B	n_1	n_2	n_3
Model of Zivi (1964)	1	1	0.67	0
Model of Wallis (1965)	1	0.72	0.40	0.08
Correlation of Lockhart et Martinelli (1949)	0.28	0.64	0.36	0.07
Correlation of Thom (1964)	1	1	0.89	0.18
Correlation of Baroczy (1965)	1	0.74	0.65	0.13

TABLE 2.14 – Values of the constants B_B , n_1 , n_2 et n_3 taken from (2.73) according to Butterworth (1975)

This very original formulation allow for the simple representation of the void fraction variation regarding the thermodynamic vapor quality.

✓ Representation of the correlation that predict the void fraction evolution

The evolution of all these laws with respect to the thermodynamic vapor quality is given in Figure 2.30. It is possible to point out that all these models predict a very fast increase of the void fraction with the thermodynamic vapor quality. Thus for a thermodynamic vapor quality of 0.2, the whole set of correlations predict a void fraction higher than 60% for a duct having a hydraulic diameter of 1.4 mm, a mass velocity of $100 \text{ kg.m}^{-2}.\text{s}^{-1}$ for Forane 365 HX at 70 kPa (relative pressure).

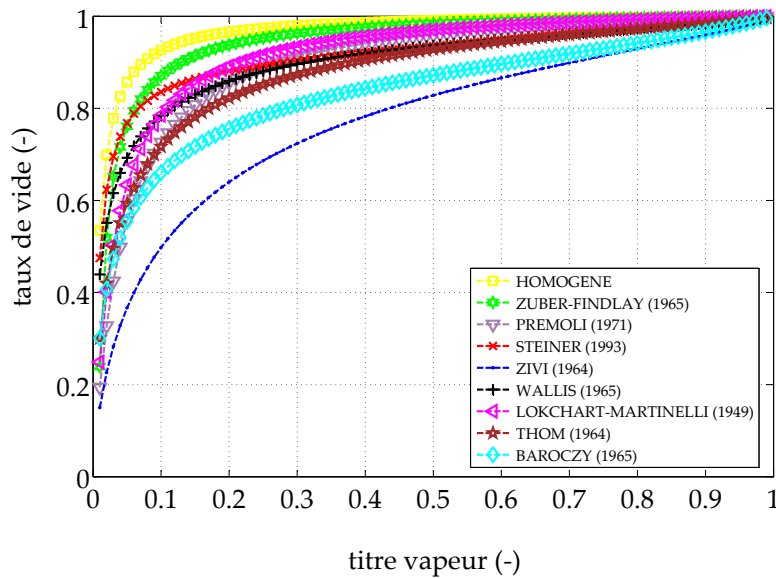


FIGURE 2.30 – Representation of the void fraction evolution regarding the thermodynamic vapor quality for the preceding correlations for a duct having a hydraulic diameter of 1.4 mm, a mass velocity of $100 \text{ kg.m}^{-2}.\text{s}^{-1}$ for Forane 365 HX at 70 kPa (relative pressure)

2.5 Prediction of the heat transfer coefficients evolution

2.5.1 Presentation of the theoretical data

The evolution of the heat transfer for convective boiling is related to a chronology of the vapor and liquid phase repartition. Following to ONB, the bubble flow regime is dominant. It is then followed by the plug/slug flow toward the annular flow and from annular flow up to dispersed flow (fog) (Figure 2.31).

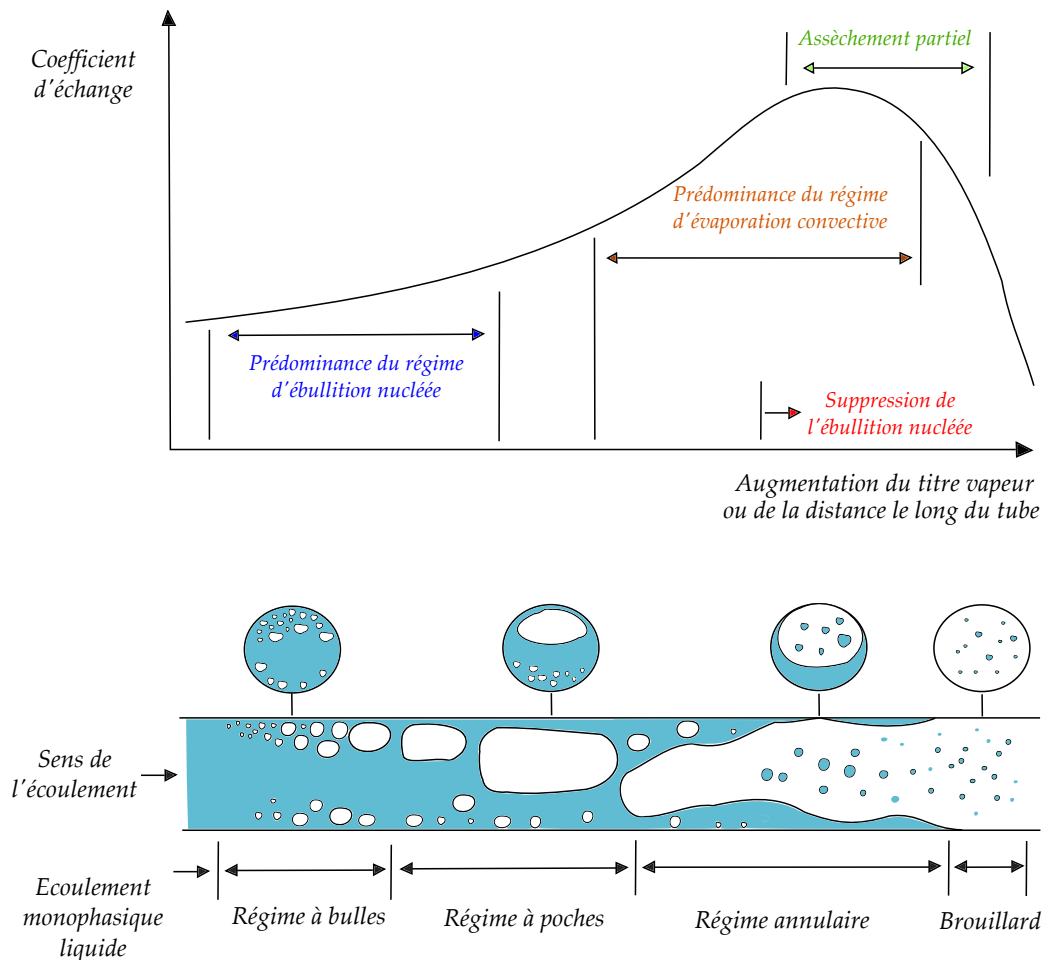


FIGURE 2.31 – Variation of the heat transfer coefficients and of the flow regime along a horizontal tube (Carey (2008))

It is often necessary to consider different mechanisms of heat transfer that evolved with the thermodynamic vapor quality (or with the considered location along the flow) during the convective boiling. Figure 2.31 showed that the nucleated boiling regime drove the heat transfer for low thermodynamic vapor qualities and led to a very moderated increase of the heat transfer rate. For larger thermodynamic vapor qualities, the flow goes rapidly in the annular configuration, and the heat transfer mechanism are controlled by the interface vaporization that allow

for the enhancement of the heat transfer coefficient. This is due to the decrease of the liquid thin film that lead to a decrease of the thermal resistance. For the moderated thermodynamic vapor qualities, the two mechanism may control simultaneously the heat transfer rate. From a specific thermodynamic vapor quality (or a specific location), the liquid vaporization at the interfaces may become so important that the nucleate boiling regime can be fully suppressed. From this moment, the vaporization mechanism become the single process that drive the heat transfer rate. During the last stages of the annular flow, the core vapor acceleration produced very often droplets entrainment that have been taken from the liquid film and caused by the appearance of Kelvin-Helmholtz instability (Revellin et Thome (2008)). For higher thermodynamic vapor quality, these breaks may lead to a localized disappearance that is called partial dryout. It is possible to fully dry this thin film for the most unfavorable conditions³⁷.

From their literature review Webb et Gupte (1992) listed three modelling for defining the importance of the heat transfer mechanism that can be encountered in convective boiling :

a) Superposition model :

$$h_{diph} = h_{nb} + h_{cv} \quad (2.74)$$

where h_{nb} is the heat transfer coefficient due to the nucleate boiling and h_{cv} , the one due to the convective flow contribution.

b) Asymptotic model :

$$h_{diph}^n = h_{nb}^n + h_{cv}^n \quad (2.75)$$

c) Intensification model :

$$h_{diph} = \Psi h_L \quad (2.76)$$

In the following paragraphs some of the most known model will be presented.

37. A complementary definition of these two mechanisms is given in §2.2.4

2.5.2 Correlations taken from literature

a) Superposition model

☞ *Chen (1966) correlation and adaptation to the mini-channels cases by Zhang et al. (2004)*

Chen (1966) defined the superposition model by considering that the heat transfer coefficient for saturated convective boiling was the sum of a microscopic (nucleate boiling) and macroscopic (heat transfer by convection) contribution. Regarding the flow conditions, one of the contribution may be increased or decreased. Using the Figure 2.31, it is more simple to understand the analysis made by Chen (1966) which has weighted the heat exchange coefficient due to nucleate boiling (h_{nb}) by a suppression factor S and the heat transfer coefficient due to convective vaporization (h_{cv}) by a intensification factor F :

$$h_{diph} = Sh_{nb} + Fh_{cv} \quad (2.77)$$

The heat transfer coefficients for the nucleate boiling and convection vaporization were given by Forster et Zuber (1955) (the coefficients have been determined for pool boiling for nucleate boiling regime) and Dittus et Boelter (1930) respectively.

$$\begin{cases} h_{nb} = 0.00122 \left(\frac{\lambda_l^{0.79} c_{pl}^{0.45} \rho_l^{0.49}}{\sigma^{0.5} \mu_l^{0.29} h_{lv}^{0.24} \rho_v^{0.24}} \right) [T_p - T_{sat}(P_l)]^{0.24} [P_{sat}(T_p) - P_l]^{0.75} \\ h_{cv} = 0.023 Re_l^{0.8} Pr_l^{0.4} \left(\frac{\lambda_l}{d_h} \right) \end{cases} \quad (2.78)$$

with λ_l , c_{pl} , ρ_l , ρ_v , σ , μ_l , h_{lv} , T and P that are given in SI unit.

The suppression and intensification factors are defined following :

$$\begin{cases} S = (1 + 2.53 \times 10^{-6} Re_{hom}^{1.17})^{-1} \\ F(X_{tt}) = 2.35 \left(\frac{1}{X_{tt}} + 0.213 \right)^{0.736} & \text{if } X_{tt}^{-1} > 0.1 \\ F(X_{tt}) = 1 & \text{if } X_{tt}^{-1} \leq 0.1 \end{cases} \quad (2.79)$$

X_{tt} is the Lockhart et Martinelli (1949) parameter, obtained when the liquid and vapor phases are considered in turbulent regime. Thus using the equations (2.46) and (2.34), it is possible to obtain :

$$X_{tt} = \left(\frac{1-x}{x} \right)^{0.9} \left(\frac{\rho_v}{\rho_l} \right)^{0.5} \left(\frac{\mu_l}{\mu_v} \right)^{0.1} \quad (2.80)$$

The Chen (1966) analysis was based on 395 experimental data points for vertical flows for various fluids (water, methanol, pentane, benzene, heptane, cyclo-hexane). This correlation take

more into account the physical mechanism that occurred during the convective boiling than the other superposition correlations. It is possible to point out that this correlation did not give good results for refrigerants. Zhang *et al.* (2004) have studied 13 different databases and compared the most often used correlations for the prediction of the transfer coefficient for the conventional systems. According to the authors, this is the Chen (1966) correlation that allow for the obtaining of the best results. However for the micro-systems, the authors point out that the Reynolds number are generally lower than 3000, what match with transition or laminar flow. They specified that this value is no consistent with the original development of Chen (1966), particularly for the determination of the intensification factor of convective component. Thus the authors defined F as :

$$F = 0.64 \left(1 + \frac{20}{X_{tt}} + \frac{1}{X_{tt}^2} \right)^{0.5} \quad (2.81)$$

Zhang *et al.* (2004) made the assumption that nucleate boiling took place in channel of small dimensions and they said that the suppression factor follow the same expression compared to the one given in (2.79). They kept the heat transfer coefficient expression [equation (2.78)] that have been defined for nucleate contribution.

☞ *Gungor et Winterton (1986) correlation*

Gungor et Winterton (1986) used the same approach compared to Chen (1966) for defining their correlation. The authors used 4202 experimental data points for saturated boiling condition and 946 for subcooled boiling for numerous fluids (HCFC22, CFC11, CFC12, CFC113, CFC114, water, ethylene glycol, n-butanol and ethanol), for upward or downward flow inside horizontal or vertical tubes. Their correlation can be written as :

$$h_{diph} = \left(1 + 3000Bo^{0.86} + 1.12 \left(\frac{x}{1-x} \right)^{0.75} \left(\frac{\rho_l}{\rho_v} \right)^{0.41} \right) h_{cv} \quad (2.82)$$

with Bo that is the boiling number.

b) Asymptotic model

☞ *Liu et Winterton (1990) correlation*

Liu et Winterton (1990) used an asymptotic model of second order for correlating the heat transfer coefficient evolution. Their correlation was based on 5193 experimental data points (whose 991 for subcooled conditions), that came from 30 different databases for numerous

Chapitre 2. Literature review on the boiling in mini-channels

fluids (water, alcohols, CFC11, CFC12, HCFC22, CFC113, CFC114). This correlation can be written as :

$$h_{diph} = \left[(Sh_{nb})^2 + (Fh_{cv})^2 \right]^{\frac{1}{2}} \quad (2.83)$$

The heat transfer coefficient were defined following :

$$\begin{cases} h_{nb} = 55P_r^{0.12-0.2\log(R_p)}(-\log(P_r))^{-0.55}M^{-0.5} \times (q'')^{2/3} \\ h_{cv} = 0.023Re_l^{0.8}Pr_l^{0.4} \left(\frac{\lambda_l}{d_h} \right) \end{cases} \quad (2.84)$$

P_r is the reduced pressure, R_p (μm) is the mean height of the wall roughness, M ($g.mol^{-1}$) the fluid molar mass and q'' ($W.m^{-2}$) the heat flux. The suppression and intensification factors were defined as :

$$\begin{cases} S = (1 + 0.055F^{0.1}Re_l^{0.16})^{-1} \\ F = \left[1 + xPr_l \left(\frac{\rho_l}{\rho_v} - 1 \right) \right]^{0.35} \end{cases} \quad (2.85)$$

c) Intensification model

Shah (1976) correlation

For vertical or horizontal saturated flows, Shah (1976) proposed a correlation for the determination of the heat transfer coefficients that were determined from the analysis of 780 experimental data points that come from 19 different experimental databases. The fluids that have been used for the development of this analysis took in account : CFC11, CFC12, HCFC22, CFC113, water and cyclohexane. The author proposed the following relation :

$$h_{diph} = h_l \times \max(\psi_{cv}, \psi_{nb}) \text{ or } h_{diph} = h_l \times \max(\psi_{cv}, \psi_{bs}) \quad (2.86)$$

ψ_{nb} , ψ_{cv} , ψ_{bs} , are, the intensification factors for the purely nucleate boiling regimes, convective evaporation and boiling with nucleation suppression. These three factors were dependent on the convection (Co), boiling (Bo) and Froude of liquid phase (Fr_l) numbers, defined as :

$$\begin{cases} Co = \left(\frac{1-x}{x} \right)^{0.8} \left(\frac{\rho_v}{\rho_l} \right)^{0.5} \\ Bo = \frac{q''}{Gh_{lv}} \\ Fr_l = \frac{G^2}{\rho_l^2 g d_h} \end{cases} \quad (2.87)$$

Section 2.5. Prediction of the heat transfer coefficients evolution

The values of the intensification factors are given following :

$$\psi_{cv} = 1.8N_s^{-0.8} \quad (2.88)$$

N_s is a parameter that has been defined by Shah (1976) which depends on the Froude number and is calculated for horizontal or vertical flows as :

$$N_s = Co \quad \text{for } Fr_l \geq 0.04 \quad (2.89a)$$

$$N_s = 0.38Fr_l^{-0.3}Co \quad \text{for } Fr_l < 0.04 \quad (2.89b)$$

Pour $N_s > 1$:

$$\psi_{nb} = 1 + 46Bo^{0.5} \quad \text{for } Bo < 0.0003 \quad (2.90a)$$

$$\psi_{nb} = 230Bo^{0.5} \quad \text{for } Bo > 0.0003 \quad (2.90b)$$

Pour $N_s \leq 1$:

$$\psi_{bs} = F_sBo^{0.5} \exp(2.74Co^{-0.1}) \quad \text{for } 0.1 < N_s \leq 1 \quad (2.91a)$$

$$\psi_{bs} = F_sBo^{0.5} \exp(2.47Co^{-0.15}) \quad \text{for } N_s \leq 0.1 \quad (2.91b)$$

F_s is a parameter that is boiling number dependent :

$$F_s = 14.7 \quad \text{for } Bo \geq 11 \times 10^{-4} \quad (2.92a)$$

$$F_s = 15.4 \quad \text{for } Bo < 11 \times 10^{-4} \quad (2.92b)$$

☞ *Kandlikar et Balasubramanian (2003) correlation (adaptation to the mini-channels cases)*

Kandlikar et Balasubramanian (2003) have extended the Kandlikar (1990) correlation to the case of mini-channels, where the heat transfer coefficients for boiling flow were determined regarding the dominant mechanism between the nucleate boiling and the convective evaporation. Kandlikar (1990) based its analysis on 5246 experimental data points that are coming from 24 independent databases. A general form of this correlation can be written as :

$$h_{diph} = \max(h_{nb}, h_{cv}) \quad (2.93)$$

The parameters h_{nb} and h_{cv} were obtained following :

$$h_{nb} = 0.6683 \left(\frac{\rho_l}{\rho_v} \right)^{0.1} x^{0.16} (1-x)^{0.64} f(Fr_l) h_l + 1058Bo^{0.7} F_k (1-x)^{0.8} h_l \quad (2.94a)$$

$$h_{cv} = 1.1360 \left(\frac{\rho_l}{\rho_v} \right)^{0.45} x^{0.72} (1-x)^{0.08} f(Fr_l) h_l + 667.2 Bo^{0.7} F_k (1-x)^{0.8} h_l \quad (2.94b)$$

$f(Fr_l)$ and Bo are, a function that depends on the Froude and the boiling numbers respectively. These parameters have been defined in equation (2.87). F_k is a parameter that is dependent on the couple fluid/wall that give an estimation of the surface effects on the heat transfer rate³⁸. h_l is the heat exchange coefficient calculated using single-phase flow condition for all the duct.

Kandlikar et Balasubramanian (2003) modified the estimation of the h_l value by specifying that for channels of small dimensions, the turbulent flow regime is not often reached ($Re < 3000$). This situation make the use of the Gnielinski (1976) or the Petukhov et Popov (1963) correlations not adapted. They proposed to replace them by the laminar correlation for the thermal aspect. In addition, the use of the Froude number for channels of small dimension is not relevant and the authors proposed to set $f(Fr_l) = 1$. For the flows for which the Reynolds numbers are lower to 1600, h_l is calculated thanks to equations (1.14) and (2.95) :

$$h_l = \frac{Nu \lambda_l}{d_h} \quad (2.95)$$

For transition flows ($1600 < Re < 3000$), it is necessary to realize an interpolation between the correlations used for fully developed regime (thermal point of view) and the transition regime correlations. Finally, when $Re < 100$, the authors have recommended to use the equation (2.94a) only.

Kandlikar et Balasubramanian (2003) gave some values of the F_k parameter for specific fluids. They are reported in Table 2.15 :

Fluide	Water	R11	R12	R22	R134a	Nitrogen
F_k	1	1.3	1.5	2.2	1.63	4.7

TABLE 2.15 – F_k values according to Kandlikar et Balasubramanian (2003)

When F_k is unknown the authors advised to use the pre-factor defined in the Forster et Zuber (1955) correlation defined for pool boiling conditions.

✓ *Representation of the correlation that predict the heat transfer evolution*

The evolution of the whole set of correlation have been given on Figure 2.32.

38. This number can be estimated using the Forster et Zuber (1955) correlation that has been defined in equation (2.78) for pool boiling experiments

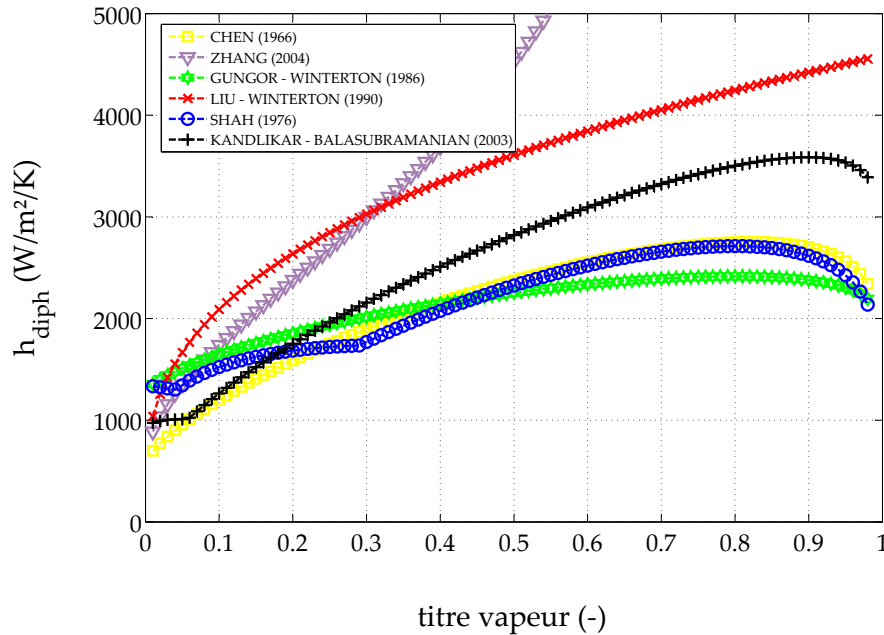


FIGURE 2.32 – Heat transfer variation regarding the thermodynamic vapor quality for a duct having a hydraulic diameter of 1.4 mm , a mass velocity of $100\text{ kg}\cdot\text{m}^{-2}\cdot\text{s}^{-1}$ and a heat flux of $4800\text{ W}\cdot\text{m}^{-2}$. The working fluid is Forane 365 HX at a saturation pressure of 70 kPa

In a general point of view, the correlations predicted a global increase of the heat transfer coefficient when compared to the Dittus et Boelter (1930) correlation, that has been obtained for a single-phase liquid flow. The correlations of Chen (1966) and Gungor et Winterton (1986) have variations that are qualitatively similar with a progressive increase of the heat transfer coefficients followed by a decrease of its values for thermodynamic vapor qualities close to 1. When referring to the analysis that have been made for macro-scale flows, this behavior is characteristic of the convective evaporation mechanism. The decrease of the heat transfer coefficients for high thermodynamic vapor quality is related to the dryout that may occurred inside the flow. Contrary to these evolutions the correlation of Liu et Winterton (1990) predicted an increase of the heat transfer coefficients for the whole range of thermodynamic vapor quality. This behavior is in agreement with the Zhang *et al.* (2004) correlation that predict an increase of this coefficient. These results may seemed surprising regarding the flow physics and are related to the mathematical construction of these correlations (amplification (F) parameter of the Zhang *et al.* (2004) and Liu et Winterton (1990) correlations). The correlations of Shah et London (1978) and Kandlikar et Balasubramanian (2003) highlighted, the influence of the nucleate boiling and of the convective boiling on the heat transfer rate³⁹. For low thermodynamic

39. The Shah et London (1978) correlation take into account an intermittent mechanism which considered the simultaneous impact of the nucleate boiling and the convective boiling

Chapitre 2. Literature review on the boiling in mini-channels

vapor qualities, the heat transfer coefficients evolved slowly with vapor quality, then increased for the moderate to high vapor quality and finally decrease for vapor qualities close to 1. These two last correlations seemed to better take into account the physical phenomena that occurred during the convective boiling.

➤ Impact of the duct hydraulic diameter

As showed in Figure 2.33, the whole set of correlation predict an increase of the heat transfer coefficients when the hydraulic diameter of the duct is reduced.

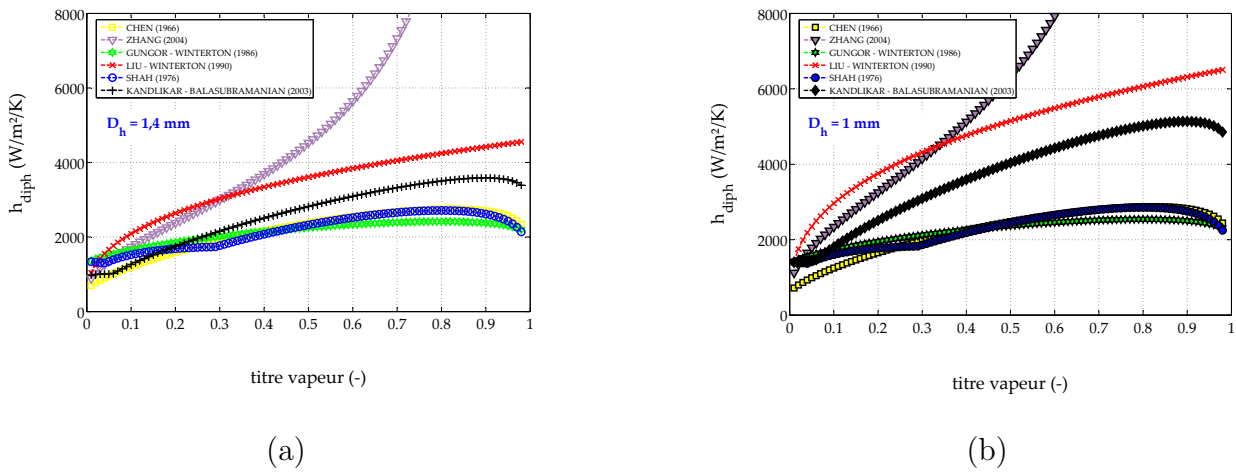
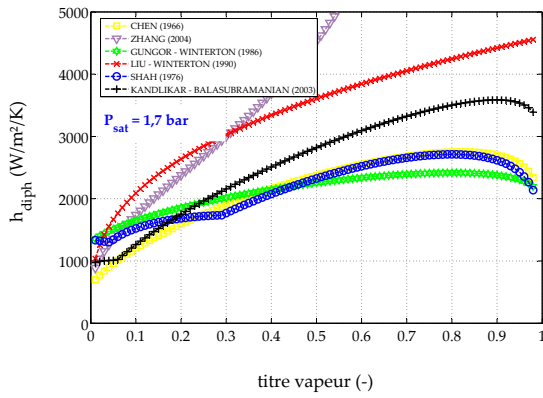


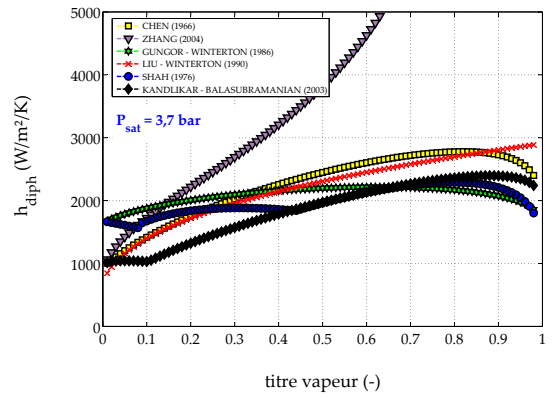
FIGURE 2.33 – Representation of the correlation for the evolution of the heat transfer coefficients for Forane 365 HX that flowed at a mass velocity of $100 \text{ kg m}^{-2} \text{ s}^{-1}$, a heat flux of 4800 W.m^{-2} , a saturation pressure of 70 kPa in a duct of : (a) 1.4 mm (b) 1 mm

It could be relevant to study the impact of other parameters. Thus, using the data from Figure 2.34, the impact of the saturation pressure, mass flow and heat flux on the heat transfer coefficients will be analyzed.

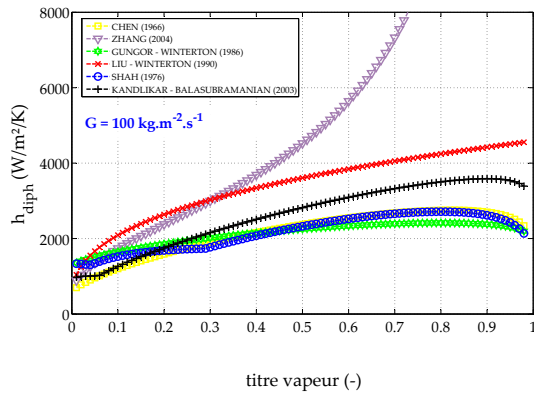
Section 2.5. Prediction of the heat transfer coefficients evolution



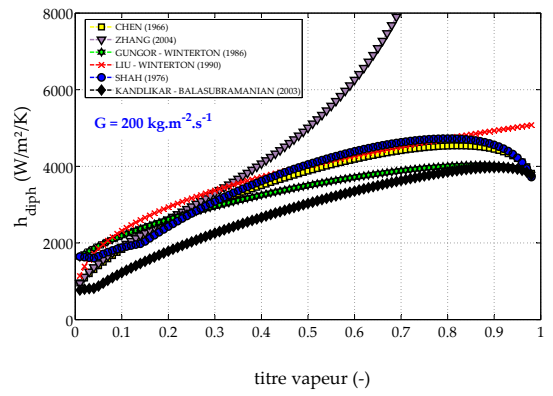
I - (a)



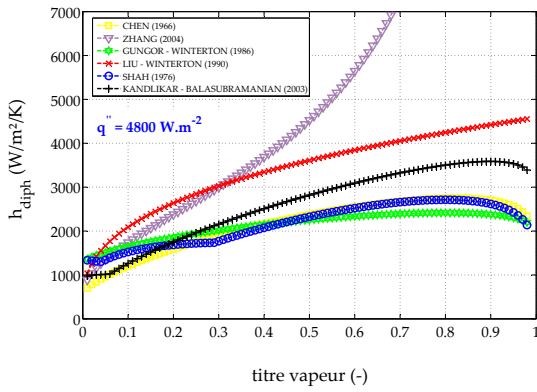
I - (b)



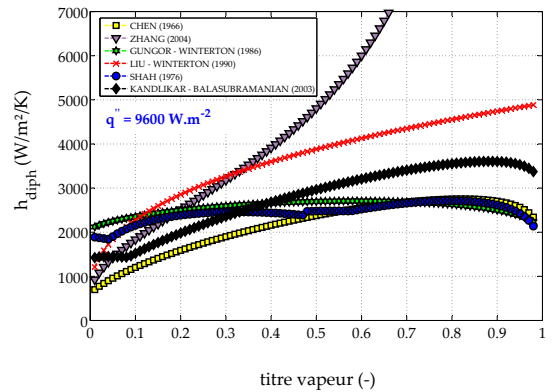
II - (a)



II - (b)



III - (a)



III - (b)

FIGURE 2.34 – Correlation predictions for the determination of the heat transfer coefficients for Forane 365 HX : **I** - that flow in a duct of 1.4 mm , a mass velocity of $100\text{ kg m}^{-2}\text{ s}^{-1}$, a heat flux of 4800 W.m^{-2} and a saturation pressure of : (a) 70 kPa (b) 370 kPa , **II** - that flow in a duct of 1.4 mm , at a saturation pressure of 70 kPa , a heat flux of 4800 W.m^{-2} and a mass velocity of : (a) $100\text{ kg m}^{-2}\text{ s}^{-1}$ (b) $200\text{ kg m}^{-2}\text{ s}^{-1}$, **III** - that flow in a duct of 1.4 mm , a mass velocity of $100\text{ kg m}^{-2}\text{ s}^{-1}$, a saturation pressure of 70 kPa and a heat flux of : (a) 4800 W.m^{-2} (b) 9600 W.m^{-2}

➤ Impact of the saturation pressure

The results that have been given in Figure 2.34 showed surprisingly the only two correlations (Gungor et Winterton (1986) and Chen (1966)) predicted an increase of the heat transfer rate with the increase of the saturation pressure. This intensification behavior is in agreement with the experimental data that have been reported in § 2.3.3 where the heat transfer coefficient increase with the working pressure. It is consequently surprising that numerous correlations predicted a decrease of the heat transfer with the pressure.

➤ Impact of the mass flow

The whole set of correlations predict an increase of the heat transfer coefficient when the mass flow is increased, except for the Kandlikar et Balasubramanian (2003) correlation which predict a decrease for small thermodynamic vapor quality.

➤ Heat flux impact

The increase of the heat transfer rate from the wall lead generally to an increase of the heat transfer coefficient. It is possible to note that the impact of this operating condition is strong for low to moderate thermodynamic vapor qualities and weaker for higher vapor quality for the Kandlikar et Balasubramanian (2003) and Shah et London (1978) prediction. This behavior supposed that the model considered that the heat flux did not play a role on the flow that take place at low thermodynamic vapor qualities (\rightarrow nucleate boiling regime). It should be highlighted that the Chen (1966) correlation, did not evolved much when the heat flux is modified.

2.6 Chapter 2 conclusions

The data that have been presented in this chapter showed that the evolution of the internal convective boiling phenomena depends on a large number of parameters. It was noticed that the operating conditions were the most often studied parameters for the analysis of the variations of the pressure drops and heat transfer coefficients. Indeed, every modification of these operating conditions can allow for the intensification (or degradation) of these associated pressure drops or heat transfer coefficients. The example of the saturation pressure showed that when its value is increased, this lead generally to the intensification of the heat transfer rate and to the reduction of the pressure drop for experiments. These operating conditions may influenced the convective boiling, from its onset up to the dryout occurrence. The knowledge of the wall heat transfer rate allowing for the onset of nucleate boiling (ONB) is very important for sizing the cooling system. It is also very key to determine the conditions for reaching the critical heat flux (CHF) condition in order to avoid the deterioration of the heat exchanger.

It can be point out that apart from the operating conditions, the fluid wetting properties with the wall may impact the evolution of the conditions that lead to ONB or CHF also.

Nowadays, very few studies have been focused on the specific influence of the duct geometry (particularly when the cross section are different to the circular ones), on the evolution of the pressure drops or the heat transfer coefficients. Yen *et al.* (2006) showed that changing the cross section of a mini-channel from a circular one to a rectangular one for similar hydraulic diameter ($\approx 210\mu m$) can modify significantly the evolution of the heat transfer rate for a convective boiling flow. For the mini-channels, the pair of geometrical parameters that seemed to be key is the aspect ratio and the hydraulic diameter. Indeed, if the bubble detachment diameter is larger than the mini-channel width or its height, this bubble will be confined only in one direction, but would be able to move more or less freely in the other one what should alleviate the confinement. One can note that Agostini (2002) affirmed that the hydraulic diameter would not allow for the characterization of the confinement for mini-channels by itself. The author proposed in his study to use the smaller dimension of the mini-channel for characterizing the possible confinement during boiling.

This literature survey allow for the affirmation that many efforts were made to better understand the convective boiling phenomena in mini-channel. However, the impact of the geometrical parameters, and in particular for the case of rectangular mini-channels, have not been studied much. Thus, in the context of this experimental study, it has been decided to pay attention particularly to the impacts of the aspect ratio and of the hydraulic diameter on the evolution of the pressure drops and heat transfer rates for convective boiling situations. A visualization system, that have been defined during this thesis work allowed for the study of the flow regime transition regarding the mass flow and heat flux conditions. All of the elements that help us to define the experimental setup and the fluid selection will be presented in **Chapter 3**.

Deuxième partie

EXPERIMENTAL TECHNIQUES

Description of the experimental approach

3.1	Goal of the study and experimental approach	105
3.2	Working fluid selection	106
3.3	Preliminary cautions for studying a boiling flow	111
3.4	Working fluid selection	111
3.4.1	General description of the fluid	112
3.4.2	Thermophysical properties of Forane 365 HX	112
3.5	Chapter 3 conclusions	115

Summary :

THE data that have been given during the state of the art study have demonstrated that the physical phenomena that took place for internal flows in boiling conditions are not well understood when the geometrical dimensions are reduced. The impact of the geometrical parameter on the evolution of the heat transfer and friction coefficients have been studied in **Part III** of this manuscript. The aim of this chapter is to present the steps that lead our work during the experimental set-up montage. The different modifications of the test sections, that are related to the working fluid selection, the geometrical mini-channels dimensions selection, up to the test section instrumentation are presented in this chapter.

3.1 Goal of the study and experimental approach

The state of the art review (Chapter 2) showed that during the forced convective boiling, numerous parameters can allow for the improvement of the thermal system performances. Generally, the scale reduction should lead to the increase of the amplitude of the heat transfer rate and to a higher thermal efficiency (better mixing due to the smaller diffusion distances, the increase of the heating due to the reduction of the volume/surface ratio regarding the single phase condition) according to the state of the art review. However, for internal forced boiling conditions, numerous characteristics have to be specified, whose the conditions leading to ONB and to CHF. These to last conditions allow for the definition of all the range of effective working of a heat exchanger in boiling condition. Still nowadays, and after our review, it is particularly difficult to evaluate the impact of the geometrical parameters only¹ on the hydrodynamic or thermal behaviors, for an internal boiling flow.

The goals of this experimental study are to answer the following questions :

- ▷ Is the needed heat flux that lead to ONB has the same value for different mini-channel geometry ?
- ▷ Are the conditions that led to CHF are impacted by the geometrical parameters ?
- ▷ Are the pressure drops variations have same profile for channel of same hydraulic diameter but of different cross section (or aspect ratio) ?
- ▷ Are the related heat transfer coefficients the same for channel of same hydraulic diameter but different cross section (or aspect ratio) ?
- ▷ Is a geometrical reference parameter can be defined for boiling conditions in mini-channels ?

For fully describe the heat transfer rate and the pressure drops variations for a boiling flow conditions, it is necessary to determine the evolution of specific physical measurements that are : flow rate, pressure, wall and fluid temperatures, void fraction and local heat flux distribution inside the mini-channel. The measurements of all these parameters are difficult in an experimental point of view. Taking into account this fact, it has been decided to do choices (that will be detailed in **Chapter 4**) in order to realize this experimental study.

Our approach has consisted in the measurement of some of these experimental values and to the assessment of the others² in order to determine the pressure drops and the heat transfer coefficients. An interesting point of this study is related to the simultaneous measurements coupled with flow regime visualizations. This allow for the better understanding of the evolution

1. In particular when the geometry gets further compared to circular cross section, where less data point exist

2. As for example the void fraction variation with the thermodynamic vapor quality.

of the pressure drop values and of the heat transfer mechanisms related to internal convective boiling.

3.2 Working fluid selection

The methodology for working fluid selection has been based on the possibility to use it for boiling conditions respecting some specifications for the targeted application. Indeed, the constraints related to the use of a refrigerant for the fuel cell cooling have been detailed in the following paragraphs :

① Respect of the environmental regulations

Today, for the selection of a fluid in the context of an industrial application, some indicators have been defined for evaluating the fluid impact in the case where it will be released to atmosphere. Thus, regarding the current and future regulations, it is necessary to check that the fluid does not contribute to ozone depletion [Ozone Depletion Potential (ODP)] and that it does contribute very weakly (or not at all) to global warming [Global Warming Potential (GWP)].

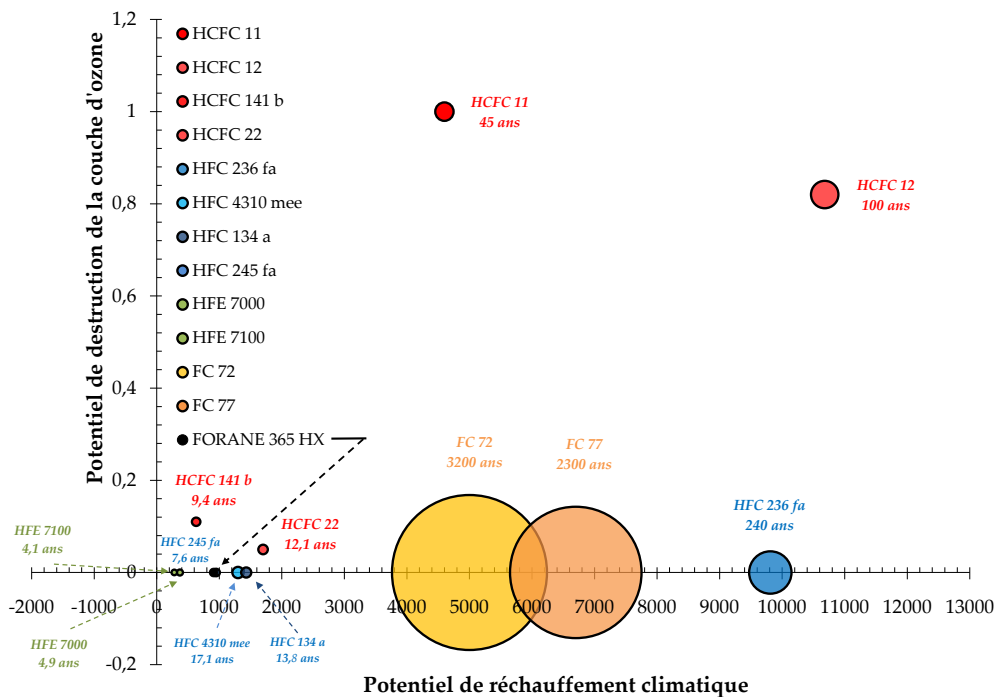


FIGURE 3.1 – ODP, GWP and lifetime of selected refrigerant in atmosphere

These two last indicator were considered as very important since the Montreal (1987) (**goal** : stop ozone depletion) and Kyoto (1997) (**goal** : reduction of the emission of global warming

gases) protocols. Moreover, the lifetime of a chemical component in atmosphere is an important parameter to consider to quantify more truly its impact. Some ODP, GWP and refrigerants lifetimes are give in Figure 3.1³.

② **Safety and easiness of use**

For the targeted application, it is necessary that the fluid fulfill conditions of use. Thus the fluid must be non flammable, non explosive⁴, with low (or no) toxicity for human being and environment and finally compatible with a large range of materials.

③ **Dielectric fluid**

One can note that the whole set of fluid has the capacity to be more or less polarized when subjected to an electrical field around them. This polarization can produce current leakage in the refrigerant when this fluid is used in a fuel cell for example.

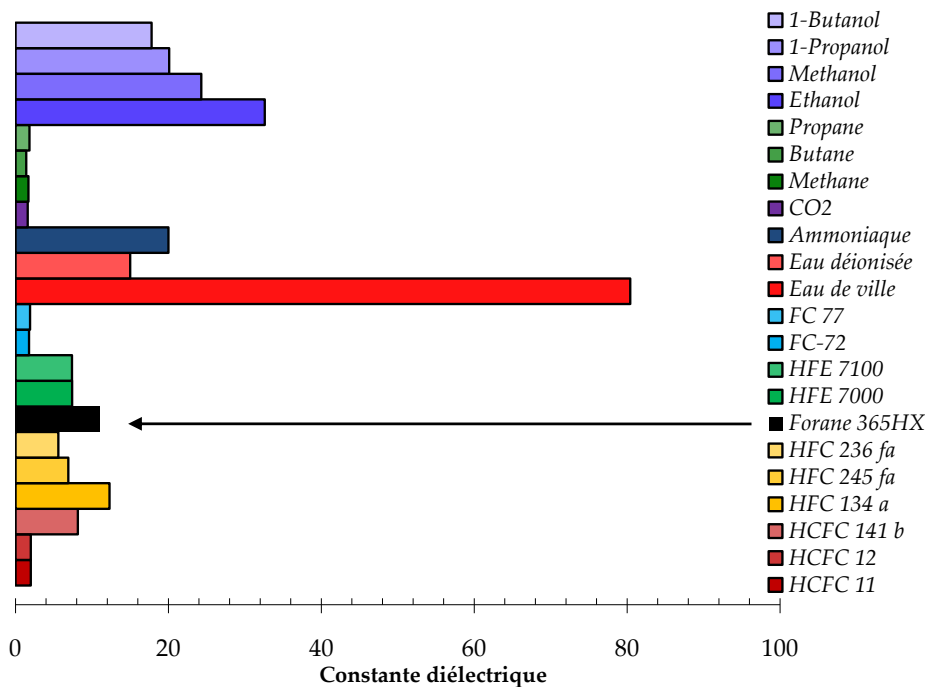


FIGURE 3.2 – Dielectric constant values for a selection of fluids

The aptitude of the fluid to be polarized can be expressed using the dielectric constant value

3. One can note that for natural fluids (Hydrocarbons, Water, Ammonia, CO₂) ODP and GWP values are generally very low. These characteristics show the interest of using them, instead of the difficulties that can be generated by the use of some of them.

4. This characteristic applied particularly to fluids that must work under pressure for being used in liquid phase

(κ). This constant represent the ratio between the fluid capacity to transport an AC current compare to the vacuum capacity to drive the same current. This constant can be expressed as :

$$\kappa = \frac{\epsilon}{\epsilon_0} \quad (3.1)$$

It should be underline that the electrical conduction generally increase with the dielectric constant. As a consequence it is necessary to find a fluid whose dielectric properties are low for avoiding the fuel cell current leakage. Some values of dielectric constants for sereval fluid are given in Figure 3.2.

④ **Antifreeze properties**

The fluid antifreeze properties are particularly important when considering fuel cell usage. This properties make water not so well adapted as a coolant⁵, despite its very good thermophysical properties. Indeed, for the working of the fuel cell in « extreme » conditions (temperature lower to 0°C) a fluid whose crystallization point is much lower is usually looked for.

⑤ **Boiling point ranged between 60 - 90°C**

During its assembly, the fuel cell is generally tightly attached at high pressures (usually the maximal pressure is around 4 bar) in order to ensure the correct working conditions of the membrane/electrode assembly (*MEA*). Moreover, in order to increase the electro-chemical Nerst potential reaction, the gases entrance (air, hydrogen) may occur under pressure. The use of the refrigerant (subjected to a pressure higher than atmospheric pressure) could be imagined as soon as these pressures are not above the assembly constraints⁶. In this context, the fluid may be used for thermodynamic compression vapor cycles for increasing the efficiency of the heat transfer rate. As a consequence, it is essential to know the working temperature variation regarding the related pressure.

5. Generally, the adding of additives which are mixed with water as for example ethylene glycol, glycerol etc... allow for the decrease of the crystallization temperature. However these products are very often criticized for their toxicity regarding environment. In addition, the additives are usually composed of one or several hydroxylic groups that lead to the increase of the dielectric constant (for ethylene glycol and glycol this constant reach a value above to 35)

6. A schematic that showed the location of the cooling system is given in Chapter 7

For illustrating this aspect, the saturated temperatures variations with respect to the saturated pressures for several fluids which have been very often cited in the literature have been given on Figure 3.3. It can be noted that during the fuel cell working water is produced and its management is still complex. Indeed, for ensuring the correct working of these fuel cells, it is necessary to make them work for temperatures ranged between 60°C and 90°C for ensuring at the same time sufficient membrane humidity, that allow for their working, and avoid the membrane dryout (which would lead to the rapid reduction of the reaction performances). This last point impede the working conditions above 100°C (if Nafion[®] is used as proton membrane exchange).

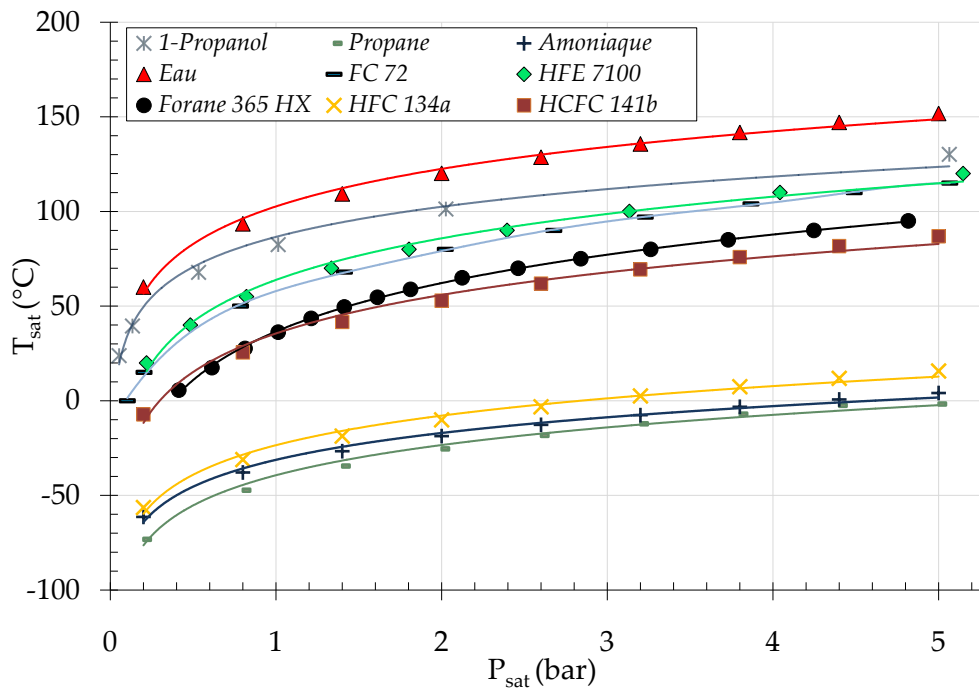


FIGURE 3.3 – Evolution of the saturated temperature with the working pressure

⑥ High latent heat

This is a very important point when choosing a working fluid. This thermophysical property expresses the energy quantity that should be brought for changing one kilogram of fluid into vapor. Therefore, for high latent heat, the heat transfer rate will be better during the phase change for a similar evaporation rate.

⑦ **High specific heat and high thermal conductivity**

The specific heat expresses the fluid capacity to store thermal energy and its thermal conductivity its capacity to conduct it. It is important that the values of this couple be the highest possible for allowing an efficient heat transfer rate, particularly in the subcooled zones⁷.

⑧ **Balance between the viscosities and the mass densities**

This set of thermophysical properties is important for the characterization of the pressure drops of a two-phase flow. For a single-phase flow the reduction of the liquid viscosity generally allow for the reduction of the pressure drops for an internal flow. In the two-phase flow case, it may be useful to study the couple vapor viscosity / vapor mass density and liquid viscosity / liquid mass density. Indeed, the knowledge of the these terms is needed for the evaluation of the flow regimes which are developed through the duct and that lead the pressure drops. The results given by Revellin et Thome (2006) and Jassim et Newell (2006) showed that when the superficial vapor velocity is lower, the two-phase pressure drop is smaller also.

In Table 3.1 some values of thermophysical properties for several fluids at a saturation temperature of 85°C have been reported.

Fluid	P_{sat}	T_{fus}	ρ_l	ρ_v	h_{lv}	c_{pl}	c_{pv}	μ_l	μ_v	λ_l	λ_v
Unit	bar	°C	kg/m ³	kg/m ³	kJ/kg	kJ/kg.K	kJ/kg.K	μkg/m.s	μkg/m.s	mW/m.K	mW/m.K
C3H7OH	0.93	-126.2	740	2	715	3.2	1.6	450	9.5	143	20
C3H8	34.3	-187.7	354	98.7	133.4	5.4	5.7	44.2	12.9	68.3	38.6
NH3	46.1	-77.6	495	38.4	800.5	6	5.7	74.2	12.2	324.1	40
H2O	0.57	0	969	0.35	2282	4.2	2	333.3	11.7	672.8	23.5
FC-72	2.3	-90	1518	N/A	75.6	1.14	N/A	210	N/A	50.6	N/A
HFE-7100	2.1	-135	1364	19.4	103	1.3	N/A	307	12.2	56.5	N/A
F365 HX	3.7	< -35	1084	22.9	148.5	1.5	1.1	245	11.4	86	15.6
HFC-134a	29.3	-101	838	217	82.5	2.3	2.4	81.3	16.7	54.8	26.2
HCFC-141b	4.7	-103.5	1109	21	191.6	1.25	0.93	219.3	11.1	74.9	14.7

TABLE 3.1 – Thermophysical properties of some fluid for a saturation temperature of 85°C

7. One can note that for saturated boiling conditions, the contribution of the latent heat is more significant than the contribution related to the specific heat during the heat transfer

3.3 Preliminary cautions for studying a boiling flow

The analysis that has been done during the state of the art review showed that the conditions for the usage of a working fluid, must be considered with caution. Indeed, according to the literature, the repeatability of a result in boiling conditions seemed to be related to the ability of the fluid to stay stable in a chemical point of view. This is for this reason that pure fluid are generally used in industrial applications in comparison to mixed fluid, which can be zeotropic. Indeed, for the zeotropic mixing, the component that constitute the mixing have different evaporative properties. Thus the most volatile component evaporates more easily and in case of lost, the mixed thermophysical properties evolved toward the less volatile fluid characteristics.

Besides, one can note that a large part of fluids is more or less sensitive to dissolved gases. In this context, Steinke et Kandlikar (2004) have experimentally demonstrated, that dissolved oxygen in water can impact significantly the conditions leading to onset of nucleate boiling. The results of these authors allow for the demonstration that above a threshold dissolved gases concentration ($> 5.4 \text{ ppm}^8$), the onset of nucleate boiling may took place for temperature that can be 10°C lower compare to normal saturated conditions⁹. In addition, Li *et al.* (2004) have showed in a numerical study that the impact of dissolved gases may lead to the reduction of onset of nucleate boiling by almost 35°C . However, it can be underlined that You *et al.* (1995) which used *FC-72* as working fluid, for pool boiling conditions, have obtained less alarmist results. Indeed, these authors have demonstrated that the dissolved gases concentration influenced the boiling phenomena, only when it was relatively high ($> 427 \text{ ppm}$). As a consequence, it seemed that the working fluid selection and corollary its capacity to capture dissolved gases may be significant on boiling characteristics. Thus, in the absence of data regarding the dissolved gases concentration for the selected fluid, an experimental technique has been built (§ 4.1.2) for allowing the limitation of the dissolved gases concentration influence in boiling conditions during our study.

3.4 Working fluid selection

In a first step, water has been chosen (because its thermophysical properties are well known) in order to validate the experimental set-up for single phase flow conditions. Then for the convective boiling conditions, it was necessary to select another fluid according to the specifications which have been given in § 3.2. In the following paragraphs, some of the points that have led to the working fluid selection will be detailed .

8. part per million

9. For water $T_{sat} \approx 100^\circ\text{C}$ at P_{atm}

3.4.1 General description of the fluid

Forane 365 HX (fabricated by Arkema) has been selected for this study. This fluid is recommended for the replacement of R141b. According to the supplier, its main applications are related to the particle removal, to drying, to rinsing and to the heat transfer. Forane 365 HX is the result of the mixing of HFC 365mfc¹⁰ ($C_4H_5F_5 \geq 75\%$) and HFC 4310mee ($C_5H_2F_{10} < 25\%$) that make an azeotropic mixture (\rightarrow that stay stable along the time). One of the main objective of this combination is to make the fluid non-flammable. In addition, Forane 365 HX does not have flash point, is non-explosive and has low toxicity for human being. The vapor gases that are released by this fluid are non-irritant for skin or eyes. Arkema recommend a mean exposure value of 500 ppm. Elements related to the resistance of metals, elastomers and plastics can be found in Appendices A.

3.4.2 Thermophysical properties of Forane 365 HX

The work that has been done during the state of the art review allow for the selection of about thirty fluids that have been used in boiling conditions for ducts of small dimensions. The variation of these fluids' thermophysical properties with working pressure have been analyzed with caution for making our selection. For the considered applications, the system working pressure must be comprised between the atmospheric pressure and a pressure of 4 bar (relative pressure) as it has been discussed in § 3.2. On Table A.1, the thermophysical properties of Forane 365 HX for a relative pressure 0.7 bar has been reported.

Fluide	T_{sat}	ρ_l	ρ_v	h_{lv}	c_{pl}	c_{pv}	μ_l	μ_v	λ_l	λ_v	Pr_l	Pr_v	σ
Unités	$^{\circ}C$	kg/m^3	kg/m^3	kJ/kg	$kJ/kg.K$	$kJ/kg.K$	$\mu kg/m.s$	$\mu kg/m.s$	$mW/m.K$	$mW/m.K$	S.U	S.U	mN/m
F365 HX	55	1160	10.2	160.8	1.42	1.01	416.5	10.1	94	13.1	6.3	0.78	11.5

TABLE 3.2 – Thermophysical properties of Forane 365 HX at 170 kPa

One can notice that the values of specific heat at constant pressure and of viscosity have been obtained experimentally regarding the fluid temperature for single phase conditions. The technics and the measurements that have been used for obtaining these thermal properties will be reviewed in next sections. It can be highlighted that the supplier did not gave the melting temperature of this fluid. However, the melting temperature of HFC 4310mee is of $-35^{\circ}C$ and the one of HFC 365mfc is of $-80^{\circ}C$. Thus, during this work it has been assumed that the melting temperaute of the mixture was below $-35^{\circ}C$.

🔍 Specific heat measurement : $\mu DSC7$ description

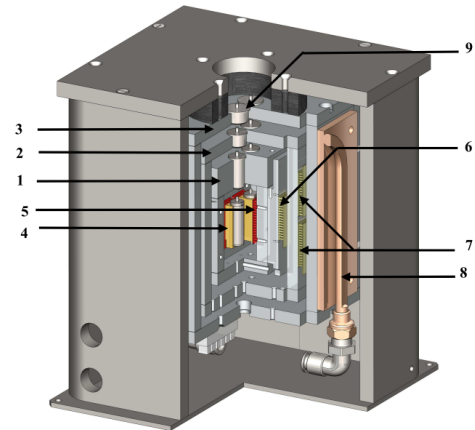
10. United State Environmental Protection Agency (USEPA) consider that this coumpound may be used as a refrigerant in the future - <http://www.epa.gov>

The whole set of measurements that is given here have been made in the « Centre Scientifique et Technique du Bâtiment (CSTB) » that is localized on the campus of the Grenoble University. During the experimental campaigns, Hébert Sallée and Colas Hasse (employees of CSTB) helped a lot for making these measurements possible. For obtaining the specific heat values, a calorimeter that is commercialized by SETARAM was used.

A picture of this equipment is reported on Figure 3.4a.



(a)



(b)

FIGURE 3.4 – (a) Micro-calorimeter localized at CSTB for the measurement of the liquid specific heat (b) Cross section view of the device

The calorimetric sensor internal walls are made in aluminum (1,2,3) and the montage allowed for the insulation of the measuring cells regarding environment (indeed each walls are separated by air). The specific heat measurement is made according to a differential analysis. Indeed, two cells (made in Hastelloy C276¹¹) were inserted into the $\mu DSC7$. Each cells is surrounded by a plain fluxmeter (5), whose signal is regularly evaluated by the device. The electrical signal which is emitted by these fluxmeters is proportional to the heat transfer between the cell that contain the sample and the calorimetric block. In a first stage, a blank measurement is made between two empty cells for evaluation of the impact of the cells only on the measurement of the specific heat. Once this measure is made, the fluid was added to the measuring cell whereas the reference cell was kept empty. The calorimeter is thermally linked to the regulation enclosure that set the intermediate temperature of the calorimeter. Parts (6,7) that used Seebeck effect for heat dissipation are placed between the block and the enclosure. The whole system is regulated by

11. Material whose main properties are to withstand the high temperature and to be resistant to corrosion

Chapitre 3. Description of the experimental approach

a water flow (8) whose temperature is controlled and this flow is located on the external walls of the equipment. The liquid specific heat can be then evaluated using the following equation :

$$C_p = \frac{Q_{\mu DSC}}{\beta_c m} \quad (3.2)$$

where $Q_{\mu DSC}$ is the thermal power that enters or flows out from the sample (corrected by the curve of reference), β_c the heating ramp into the sample and m the sample mass.

All the measurements were made for heating and cooling situation, in a range of temperature comprised between 5 and 40°C, and have showed excellent repeatability.

☞ Liquid viscosity measurement using a capillary viscometer

The viscosity measurements were made using a viscometer for dilution series by SCHOTT. These measurements were made with Yannick Molmeret (From the « Laboratoire de Rhéologie ») and Denise Foscallo (From the « Laboratoire d'Électrochimie et de Physico-chimie des Matériaux et des Interfaces (LEPMI) »). On Figure 3.5, the schematic of the experimental device that was used is given.

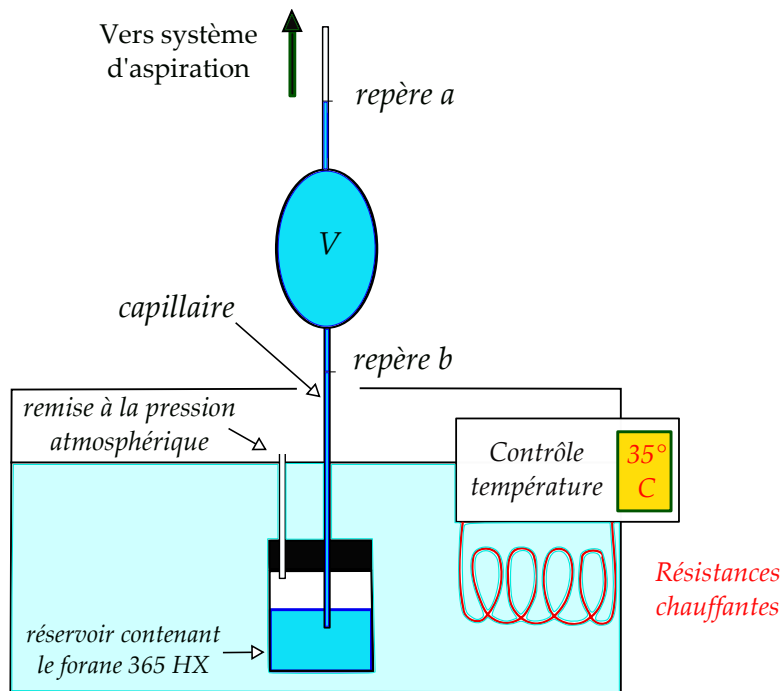


FIGURE 3.5 – Device that allow for the measurement of the viscosity of Forane 365 HX

The measuring principle is the following one :

The measuring sample is placed in a glass reservoir that has two opening whose one can be put at atmospheric pressure and the other one linked to a suction system that allow the Forane to enter. This reservoir was placed inside a thermal bath in order to control the sample temperature. This temperature was varied between $20^{\circ}C$ and $40^{\circ}C$ during the realized experiments. One can note that the capillary diameter selection is important because its allow for the guarantee of the measurement accuracy that is based on the fact to have a laminar flow. Indeed, for all the dynamic viscosities calculation, the assumption related to a Poiseuille flow were made. It can be highlighted that for the whole set of made experiments, the working fluid was considered as having a Newtonian behavior. Formerly to the experiments, the liquid sample was filtered through a mesh having a pore size of 0.4 mm .

As showed in Figure 3.5, the capillary consisted of a reservoir having a volume V . Once the Forane 365 HX filled this reservoir and reached a level slightly higher than the marker a , the liquid suction system was stopped. Then the system released the working fluid and as soon as the free surface of the Forane went below the marker a , a stopwatch was started. Indeed the fluid viscosity was related to the time during which its flow up to the marker b . Photoelectric diodes were placed on these markers for determining the passage of the liquid free surface. Thus, once this surface reached the marker b , the stopwatch was stopped in a automatic way. The law relating the dynamic viscosity and the time during which the liquid flow from marker a to marker b can be written as follow :

$$\mu = \frac{\pi R^4 g}{8V} \rho_l t = k \rho_l t \quad (3.3)$$

where R is the capillary radius, g the gravity acceleration, V the capillary reservoir volume, ρ_l the fluid mass density, t the characteristic time for the draining of the capillary and k a standardization constant that is related to the capillary that has been used (this value is given by the supplier). The whole set of tests that has been made showed a very good repeatability and allow for the validation of the realized experiments.

3.5 Chapter 3 conclusions

In this chapter, it was possible to state more precisely, the goal of this PhD thesis work. Thus, after the selection of the working fluid, it was possible to give the description of the experimental test section in which the experiments related to convective boiling measurements were made. This description will be given in Chapter 4

Experimental set-up description

4.1	Hydraulic test loop presentation	119
4.1.1	General description	119
4.1.2	Degassing system	121
4.1.3	Preheating method	124
4.1.4	Test section description	124
4.1.5	Mini-channels sizing	126
4.2	Data acquisition of the experimental measurements	127
4.3	Cameras acquisition system description	128
4.4	Presentation of the list of made experimental tests	130

Summary :

A TEST section has been built for studying the internal convection boiling phenomena in mini-channels of different dimensions. The originality of this work was mainly related to the possibility of analyzing several geometrical parameters on a same experimental device. The studied dimensions ($0.727\text{mm} < D_h < 1.4\text{mm}$) allow for the analysis of the confinement effect on convective boiling flows. A detailed description of the test section is then given as well as the geometrical characteristics of the studied mini-channels. The data acquisition system has been presented also in this chapter. The visualization techniques will be describe in a dedicated section.

4.1 Hydraulic test loop presentation

4.1.1 General description

For realizing convective boiling experiments, it was decided to improve the laboratory existing experimental set-up used for single phase flows. This experimental set-up was built during the work done by Gao *et al.* (2002). Bavière (2005) has then improved it during his PhD work and has studied liquid single phase flow in « micro-channels¹ » of different hydraulic diameters. Finally Gamrat (2007) has conducted complementary experiments and made a numerical study related to the impact of the wall roughness on the flow hydrodynamic and thermal behaviors.

« The reader may note that all these studies prior to this study were done for single-phase flow conditions. »

A general schematic of the hydraulic test loop allowing for the study of the convective boiling is given on Figure 4.1. This test loop consisted of two hydraulic loops that can work separately as closed loop. The EMC (« Ébullition en Mini/Micro Conduites ») loop allow for the study of the boiling in channels of small dimensions. The other hydraulic loop allow for the degassing of Forane 365 HX prior to the tests made in the EMC loop². It is possible to highlight that the visualization system was not represented on this schematic for clarity. The description of this system will be made in paragraph (§ 4.3).

1. At the moment of his study, the author has identified the channels whose hydraulic diameters were below 1 mm as micro-channels. However, it should be highlighted that for the realized experiments, Bavière (2005) showed that no flow modifications due to micro-effects were noticeable even at these scales

2. One can notice that the lengths of the lines that had been presented in Figure 4.1 did not correspond to a real distance between the different elements of the general loop

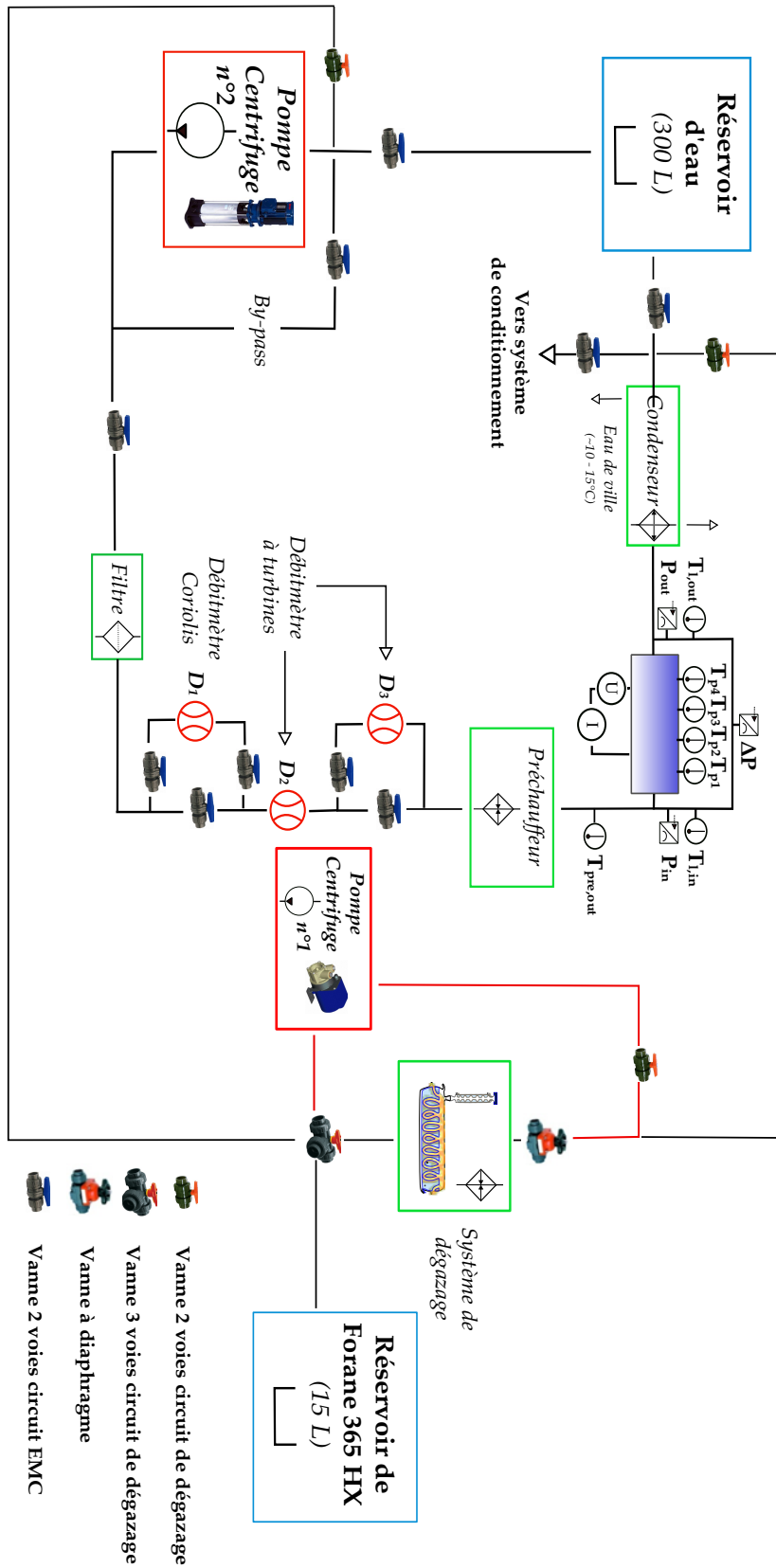


FIGURE 4.1 – Hydraulic test loop fabricated for studying Forane 365 HX convective boiling

The EMC test loop included :

- ▣ a centrifugal pump (Movichrom N CN 3/12, 10 *bars*, 20 $l.min^{-1}$),
- ▣ a particle filter (« Filtration SASU ») with a pore diameter of 5 μm , that was fabricated in stainless steel,
- ▣ three flowmeters (Kobold PEL L45, Kobold PEL LO1 and Bronkhorst LFM L2, full scales : 6 $l.m^{-1}$, 0.2 $l.m^{-1}$ and 0.017 $l.m^{-1}$ respectively),
- ▣ three absolute pressure sensors (two MBS 3000, 16 *bars*, and one Keller PR21S, 2 *bars*),
- ▣ two differential pressure sensors (inductive sensor HBDM PD1, 0.1*bar*) and one piezo-electric sensor (LEGI home-made, 0.7 *bar*),
- ▣ six type T thermocouples whose two were used for the fluid inlet or outlet temperature measurements (regarding the test sections) and four for the measurement of the wall temperature at 1 *mm* of the solid-liquid interface,
- ▣ ten two-way valves in PVC-U (Georges Fisher, 16 *bars*) for controlling the hydrodynamic conditions and the fluid flow in the EMC loop.

A degassing system was then fabricated for reducing the uncertainties related to the impact of the dissolved gases. This system is included in a new loop that will be presented in the following paragraph.

4.1.2 Degassing system

The state of the art review showed that the effect of the dissolved gases may be significant on the convective boiling phenomena. Thus, in order to better controlled this phenomenon, a degassing system that allow for the extraction of the confined in Forane 365 HX. It should be noted that for the single phase flow, the dissolved gases did not seemed to have any impact (Steinke et Kandlikar (2004)). In order to realize this degassing process, a specific test loop was made. It comprised the following elements :

- ▣ a centrifugal pump (Totton Pumps HPR6, 3 l/min),
- ▣ a reservoir of 15 L with a closing valve in EPDM (Safi Vannes, 16 *bars*),
- ▣ a cylindrical glass reservoir (degassing reservoir) comprising an internal coil (Dumas SA, $\approx 11 l$) and topped with a six-bulb condenser,
- ▣ a thermal bath (Julabo F25, $-25^{\circ}C$ at $200^{\circ}C$, 4.5 l),
- ▣ a diaphragm valve in PVC-U with a EPDM membrane (Georges Fisher, 16 *bars*) for controlling the system working pressure when the EMC test loop was used,

Chapitre 4. Experimental set-up description

- a three-way valve in PVC-U (Georges Fisher, 16 bars) for driving the fluid toward the degassing reservoir or toward the EMC loop,
- two two-way valves in PVC-U (Georges Fisher, 16 bars) for isolating either the degassing test loop or the EMC loop.

The whole description is given in a summarized manner on Figure 4.2. The experimental procedure for extracting the dissolved gases from Forane 365 HX follow the successive steps :

(a) Forane 365 HX was stored in the reservoir of 15 L then using the centrifugal pump *n*^o1 (Figure 4.1), it was sent to the cylindrical glass reservoir of 560 mm length, 160 mm of diameter with a glass thickness of 7 mm. This reservoir is topped with a six-bulb condenser where water flows in counterflow at a temperature ranged between 10 and 15°C.

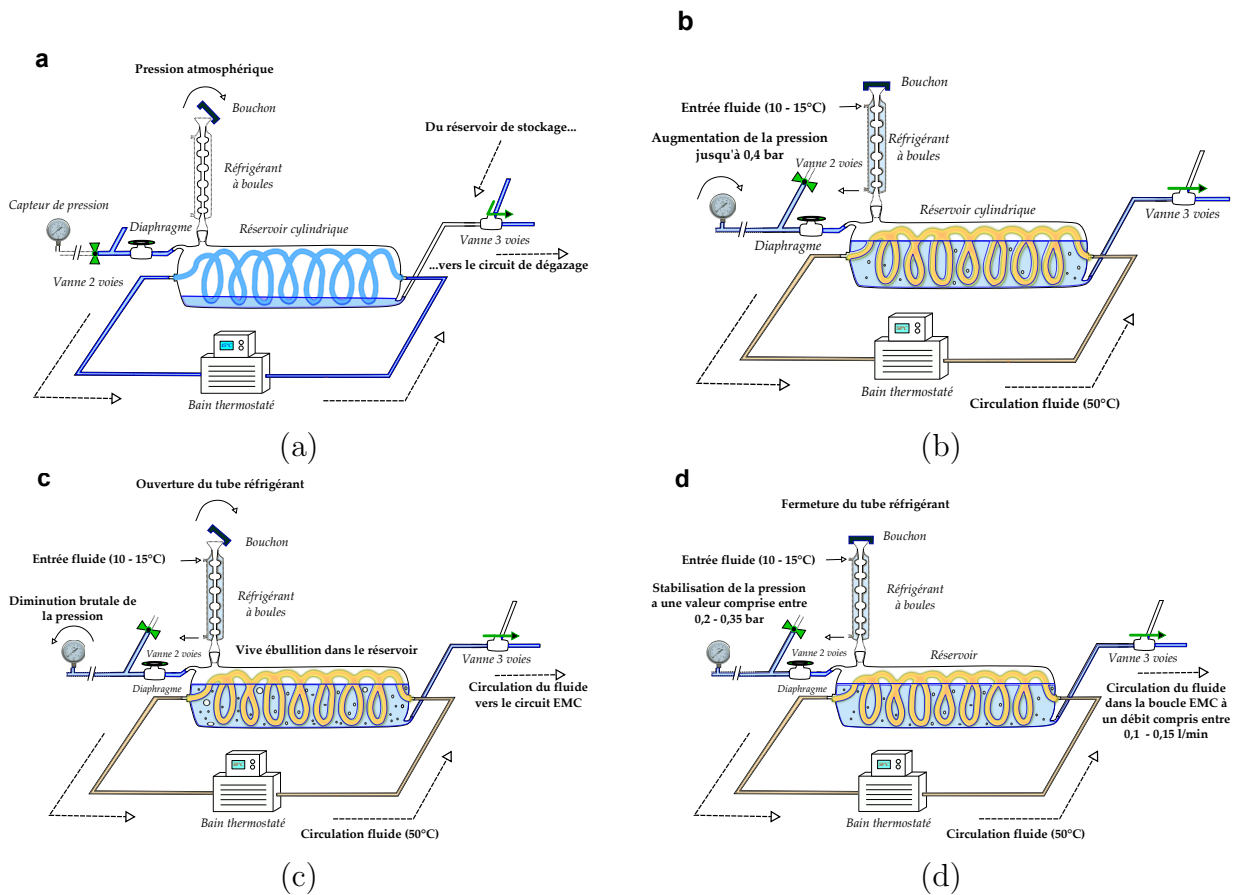


FIGURE 4.2 – Forane 365 HX degassing procedure (a) Cylindrical reservoir filling. (b) Fluid in boiling condition and pressurization. (c) Pressure release and removal of the dissolved gases. (d) Fluid flow inside the EMC loop

(b) Once the reservoir was filled with Forane 365 HX, hot water at 50°C was sent through the serpentine which was inside the reservoir. When this water flow was initiated, the top

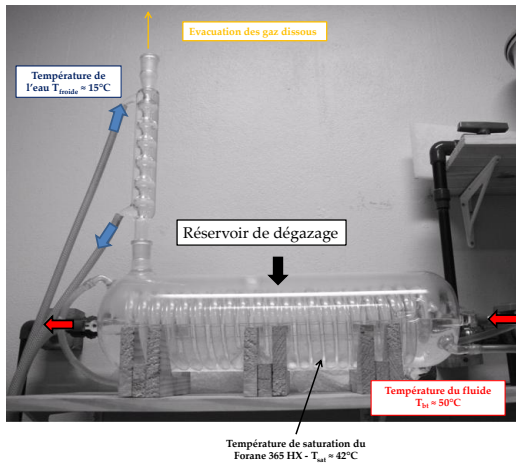
Section 4.1. Hydraulic test loop presentation

of the condenser was closed using a cover that was sized for this purpose. This water flow allows, the Forane 365 HX that was inside the glass reservoir, to gradually enter in boiling (at atmospheric pressure, Forane 365 HX boiled at about forty degrees). The phase change generated by the water flow at 50°C led to pressure increase inside the reservoir due to the closing of the condenser.

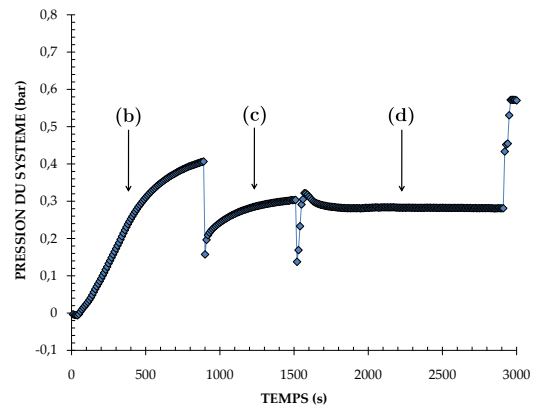
(c) When this pressure reached 0.4bar , the cover which was placed on top part of the condenser was removed and the gas under pressure that was at the free surface of Forane 365 HX in the glass reservoir released to the atmosphere. This action led to the appearance of a strong boiling in the reservoir that was suddenly submitted to atmospheric pressure. The cover was then placed again on the top part of the condenser and the procedure was then repeated a second time³. The full time of the procedure was about 30 minutes.

(d) After step (c), the centrifugal pump ($n^{\circ}2$, the pump $n^{\circ}1$ was then stopped) was started and made the degassed fluid flowed in the **EMC** loop. This flow was maintained for 20 minutes for continuous degassing purposes as the fluid may be in contact with air that was entrapped in the loop. Once this process was made, it was assumed that the impact of the dissolved gases was small on the studied boiling phenomena in the mini-channel.

On Figure 4.3a a picture of the degassing reservoir has been given. The evolution of the pressure during the degassing procedure followed the trend of the experimental data given on Figure 4.3b. The increase that can be noticed for a time of about 3000 seconds was related to the pressurization of the hydraulic loop due to the closing of the diaphragm valve.



(a)



(b)

FIGURE 4.3 – (a) Picture of the degassing reservoir (b) Evolution of the pressure during Forane 365 HX degassing process

3. One can note that the increase of pressure is slower and did not reached 0.4bar always during this second stage

4.1.3 Preheating method

In order to control the test section fluid inlet temperature, a heating technique that allow for the increase of the fluid temperature was developed. A PID system was used for the regulation.

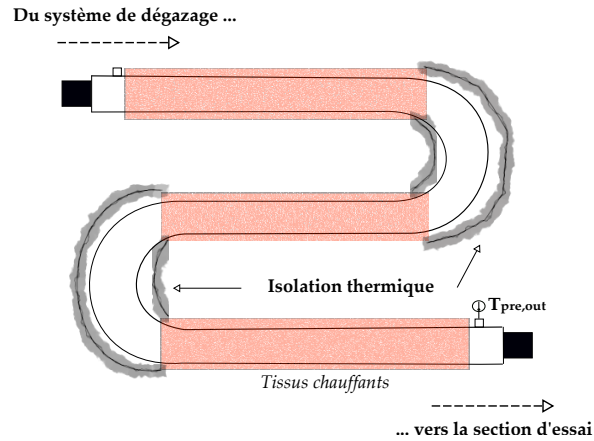


FIGURE 4.4 – Preheater representation

This pre-heater (Figure 4.4) is made using copper tubes having 20 mm of diameter, having straight lengths of 250 mm and having two U-shape turns with a radius of curvature of 50 mm . Heating tapes were stuck on the tube walls and allow for their heating. These tapes were controlled by the PID regulator (SA 200) that allow for the regulation of the heat flux needed for reaching the setpoint temperature ($T_{pre,out}$). The PID parameters were tuned using the Ziegler-Nichols method.

4.1.4 Test section description

The test section that was used derived from the different adaptations made by Gao *et al.* (2002), Bavière (2005) and Gamrat (2007) (§1.4.1). It was composed of three different parts : two brass blocks, separated by a stainless hollowed steel plate 301. The machined blocks constituted the main channel walls and the plate has a specific thickness b , which set the distance in between the two blocks. The fluid heating was ensured by four heating cartridges that were inserted in the lower block. These cartridges were placed in housing that were thermally insulated. Each of these housing was equipped with a type T thermocouple of 0.5 mm of diameter. These thermocouples were placed into drill holes of 4 mm of diameter that were formerly filling with a thermal grease and whose ends was located at 1 mm from the solid/liquid interface. The four thermocouples were placed at a regular interval of 20.5 mm in the lower block. One can note that the first thermocouple was located at 5.5 mm from the channel entrance. Probes of same type were used for measuring the mixed temperatures at the test section inlet and outlet. The whole set of thermocouples was calibrated several times during this experimental work.

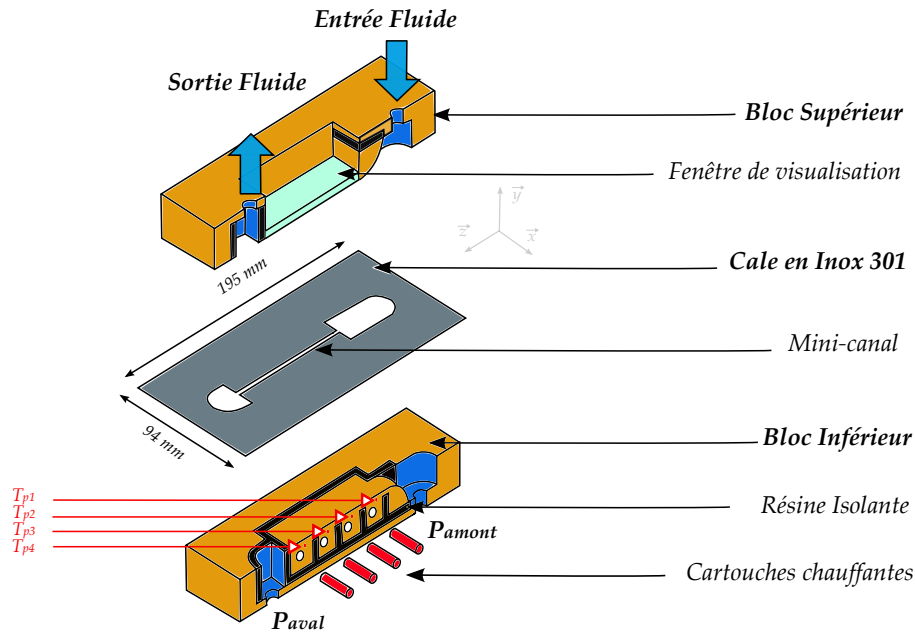


FIGURE 4.5 – Simplified representation of the test section

The pressure sensors were placed upside down below the test section in order to allow for the rapid release of the vapor bubbles that were created during the convective boiling in the test section. Indeed, for boiling conditions the vapor bubbles that were created in the mini-channel were driven by the flow to the outlet reservoir. The buoyancy forces led the bubbles to rise toward the top part of this reservoir and these bubbles can be extracted more easily from the test section. These sensors were calibrated on a regular basis during this work.

A visualization window⁴ (Figure 4.5) has been inserted in the top block of this test section. This window has showed a very good chemical compatibility with Forane 365 HX all along the test campaigns. It was made in zinc sulfide (ZnS) that is a semi-transparent material ($> 65\%$) for wavelengths related to visible light (wavelengths ranged between 380 and 780 nm) and semi-transparent ($> 70\%$) to infrared radiation (IR) (wavelengths ranged between 0.78 and $10\text{ }\mu\text{m}$). The usage of this window led to wall heat fluxes that were asymmetric between the two main walls of the mini-channel.

The lower block wall was textured by means of an electrochemical technique (deposition of a nickel thin film of $2\text{ }\mu\text{m}$ of thickness, with embedded silicon carbides particles having diameter that was between $5\text{ }\mu\text{m}$ to $7\text{ }\mu\text{m}$), on a specific active area. The fabrication of this micro-structure during the work of Bavière (2005) allow for the study of the impact of the roughness on the pressure drop and on heat transfer coefficients. The assembly of the test section was possible using 14 screws spaced regularly at the blocks' rims. The tightening was ensured using a torque

4. The layouts of the top block which comprised this window can be found in Annexe B.

wrench that allow for the repeatability of the mounting or disassembly operations. A torque of about 20 $N.m$ was applied on all the screws during these operations.

4.1.5 Mini-channels sizing

For analysis the impact of the geometrical parameter on the internal convective boiling, it was necessary to wisely select the mini-channels dimensions. Indeed, the influence of the geometry on the convective boiling phenomena has been barely studied in the state of the art review that was analysed. Thus, during this study different mini-channel dimensions were defined for evaluating the impacts of the aspect ratio and of the hydraulic diameter on the variations of the pressure drops and of the heat transfer coefficients. In addition, these dimensions were selected in order to make the comparisons between the channels possible. According to the state of the art review, the evolution of the flow regimes is related to the experimental conditions, but also to the geometry of the mini-channels. Thus, from the existing experimental set-up, it was decided to use for all the made experiments, the available test section whose length was 94 mm . The different mini-channels widths (a) and heights (b) were selecting for allowing the bubbles confinement to be significant enough. This was made in order to permit the visualization of the whole set of flow regime, from onset of nucleate boiling to wall dryout.

The state of the art review suggested that the hydraulic diameter was a necessary but not sufficient parameter⁵ for characterizing the hydrodynamic behavior for internal boiling conditions in mini-channels. In this sense, the simultaneous impacts of the hydraulic diameter and of the aspect ratio⁶ should, according to our analysis, play an important role on these flows. Thus, the geometrical dimensions of the mini-channels used during this study have been defined to allow for the evaluation of the impact of the hydraulic diameter and of the aspect ratio on the behavior of the boiling flow. The dimensions of the four selected mini-channels are given in Table 4.1.

Mini-channel	Height (μm)	Width (μm)	D_h (μm)	γ
C_1	1006 ($\pm 4 \mu m$)	2274 ($\pm 10 \mu m$)	1394	0.442
C_2	816 ($\pm 6 \mu m$)	5613 ($\pm 10 \mu m$)	1424	0.145
C_3	814 ($\pm 6 \mu m$)	7983 ($\pm 10 \mu m$)	1476	0.103
C_4	421 ($\pm 2 \mu m$)	4101 ($\pm 10 \mu m$)	764	0.101

TABLE 4.1 – Dimensions of the different selected plates

This table gives a nomenclature that will be used several time in this manuscript. The thickness

5. This is particularly true when the shape of the duct get away from circular cross section

6. For the range of mini-channels whose either the width or the height is larger to bubble detachment diameter, the aspect ratio has an impact on the behavior of the flow

measurement were done using micrometric touch probe (Heidenhain, $\pm 1 \mu m$), on a flat marble. The results that are given in this table were obtained for 10 experimental data point all along the plates' hollow. One can note that these channels thickness is not fully constant along the hollow what explained the different uncertainties. The mean width values have been obtained using the image analysis made with a binocular microscope.

4.2 Data acquisition of the experimental measurements

During this work, the whole data acquisition has been transferred from TestPoint software toward Labview 7.1 software. Indeed, all modification of the code source under TestPoint was very few intuitive and generated cumbersome procedures. Moreover, the implementation of the data related to initialisation measurements (pressure sensors), the addition of acquisition channels for the temperature measurements, or the development of images acquisition technique using the camera were not possible easily on this same software. Thus it was decided to transfer the whole code (an to adapt it) on Labview 7.1. The basis on this work can be found in Valdenaire (2008).

The whole data measurement acquisition was made using a Keithley 2700, which has 40 channels distributed on two different electronic boards. The connection between the PC and system acquisition was realized through a RS232 protocol. The software function can be summarized according to the seven following points :

- ① Flow steady state detection after selection of the operating conditions,
- ② Saving of all the instantaneous data of the whole set of realized experiments,
- ③ Mean value determination of the whole set of measured parameters on the x last experimental data point from a selected time and saving of these data in a indexed table,
- ④ Automatic evaluation of all the thermophysical properties of water or Forane 365 HX regarding the fluid mean temperature (single-phase) or regarding the saturated pressure (boiling),
- ⑤ Estimation of the heat transfer rate from wall to fluid (single-phase) in real time,
- ⑥ Instantaneous display of the pressure drops or heat transfer coefficients (single-phase) and automatic representation of these points on a chart for the steady state conditions,
- ⑦ Instantaneous calculation of the flow velocity in the channel, of the system pressure and vapor quality estimation (boiling).

4.3 Cameras acquisition system description

During the montage of the hydraulic test loop and for the boiling conditions, an video acquisition system was designed. This system was composed of :

▣ a binocular microscope (Nikon SMZ 1500), equipped with a lens (Nikon APO HR \times 0.5),

The selection of a binocular was made in order to obtain a very precise visualization. The field of view was squared and can be varied from 3.9mm to 58.7mm of sidelength. Regarding the used lens it was possible to enlarge or reduce this field of view. One of the most significant point related to the use of this binocular was to make local analysis and more global observations of the two-phase flow possible.

▣ two sources of cold lights (Schott KL2500) with two flexible optical fibers having a length of 100 cm that were used to guide the light,

During the development of the boiling flow in mini-channel, the liquid or vapor velocities may become important. Thus in order to visualize these phenomena, it was necessary to lighten them intensively. In addition, for avoiding to add a supplementary heat flux, two optical fibers linked to two cold sources of 250 W , allow for the driving of this light flux without bringing heat to the test section.

▣ a CCD camera (Jai Pulnix 1327 TM, 1392×1040 , 30 im/s) and a CMOS camera (AOS MOTIONeer, 640×512 , 1000 im/s),

Two camera were used for this analysis. The selection was mainly due to the sensor sensitivity regarding the light. Thus, when the mass velocities were about $400\text{kg.m}^{-2}.\text{s}^{-1}$ or at very important vapor qualities it was particularly complex to observe the liquid/vapor phases arrangement. For the first camera (Pulnix 1327 TM) the shutter was set to a value ranged between $100\text{ }\mu\text{s}$ and $160\text{ }\mu\text{s}$ whereas for the second one (AOS MOTIONeer) it was set to a value between $400\text{ }\mu\text{s}$ and $1000\text{ }\mu\text{s}$.

▣ a guide rail allowing for millimeter displacements that support the test section.

A picture that showed the location of the binocular, of the optical fibers and of the camera is given on Figure 4.6.

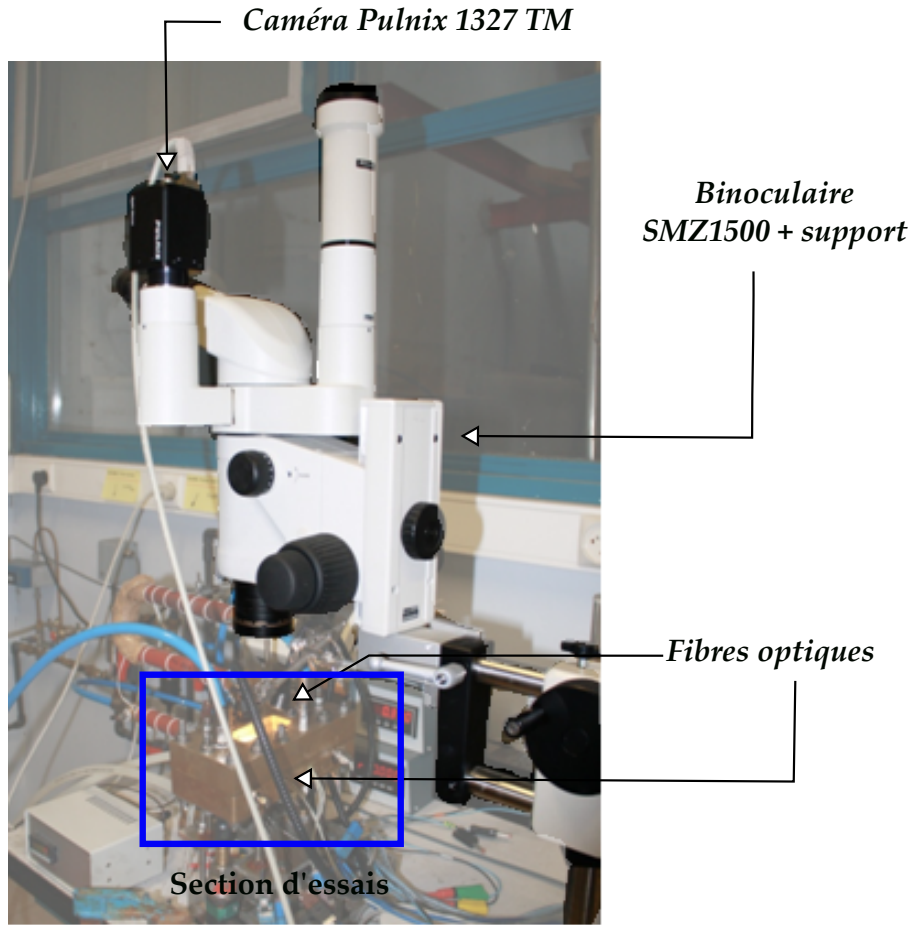


FIGURE 4.6 – Location of the visualization system above the test section

The whole visualization system montage has been presented on Figure 4.7.

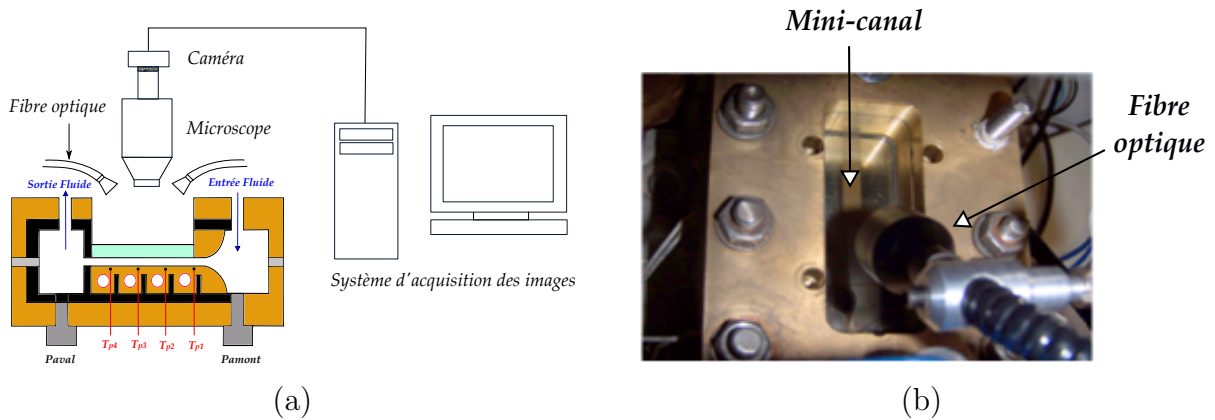


FIGURE 4.7 – (a) Presentation of the visualization experimental set-up (b) Bird eye's view of the test section

The mini-channel viewable zone (through the window) was comprised between the locations of wall thermocouple $n^{\circ}1$ to wall thermocouple $n^{\circ}4$. However during the made experiments it

Chapitre 4. Experimental set-up description

was not possible to position the binocular above thermocouple $n^{\circ}1$ or $n^{\circ}4$ because of the lack of light. The effective visualizing zone is reported on Figure 4.8. It has been reported also, the location of the pressure sensors and of the inlet and outlet test section temperature sensors.

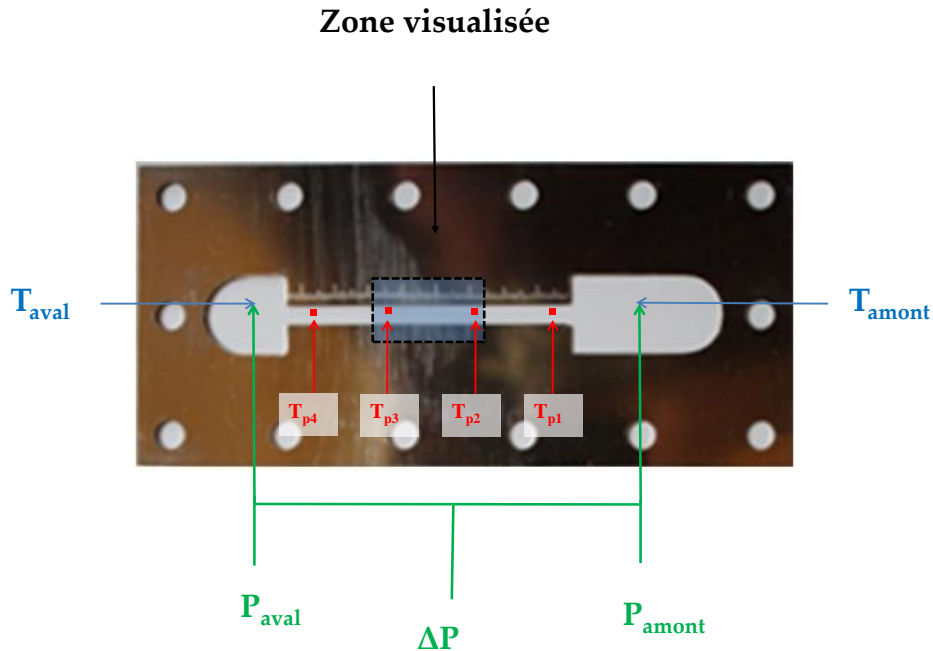


FIGURE 4.8 – Visualization region

4.4 Presentation of the list of made experimental tests

During this study several tests were made in order to characterize the test section for boiling conditions. It should be highlighted that this study was exploratory and numerous operational conditions were tested. An attention was paid particularly on the onset of nucleate boiling and on critical heat flux determination (using the data given by the boiling curves) regarding the working conditions. The study of the impact of the vapor thermodynamic quality on heat transfer coefficients for « constant » heat fluxes conditions was done to a lesser extent also. Next to this paragraph, tables that summarized all the made experiments for the convective boiling conditions have been given.

Section 4.4. Presentation of the list of made experimental tests

☞ Onset of nucleate boiling

C_1 mini-channel (1 mm × 2.3 mm)	G (kg.m ⁻² .s ⁻¹)				
	200	300	400	500	600
$P_{sat} = 0.7 \text{ bar} - \Delta T_{sub} = 15^\circ C$	✓	✓	✓	✓	✓

C_2 mini-channel (0.816 mm × 5.6 mm)	G (kg.m ⁻² .s ⁻¹)				
	100	200	300	400	500
$P_{sat} = 0.7 \text{ bar} - \Delta T_{sub} = 15^\circ C$	✓	✓	✓	✓	✓

C_3 mini-channel (0.814 mm × 8 mm)	G (kg.m ⁻² .s ⁻¹)				
	400	500	600	700	800
$P_{sat} = P_{atm} - \Delta T_{sub} = 14^\circ C$	✓	✓	✓	✓	✓
$P_{sat} = P_{atm} - \Delta T_{sub} = 10^\circ C$	✓	✓	✓	✓	✓
$P_{sat} = P_{atm} - \Delta T_{sub} = 5^\circ C$	✓	✓	✓	✓	✓
	100	200	300	400	500
$P_{sat} = 0.7 \text{ bar} - \Delta T_{sub} = 15^\circ C$	✓	✓	✓	✓	✓

C_4 mini-channel (0.421 mm × 4 mm)	G (kg.m ⁻² .s ⁻¹)				
	100	200	300	400	500
$P_{sat} = 0.35 \text{ bar} - \Delta T_{sub} = 15^\circ C$	✓	✓	✓	✓	✓
$P_{sat} = 0.5 \text{ bar} - \Delta T_{sub} = 15^\circ C$	✓	✓	✓	✓	✓
$P_{sat} = 0.7 \text{ bar} - \Delta T_{sub} = 15^\circ C$	✓	✓	✓	✓	✓

☞ Study of the boiling curves and incipience of critical heat flux

C_1 mini-channel (1 mm × 2.3 mm)	G (kg.m ⁻² .s ⁻¹)				
	200	300	400	600	800
$P_{sat} = 0.7 \text{ bar} - \Delta T_{sub} = 15^\circ C$	✓	✓	✓	✓	✓

C_2 mini-channel (0.816 mm × 5.6 mm)	G (kg.m ⁻² .s ⁻¹)				
	200	300	400	600	800
$P_{sat} = 0.7 \text{ bar} - \Delta T_{sub} = 15^\circ C$	✓	✓	✓	✓	✗

C_3 mini-channel (0.814 mm × 8 mm)	G (kg.m ⁻² .s ⁻¹)				
	100	200	300	400	600
$P_{sat} = 0.7 \text{ bar} - \Delta T_{sub} = 15^\circ C$	✓	✓	✗	✗	✗

Chapitre 4. Experimental set-up description

C_4 mini-channel ($0.421\text{ mm} \times 4\text{ mm}$)	G ($\text{kg}\cdot\text{m}^{-2}\cdot\text{s}^{-1}$)				
	200	300	400	600	800
$P_{sat} = 0.7\text{ bar} - \Delta T_{sub} = 15^\circ\text{C}$	✓	✓	✓	✓	✓
$P_{sat} = 0.7\text{ bar} - \Delta T_{sub} = 7^\circ\text{C}$	✗	✓	✗	✓	✗

Troisième partie

EXPERIMENTAL RESULTS

Single-phase flow in mini-channels

5.1	Study of the friction coefficients in mini-channel	137
5.1.1	Methodology and study description	137
5.1.2	Experimental determination of the friction coefficients	137
5.1.3	Experimental uncertainties	138
5.1.4	Measurements and results	140
5.2	Study of the heat transfer coefficients in mini-channel	148
5.2.1	Methodology and study description	148
5.2.2	Determination of the heat transfer coefficients	148
5.2.3	Experimental uncertainties	150
5.2.4	Measurements and results	152
5.3	Conjugated (heat/flow) numerical analysis	165
5.3.1	Numerical results	165
5.3.2	Correction of the experimental data	171
5.4	Chapitre 5 conclusions	174

Summary :

THIS chapter gives the whole experimental methodology and the results that were obtained for the pressure drops¹ and the heat transfer coefficients variation in mini-channels. The presented data have been limited to the results related to the hollowed test plates² $C_1(a = 2.3 \text{ mm} - b = 1 \text{ mm})$ and $C_2(a = 5.6 \text{ mm} - b = 0.816 \text{ mm})$. Two working fluids (demineralised water and forane 365 HX) have been used for all the single-phase flow analysis. The results were compared to the correlations that have been defined in the state of the art review. The obtained results allow for the demonstration that the pressure drops coefficients were in very good agreement with the predictive methods for the two working fluids. A deviation for the

1. These coefficients were obtained for a adiabatic flow

2. The raw experimental results for plate $C_3(a = 8 \text{ mm} - b = 0.814 \text{ mm})$ and $C_4(a = 4 \text{ mm} - b = 0.421 \text{ mm})$ have been reported in Annexe D

experimental heat transfer coefficients has been noticed when the laminar regime was reached. In order to better understand this behavior, a numerical model was built with the aim to use few simplifying assumptions. The results from this model suggested that these deviations were due to non-homogeneous heat flux along the mini-channel walls for the small flow rate. The intensity of this heat flux was generally higher close to the channels entrance, depending on their geometries and on the selected fluid. After this numerical study and using an equation that was Reynolds-dependent, the mean heat flux evolution at the solid/liquid interface was formalized. Finally a method for correcting the experimental data has been proposed.

5.1 Study of the friction coefficients in mini-channel

5.1.1 Methodology and study description

The mini-channel was made by the assembly of three elements : lower block, hollowed plate and top block. The fluid flow was in contact with three surface of reference which are : a nickel thin film that was deposited on the lower block, the surfaces of the hollowed plate and the window visualization made in zinc sulfide (ZnS) for the top wall. In function of each of these surfaces, the roughness height (ε) may evolved. This data may be important for the experimenter as it can impact the flow nature, and particularly the transition to turbulence when the scale become smaller. Indeed, when the characteristic dimensions of the cross section were reduced, the value of the relative roughness become important and it was necessary to estimate correctly its value. For the considered test section, the experimental conditions were semi-rough because the window surface was considered as smooth. Similarly to this window surface, the lateral side of the mini-channels were considered as smooth. For the study of the friction coefficients, the analysis has been restricted to adiabatic flow conditions.

5.1.2 Experimental determination of the friction coefficients

The evolution of the friction coefficients (for an internal flow) depends on :

- ▷ channel geometrical parameters (hydraulic diameter (d_h), length (L) and wall roughness)
- ▷ flow velocity (u) in the channel
- ▷ fluid mass density (ρ_l) and viscosity (ν_l).

The thermophysical properties of a liquid are, for single-phase flow, more sensitive to the temperatures than to the pressure variations. Thus, these properties has been estimated using the mean fluid temperature measured at the entrance and at the outlet of the test section, for water and forane 365 HX.

Finally, the friction coefficient can be calculated using :

$$f = \frac{\Delta P d_h}{2\rho u^2 L} \quad (5.1)$$

The reader could noticed that the test section entrance is made with a convergent that allow for the limitation of fluid detachment at channel entrance. The expression related to the fluid acceleration, due to this convergent led to a decrease of the pressure term that is used for the calculation of the friction coefficient which was defined in equation (5.1).

The Poiseuille number can be determined by making the product between the friction coefficient and the Reynolds number :

$$Po = fRe \quad (5.2a)$$

$$Re = \frac{ud_h}{\nu} \quad (5.2b)$$

This Poiseuille number will be compared to the theoretical laws given by literature (equations (1.7)) and (1.9).

5.1.3 Experimental uncertainties

In this paragraph, the method for determining the experimental uncertainties is presented for one specific parameter. The calculation of the uncertainties related to the other parameter has been detailed in the appendices. The knowledge of the uncertainty on a defined function $f(X_1, X_2, X_3, \dots, X_i)$ is related to uncertainties of the variables that define the function. Kline et McClintok (1953) have defined a general rule named : « error propagation », that allow for the rigorous determination of the global error that is made on each variable of this function. If the different variables of f are non-dependent, the measurement uncertainty $i_{(f)}$, can be calculated using :

$$i_{(f)} = \pm \sqrt{\sum_{n=1}^{n=i} \left(\frac{\partial f}{\partial X_n} i_{(X_n)} \right)^2} \quad (5.3)$$

where $i_{(X_n)}$ is the measurement uncertainty on X_n .

The calculation of the experimental uncertainty was given as an example for the Poiseuille number. By combining equations (5.1) and (5.2b), equation (5.2a) become :

$$Po = \frac{\Delta P d_h^2}{2\rho\nu L} \quad (5.4)$$

By expressing the mass flow rate \dot{m} and the hydraulic diameter regarding the hollowed plate width (a) and thickness (b), the equation (5.4) become :

$$Po = \frac{2\Delta P (a \times b)^3}{\dot{m}\nu L (a + b)^2} \quad (5.5)$$

The uncertainties related to the Poiseuille number can be determined by calculating the whole set of partial derivatives of this function according to :

$$\left\{ \begin{array}{l} i_{(Po)} = \pm \sqrt{\left(\frac{\partial Po}{\partial \Delta P} \right)^2 i_{(\Delta P)}^2 + \left(\frac{\partial Po}{\partial a} \right)^2 i_{(a)}^2 + \left(\frac{\partial Po}{\partial b} \right)^2 i_{(b)}^2 + \dots} \\ \dots \left(\frac{\partial Po}{\partial \dot{m}} \right)^2 i_{(\dot{m})}^2 + \left(\frac{\partial Po}{\partial L} \right)^2 i_{(L)}^2 + \left(\frac{\partial Po}{\partial \nu} \right)^2 i_{(\nu)}^2 \end{array} \right. \quad (5.6)$$

Section 5.1. Study of the friction coefficients in mini-channel

The uncertainties $i_{(X_n)}$, on each of these parameters are determined either using a data given by the supplier (technical specifications on : flow-meters, pressure sensors, geometrical dimension of the hollowed plates), or thanks to calibrations that were made on the constitutive elements of the test section (thermocouples, hollow plates dimensions, pressure sensors). Thus, we determined the measurement uncertainty on the Poiseuille number for the whole set of hollowed plates and the results were given for $C_1(a = 2.3 \text{ mm} - b = 1 \text{ mm})$ and $C_2(a = 5.6 \text{ mm} - b = 0.816 \text{ mm})$, on the whole range of Reynolds numbers that were comprised between 200 and 8000³.

Using the Tables (5.1) and (5.2) the reader may notice that the experimental uncertainties reached their maximum values when the Forane 365 HX was used. For understanding the reasons for the increase of this uncertainty, the main contribution for this global uncertainty was represented for the determination of the Poiseuille number. One can noticed that the range of Reynolds numbers has been given regarding this main contribution.

Reynolds number range	Mean dP_0/P_0 on the range of Reynolds (%)	Main contribution	Contribution to global uncertainty (%)
$C_1 - a = 2.3 \text{ mm} - b = 1 \text{ mm}$			
233 - 2134	$\pm 15.5 \%$	ΔP	76.7 %
2134 - 2717	$\pm 5.3 \%$	b	39.6 %
2717 - 3361	$\pm 15.3 \%$	\dot{m}	89 %
3361 - 4948	$\pm 17.8 \%$	ΔP	56 %
4948 - 7157	$\pm 10.9 \%$	\dot{m}	43.7 %
$C_2 - a = 5.6 \text{ mm} - b = 0.816 \text{ mm}$			
174 - 1528	$\pm 18.6 \%$	ΔP	83.5 %
1528 - 2961	$\pm 10.9 \%$	\dot{m}	68.1 %
2961 - 7123	$\pm 13.7 \%$	ΔP	65 %

TABLE 5.1 – Main contributions to the global uncertainty (water)

After analyzing the data given on Tables (5.1) and (5.2), it has been noted that the contributions that have impacted particularly the Poiseuille number calculation were ΔP and \dot{m} . These two measured values were dependent of the working fluid thermophysical properties. The main difference between these two fluid, when determining the frictions coefficient, came from viscosity. Indeed, forane 365 HX has dynamic viscosity that is about 1.75 time smaller than the one of water. Thus for a given Reynolds number, its used has led to smaller pressure drops and flow rate. Consequently, at smaller flow rate, the uncertainties on the measurements of the differential pressure and flow rate had been larger for forane 365 HX than for water.

3. The data related to the uncertainty on the Reynolds number were not represented as these uncertainties were very low for this range of studied Reynolds numbers

Reynolds number range	Mean dP_o/P_o on the range of Reynolds (%)	Main contribution	Contribution to global uncertainty (%)
$C_1 - a = 2.3 \text{ mm} - b = 1 \text{ mm}$			
495 - 3452	$\pm 27.8 \%$	ΔP	86.3 %
3452 - 5701	$\pm 11.9 \%$	b	62.7 %
5701 - 6867	$\pm 19.2 \%$	\dot{m}	84.2 %
$C_2 - a = 5.6 \text{ mm} - b = 0.816 \text{ mm}$			
363 - 2974	$\pm 30.7 \%$	ΔP	88.7 %
2974 - 6999	$\pm 11.8 \%$	\dot{m}	61.1 %
6999 - 8270	$\pm 14.3 \%$	ΔP	82.5 %

TABLE 5.2 – Main contributions to the global uncertainty (forane 365 HX)

For these two working fluids, the experimental uncertainty on the calculation of the Poiseuille number increased significantly when the flow rate was reduced due to the low measured differential pressures. For avoiding the too large uncertainties, the tests had been limited, to the calculation of Poiseuille numbers for Reynolds numbers larger than 150, for water and 350 for forane 365 HX.

5.1.4 Measurements and results

The first made experiments were done using demineralized water in order to obtain data points of reference before making the experiments with forane 365 HX. The experimental data that had been obtained were then compared to the theoretical laws of Shah et London (1978) and of Blasius (1913) that have been presented in Chapter 1. It was possible to notice that for our experimental set-up, the studied flow was mainly in developing conditions for the hydrodynamic boundary layers, during the laminar regime. Indeed, these results were due to the small length of the channels. Considering this, the experimental data were then compared to the correlations that have been established for conditions related to the development of the hydrodynamic boundary layer during this flow regime.


 Working fluid : water

Figure 5.1 showed the friction coefficient that have been obtained for C_1 mini-channel ($a = 2.3 \text{ mm} - b = 1 \text{ mm}$) for three different tests made with water. It can be highlighted that for the whole set of studied Reynolds numbers, the experimental data points showed a very good repeatability behavior (except for the lower Reynolds numbers values (< 600)). Indeed, the discrepancies that were observed for the small values of flow rate were related to the small variation of pressures between the test section inlet and outlet (about 200 Pa for the lower

Section 5.1. Study of the friction coefficients in mini-channel

values of Reynolds numbers whereas the sensor sensitivity was about $100 Pa$ according to the manufacturer), as specified in former paragraph. Otherwise, the made measurements were repeatable for the main part of Reynolds numbers range what showed that the measurement technique was reliable.

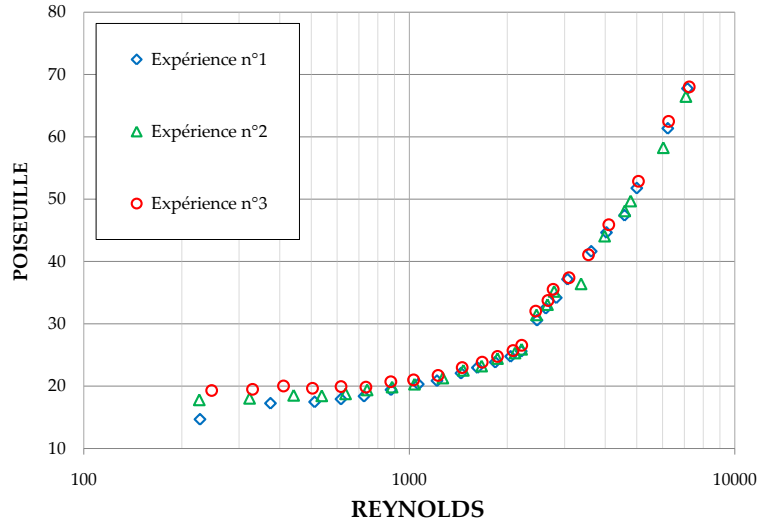


FIGURE 5.1 – Poiseuille number regarding the Reynolds number - Repeatability tests for C_1 plate ($a = 2.3 mm$, $b = 1 mm$); working fluid : water

The obtained experimental results showed two different trends depending on the flow regime that was developed inside the channel. For the laminar regime, the Poiseuille number variation was small regarding the Reynolds number. When the turbulent regime was reached, the Poiseuille number increase rapidly with this Reynolds number. After these repeatability tests, the results were then compared to the data from the literature. These results have been presented in the following paragraphs.

On Figure 5.2, the obtained results that have been obtained for C_1 mini-channel ($a = 2.3 \text{ mm} - b = 1 \text{ mm}$) have been reported. In order to evaluate the differences with the data from the literature, the correlations of Shah et London (1978) and Blasius (1913) were given on this same chart. For the laminar flow ($Re < 2400$), the experimental data points were in very good agreement with the evolution predicted by Shah et London (1978) with an absolute mean error⁴ of less than 3%.

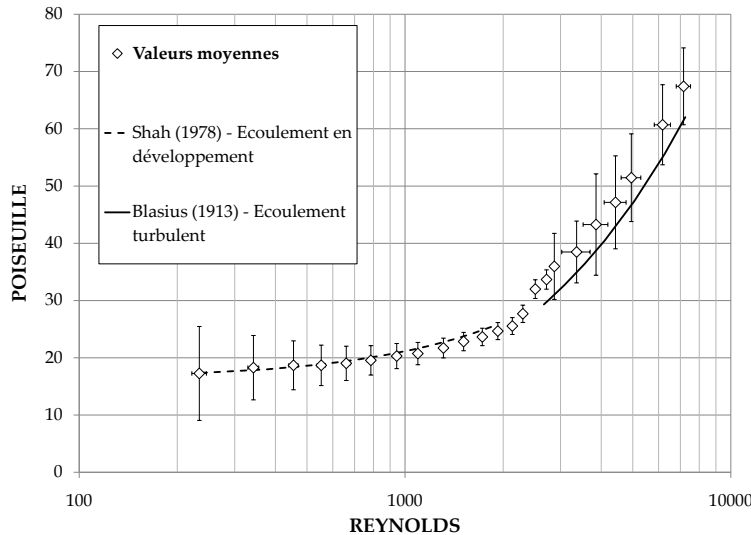


FIGURE 5.2 – Poiseuille number regarding the Reynolds numbers for C_1 mini-channel ($a = 2.3 \text{ mm}$, $b = 1 \text{ mm}$); working fluid : water

A more significant difference (AME equaled 10.5%) was noticed with Blasius (1913) prediction. This difference that was observed with this correlation was supposed to be due to an uncertainty on the measured pressure difference for larger Reynolds numbers. Indeed, when the flow rate was increased, the differential pressure was calculated, without using the inductive sensor (full scale equaled 0.1 bar with a measure precision of 1% of this full scale), but using other pressure sensors (whose full scale equalled 0.7 bar or 2 bar regarding the used sensor). As a consequence, the use of these sensors induced larger uncertainty for large Reynolds numbers. However the reader may notice that the error bars intercepted the correlation that has been established by Blasius (1913).

4. the acronym AME will be used in the remaining sections of this manuscript to notify this error

The whole set of experimental data points that were obtained for this experimental campaign has been reported on Figure 5.3.

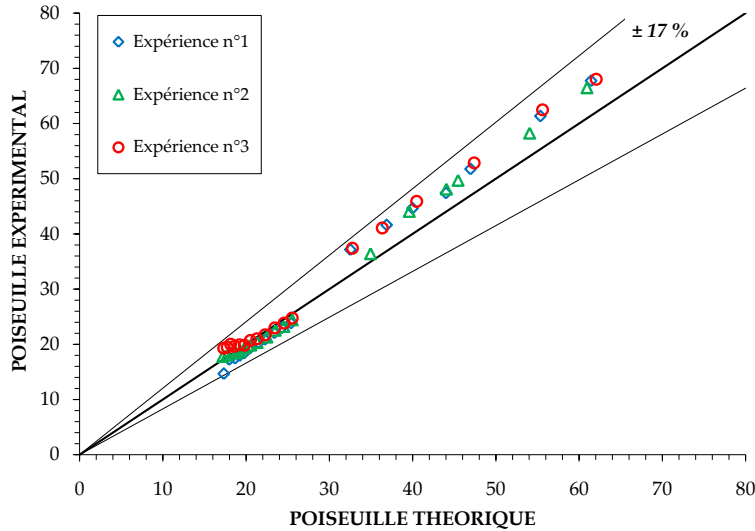


FIGURE 5.3 – Comparison between the experimental / theoretical Poiseuille numbers for C_1 mini-channel ($a = 2.3 \text{ mm}$, $b = 1 \text{ mm}$); working fluid : water

The data that have been obtained for this configuration showed that 100% of the experimental data points were predicted at $\pm 17\%$ by using these two correlations. When referring to the Shah et London (1978) correlation only, 90% of the experimental data points were predicted at $\pm 5\%$ showing the very good agreement with this correlation.

The results from the tests made for the C_2 mini-channel ($a = 5.6 \text{ mm} - b = 0.816 \text{ mm}$) have been reported on Figure 5.4. The data were in very good agreement with the two predictive tools. Mean differences of 4.5% regarding the Shah et London (1978) correlation and of 5.2% compared to the Blasius (1913) correlation have been noticed. The reader may observe that almost 92% of the experimental data points were predicted at $\pm 12\%$ using these two correlations (Figure 5.5).

After this study, it was possible to conclude using the whole set of results obtained for plates C_1 ($a = 2.3 \text{ mm} - b = 1 \text{ mm}$) and C_2 ($a = 5.6 \text{ mm} - b = 0.816 \text{ mm}$) that the correlations from the literature were also applicable for our experimental set-up when water was used as working fluid.

Working fluid : forane 365 HX

The experimental results that are given in this paragraph were obtained using forane 365 HX. It can be highlighted that the small viscosity of the fluid impact significantly the experimental

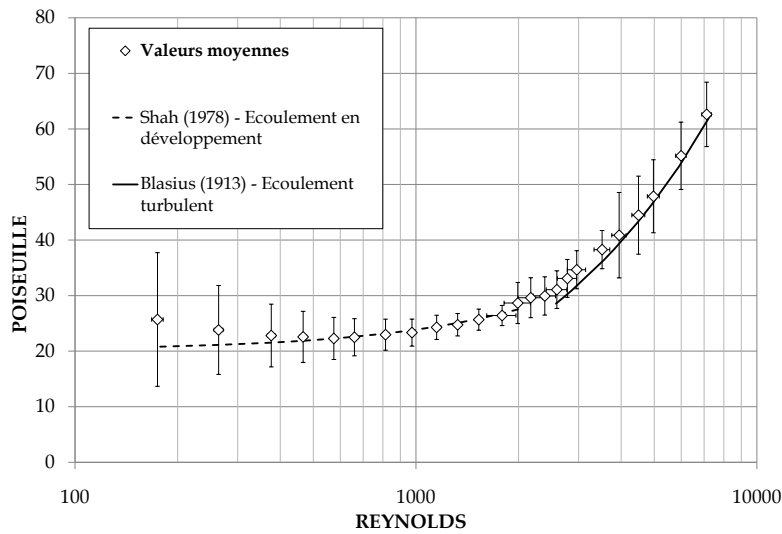


FIGURE 5.4 – Poiseuille number regarding the Reynolds number for C_2 mini-channel ($a = 5.6 \text{ mm}$, $b = 0.816 \text{ mm}$); working fluid : water

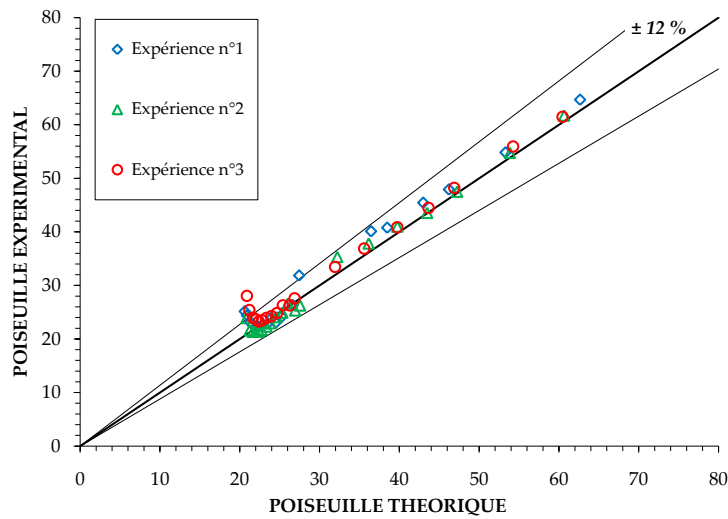


FIGURE 5.5 – Comparison between the experimental / theoretical Poiseuille numbers for C_2 plate ($a = 5.6 \text{ mm}$, $b = 0.816 \text{ mm}$); working fluid : water

uncertainties (variations of the pressures between the inlet and the outlet of the test section were smaller). Thus, the flow rate reduction was limited to Reynolds numbers that were higher than for water case as specified in § 5.1.3. The results that are reported on Figure 5.6 showed that the AME was about 10.7% regarding the Shah et London (1978) law and equaled 6.6% in comparison to the Blasius (1913) correlation for the C_1 mini-channel ($a = 2.3 \text{ mm} - b = 1 \text{ mm}$).

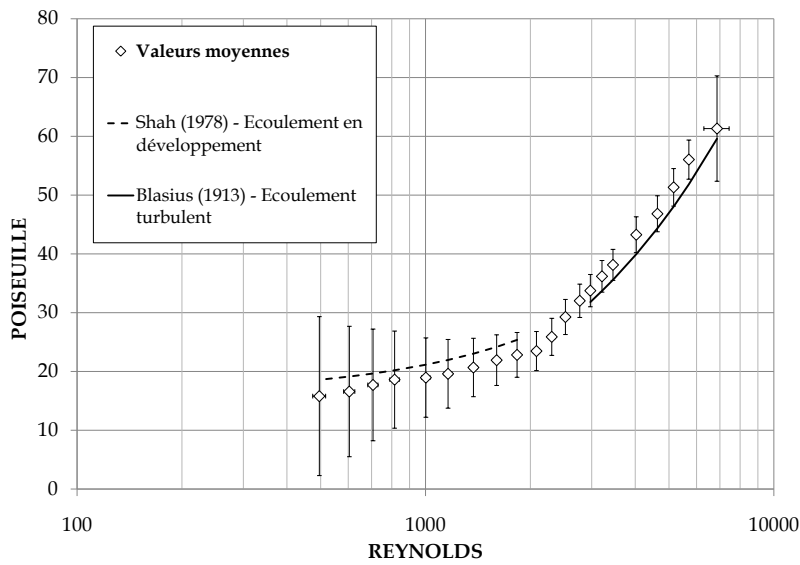


FIGURE 5.6 – Poiseuille number regarding the Reynolds numbers for C_1 plate ($a = 2.3 \text{ mm}$, $b = 1 \text{ mm}$); working fluid : forane 365HX

The experimental data points given on Figure 5.7 showed that 100% of the data point were predicted at $\pm 16\%$ using the two correlations.

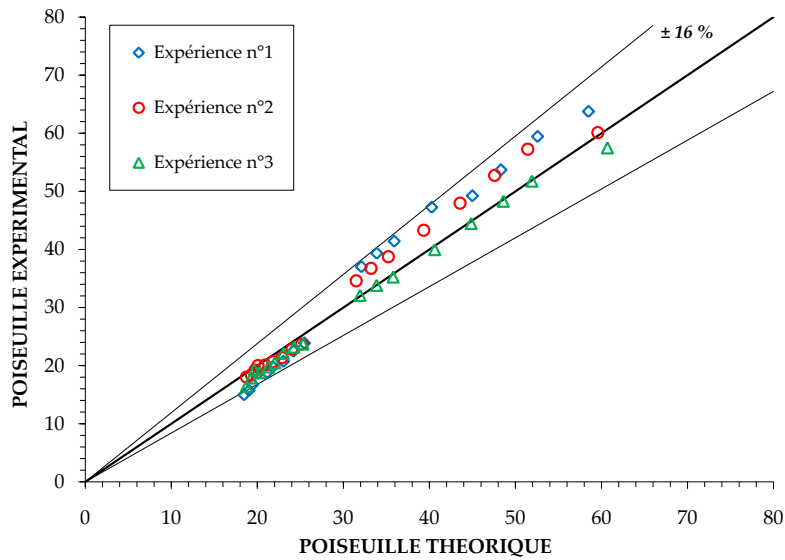


FIGURE 5.7 – Comparison between the experimental / theoretical Poiseuille numbers for C_1 plate ($a = 2.3 \text{ mm}$, $b = 1 \text{ mm}$); working fluid : forane 365 HX

The results for the C_2 mini-channel ($a = 5.6 \text{ mm} - b = 0.816 \text{ mm}$) were in very good agreement with the theoretical data. The error calculations gave an AME of 3.7% compared to

Chapitre 5. Single-phase flow in mini-channels

the Shah et London (1978) prediction and of 5.8% compared to the Blasius (1913) correlation (Figure 5.8).

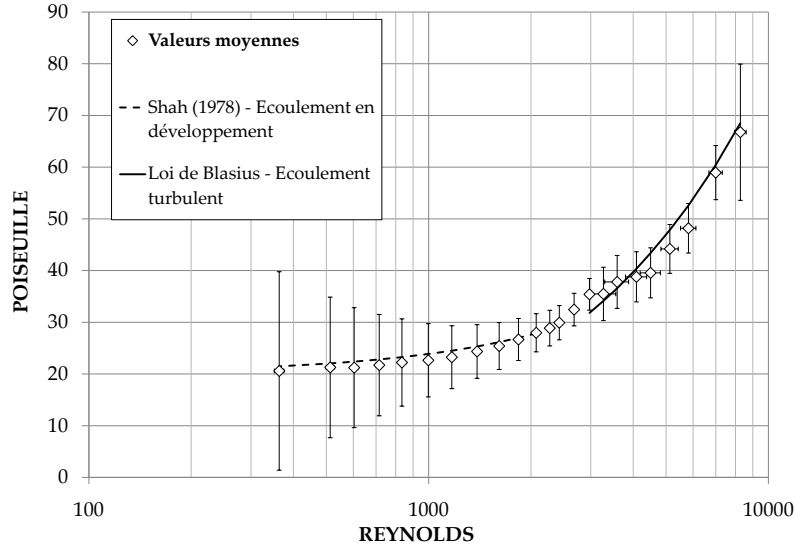


FIGURE 5.8 – Poiseuille number regarding the Reynolds number for C_2 plate ($a = 5.6 \text{ mm}$, $b = 0.816 \text{ mm}$); working fluid : forane 365 HX

Figure 5.9 showed that 95.5% of the experimental data points were predicted at $\pm 10\%$ using these two correlations.

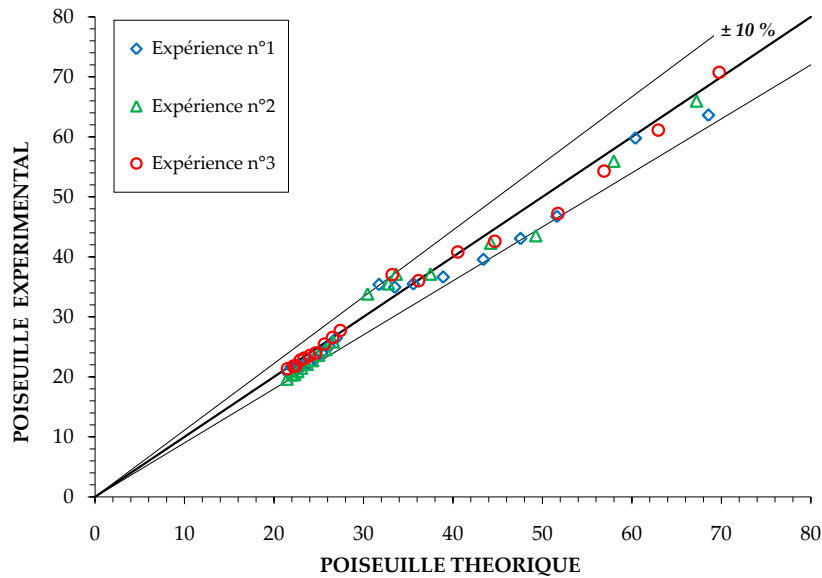


FIGURE 5.9 – Comparison between experimental / theoretical Poiseuille number for C_2 plate ($a = 5.6 \text{ mm}$, $b = 0.816 \text{ mm}$); working fluid : forane 365 HX

Summary on the pressure drop evolution for a single-phase flow

During this experimental study, it was confirmed that the established correlations for the friction coefficients determination for the macro-scale flow were valid for the mini-channels that have been studied also. This results was validated for water and forane 365 HX used as working fluids. The study of the critical Reynolds numbers allow for the demonstration that the transition from laminar to turbulent flow was not modified for the tested conditions regarding the usual data from the literature.

On Table 5.3 the results that have been obtained during the experimental friction coefficients calculation have been summarized.

Tested plate	Fluid	Shah et London (1978)	Blasius (1913)	Crit. Reynolds
C_1	water (demin.)	MAE = 3 %	MAE = 10.5 %	2134 - 2510
	forane 365 HX	MAE = 10.7 %	MAE = 6.6 %	2081 - 2521
C_2	water (demin.)	MAE = 4.5 %	MAE = 5.2 %	2387 - 2780
	forane 365 HX	MAE = 3.7 %	MAE = 5.8 %	2072 - 2679

TABLE 5.3 – Summary of the data given in the § 5.1.4 and critical Reynolds numbers

The results that have been obtained showed a very good agreement with the correlations presented in the literature review as showed by the data given in the previous table. For this part of this work, no impact of the wall roughness, regarding the comparison made between experiments and theory were noticed. In addition, these predictive tools were relevant for the data that have been obtained for the experiments realized with C_4 plate ($a = 4 \text{ mm} - b = 0.421 \text{ mm}$)^a. Therefore it was concluded that the impact of the wall roughness relatively to the height of the studied channels did not had a huge impact on the friction coefficients determinations in our configuration.

^a. Appendice D

5.2 Study of the heat transfer coefficients in mini-channel

5.2.1 Methodology and study description

In this paragraph, the experimental study that has been made to characterize the heat transfer rate by forced convection in the mini-channels is presented. It is important to notice that this analysis is a continuation of the analysis made by Bavière (2005).

Bavière *et al.* (2006) have showed previously that it can exist an experimental bias due to the measurement of the mini-channel wall temperature. This temperature allow for the estimation of the heat transfer coefficients, as it will be presented in § 5.2.2. The main difficulty related to this temperature measurement was related to the important dimension of the temperature sensors regarding the characteristic scale of the studied flows. The size of these sensors may lead to an experimental bias related to their direction regarding the heat flux streamlines, that is dependent on the amplitude of the heat transfer rate between the mini-channel walls and the fluid flow also. Bavière *et al.* (2006) have thus proposed a correlation that allow for the correction of the measured wall temperature :

$$T_{p,real} = T_{p,measured} - 0.24 \times 10^{-4} q'' \quad (5.7)$$

with q'' ($W.m^{-2}$), the heat flux on the lateral surfaces of the mini-channel and the temperatures are given in K .

The results of current study have been obtained for mini-channels having smaller widths ($a = 2.3 - 4 - 5.6$ and $8mm$) than the ones used previously ($a = 25mm$) by Bavière *et al.* (2006). The 3D effect impacted significantly the flow in our configuration. In addition, as showed by the analysis made by Maranzana that has been reported by Bigot (2005) (equation (1.24)), the difference between the thermophysical properties of water and forane 365 HX may lead to a modification of the heat flux distribution along the mini-channels walls.

5.2.2 Determination of the heat transfer coefficients

The evolution of the heat transfer coefficient (for an internal flow) depends on several parameters namely :

- ▷ the mini-channel wall heat flux (q''),
- ▷ the test section inlet liquid temperature (T_{amont}),
- ▷ the mass flow rate (\dot{m}),

Section 5.2. Study of the heat transfer coefficients in mini-channel

▷ the constitutive laws that characterize the variation of the fluid thermophysical properties (specific heat (c_p) and thermal conductivity (λ_l)⁵),

▷ the longitudinal position where the wall temperature was measured (z_i).

For determining the evolution of the heat transfer coefficients, the outlet temperature (T_{aval}) was measured whereas the difference between the wall and the fluid mixture temperature on the channel cross section ($T_p(z) - T_l(z)$) has been calculated. Similarly to the study made for analyzing the friction coefficient, the fluid specific heat and thermal conductivity have been estimated using the mean fluid temperature upstream and downstream the test section. By neglecting the thermal power due to the viscous dissipations, the wall convective heat flux can be approximated following :

$$\Phi_{conv} \approx \dot{m}c_p(T_{aval} - T_{amont}) \quad (5.8)$$

By assuming a uniform heat flux distribution at the solid/liquid interface on a length that corresponded to the heated length (L) of the channel it can be written that :

$$q'' = \frac{\Phi_{conv}}{2(a+b) \times L} \quad (5.9)$$

The increase of the fluid enthalpy on a cross section can then be expressed as :

$$T_l(z) = T_{amont} + \frac{\Phi_{conv}}{\dot{m}c_p} \frac{z}{L} \quad (5.10)$$

Using this value, the heat transfer coefficient can be calculated according to :

$$h = \frac{q''}{T_{p,real}(z) - T_l(z)} \quad (5.11)$$

where $T_{p,real}$ was obtained using equation (5.7).

Finally, the Nusselt number expression, which characterize the ratio between the convective heat transfer to the conductive one, is given as :

$$Nu = \frac{hd_h}{\lambda_{film}} \quad (5.12)$$

5. The water thermal conductivity (or the one of forane 365 HX) which has been used for the determination of the Nusselt number, was estimated regarding the local fluid temperature (T_{film}) close to the wall. This temperature has been defined by using the mean values of the local wall and fluid mixture temperatures on a channel cross section.

where d_h is the hydraulic diameter and λ_{film} , the thin liquid film thermal conductivity close to the wall⁶.

It can be observed that the variation of the Nusselt number may be changed regarding the position z_i and regarding the thermal boundary layers development. Thus for comparing the Nusselt numbers that were obtained for the four wall thermocouples, it was relevant to represent these Nusselt numbers regarding a non-dimensional length (z^* - defined on § 1.1.2). This length is a representation of the development status of the thermal boundary layers. Therefore, when the thermal boundary layers were fully developed, the Nusselt number should be of same amplitude on each of the cross sections of the flow (except for the entrance conditions). This length can be calculated using :

$$z_i^* = \frac{1}{RePr} \frac{z_i}{d_h} \quad (5.13)$$

where Pr is the Prandtl number.

It was possible to remark that for similar heat flux conditions, the liquid temperature increase was more pronounced for forane 365 HX than for water due to the difference in the specific heat values.

5.2.3 Experimental uncertainties

The measurement uncertainty on Nusselt number calculation was done using the methodology given by Kline et McClintok (1953) (error propagation) :

$$i_{(Nu)} = \pm \sqrt{\left(\frac{\partial Nu}{\partial d_h} i_{(d_h)}\right)^2 + \left(\frac{\partial Nu}{\partial \lambda_l} i_{(\lambda_l)}\right)^2 + \left(\frac{\partial Nu}{\partial h} i_{(h)}\right)^2} \quad (5.14)$$

In this paragraph the expression of each of these terms will not be detailed. In addition, for increasing the readability, it has been decided to show the variation of the experimental uncertainties for the whole set of cases that have been analyzed in this chapter.

6. It was assumed that the value of this thermal conductivity depended on the mean value of the wall and fluid mixture temperature on a cross section

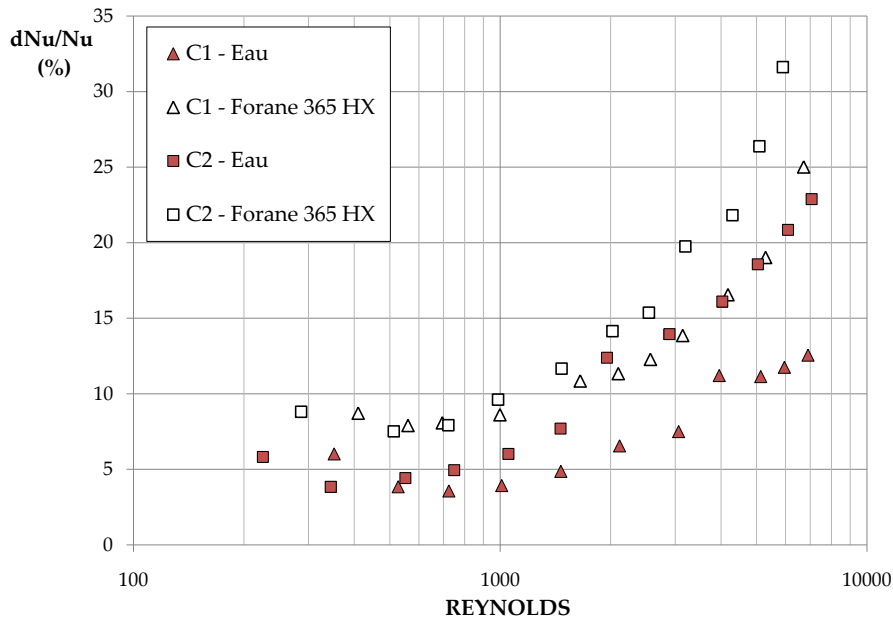


FIGURE 5.10 – Experimental uncertainties related to the Nusselt number determination

The data from Figure 5.10 showed that the measurement uncertainty increased with the Reynolds number (significant increase for Reynolds number larger than 1000). Indeed, for the more important flow rates, the difference between the channel inlet and outlet temperatures become small. The uncertainty associated with the determination of the convected thermal power became more important and led to a higher uncertainty for the determination of the Nusselt number⁷. Furthermore, whatever the fluid used, this uncertainty was more pronounced for C_2 mini-channel ($a = 5.6 \text{ mm} - b = 0.816 \text{ mm}$).

On Tables 5.4 and 5.5 are given the main contributions to total uncertainty for each of the Reynolds number window.

7. It can be highlighted that for making these direct comparisons between the two fluids Figure 5.10 cannot be used. This is related to the fact that electrical power that was imposed to the test section was different regarding the fluid that had been used. For this representation, the electrical power imposed for water was of 55 W , whereas it was of 20 W when forane 365 HX has been used

Chapitre 5. Single-phase flow in mini-channels

Window of Reynolds number	Mean dNu/Nu on the Reynolds window (%)	Main contribution	Contribution to total uncertainty (%)
C_1 - height = 1 mm - width = 2.3 mm			
352 - 526	± 5.3 %	\dot{m}	62.2 %
526 - 6903	± 8.1 %	$T_{aval} - T_{amont}$	70.5 %
C_2 - height = 0.816 mm - width = 5.6 mm			
225 - 345	± 5.7 %	\dot{m}	64.4 %
345 - 7064	± 11.8 %	$T_{aval} - T_{amont}$	69.5 %

TABLE 5.4 – Main contributions to global uncertainty (water)

For the study of the two fluids and for these two tested hollowed plates, the most important parameters for determining the Nusselt number were related to the flow rate estimation (for low value of flow rates) and mainly to the difference between the test section inlet and outlet temperatures. Indeed, these two values were important because they played an important role for the calculation of numerous parameters that have been defined in the preceding sections.

Window of Reynolds number	Mean dNu/Nu on the Reynolds window (%)	Main contribution	Contribution to total uncertainty (%)
C_1 - height = 1 mm - width = 2.3 mm			
409 - 6717	± 12.9 %	$T_{aval} - T_{amont}$	73.8 %
C_2 - height = 0.816 mm - width = 5.6 mm			
286 - 5896	± 15.9 %	$T_{aval} - T_{amont}$	82.9 %

TABLE 5.5 – Main contributions to global uncertainty (forane 365 HX)

5.2.4 Measurements and results

Similarly to the friction coefficients calculation, the results were obtained firstly for demineralized water and then for forane 365 HX as working fluid. As specified previously the difference between the thermophysical properties of these two fluids led to set different heating powers. In order to avoid the onset of nucleate boiling for single-phase conditions, the heating power

was limited 20 W for the experiments that were made with forane 365 HX. The experiments that were done with water have been made for an heating power of 55 W⁸.

Working fluid : water

In laminar flow regime, the Lee et Garimella (2006) (§ 1.1.2) correlation that predicts the evolution of the Nusselt number regarding z^* , may be re-adapted for being Reynolds number dependent. However, the reader may notice that for this case, a same Reynolds number can correspond to different state of boundary layers development and therefore to different Nusselt number regarding the position where the flow is considered in the mini-channel. Thus for drawing this law regarding the Reynolds number, it was necessary to define first a position of reference z_i . It was chosen, in a arbitrarily way, to represented the evolution of the correlation of Lee et Garimella (2006) for the $n^{\circ} 3$ wall thermocouple.

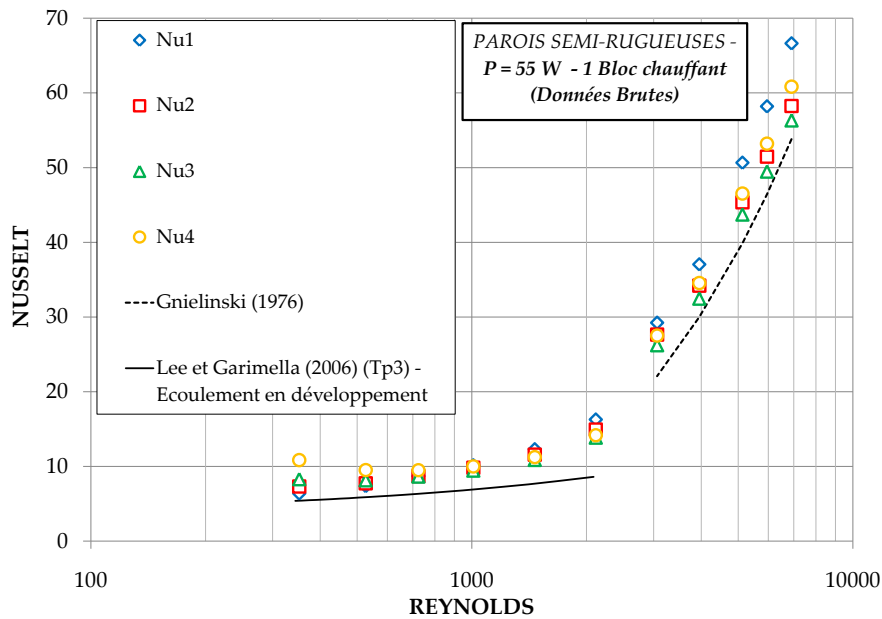


FIGURE 5.11 – Evolution of the Nusselt number regarding the Reynolds number for C_1 mini-channel ($a = 2.3 \text{ mm}$, $b = 1 \text{ mm}$); working fluid : water

Figure 5.11 showed the evolution of the Nusselt number for the C_1 mini-channel ($a = 2.3 \text{ mm} - b = 1 \text{ mm}$) with water used as fluid. An MAE of 41.8% was obtained by comparing the experimental data to the predictive method of Lee et Garimella (2006). As showed, the theoretical

8. The electrical power was not kept to 20 W for water because of the too low temperature difference between the test section inlet and outlet temperatures. For a test case realized with water with an electrical power of 36 W, a maximal uncertainty of 56% for the C_2 plate ($a = 5.6 \text{ mm} - b = 0.816 \text{ mm}$), for a Reynolds number of about 7000.

Chapitre 5. Single-phase flow in mini-channels

values tend to under-estimate the experimental data points. During these tests campaigns, the only parameter that was not controlled precisely was the heat flux distribution at the solid / liquid interface. Thus, it was though that an interesting clue that would allow for the explanation of this difference was related to the estimation of this wall heat flux (§ 5.3).

The difference compared to Gnielinski (1976) correlation (§ 1.2.2) was of 14.7%. As this difference was comprised in the error bars (Figure 5.10) no disagreement were considered between this correlation and the experimental data points. It was observed that for all the hollowed plates, the Nusselt numbers that have been obtained at the location of the thermocouple $n^{\circ}1$ was always higher than for the three other thermocouples in turbulent regime. These results were due to the location of this thermocouple ($\approx 8 \text{ mm}$ from the channel entrance), where entrance effect were more pronounced and tend to improve the heat transfer rate. In summary, it was noticed that these correlations were able to predict almost 71% of the experimental data points at $\pm 21\%$ as showed in Figure 5.12.

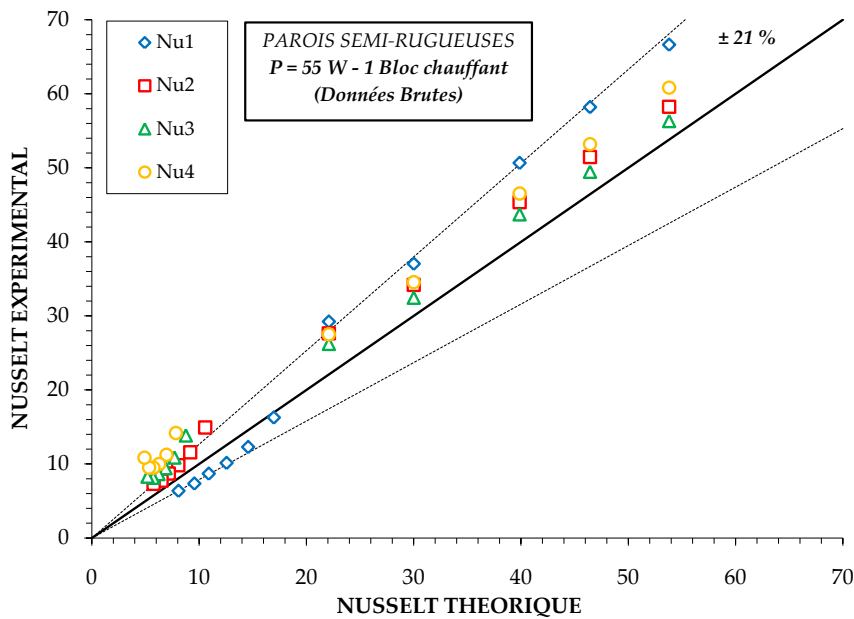


FIGURE 5.12 – Comparison between experimental / theoretical Nusselt number for C_1 mini-channel ($a = 2.3 \text{ mm}$, $b = 1 \text{ mm}$); working fluid : water

After analyzing the data that were obtained with C_1 mini-channel ($a = 2.3 \text{ mm} - b = 1 \text{ mm}$), the evolution of the heat transfer rate for C_2 mini-channel ($a = 5.6 \text{ mm} - b = 0.816 \text{ mm}$) was studied. Figure 5.13 gives the evolution of the Nusselt number in comparison with the Reynolds number for C_2 .

By comparing the experimental data to the Lee et Garimella (2006) correlation, an AME of 19.2% was obtained. This result suggested that by increasing the mini-channel width, the

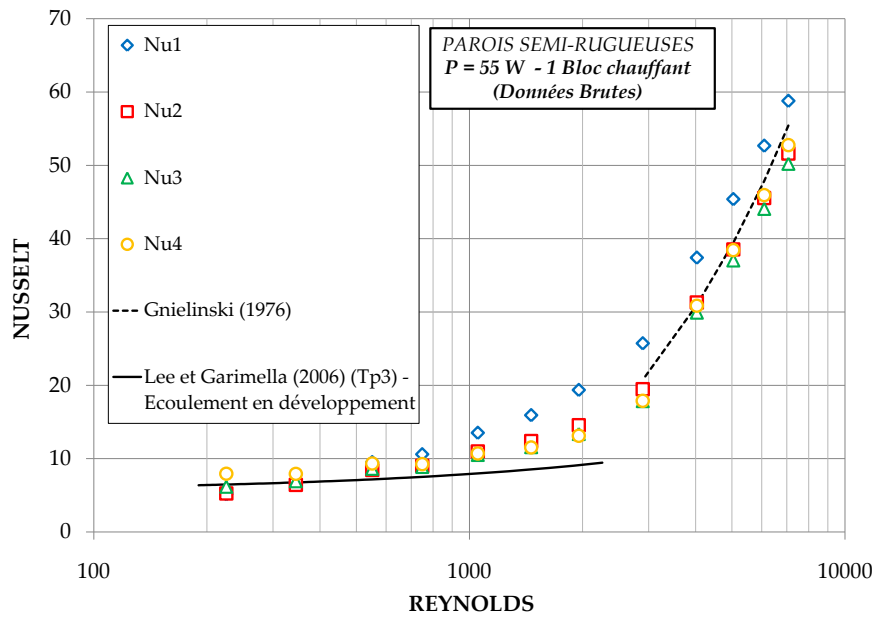


FIGURE 5.13 – Evolution of the Nusselt number in function of Reynolds number for C_2 mini-channel ($a = 5.6 \text{ mm}$, $b = 0.816 \text{ mm}$); working fluid : water

difference between the predictive method of Lee et Garimella (2006) and the experiments tend to be reduced. This behavior remain compliant with the number that has been defined in Bigot (2005). The difference between the data and the Lee et Garimella (2006) approach was supposed to be due to the wall heat flux distribution at the solid / liquid interface that was not measurable during the experiments. However, a numerical analysis that allow for the estimation of this distribution has been discussed in § 5.3.

The deviations between the experimental data points and the Gnielinski (1976) correlation were acceptable (regarding the measurement uncertainties that have been given in Figure 5.10) and reached 7.9%. These correlations predicted 68.8% of the experimental data points at $\pm 15\%$ as showed in Figure 5.14.

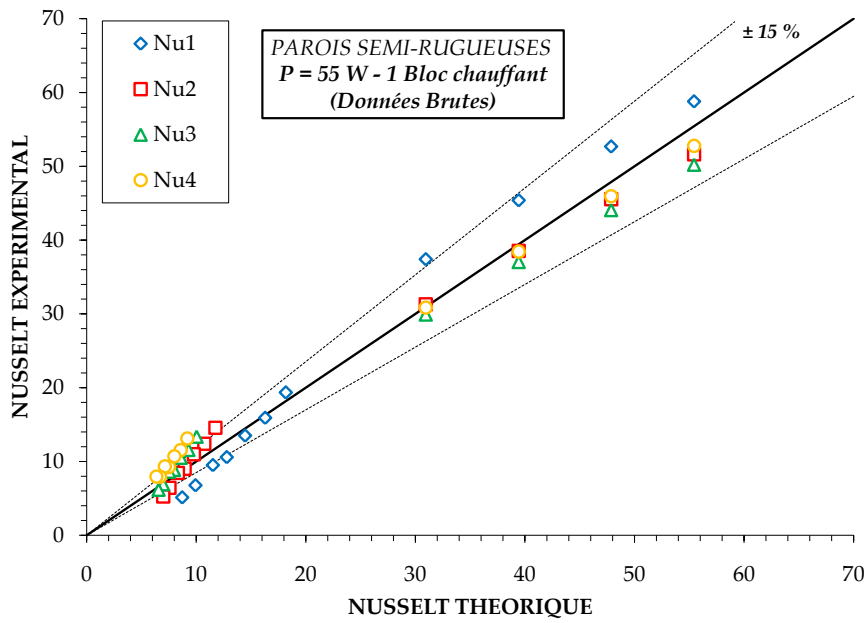


FIGURE 5.14 – Comparison between the experimental / theoretical Nusselt numbers for C_2 mini-channel ($a = 5.6 \text{ mm}$, $b = 0.816 \text{ mm}$) ; working fluid : water

During this study, made with these two hollowed tests plates, it was observed that when the turbulent regime took place ($Re > 3000$), the Gnielinski (1976) correlation predict relatively well the data points that were obtained experimentally (regarding the experimental uncertainties - Figure 5.10). However, when the flow regime became laminar, a difference may be noticed between the experimental data points and the Lee et Garimella (2006) correlation. For studying more deeply the evolution of the Nusselt number in laminar regime, or for analyzing the occurrence of the critical Reynolds number (transition to turbulence), it was more straight to represent the evolution of the Nusselt number in function of z^* (equation 5.13), which expressed, the status of the thermal boundary layers development. Figure 5.15 shows the Nusselt number variation for all the thermocouples.

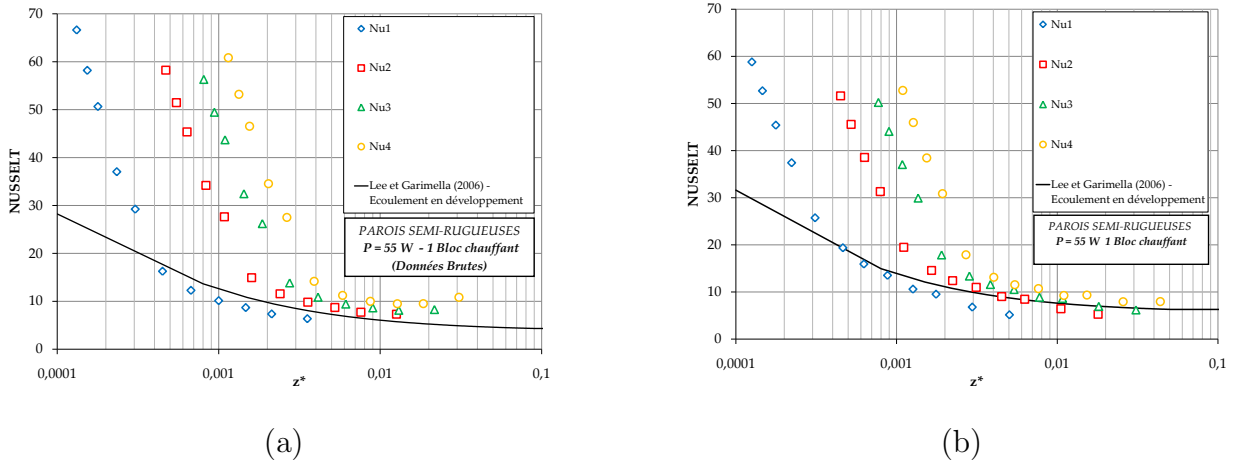


FIGURE 5.15 – Evolution of the Nusselt number in function of z^* with water for : (a) C_1 mini-channel ($a = 2.3 \text{ mm} - b = 1 \text{ mm}$) and, (b) C_2 plate ($a = 5.6 \text{ mm} - b = 0.816 \text{ mm}$)

The laminar regime (z^* is high and the Nusselt number variation is small) and the turbulent regime (z^* is small and the Nusselt number variation is large) can be easily determined on this figure. The transition to turbulence can be located by analysing the change of slope that took place during the evolution of the experimental Nusselt number on Figure 5.15. Thus, it was calculated that the critical Reynolds number was comprised between 2115 and 3063 for C_1 and between 1954 and 2893 for C_2 . It was noticed, that the experimental Nusselt numbers were generally over-estimated, then under-estimated in the direction T_{p1} to T_{p4} .

The reader may noticed that the Lee et Garimella (2006) correlation predict a complete thermal boundary layer development for a z^* equaled to 0.05 for C_1 mini-channel ($a = 2.3 \text{ mm} - b = 1 \text{ mm}$) and equivalent to 0.023 for C_2 mini-channel ($a = 5.6 \text{ mm} - b = 0.816 \text{ mm}$). This means that above these values, a same z^* should correspond to a common Nusselt number, what was not observed experimentally. It was though that this phenomena may be due to the heat flux repartition at the solid / liquid interface. This idea was the most promising for explaining these evolutions. Therefore, this heat flux distribution was analysed using a numerical approach that is presented in § 5.3.

In addition, by observing more closely the number defined by Maranzana *et al.* (2004) that was later modified by Bigot (2005), it was concluded that the conduction effect of the heat flux through the walls may become significant for low value of flow rates, what may be the cause of the deviations that were observed for our experimental data points in these situations. It can be recalled that his number was written as :

$$M' = \frac{\lambda_p}{\rho_l c_{pl} u L} \frac{e_p \times l_p}{a \times b} \quad (5.15)$$

where ρ_l is the liquid mass density, c_{pl} the liquid specific heat, u the flow rate in the duct and l_p , the heated length of the plate. The whole set of geometrical dimensions has been given on Figure 1.5. The variation of this number M' , during the current analysis has been reported on Figure 5.16.

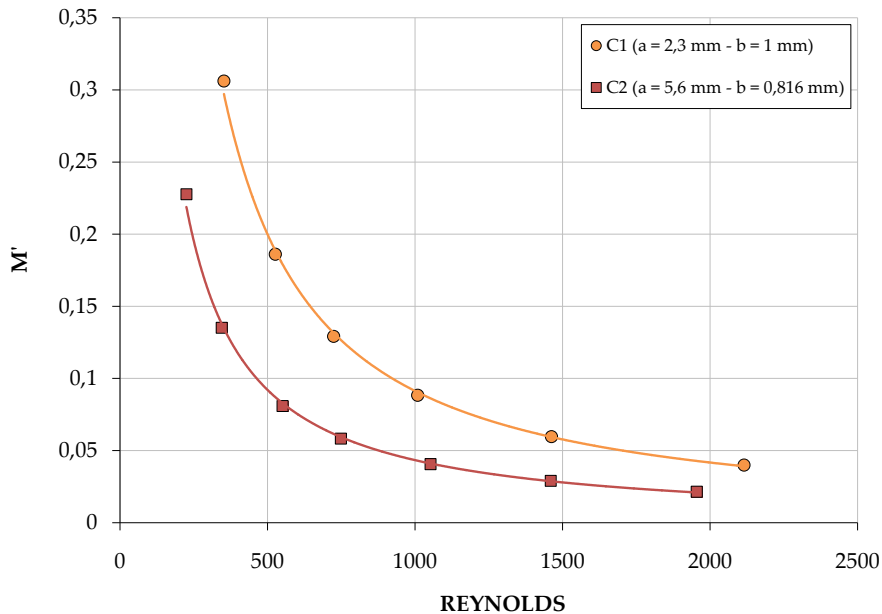


FIGURE 5.16 – Evolution of the Maranzana *et al.* (2004) number modified by Bigot (2005) for C_1 and C_2 mini-channels with water as working fluid

The numerical study made by these authors was initially realized for a plain 2D channel (channel width was considered as large). The results that have been obtained suggested that when M' (equation (1.23)) was larger than 0.05, the conduction heat flux was no more negligible compared to the longitudinal heat flux. For these case, the temperature profile can become distorted compared to a linear evolution. Therefore, according to this approach, specific analysis is required for Reynolds number lower to 1500. This analysis regarding the heat flux distribution was done using an numerical approach that ha been discussed in § 5.3.

Working fluid : forane 365 HX

In order to compare the working fluid impact on the heat transfer rates in the mini-channels, forane 365 HX was used inside the same experimental device. Figure 5.17 showed the evolution of the Nusselt number in function of the Reynolds number for C_1 mini-channel ($a = 2.3\text{mm} - b = 1\text{mm}$).

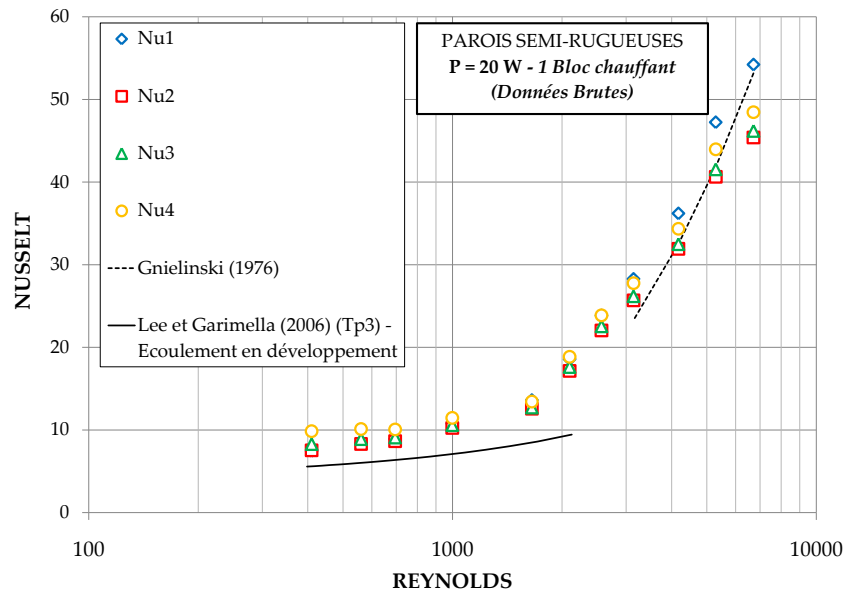


FIGURE 5.17 – Evolution of the Nusselt number in function of the Reynolds number for C_1 mini-channel ($a = 2.3 \text{ mm}$, $b = 1 \text{ mm}$); working fluid : forane 365 HX

Similarly to the results that were obtained for water, a high AME was obtained for forane 365 HX during the laminar regime (46.6% in comparison with the Lee et Garimella (2006) prediction). For the turbulent regime, an AME of 13.1% was obtained compared to the Gnielinski (1976) correlation.

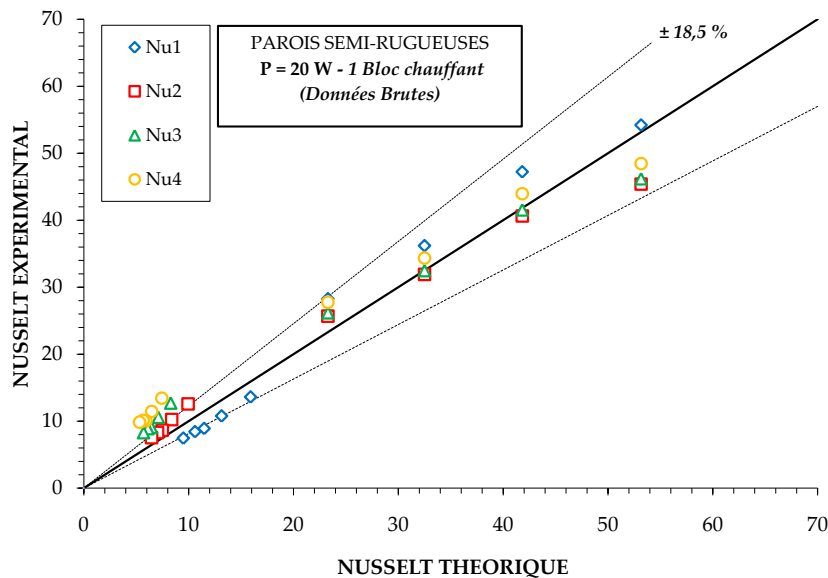


FIGURE 5.18 – Comparison between experimental / theoretical Nusselt number for C_1 mini-channel ($a = 2.3 \text{ mm}$, $b = 1 \text{ mm}$); working fluid : forane 365 HX

Chapitre 5. Single-phase flow in mini-channels

These two correlations were able to predict 68.2% of the experimental data points at $\pm 18.5\%$ as showed in Figure 5.18.

After studying the results that have been obtained for C_1 mini-channel ($a = 2.3 \text{ mm} - b = 1 \text{ mm}$), the impact of the channel geometry was analyzed on the heat transfer rate by using C_2 mini-channel ($a = 5.6 \text{ mm} - b = 0.816 \text{ mm}$). The experimental data that have been reported on Figure 5.19 give the evolution of the Nusselt number in function of the Reynolds number for C_2 .

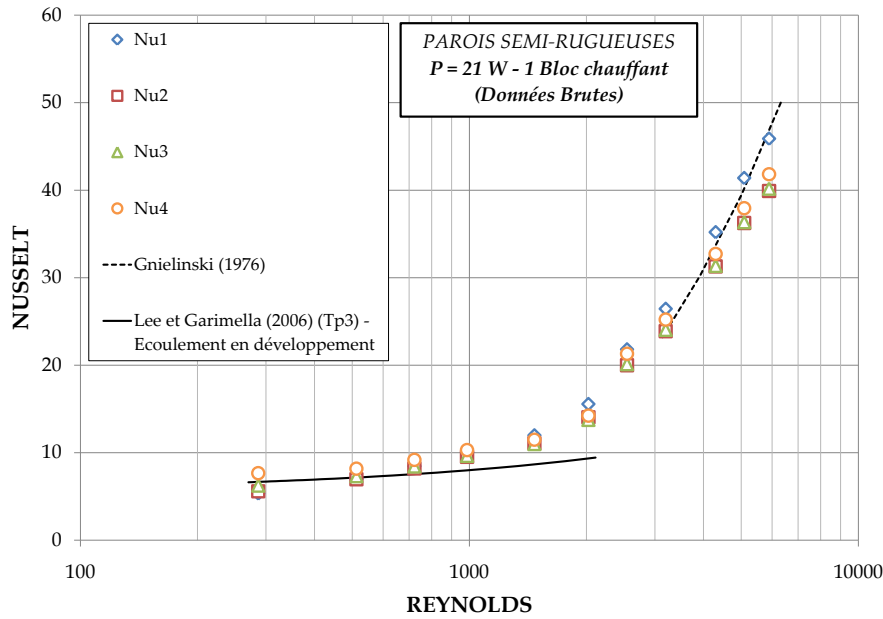


FIGURE 5.19 – Evolution of the Nusselt number regarding the Reynolds number for C_2 mini-channel ($a = 5.6 \text{ mm}$, $b = 0.816 \text{ mm}$); working fluid : forane 365 HX

Still here, and similarly for water used as working fluid, it was observed that the increase of the mini-channel width allow for the reduction of the difference between the experimental data points and the Lee et Garimella (2006) correlation. Thus, an AME of 21.4% was calculated for this flow regime. When the flow become turbulent, the AME dropped to 8.3% compared to the Gnielinski (1976) prediction.

These correlations can predict 69.4% of the experimental data points at $\pm 15\%$ as showed in Figure 5.20.

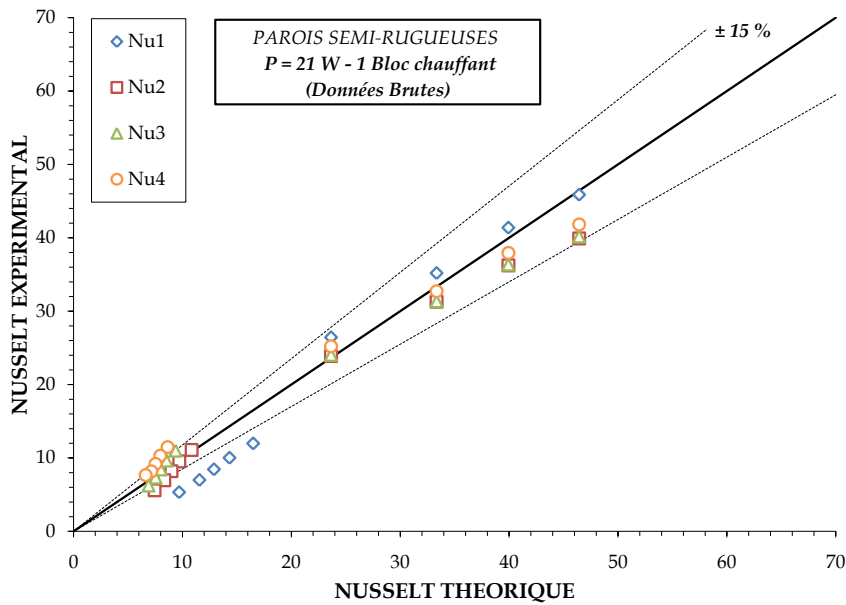


FIGURE 5.20 – Comparison between the experimental / theoretical Nusselt number for C_2 mini-channel ($a = 5.6 \text{ mm}$, $b = 0.816 \text{ mm}$); working fluid : forane 365 HX

Figure 5.21 showed the evolution of the thermal boundary layers development by representing the Nusselt number in function of the non-dimensional thermal length, z^* . The theoretical conditions that led to the full development of the thermal boundary layers did not depend on the aspect ratio variation according to the Lee et Garimella (2006) approach. Therefore, the non-dimensional thermal lengths that correspond to this full development will be kept the same compared to the case with water as working fluid.

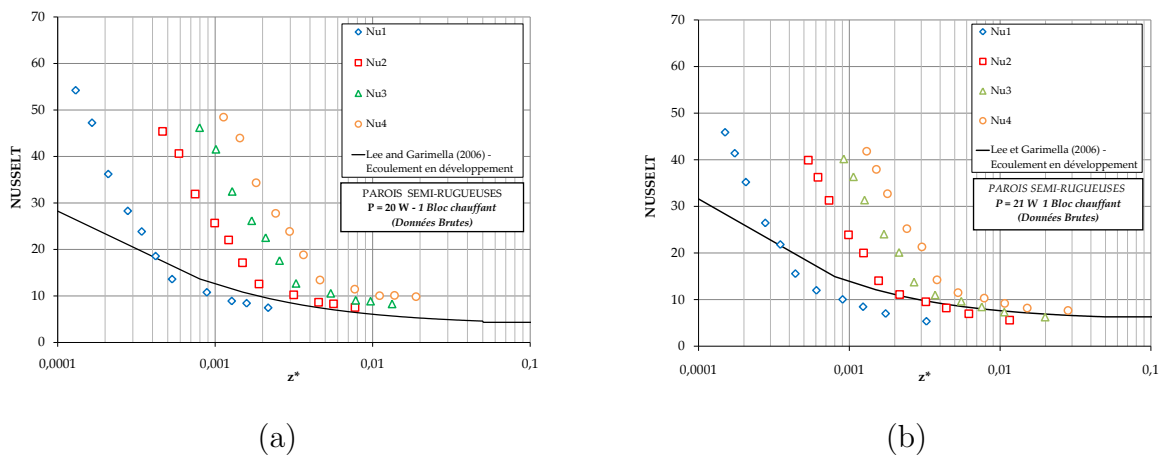


FIGURE 5.21 – Evolution of the Nusselt number in function of the number z^* with forane 365 HX for : (a) $C_1(a = 2.3 \text{ mm} - b = 1 \text{ mm})$ (b) $C_2(a = 5.6 \text{ mm} - b = 0.816 \text{ mm})$

For these tests, the critical Reynolds number was comprised between 1651 and 2097 for C_1 and between 2023 and 2542 for C_2 . It can be noticed that according to the evolution of the number M' (equation 5.15), the heat flux conduction effect in the wall of the test section seemed to become more significant for the study made with forane 365 HX as working fluid. On Figure 5.22, the evolution of this number regarding the Reynolds number was reported.

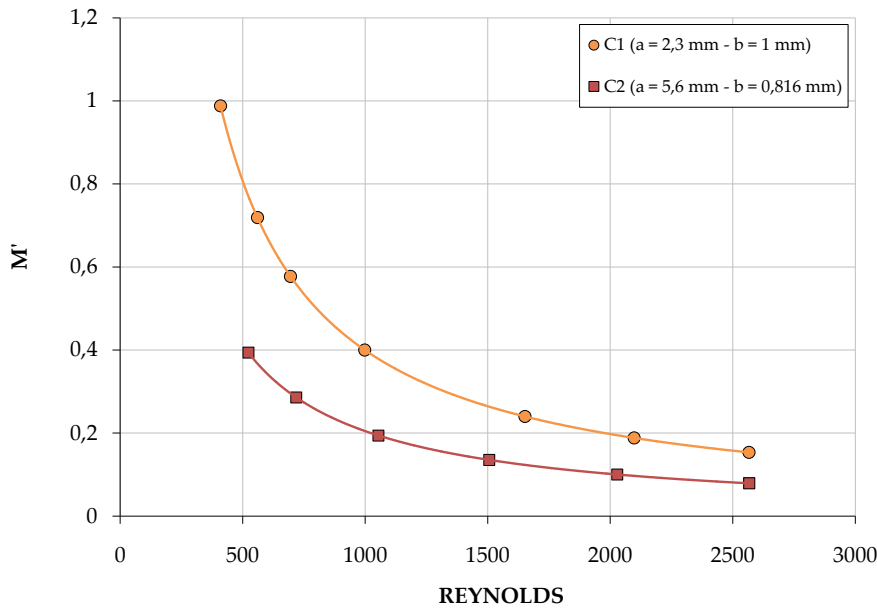


FIGURE 5.22 – Evolution of the number defined by Maranzana *et al.* (2004) and modified by Bigot (2005) for C_1 and C_2 mini-channels for forane 365 HX as working fluid

The data given in Figures 5.16 and 5.22, showed that the impact of the conduction heat flux should be more pronounced for forane 365 HX than for water as working fluid. Therefore, for the use of forane 365 HX, the evolution of the heat flux distribution at the mini-channel solid/liquid interface should be different compared to an homogeneous distribution.

Regarding these experimental results, it was estimated as more relevant to build a numerical model (§ 5.3) that was able to determine what was the distribution of the heat flux along the mini-channel walls in the case of laminar flow regime. This study was preceded by the preliminary numerical analysis that was made by Lancereau (2008). These first numerical results were obtained using Fluent 6 (2001) on a simplified model⁹ of the test section, in order to give the information regarding the repartition of the wall temperatures profiles. During this work, Lancereau (2008) evaluated the variation of the heat flux profiles at the solid/liquid interface. The numerical results have allow for the consolidation of the idea that the experimental heat flux may differ from a homogeneous distribution due to the axial conduction of the heat flux through

9. The mini-channel only was represented

the test section wall. However, due to the partial representation of the test section, several assumptions were made, particularly on the entrance boundary conditions. As a consequence, a singular effect that led to a very important heat flux at the mini-channel entrance appeared for these numerical data and it was not possible to obtain qualitative values related to this heat flux distortion compared to the experimental set-up. Therefore, it was decided, taking advantage of this model, to represent in a more detailed way the test section that was used and to limit as much as possible the simplifying assumptions.

Summary on the heat transfer coefficients determination for single-phase flow

The experimental heat transfer coefficients that were obtained for single-phase flow conditions have been in good agreement with the Gnielinski (1976) correlation, that has been defined for turbulent conditions. However these coefficients were less well predicted for laminar flows. At the end of the analysis, it was guessed that this behavior was due to the impact of the heat flux distribution that may differ compared to a homogeneous repartition that took place more specifically at low flow rates. In addition, it was noticed that the theoretical heat transfer coefficients predicted relatively better the data that were obtained for C_2 mini-channel ($a = 5.6\text{ mm}$, $b = 0.816\text{ mm}$) compared to those obtained for C_1 mini-channel ($a = 2.3\text{ mm}$, $b = 1\text{ mm}$) for laminar flow regime. Therefore, it was though that the mini-channel geometry impact could allow for the modification of this heat flux repartition.

The whole set of results that was obtained in this paragraph may be summarized according to the data reported in Table 5.6.

Plate	Fluid	Lee et Garimella (2006)	Gnielinski (1976)	Crit. Reynolds
C_1	water (demin.)	AME = 41.8 %	AME = 14.7 %	2115 - 3063
	forane 365 HX	AME = 46.6 %	AME = 13.1 %	2023 - 2542
C_2	water (demin.)	AME = 19.2 %	AME = 7.9 %	1954 - 2893
	forane 365 HX	AME = 21.4 %	MAE = 8.3 %	1651 - 2097

TABLE 5.6 – AME regarding heat transfer coefficient correlations and critical Reynolds number

The results that have been given in this table showed that the difference between the correlations of reference remained approximately the same (considering the mean values) whatever the fluid used or the flow regime that was developed through each of these mini-channels. It was reported that the difference that were noticed as most significant were obtained for laminar flow regime.

Finally, it was demonstrated that the Nusselt numbers may evolved, in function of the non-dimensional length (z^*), when the thermal boundary layer development was complete in a theoretical point of view. Therefore, in order to better understand these experimental results and to corroborate (or not) this assumption related to the heat flux distribution, a numerical model that allow for the representation of the heat transfer rate on the mini-channel wall was built (§ 5.3).

5.3 Conjugated (heat/flow) numerical analysis

In this paragraph, the results from the numerical analysis regarding the flow that took place inside the tests section¹⁰ for imposed heat flux conditions have been reported. The aim of this study was to estimate numerically the mean heat flux distribution on the heat exchange surface of the different mini-channels. This work resulted in the definition of an estimation factor that allow for the correction of the fluid enthalpy increase and of the wall temperatures inside the mini-channels. The numerical model description as well as the mesh sensitivity calculation have been given in Appendix E.

5.3.1 Numerical results

After modeling the test section and the flow that took place inside the different mini-channels, the heat flux distribution at the solid/liquid interface was studied for similar conditions compared to experiments. The main difficulty regarding this study was related to the fact that three different heat transfer surfaces were in contact with the working fluid. This induced a modification of the heat transfer rate that was exchanged on each of these surfaces. The heat flux rate was always more important for the lower surface that was in brass (which contained the heating cartridges). In this paragraph, the data that have been obtained for C_2 mini-channel ($a = 5.6 \text{ mm} - b = 0.816 \text{ mm}$) have been given. Indeed, for this plate, the impacts of numerous operating conditions were evaluated whereas for the other plates, only the impacts of the flow rate and of the working fluids have been analyzed.

☞ *Impact of the flow rate on the heat flux distribution*

The impact of the flow rate on the evolution of the heat flux distribution was reported on Figure 5.23¹¹, with water as working fluid and with a dissipated power of 55 W.

On this figure, \bar{q}'' was the ratio between the heat flux at the location z and the mean heat flux and \bar{z} was the ratio between a location z (located in the mini-channel) to the total heated length :

$$\begin{cases} \bar{q}'' &= q'' / q_{moy} \\ \bar{z} &= z / L \end{cases} \quad (5.16)$$

10. This modeling, realized under specific assumptions has been presented in Appendix E

11. This distribution resulted from the heat flux integrated on all the lateral surfaces of the mini-channel

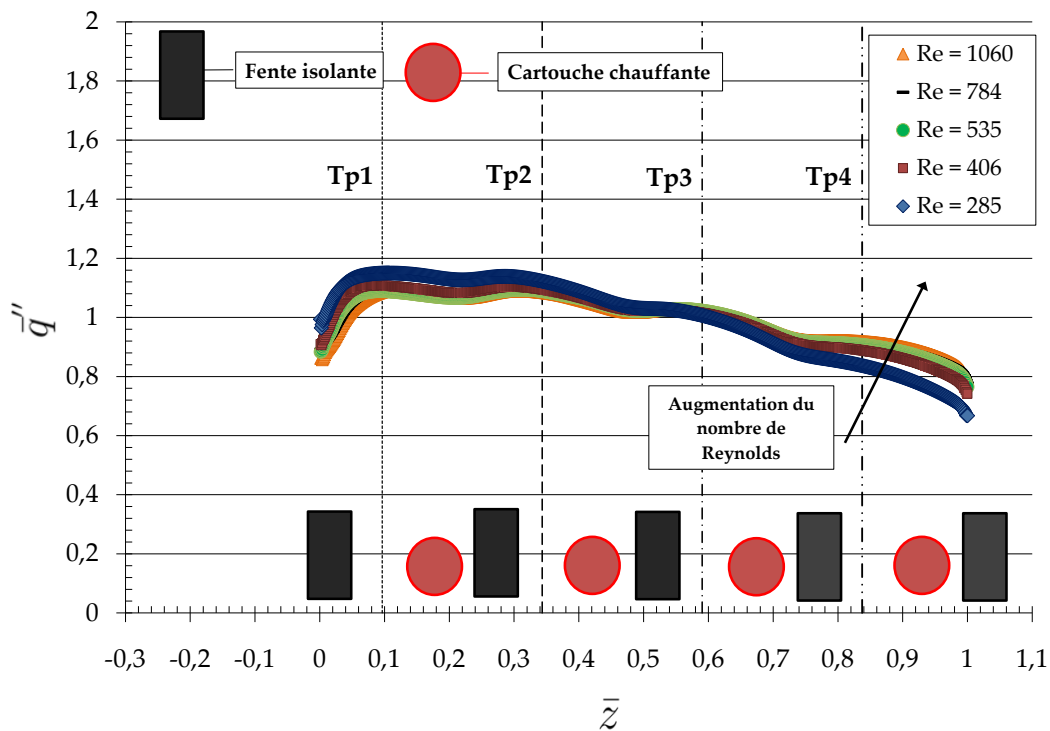


FIGURE 5.23 – Heat flux distribution at the solid/liquid interface in function of the Reynolds number for C_2 mini-channel ($a = 5.6 \text{ mm} - b = 0.816 \text{ mm}$) with water as working fluid for a dissipated power of 55 W

The data taken from Figure 5.23, showed that the mean heat flux distribution evolved with the imposed Reynolds number. The noticeable waves on this distribution were due to the heat flux attenuation related to the insulated compartment where the heating cartridges were inserted. The location and the width of these compartments were represented at scale on this figure. The cartridges and thermocouples locations have been given on this figure also. The numerical results suggested that the heat flux increased slightly at the channel entrance (and consequently decrease near the outlet) when the flow rate was reduced. Indeed, it was deduced, similarly to other studies (Maranzana *et al.* (2004), Bigot (2005) among others) that this behavior was due to the axial heat flux conduction that became more significant at the channel entrance when the flow rate diminished. However, when the flow rate was increased (Reynolds number higher than 406 for this hollowed plate), the impact of the flow rate become smaller regarding this heat flux distribution.

During the study, it was noticed that the liquid convected power in the mini-channel was generally under-estimated regarding the experimental data points (15% average). It was though that this result was caused by the absence of an additional thermal insulation that overlain the lower block. Therefore, it was assumed regarding the experimental point of view that this insulation allow for the limitation of the thermal losses with the environment. However for

Section 5.3. Conjugated (heat/flow) numerical analysis

making sure that the modeling was realistic and particularly regarding the estimation of the heat flux, a comparison between the wall temperatures that were obtained numerically and in experiments was made. Indeed, these wall temperatures variations were inherently related to the heat flux at the solid/liquid interface. Therefore, on Figure 5.24, the representation of the difference between the wall temperature T_{p_i} and the temperature located at $z = 0.008$ (T_{p_1}) for C_2 mini-channel with water as working was given.

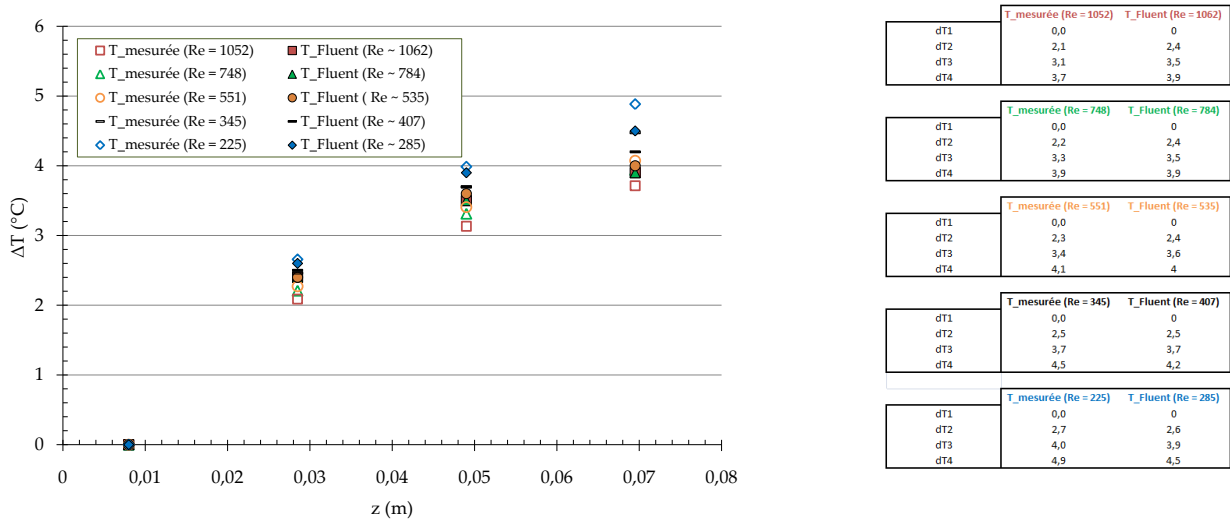


FIGURE 5.24 – Evolution of the differences between the wall temperature and the temperature measured with thermocouple $n^{\circ}1$ along the mini-channel wall for C_2 mini-channel ($a = 5.6\text{mm} - b = 0.816\text{mm}$) for water as working fluid

As it can be noticed, the difference between the evolutions that were obtained with the numerical model and the one obtained through the experiments were relatively small on all the range of studied flow rates. Therefore, these results may lead to suppose that the heat flux was very similar between experiments and modeling. Also, for representing this heat flux, an evolution law that allow for its estimation was defined. This law was Reynolds-dependent, exponential type and can be written according to :

$$\bar{q}'' = \exp(f_1(Re)\bar{z} + f_2(Re)) \quad (5.17)$$

For example, this approximating law has been drawn on Figure 5.25 for C_2 mini-channel ($a = 5.6\text{mm} - b = 0.816\text{mm}$), for water as working fluid and for a Reynolds number equaled to 1060. It should be highlighted that the difference between this law and the numerical profile was lower to 5% (in average) for the whole set of tested cases on the range of \bar{z} that corresponded to the distance included between the wall thermocouples $n^{\circ}1$ and $n^{\circ}4$ for this tests plate.

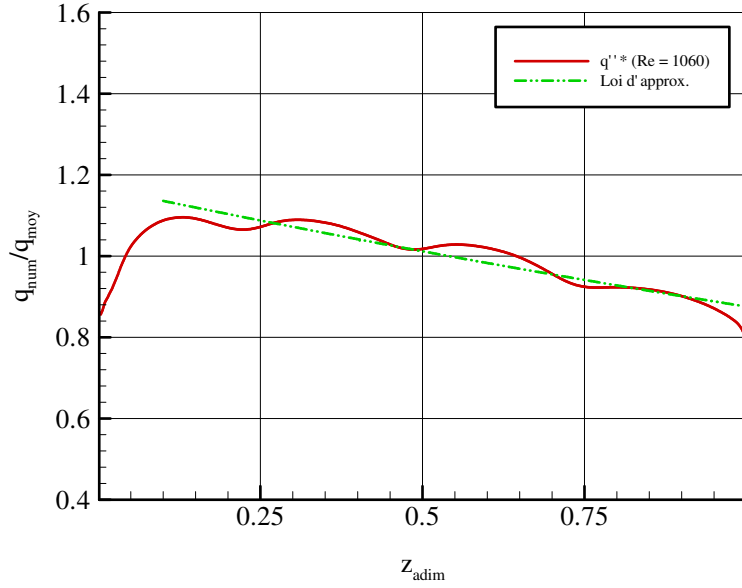


FIGURE 5.25 – Approximation of the heat profile distribution at the solid/liquid interface using an exponential-type law for C_2 mini-channel ($a = 5.6\text{ mm} - b = 0.816\text{ mm}$), for water as working fluid and for a Reynolds number of 1060

For the example of the results that were given for this tests plate, the function $f_1(Re)$ and $f_2(Re)$ that expressed the heat flux evolution in function of the flow rate can be written as¹² :

$$f_1(Re) = -1.82 \times 10^7 \times Re^{-16/5} - 0.2842 \quad (5.18a)$$

$$f_2(Re) = 8.64 \times 10^6 \times Re^{-16/5} + 0.1518 \quad (5.18b)$$

Once this correlation was determined, the fluid enthalpy increase from the mini-channel entrance up to the defined location could be determined. This increase can be calculated with an energy balance that was made on the mini-channel (slight modification of equation (2.24)) according to :

$$T_l(z) = T_{l,in} + \frac{q''_{moy} S}{c_p \dot{m}} \times \int_0^z \exp\left(f_1(Re) \frac{z}{L} + f_2(Re)\right) dz \quad (5.19)$$

The same idea was used when other geometries or other fluid (forane 365 HX) were used. Therefore, these studies were not detailed through this paragraph. However, after the calculation

12. These equations were valid only for the range of \bar{z} comprised between the wall thermocouple location (TP_1) and (TP_4).

of this new evolution law regarding the fluid enthalpy increase, its impact on the heat transfer coefficients was analyzed. This study that allow for the correction of the experimental data will be detailed in § 5.3.2.

Impact of the working fluid on the heat flux distribution

After the analyze regarding the impact of the flow rate on the distribution of the heat flux density at the solid/liquid interface, the working fluid impact on this distribution was studied. For making this comparison, the electrical power¹³ was set to 22 W and the flow velocity to a value in the range 0.42 – 0.45 m.s⁻¹ for the two selected fluids.

These data have been drawn on Figure 5.26.

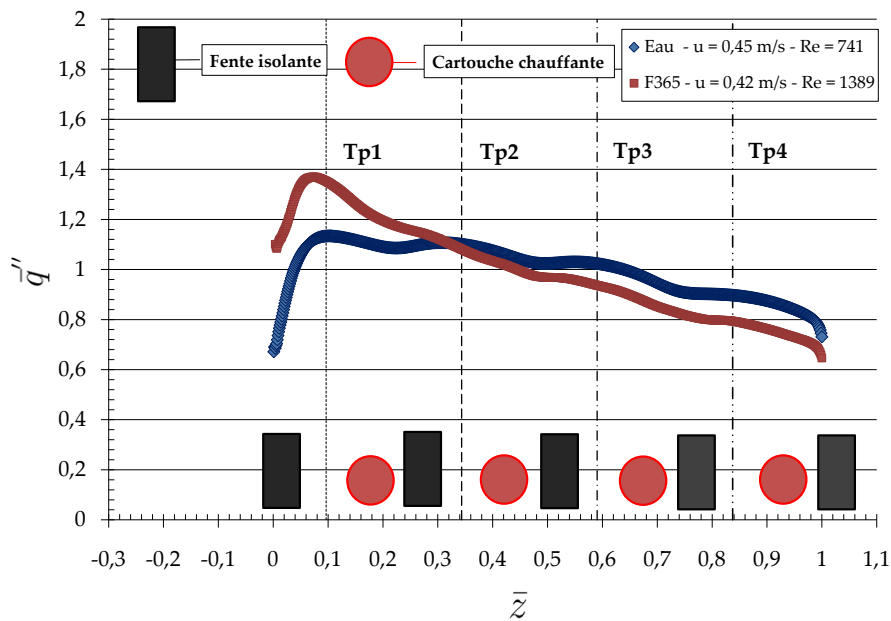


FIGURE 5.26 – Impact of the fluid on the heat flux distribution at the solid/liquid interface of the mini-channel C_2

The data that have been given on this figure showed all the importance of the working fluid selection for studying the heat transfer for a forced convected flow in mini-channels. Indeed, the evolution of the heat flux distribution at the solid/liquid interface was modified when the working fluid was modified. The difference that was reported for this plate may reached a maximal value of 25% between water and forane 365 HX at the mini-channel entrance. It was noticed that the main difference between the heat convection terms came from the specific heat. Therefore, similarly to Maranzana *et al.* (2004), this result showed that the increase of

13. This electrical power has been reduced to make realistic comparison with forane 365 HX.

the specific heat should lead to the homogenization of this heat flux distribution. The functions $f_1(Re)$ and $f_2(Re)$ for forane 365 HX and inside the mini-channel C_2 were expressed as :

$$f_1(Re) = -0.154 \times Re^{1/5} - 1.33 \quad (5.20a)$$

$$f_2(Re) = 0.935 \times Re^{-17/10} + 0.187 \quad (5.20b)$$

Impact of the channel geometry on the heat flux repartition

Figure 5.27 reports the impact of the channel geometry on the heat flux distribution at the solid/liquid interface for water as working liquid.

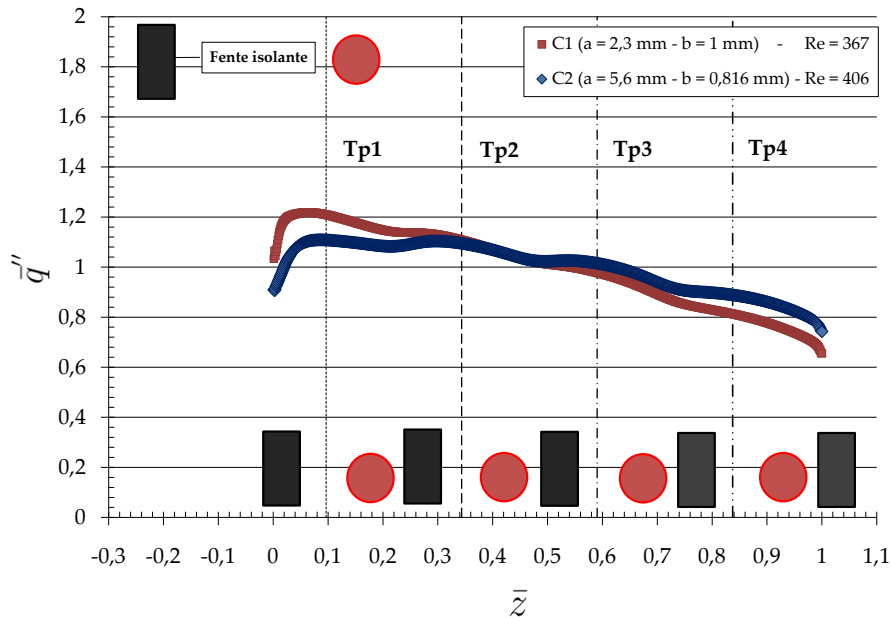


FIGURE 5.27 – Influence of the geometry on the heat flux distribution at the solid/liquid interface for C_1 ($a = 2.3 \text{ mm} - b = 1 \text{ mm}$) and C_2 ($a = 5,6 \text{ mm} - b = 0,816 \text{ mm}$) mini-channels

The data that have been reported on this figure showed that the common impact of the mini-channels width (a) and height (b) could lead to a more homogeneous heat flux distribution. We thought that this homogenization could be explained by the reduction of the impact of the entrance effects. Indeed, these effects tend to be reduced when the channel width increase (case of the C_2 mini-channel ($a = 5.6 \text{ mm} - b = 0.816 \text{ mm}$) regarding the C_1 mini-channel ($a = 2.3 \text{ mm} - b = 1 \text{ mm}$)) and lead consequently to a reduction of the heat flux transferred at the mini-channels entrance. The expression of the functions $f_1(Re)$ and $f_2(Re)$ for C_1 plate ($a = 2.3 \text{ mm} - b = 1 \text{ mm}$) with water as working fluid can be expressed according to :

$$f_1(Re) = 0.955 \times Re^{1/10} - 2.31 \quad (5.21a)$$

$$f_2(Re) = 1.6 \times Re^{-1/10} - 0.6 \quad (5.21b)$$

Similarly than for water used as working fluid, it was proposed using this numerical model an expression for the functions $f_1(Re)$ and $f_2(Re)$ for evaluating the heat flux distribution for forane 365 HX which flowed in the C_1 mini-channel ($a = 2.3 \text{ mm} - b = 1 \text{ mm}$). These functions could be expressed as :

$$f_1(Re) = -3.96 \times 10^{-7} \times Re^{3/2} - 0.738 \quad (5.22a)$$

$$f_2(Re) = 4.41 \times 10^{-4} \times Re^{3/5} - 0.298 \quad (5.22b)$$

5.3.2 Correction of the experimental data

After the determination of the heat flux distribution for the mini-channels, it was assumed that these laws were representative of the evolution of the heat flux distributions that were obtained experimentally. In this context, the mean thermal power transferred between the four walls of the mini-channels and the working fluid was modified and can be calculated along the exchange surfaces. Using this heat flux, the measured wall temperatures were corrected also (using the Fourier relation (1822)) for the estimation of the temperatures at solid/liquid interface. In addition, the determination of the heat flux distribution allow for the calculation of the fluid enthalpy increase from the mini-channel entrance, as presented through equation 5.19. Consequently, and using these three parameters, it was possible to determine the corrected heat transfer coefficients values. The evolution of the experimental Nusselt numbers has been given on Figure 5.28.

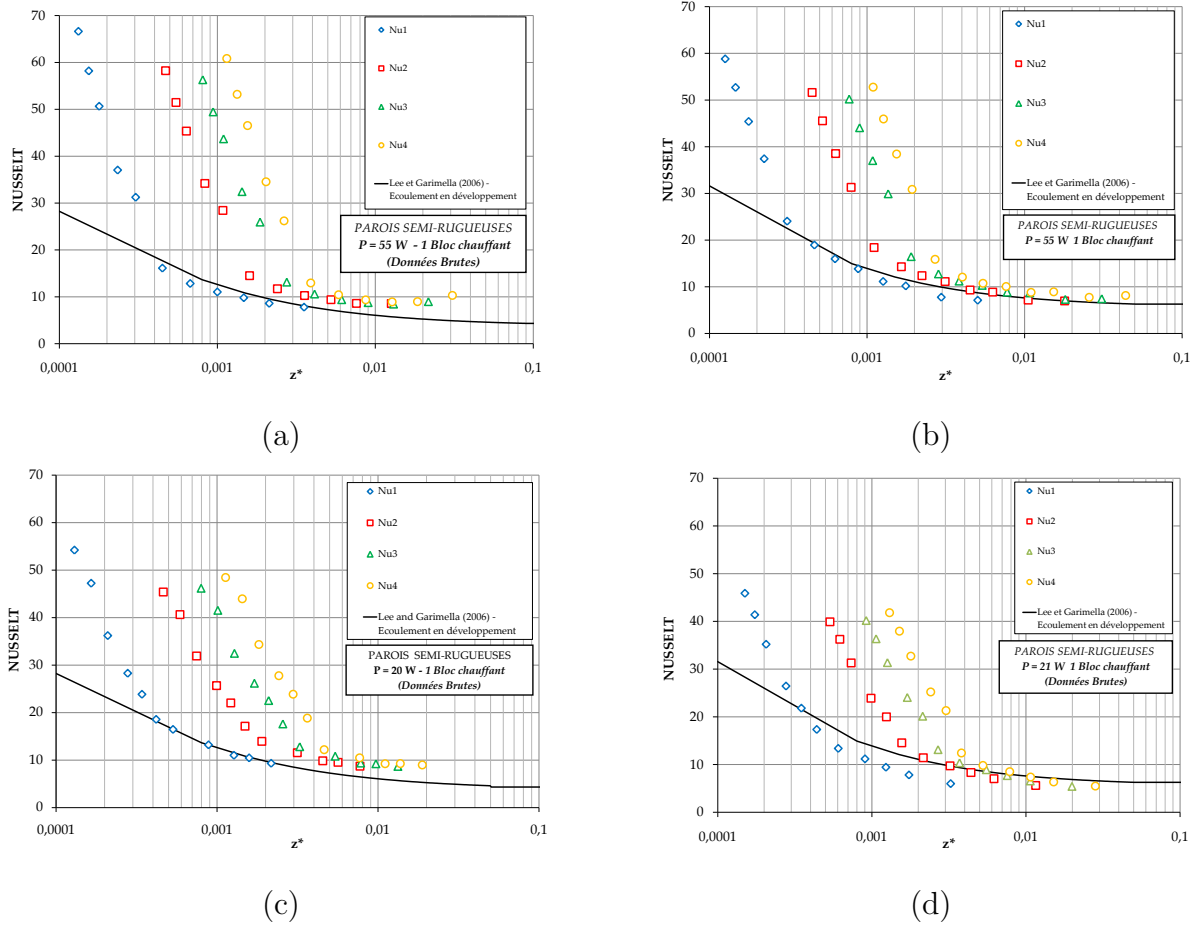


FIGURE 5.28 – Evolution of the Nusselt number in function of the non-dimensional length, z^* , considering a non-uniform heat flux distribution for water with : (a) C_1 (b) C_2 mini-channels, and for forane 365 HX with : (c) C_1 (d) C_2 mini-channels

Using this approach, the reader may noticed that the differences between Lee et Garimella (2006) correlation and the experimental data were slightly reduced compared to the initial analysis (Table 5.6). A summary of these results may be found in Table 5.7.

Plate	Fluid	Lee et Garimella (2006)
C_1	water (demin.)	AME = 38.8 %
	forane 365 HX	AME = 38.1 %
C_2	water (demin.)	AME = 15.1 %
	forane 365 HX	AME = 16.1 %

TABLE 5.7 – AME for the comparison between experiments and Lee et Garimella (2006) correlation

The data that have been reported on Table 5.7, showed that the differences that were observed between the experimental data and the Lee et Garimella (2006) prediction still remained significant. Therefore, it was concluded that this correction was not sufficient for explaining the differences that were noticed between this predictive method and our experimental values using the single heat flux distribution aspect. As a consequence it was thought that this difference should be mainly due to the operating conditions. Indeed, for our experimental tests, the heat flux condition that was imposed on the channel wall remain quite far from the ideal condition defined by Lee et Garimella (2006). Indeed, the authors have represented in their modeling an uniform heat flux distributed on the whole exchange surface of the mini-channels. However, according to the data Shah et London (1978) (Chapter VII, Table 44 of this book), the impact of the heated wall number may have a very noticeable influence on the evolution of the Nusselt number. As a consequence, it may be thought that the impact of the heat transfer rate that evolved between the walls may impact the heat transfer rate and led to difference, by comparison with the Lee et Garimella (2006) data.

Beside the comparisons made with the literature data, the results of Figure 5.28 showed a very interesting evolution when the heat flux repartition was not considered as uniform. Indeed, for the whole set of corrected data, it seemed to have a non-dimensional length z^* ¹⁴ from which it can be noticed very small variations of the Nusselt number regarding z^* . Therefore, this result suggested that the mechanism that took place usually after full development of the thermal boundary layers should be better taken into account when a non-uniform heat flux distribution is considered.

Moreover, we have obtained using this numerical work a very essential results for further study. Indeed, it was observed that for all the made tests, the heat flux integration from the mini-channel entrance up to the location of the wall thermocouple $n^{\circ}3$ gave a very close value of the mean heat flux density, q''_{moy} , between the wall and the working fluid between the mini-channel inlet and outlet. This mean heat flux may be written as :

$$q''_{moy} = \frac{\Phi_{conv}}{S_{lat}} \quad (5.23)$$

where Φ_{conv} is the mean flow convected power and S_{lat} the mini-channel lateral surface. The differences that were noticed were approximately comprised between $\pm 10\%$ regarding the mean heat flux. Thus, when the fluid flow reach this point, it was assumed in the remaining part of this work that the heat flux transferred in the cross section of the thermocouple $n^{\circ}3$ equaled its mean integrated values along the mini-channel.

14. It could be recalled that a same thermal non-dimensional length, z^* , correspond to a same state of thermal boundary layer development, when the flow is fully developed.

5.4 Chapitre 5 conclusions

The results that have been given in this chapter relied on the data that were obtained for $C_1(a = 2.3 \text{ mm} - b = 1 \text{ mm})$ and $C_2(a = 5.6 \text{ mm} - b = 0.816 \text{ mm})$ mini-channels. Two tests fluids were studied in this work : water and forane 365 HX. The collected data allow for the characterization of the tests section. This preliminary analysis was important before the study that was made in a boiling configuration where numerous parameters whose the transfer rate to the fluid were determined indirectly. During this work, the evolution of the friction coefficients as well as the heat transfer coefficients were analyzed for single-phase flow conditions. Regarding these two tests configuration, a detailed description will be given below.

▷ The **determination of the friction coefficients** was made for adiabatic conditions for all the studied cases of this work. It was noticed that the results that were obtained during these experiments were in good agreement with the Shah et London (1978) correlation for the laminar regime and with the one of Blasius (1913) for the turbulent regime. In addition, the modification of the cross section did not impacted the performance of these predictives tools for these flows configurations. Consequently, as other studies of the literature showed it, this one confirmed that the law which were defined for conventional flows ($d_h > 3 \text{ mm}$) allow for the prediction of the experimental friction coefficients for these mini-channels.

▷ The **heat transfer coefficients calculation** were made for the whole set of tests plates. For this work we observed a significant difference between the correlations that predicted the heat transfer coefficients evolution and the experimental data for the flows in laminar regimes. During the analysis, it was shown using a numerical study that this behavior was not caused only by a non-homogeneous heat flux distribution at solid/liquid interface. Indeed, after estimating the evolution of the mean heat flux distribution at the interface for the whole set of test plates, it was proposed to approximate them using exponential-type laws. Once these laws were determined, a correction method for determining the experimental data was defined. The obtained results have allowed for the propositions of three conclusions that are given below :

① The differences that were noticed between the Lee et Garimella (2006) correlation and the experimental data are mainly due to the fact that the conditions that were imposed to the channel walls were not homogeneous compared to the ones defined by these authors.

② The consideration of the heat flux repartition that was obtained numerically, allow for the better consideration of the thermal boundary layers development. Indeed, above a treshold non-dimensional length, z^* , the Nusselt number value variation is small after correction of the experimental data.

③ There is a region in the mini-channel where the heat transfer is very close to the mean heat flux density. This region is located near the wall thermocouple n^o3 .

This last observation, important for the rest of this study, allow for the specification of a reference region where it was decided to study all the phenomena related to boiling conditions. Therefore, we made the assumption that in this region (near the wall thermocouple $n^{\circ}3$), the heat transfer rate equaled to its mean value (equation 5.23).

Boiling flows in mini-channels

6.1	Fundamental estimations in convective boiling conditions	178
6.1.1	Experimental determination of the transferred heat flux	178
6.1.2	Reference fluid temperature determination	180
6.1.3	Measurement uncertainties	181
6.2	Study of the ONB in the mini-channels	183
6.2.1	Study description and methodology	183
6.2.2	Measurements and results	183
6.3	Flow regime visualization in mini-channels	194
6.4	Evolution of boiling curves with wall heat flux	206
6.4.1	Boiling curves presentation	207
6.4.2	Pressure drop evolution	212
6.4.3	Evolution of the heat transfer coefficients	227
6.4.4	Conditions that lead to wall dryout	238
6.5	Chapter 6 conclusions	244

Summary :

THIS chapter gives the results that were obtained during the analysis made for internal convective boiling conditions. In this first paragraph, the methodology that allow for the determination of the thermal energy that was transferred to the fluid during boiling has been presented. In order to determine the heat exchange amplitude, a procedure for estimating the fluid temperature close to wall location. This calculation was possible thanks to the determination of the saturation pressure. Once these fundamental parameters were obtained, the impact of the operating conditions as well as the one of the geometrical parameters on the onset of nucleate boiling (ONB) or on critical heat flux (CHF) were determined. Pictures of the boiling flow were deeply analyzed and their allow for the better understanding of some of the mechanisms that took place during the convective boiling in the mini-channels. Finally, correlations for predicting the dryout evolution, pressure drops and the heat transfer coefficients for the mini-channels were proposed.

6.1 Fundamental estimations in convective boiling conditions

6.1.1 Experimental determination of the transferred heat flux

In this work, one of the main constraints that was encountered during the convective boiling was related to the determination of the thermal power that was transferred to the fluid. Indeed the direct physical measurements often did not exist for obtaining these thermal powers. This difficulty increases all the more when thermal losses with environment exist.

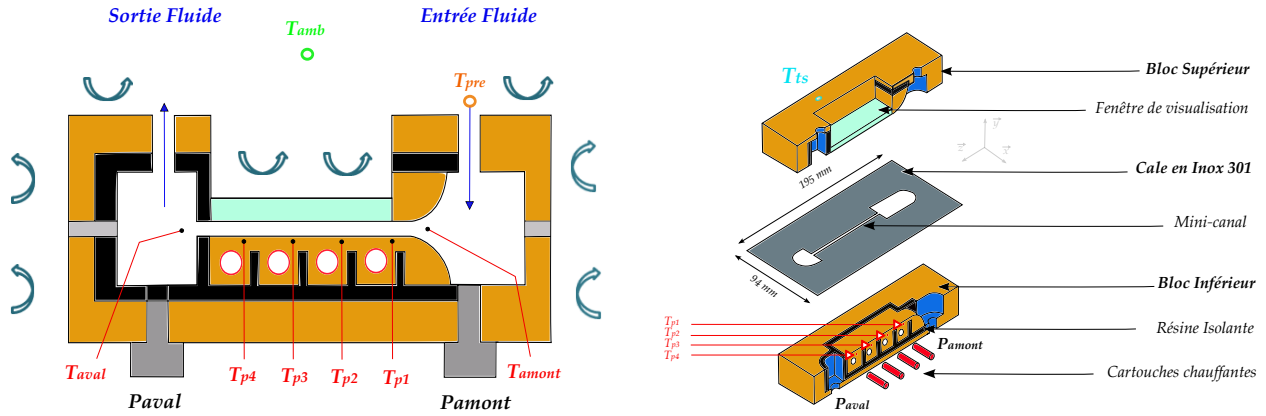


FIGURE 6.1 – Markers for the determination of the thermal power transmitted to the fluid

Therefore, for determining the thermal power that was transferred to the fluid, the different heat exchange surfaces that were used in our calculation were given on Figure 6.1. In a first stage, the electrical power that was imposed to the test section was determined thank to the knowledge of the effective current (I) and voltage (V) values that passed through the heating cartridges. This power can be calculated according to :

$$\Phi_{elec} = V.I \quad (6.1)$$

The losses with the environment can be deduced using the relation :

$$\Phi_{pertes} = h_{nat} S_{ts} (T_{ts} - T_{amb}) \quad (6.2)$$

where h_{nat} is the heat transfer coefficient by natural convection with the ambient, S_{ts} , the test section external surfaces, T_{ts} , a mean temperature of this external surface¹ and T_{amb} was the ambient temperature. The heat transfer coefficient by natural convection h_{nat} was comprised between 11 and 18, $5W.m^{-2}.K^{-1}$ for the whole set of experiments. For obtaining the value of this

1. The location of the thermocouple placed on the test section external surface was chosen after testing different location of temperature measurement. This was done in order to represent at the best as possible the mean temperature surface.

Section 6.1. Fundamental estimations in convective boiling conditions

coefficient, it was realized formerly to the two-phase flows tests, single-phase flow experiments where the convected thermal power was determined (Φ_{conv}) from the entrance to the outlet of the test section. This thermal power could be expressed using :

$$\Phi_{conv} \approx \dot{m}c_p(T_{aval} - T_{pre}) \quad (6.3)$$

In addition, it was noticed that the external test section temperature may varied slightly, even when, the stability criteria was reached. This temperature variation was synonymous to different energy storage (or release) in the test section on the time range where the average measurement was done. During this analysis, the convected power could be determined directly using the temperature difference between the inlet and the outlet of the mini-channel. However, for a boiling configuration the transmitted power could not be determined using this temperature difference. Consequently it was chosen to consider with attention the test section thermal storage (Φ_{ts}) whose formula is given as :

$$\Phi_{ts} = \left(\frac{m_{ts}}{t} \right) \times c_{p,ts} \times (T_{fin,ts} - T_{init,ts}) \quad (6.4)$$

where m_{ts} is the mass of the test section, t is the elapsed time for making the temperature goes from $T_{init,ts}$ to $T_{fin,ts}$ (on the range of 24 experiment data points used for calculating the mean temperature value : see experimental protocol in Appendix C) and $c_{p,ts}$ is the specific heat of the test section at constant pressure. Once these two power were determined, it was possible to calculate the thermal losses with the environment according to :

$$\Phi_{pertes} = \Phi_{elec} - \Phi_{conv} - \Phi_{ts} \quad (6.5)$$

Therefore, the value of the coefficient h_{nat} was deduced using the combination of equations (6.2) through (6.5). This value was determined formerly to each experiments made for boiling conditions thanks to one or several single-phase flow condition(s). When several experimental points were obtained in single-phase flow conditions, it was possible to notice that h_{nat} showed a maximal variation of $\pm 1.3 W.m^{-2}.K^{-1}$ around the mean value. Once the value of this coefficient was calculated, it was assumed to be constant for all the boiling conditions of this series.

During the experimental study, it was noticed that for specific configuration, the mini-channel inlet temperature (T_{amont}) may rose, whereas the pre-heating temperature was kept constant. For explaining this phenomenon, we examined the results given by the numerical analysis. Indeed, during this study that was made for single-phase condition (§ 5.3), it was highlighted that the heat flux distribution on the lateral surface of the mini-channels can be different from a homogeneous repartition. In addition, the amplitude of this heat flux tend to be more important toward the mini-channels entrance. Therefore, the assumption of an axial heat conduction was made and this may induced a temperature increase in the inlet reservoir

Chapitre 6. Boiling flows in mini-channels

regarding the heat flux or flow rates values. This lead us to regularly adjust the pre-heater temperature when a variation of the setpoint temperature was noticed. After several tests, it was chosen to limit the subcooling to a maximal value of $20^{\circ}C$. By supposing that we have a single-phase flow from the outlet of the pre-heater up to the test section inlet, the thermal power supplied to the fluid in the inlet reservoir by conduction may be obtained simply using :

$$\Phi_{res} = \dot{m}c_p(T_{amont} - T_{pre}) \quad (6.6)$$

Using all these elements, the thermal power that was transferred to the fluid can be determined following :

$$\Phi_{mini-canal} = \Phi_{elec} - \Phi_{res} - \Phi_{ts} - \Phi_{pertes} \quad (6.7)$$

The electrical power repartition that was supplied to the test section for C_4 mini-channel ($a = 4\text{ mm} - b = 0.421\text{ mm}$), for a mass velocity of $800\text{ kg}\cdot\text{m}^{-2}\cdot\text{s}^{-1}$ and a electrical power ranged from 70 to 220 W was reported on Figure 6.2.

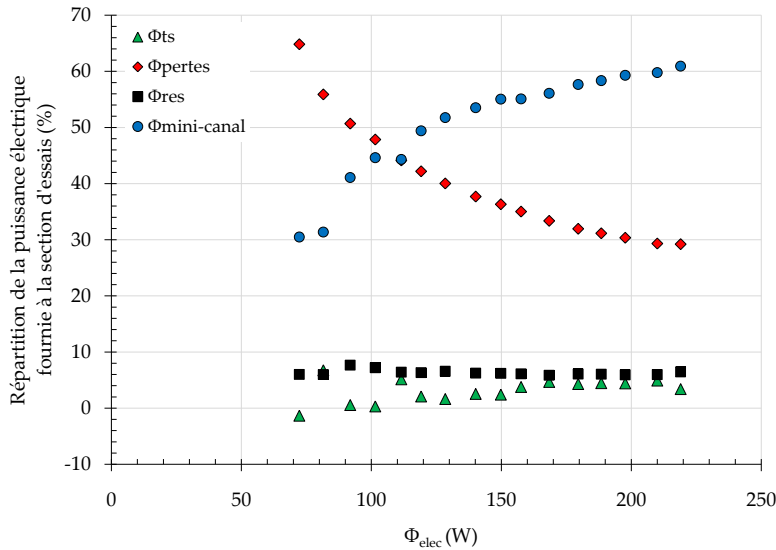


FIGURE 6.2 – Repartition of the electrical power for a boiling flow for C_4 mini-channel ($a = 4\text{ mm} - b = 0.421\text{ mm}$) according to the determination protocol to the power that was supplied to the fluid

6.1.2 Reference fluid temperature determination

During the boiling study, the knowledge of the fluid temperature on the selected mini-channel cross section was very important. Indeed, for saturated boiling, the liquid and the vapor phases were considered at saturation on a mini-channel cross section. In this configuration, the

Section 6.1. Fundamental estimations in convective boiling conditions

mixing temperature may be calculated using the saturation pressure determination along the mini-channel. Besides, if the liquid cooling or if the flow rate were important, a single phase length may occur in the mini-channel and the reference temperature was not the saturation temperature in this initial region. Two situations may occur in function of the appearance of a flow length which is not saturated before the location z_{sat} :

▷ For $z \leq z_{sat}$

The liquid temperature evolution can be obtained by taking into account the enthalpy increase from the mini-channel entrance, which is driven by the wall heat flux according to :

$$T_l(z) = T_{l,in} + \frac{\dot{q}_{moy}'' S}{\dot{m} c_p} \times \int_0^z \exp\left(f_1(Re) \frac{z}{L} + f_2(Re)\right) dz \quad (6.8)$$

▷ For $z \geq z_{sat}$

For estimating the pressure in the saturated region, it was necessary to determine the pressure drop from the mini-channel entrance up to the saturation point (single-phase flow length). During the single-phase flow experiments, the results were in excellent agreement with the correlation of Shah et London (1978) that allow for the prediction of these pressure drops (§ 5.1.4). Therefore, it was assumed that as soon as the flow was not saturated, this pressure drop followed the same evolution that was predicted by Shah et London (1978). Thus the pressure drop from the mini-channel entrance up to the saturation point may be expressed following :

$$P_{sat} = P_{in} - \frac{1}{2} \rho U^2 \left(1 + 4f \frac{z_{sat}}{d_h}\right) \quad (6.9)$$

where $\frac{1}{2} \rho U^2$ was the pressure drop caused by the fluid acceleration due to the convergent and f the friction coefficient defined by Shah et London (1978) according to equation (1.9). Once the evolution of the pressure drop was known along the mini-channels, the saturation temperature can be defined for $z \geq z_{sat}$, using a curve that relate these two values as showed in the example reported on Figure 3.3. It was then assumed that the pressure drop followed a linear behavior from the saturation point up to the mini-channel outlet.

6.1.3 Measurement uncertainties

It will be not detailed in this paragraph the procedure for the determination of the measurement uncertainties for the experiments related to boiling. It can be noticed that this procedure followed the Kline et McClintok (1953) method. On Figure 6.3 the measurement uncertainties have been given regarding the heat transfer rate to the fluid. The reader would be able to observed that this term is significantly impacted by the measurement uncertainty related to the

Chapitre 6. Boiling flows in mini-channels

heat transfer coefficient by natural convection which has been set to a value of $\pm 2 W.m^{-2}.K^{-1}$ for all our experiments.

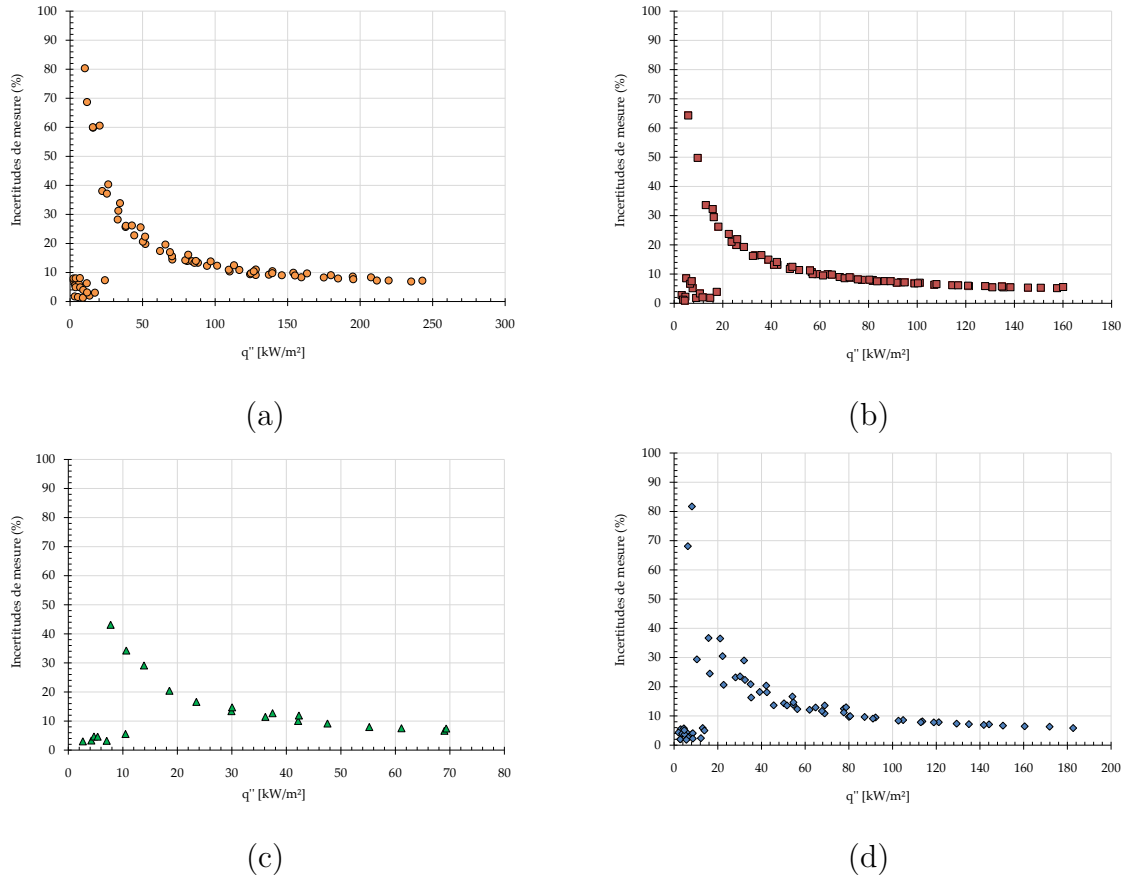


FIGURE 6.3 – Measurement uncertainties for the heat transferred to the fluid for the : (a) C_1 mini-channel ($a = 2.3 \text{ mm} - b = 1 \text{ mm}$) (b) C_2 mini-channel ($a = 5.6 \text{ mm} - b = 0.816 \text{ mm}$) (c) C_3 mini-channel ($a = 8 \text{ mm} - b = 0.814 \text{ mm}$) (d) C_4 mini-channel ($a = 4 \text{ mm} - b = 0.421 \text{ mm}$) and a sub-cooling of $15^\circ C$

The data from these charts showed that the measurements uncertainties was relatively small ($< 10\%$) for single-phase flow conditions where the power transferred to the fluid can be obtained directly. This uncertainty become then significant after the occurrence of the onset of nucleate boiling for which the power have to be determined indirectly. This uncertainty then decrease rapidly when the convected heat flux increased and became lower to 10% when the heat fluxes were larger.

6.2 Study of the ONB in the mini-channels

6.2.1 Study description and methodology

The onset of nucleate boiling (ONB) is an important data in the study of convective boiling. Indeed, from this point, the predictive tools that were defined for characterizing the single-phase flow may start to deviate.

In this paragraph, the impacts of the operating conditions on the evolution of the ONB using the image acquisition system have been analyzed. One can notice that for all the data that were obtained for boiling conditions, only forane 365 HX was used as working fluid.

6.2.2 Measurements and results

During the determination of the conditions that allow for ONB, image analysis were made simultaneously to confirm the incipience of bubbles in the mini-channels. For our experimental set-up, we noticed that the ONB was generally followed by an abrupt fluid temperature increase at the outlet of the test section (T_{aval}). It should be reminded that the flow visualization was defined in the region defined on Figure 4.8 only. Therefore, all our convected heat fluxes values were calculated at the location of wall thermocouple $n^{\circ}3$. It was then assumed that the heat flux value integrated from the channel entrance up to the location of wall thermocouple $n^{\circ}3$ was close to the heat flux conditions that were considered as homogeneous according to the discussion presented in § 5.3. As a consequence this heat flux was determined following :

$$q''_{onb(Tp_3)} = \frac{\Phi_{conv,int}}{S_{lat(Tp_3)}} \times \frac{z_3}{L} = \frac{\Phi_{conv}}{S_{tot}} \quad (6.10)$$

where $\Phi_{conv,int}$ is the convected power which was integrated on the reference length, $S_{lat(Tp_3)}$ is the lateral surface from the mini-channel entrance up to the point z_3 which is the location of wall thermocouple $n^{\circ}3$ data. L is the heated length and S_{tot} , the lateral mini-channel surface on all the heated length.

The experimental data point that have been presented in this study were the ones that precede immediately the ONB. Therefore the experimental uncertainties for the heat flux that lead to ONB were calculated for a single phase flow. This protocol has already been described in § 5.2.3. The experimental uncertainties for the calculation of wall heat flux transferred to the fluid were lower to 10%.

Chapitre 6. Boiling flows in mini-channels

During the visualizations, it was noticed that the ONB took place mostly in the mini-channel corner for all the cases that were reported in this manuscript. Images of the ONB that showed this phenomenon are given in Figures 6.4 et 6.5 for $C_1(a = 2.3 \text{ mm} - b = 1 \text{ mm})$ and $C_2(a = 5.6 \text{ mm} - b = 0.816 \text{ mm})$ mini-channels.

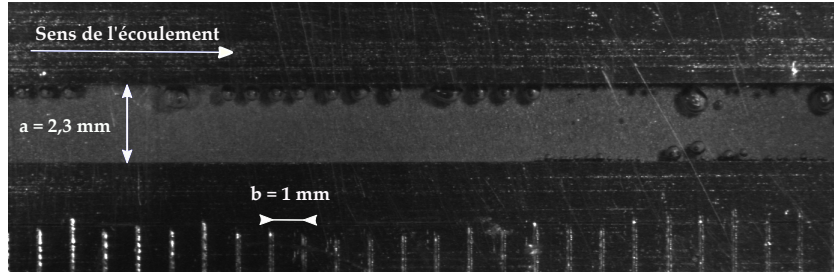


FIGURE 6.4 – ONB for $C_1(a = 2,3 \text{ mm} - b = 1 \text{ mm})$ mini-channel, for a mass velocity of $150 \text{ kg.m}^{-2}.\text{s}^{-1}$, a heat flux of 4.5 kW.m^{-2} and a subcooling of 14°C at atmospheric pressure.

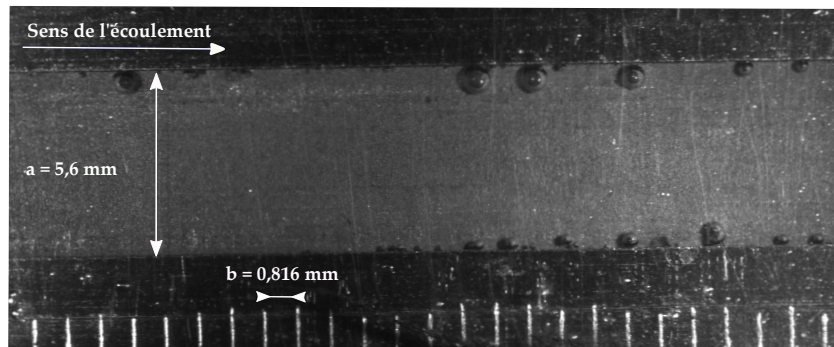


FIGURE 6.5 – ONB for $C_2(a = 5.6 \text{ mm} - b = 0.816 \text{ mm})$ mini-channel, for a mass velocity of $130 \text{ kg.m}^{-2}.\text{s}^{-1}$, a heat flux of 6.1 kW.m^{-2} and a subcooling of 12°C at atmospheric pressure.

Three main assumptions allow for the explanation of these observations :

- ① **Corner effect** : As highlighted in the study made by Li *et al.* (2004), it may be due to a corner effect which, in function of the contact angle between the fluid and the wall, may allowed for the entrapment of a gas volume. Therefore, when a heat flux was imposed to the cross section, the superheated vapor should formed bubbles in the mini-channels corners more rapidly than the vapor entrapped in the other cavities that should contain less gas.
- ② **Viscosity effect** : It may be due to a viscosity effect that slow down the fluid near the wall and lead to an increase of the temperature near the corner where the viscous effect were more significant.
- ③ **Streamline concentration** : The impact of the heat flux streamline concentration in the corner that present a geometrical singularity may generate the incipience of one or several hot spots that should be at the origin of this phenomenon.

During these experiments, the minimal heat flux that led to ONB, the influences of the inlet liquid temperature, of the saturation pressure and of the geometry were determined. For all these parameters, the main variable was the mass velocity. These analyzes will be presented in the next paragraphs.

Impact of the inlet temperature

The impact of the inlet temperature was studied at atmospheric pressure. After making the fluid degassing process, the thermal bath temperature was reduced to a value that was comprised between $35^{\circ}C$ and $40^{\circ}C$. The top cover of the condenser of the degassing reservoir was then removed. The hollowed plate that was selected for these experiments was C_3 plate ($a = 8\text{ mm} - b = 0.814\text{ mm}$). For each mass velocity, the heat flux was progressively increased up to the ONB².

Firstly, repeatability tests were made for this plate and for a subcooling of $15^{\circ}C$. The results of these two tests showed good repeatability. These data are given on Figure 6.6.

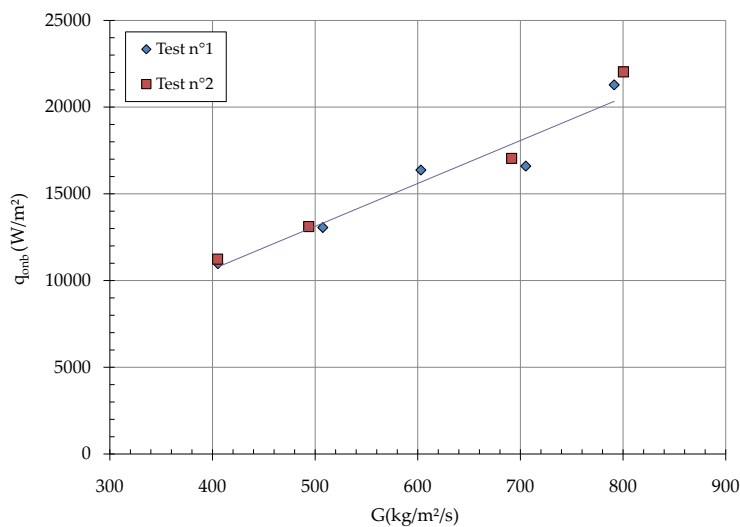


FIGURE 6.6 – Repeatability tests on the impact of the subcooling for C_3 plate ($a = 8\text{ mm} - b = 0.814\text{ mm}$)

For characterizing the influence of the inlet temperature, it was decided to set T_{amont} to three different temperatures values ($26^{\circ}C$, $30^{\circ}C$, $35^{\circ}C$). During these experimental campaigns, it was observed that forane 365 HX may reach boiling conditions, whereas the outlet fluid temperature (T_{aval}) where still slightly lower than the saturation temperature (T_{sat}). The results that are given on Figure 6.7 showed that the heat flux exchange at the mini-channels walls increased

2. The whole protocol has been described in Appendix C.

when the inlet temperature was diminished (or when the inlet liquid subcooling was increased (equation 6.11)) for a same mass velocity. It may be reminded that the relation that relate the inlet temperature to the subcooling is :

$$\Delta T_{SR} = T_{sat} - T_{amont} \quad (6.11)$$

According to our understanding, the reduction of the inlet temperature generated a reduction of the mean temperature on the flow cross section. Therefore for reaching the conditions that lead to ONB, the required energy that should be supplied to the fluid became more important.

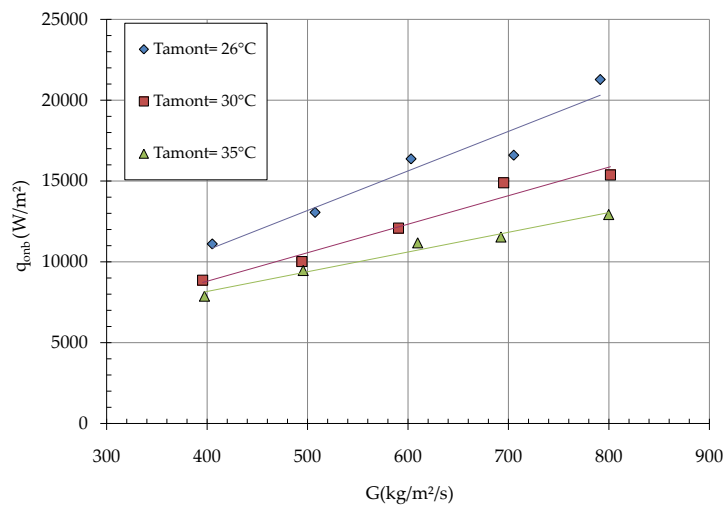


FIGURE 6.7 – Influence of the inlet temperature on the heat flux exchanged at the wall of the C_3 mini-channel ($a = 8 \text{ mm} - b = 0.814 \text{ mm}$) at atmospheric pressure

In addition, the minimal heat flux for the ONB become more important when the flow rate was increased³, what may looks trivial. Using the numerical modeling, realized for a single-phase condition § 5.3, the impact of the flow rate was evaluated on the temperature field on a mini-channel cross section located at 76 mm from the entrance. The results that were obtained (Figure 6.8) showed the flow rate impact for a convected heat flux of 1.5 kW.m^{-2} and two different Reynolds numbers.

The data given in Figure 6.8⁴ showed that the conditions for ONB became more unfavorable when the flow rate was increased. Indeed, the mean temperature on channel cross-section was smaller for a same convected power. Therefore at higher Reynolds number, for reaching a

3. It can be highlighted that, for these cases, the considered range of Reynolds number is comprised between 1000 and 2000 and the flow is either in a laminar or transition regime.

4. The aspect ratio value was not kept at scale for readability reasons. The reader may noticed that the dimensions values that correspond to the positioning of the mini-channel have been reported on Figure 6.8

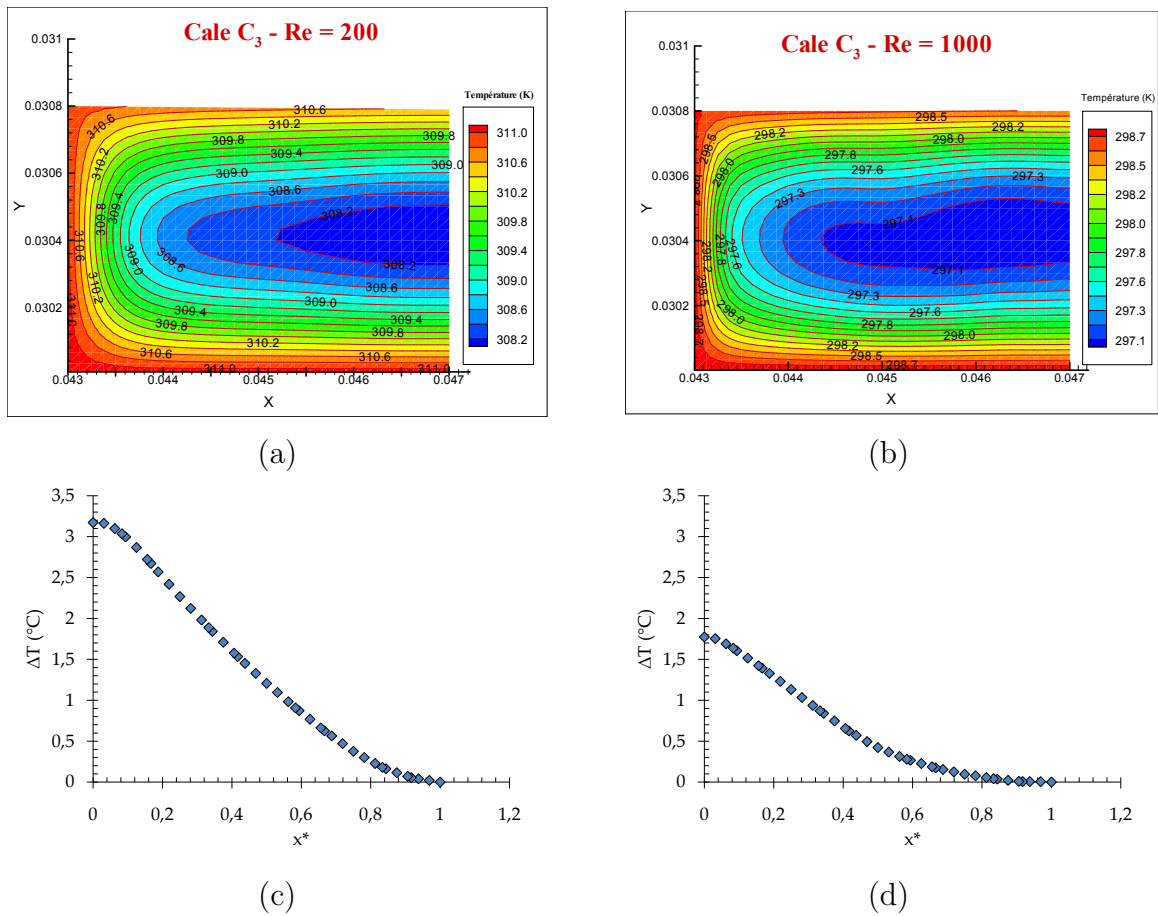


FIGURE 6.8 – Numerical results in single-phase flow. Impact of the flow rate on the temperature streamlines on a cross section located at 76 mm from the mini-channel entrance C_3 for a convected heat flux of $1.5\text{ kW}\cdot\text{m}^{-2}$ and a Reynolds number of : (a) 200 (b) 1000 - Representation of the temperature difference between the reference point and the mini-channel center on a diagonal that start from the bottom left corner up to the channel center for a Reynolds number of : (c) 200 (d) 1000

temperature field that was closer to the one that corresponds to the results that were obtained for a lower Reynolds number, it was necessary to increase the heat flux that was imposed to the flow.

It can be highlighted that the liquid temperature is more important in the corners than compared to the other locations of the mini-channel. Thus, the assumptions that were given related to the thermal effect that allow for the occurrence of the bubbles in the corner seemed to be corroborated by this numerical study. Indeed, in order that a bubble may survive without collapsing when being in contact with a cooler liquid, the temperature field around this bubble

had to be larger than the saturation temperature. According to the results of this model this situation may have the tendency to take place firstly in the corners of the mini-channels⁵.

In summary, it can be concluded that the impact of the fluid inlet temperature modification plays a significantly role on the evolution of the minimal heat flux needed for ONB. The influence of this parameter was more important than the one of the mass velocity for more than 67% of the experimental data point for this mini-channel.

Impact of the working pressure

For proceeding to the increase of the working pressure of the experimental set-up, after having realizing the degassing process, the diaphragm valve was used in order to increase the pressure drop in the loop. The working pressure was then set to a value close to 0.7 bar relatively to the atmospheric pressure. For the experiments made at atmospheric pressure, the test protocol was the same than the one presented in the preceding paragraph. It is useful to specify that the subcooling value (equation 6.11) increased with the working pressure if the inlet temperature was kept a constant value. Therefore, in order to correctly evaluate the impact of the working pressure, it was necessary to maintain the subcooling to a constant value. These tests were made on the C_3 mini-channel ($a = 8 \text{ mm} - b = 0.814 \text{ mm}$), for a subcooling on the order of 15°C for two different working pressures.

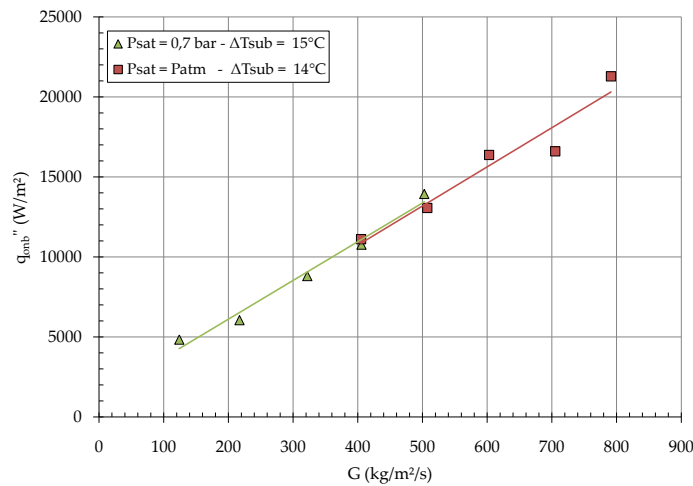


FIGURE 6.9 – Impact of the saturation pressure on the heat flux exchanged at the C_3 mini-channel ($a = 8 \text{ mm} - b = 0.814 \text{ mm}$) wall for a subcooling of about 15°C

The results that were obtained showed clearly that for this plate, the impact of the saturation pressure was relatively small on the minimal heat flux that allowed for the ONB (Figure 6.9).

5. Ghiaasiaan et Chedester (2002) named the conditions that lead to the bubbles motion from the mini-channel walls to the flow center the offset of Significant Void Fraction.

The reader may noticed that no other tests with different cross section were made during this experimental campaign. Therefore this result cannot be considered as valid for the other mini-channels.

Moreover, it can be noticed that Saitoh *et al.* (2005) have demonstrated that the working pressure impact seemed to increase when the mini-channel hydraulic diameter was reduced. Therefore, it seemed relevant to check in the future the influence of this working pressure on the ONB for mini-channel of hydraulic or/and aspect ratio that are different.

Impact of the mini-channel geometry

One of the most important point related to this thesis work concerned the impact of the geometry on the ONB. For this study, four different mini-channels that were defined in § 4.1.5 have been used. The error bars related the made measurement have been reported on Figure 6.10. These data showed that the required power to ONB can be modified only by modulating the geometrical dimensions of the mini-channel also. It was observed that this phenomenon may still occur when the aspect ratio is kept the same but the hydraulic diameter was modified. What may look surprising, it that for a same hydraulic diameter but different aspect ratio, the heat flux that led to ONB change, what has not been reported in the state of the art review that has been made. The analysis related to these results has been detailed in next paragraphs.

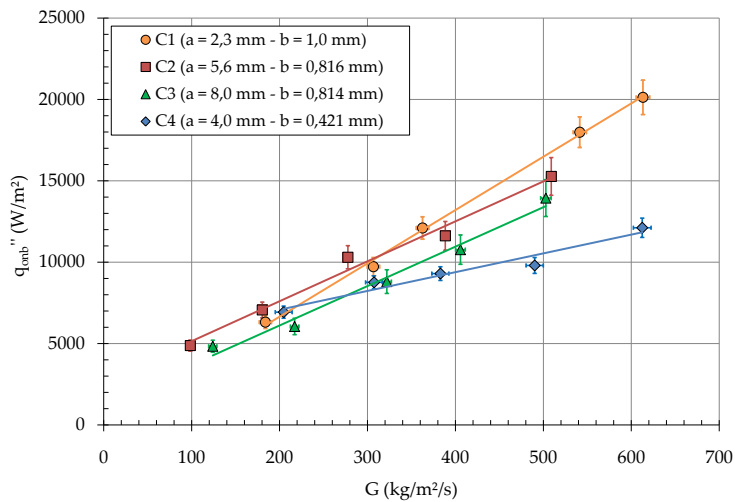


FIGURE 6.10 – Impact of the mini-channel geometry on the ONB evolution for a relative saturation pressure of 0.7 bar

➤ Impact of the mini-channel width

When comparing the impact of the flow width (a), our data were in good agreement (qualitatively) with the Liu *et al.* (2005) model. Indeed, according to these authors, the reduction of the mini-channel width led to an increase of the required heat flux needed for ONB. The same behavior was observed when comparing the data obtained for $C_2(a = 5.6 \text{ mm} - b = 0.816 \text{ mm})$ and $C_3(a = 8 \text{ mm} - b = 0.814 \text{ mm})$ mini-channel on all the range of studied mass velocities. However, it is important to highlight that Liu *et al.* (2005) studied a range of width that was comprised between 0.05 mm and 0.6 mm only.

➤ Impact of the aspect ratio

This comparison was made between $C_1(\gamma_1 = 0.435)$ and $C_2(\gamma_2 = 0.146)$ or $C_3(\gamma_3 = 0.102)$ mini-channels which has a very close hydraulic diameter compared to C_1 . For mass velocities lower than the range $200 \text{ kg.m}^{-2}.\text{s}^{-1}$ - $300 \text{ kg.m}^{-2}.\text{s}^{-1}$, the increase of the aspect ratio (b/a) seemed to lead to the ONB for smaller heat flux values. As soon as the range of mass velocities was higher, the obtained experimental results showed that the minimum heat flux that allow for the occurrence of ONB increase with aspect ratio.

In order to explain this result, the data that were obtained with the numerical model were analyzed (using single-phase flow conditions). This model showed that the flow rate impact on the evolution of the temperature field would be more pronounced for mini-channels whose aspect ratio was more significant, for the range of studied geometry. This results is reported on Figure 6.11 for Reynolds numbers and convected heat fluxes equaled to those reported in Figure 6.8.

It was observed that the mean absolute difference on the whole set of numerical data that were obtained between the data from the C_1 mini-channel and the data from the $C_3(\gamma_1 = 0.102)$ mini-channel was reduced from 104% to 79%, when the Reynolds number increased. This reduction seemed to be too poorly significant to justify the ONB characteristics for higher heat flux for $C_1(\gamma_1 = 0.435)$ mini-channel, when the flow rate increased. Indeed, the common action of the heat flux streamlines toward the corners, due to the singularity caused by the right angle of the mini-channels, coupled with a hydrodynamic effect, seemed to be needed by are not sufficient to explain what is happening in this current situation. In order to better see the flow rate impact, the evolution of the Reynolds number and of z^* (equation (1.15)) in function of the mass velocity for the four tested mini-channels was reported on Figure 6.12.

The evolutions of the Poiseuille and of the Nusselt numbers were plotted on Figure 6.13 for illustrating the flow rate impact on the hydrodynamic boundary layers development (Shah (1976) approach; equation (1.9)) and of the thermal boundary layer (Lee et Garimella (2006) approach; equation (1.17)) in the four mini-channels.

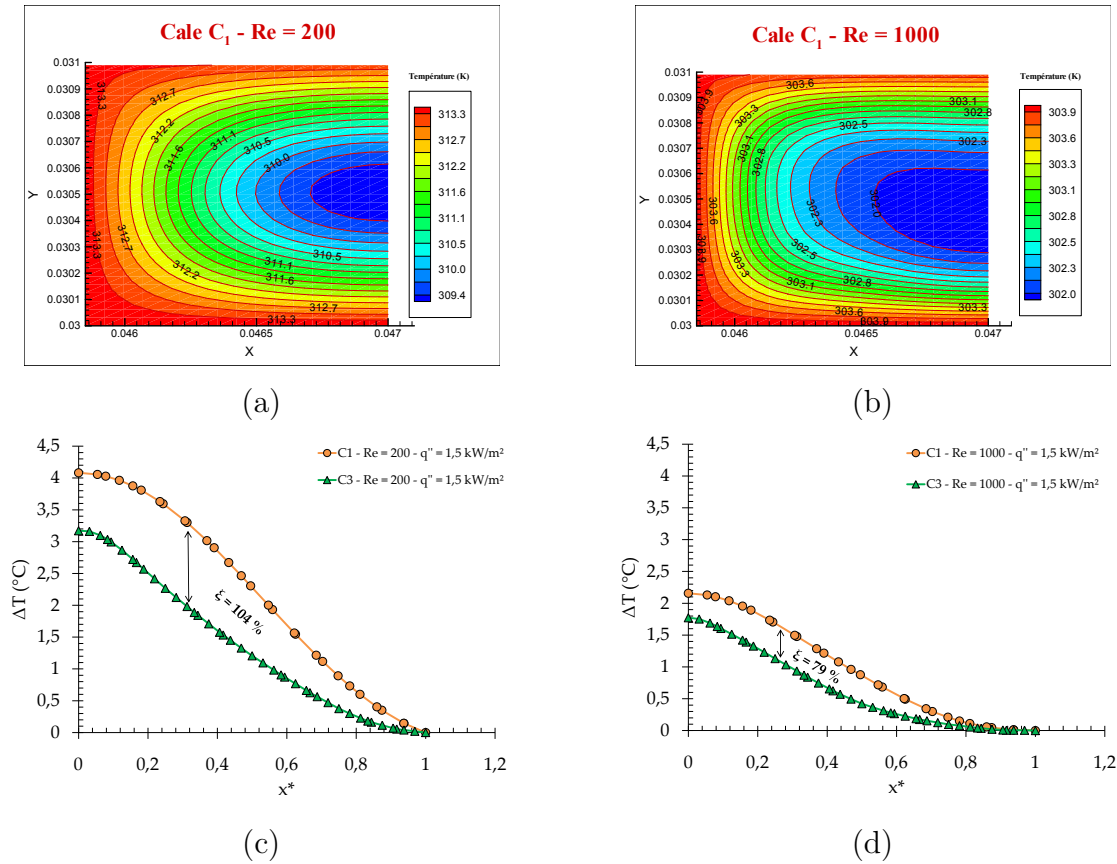


FIGURE 6.11 – Numerical results in single-phase flow. Impact of the flow rate on the temperature streamlines on a cross section located at 76 mm from the mini-channel entrance C_1 for a convected heat flux of $1.5\text{ kW}\cdot\text{m}^{-2}$ and a Reynolds number of : (a) 200 (b) 1000 - Comparison between the results obtained with C_1 ($\gamma_1 = 0.435$) and C_3 ($\gamma_1 = 0.102$) mini-channels. Representation of the temperature difference between the point located at the position x and the mini-channel center on a diagonal that starts from the bottom left corner up to the mini-channel center for a Reynolds number of : (c) 200 (d) 1000

The data taken from Figure 6.13 showed that the impact of the hydrodynamic boundary layer development was more pronounced for C_1 ($\gamma_1 = 0.435$) mini-channel than for the C_2 ($\gamma_1 = 0.146$) or C_3 ($\gamma_1 = 0.102$) mini-channels where the flow rate increases. In contrast, the rapidity of the thermal boundary layer development was similar for these mini-channels. Therefore, it was thought that the impact of the flow rate, more pronounced for C_1 leads to a more rapid increase of the dynamic pressure that acts through all the channel. In this context, the potential vapor embryos that were located in the mini-channel corner should be subjected to a higher pressure when the flow rate increases, which allows for the explanation of the observed experimental results. This was the reason why a higher heat flux for reaching ONB was required in this situation (higher flow rate).

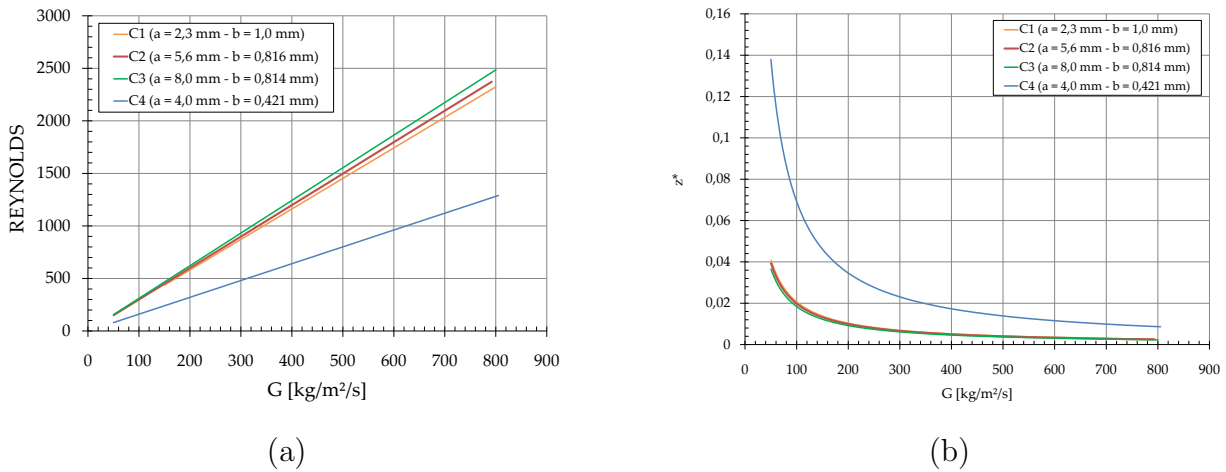


FIGURE 6.12 – Evolution of the : (a) Reynolds number and of (b) z^* in function of the mass velocity

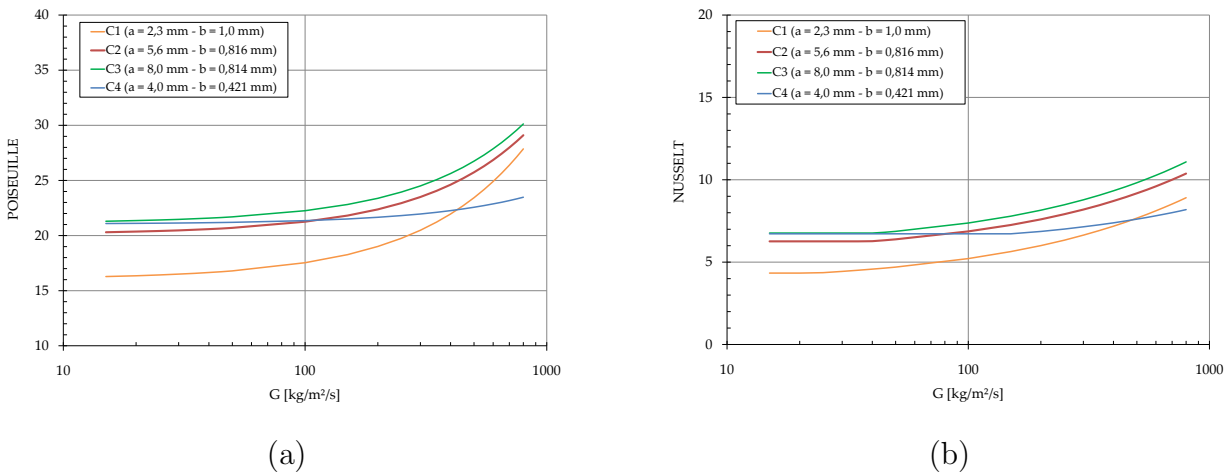


FIGURE 6.13 – Impact of the mass velocity on the properties related to : (a) hydrodynamic and (b) thermal characteristics

➤ Impact of the hydraulic diameter

From another point of view, Figure 6.13 showed the evolutions of the hydrodynamic and thermal boundary layer for C_4 ($d_h = 0.762 \text{ mm}$) mini-channel, which were very moderated compared to the other mini-channels regarded the range of the mass velocities that were studied. Indeed, for equivalent mass velocities, the Reynolds number was smaller for this mini-channel. This was due to the common impacts of the cross section and of the hydraulic diameter which were smaller than those of the other mini-channels. Therefore, the evolution of the Reynolds number was more moderated and the development of the boundary layers were more rapid than for C_4 . As a consequence, it was possible to demonstrate that the impact of the mass velocity

on the ONB was more moderated for C_4 than for other mini-channels as showed on Figure 6.10. It was possible to notice that when the mass velocity was lower to $200 \text{ kg.m}^{-2}.\text{s}^{-1}$, the minimum heat flux required for ONB was reduced for higher hydraulic diameter according to the experiments. Above this mass velocity, the opposite came true.

Summary related to the parametric study on ONB

After the study of these results, it was observed that the impact of the operating conditions may be very significant on the minimal heat flux that led to ONB. The impacts of the liquid inlet temperature and of the mass velocity were noticed as important (Figure 6.7). The obtained results suggested that the saturation pressure influence on the ONB was small for the range of studied pressures for C_3 mini-channel (Figure 6.9). In contrast, the impact of the geometry was particularly important on ONB as demonstrated in the data that were reported on Figure 6.10. These data confirmed the idea that as soon as the geometry differed from the circular cross section, the impact of the corners and of the aspect ratio for the rectangular channels may play a key role on ONB for mini-channels. Therefore it become necessary to consider with caution the impact of the whole geometry (cross section and aspect ratio) for studying the conditions that led to ONB in mini-channels.

6.3 Flow regime visualization in mini-channels

In this paragraph, the flow regimes evolution that were observed in the different studied mini-channels was analyzed. The images that have been presented were in direct relation with the boiling curves that will be introduced in § 6.4. The flow regimes that were observed have been obtained for a subcooling of $7^{\circ}C$ or $15^{\circ}C$, a relative working pressure of 0.7 bar for the whole set of studied cases. The mass velocities were comprised between $100\text{ kg.m}^{-2}.s^{-1}$ and $800\text{ kg.m}^{-2}.s^{-1}$. Most of the explanations that were given in this paragraph were based on the analysis made using high speed camera.

The flow regimes succession that was observed in the mini-channels were the following ones :

① Bubbles regime :

This flow was characterized by the presence of numerous isolated (or coalescing) spherical bubbles of small diameter regarding mini-channel hydraulic diameter. These bubbles were mostly convected to a close velocity compared to the one of the liquid flow.

② Vapor plugs regime :

The apparent diameter of the vapor bubbles became larger than the mini-channels thickness, but was kept lower than their width. For these configurations, the bubbles were flattened by the mini-channels wall in the height direction (b) and had a pancake shape.

③ Liquid slugs regime :

In this flow regime, the bubbles size reached the mini-channel width. As a consequence these bubbles were not able to continue to grow on the mini-channel cross section and have the tendency to grow in the longitudinal flow direction. In this last case, their can have the shape of a truncated cylinder. These different vapor bubbles may be separated by liquid slugs which were often composed of bubbles of smaller dimensions.

④ Churn flow regime :

When the vapor velocity increased, the vapor plugs started to break up under the strong interfacial shear stress effect. The flow went through an agitated form and reached a very unstable configuration. The boundaries of the interface of the vapor structures were more difficult to determine during this regime.

⑤ Annular flow regime :

When the heat flux transferred to the flow increased, the vaporization increases' led to the occurrence of a continuous vapor configuration at the mini-channels center. The liquid flow was now confined between the mini-channels walls and the vapor core. For high superficial vapor

velocities, a particular morphology may appear where ripples appeared at the liquid/vapor interface.

It can be specified that most of the times, some of the flow regime may took place in a very intermittent fashion. Therefore for the observations where it was noticed that one flow regime was dominant compared to the other, this is its name that was given. For the flow regime where an intermittent phenomenon was observed, it was called transition phenomenon between the flow regimes that were considered.

For all the images related to the boiling flow, the flow was going from left to right. The minimum heat flux increment that was imposed to the flow was about 3 kW.m^{-2} . Therefore, some flow regimes were not always visible during this study, this was due to the fact that the transition between them may varied very quickly regarding the heat flux.

✓ C_1 mini-channel ($2.3 \text{ mm} \times 1 \text{ mm}$)

The comments that were given in this paragraph were based on the observations that were made for the mass velocity of $300 \text{ kg.m}^{-2}.\text{s.}^{-1}$. Images showed that boiling was initiated from the mini-channel corners as already discussed in § 6.2. Immediately after ONB, these bubble tended to grow and to fill the whole cross section (Figure 6.14a). This observation was valid for all the studied mass velocities. It was though the the geometrical effect may allow to get closer to the conditions needed to move from ONB to OSV⁶ for this mini-channel. For the low heat fluxes ($12 \text{ kW.m}^{-2} \leq q'' \leq 20 \text{ kW.m}^{-2}$), the bubbles growth was higher and their diameter became rapidly larger than the mini-channel height (b) (Figure 6.14b et Figure 6.14c). Thereafter, the flow alternated between churn and annular regimes for moderated heat fluxes ($40 \text{ kW.m}^{-2} \leq q'' \leq 70 \text{ kW.m}^{-2}$ - Figure 6.14d). For the higher heat fluxes ($q'' \geq 70 \text{ kW.m}^{-2}$), the annular regime became dominant. In addition it was observed that ripples on the liquid/vapor interface appeared (Figure 6.14e). Indeed, the increase of the convected heat flux lead to the increase of the difference between the liquid and the vapor core velocities. In this context, the interfacial shear stress became more important and can make appear front instabilities as demonstrated by Revellin *et al.* (2008).

6. Onset of significant void fraction is the condition that led the bubbles to wall detachment and they flowing toward mini-channel center-line without collapsing.

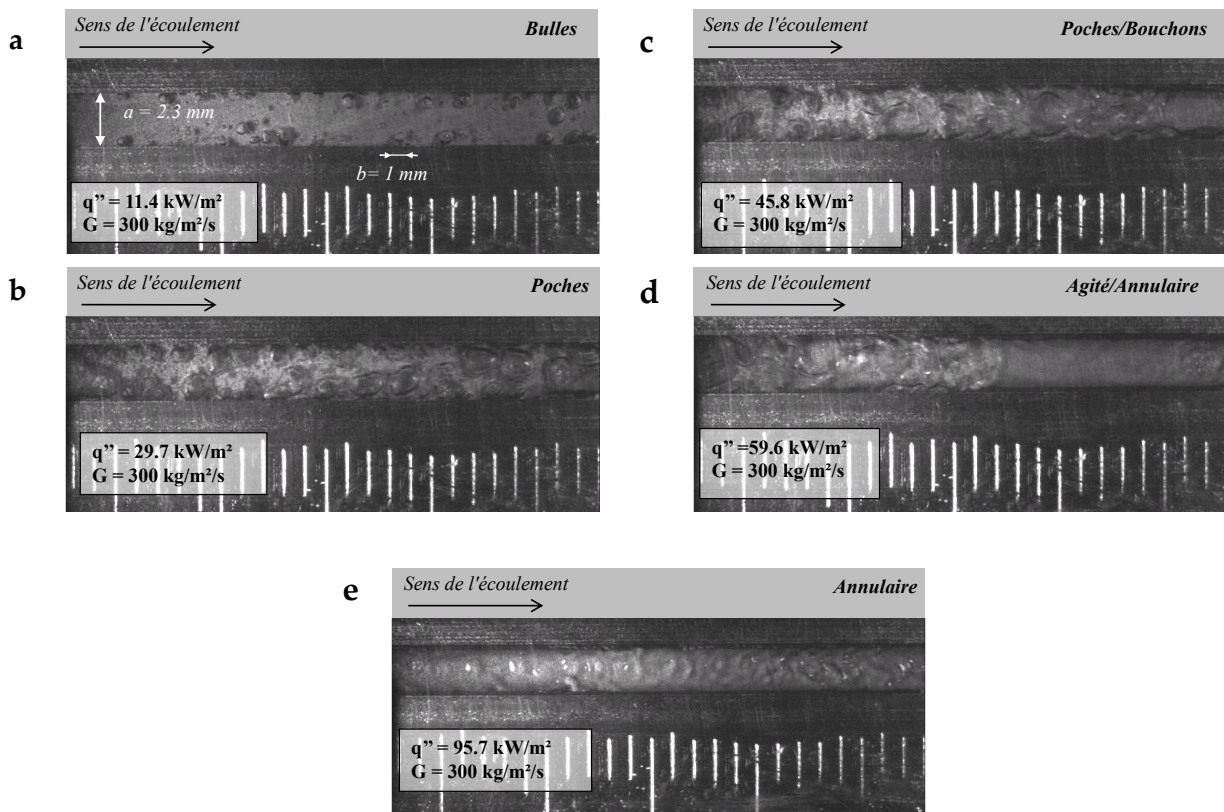


FIGURE 6.14 – Evolution of the flow regime for a mass velocity of $300 \text{ kg}\cdot\text{m}^{-2}\cdot\text{s}^{-1}$, a working pressure of 0.7 bar and a subcooling of 15°C for C_1 mini-channel ($a = 2.3 \text{ mm} - b = 1 \text{ mm}$)

It can be noticed that the flow regime transition varied strongly with the mass velocity that was imposed to the flow as showed in Figure 6.15. For all the other data that were given on histograms, the reader may observed that the maximum values that correspond to the heat flux related to the dryout were given. Therefore, it was clear that the minimum heat flux that led to dryout increase when the mass velocity was larger.

It was chosen to represent on these histograms, seven flow categories. In addition to the five presented flow regimes, it was added flow regime that had very strong interaction between them during the made observations. It was then added, the transition between the vapor plug and liquid slug regimes, and the transition between the churned and annular regimes. This classification will be kept for all the other histograms that will be presented in the following sections.

The data of the Figure 6.15 showed that the required heat flux for reaching the same transition between the flow regime was generally more significant when the mass velocity was increased. Moreover, the range of heat fluxes for which the flow had two distinct phase with vapor structures that had closed interface (bubbles, plugs, slugs) became larger, when the flow rate was

increased. Indeed, when the imposed wall heat fluxes were small, the flow rate increase allow the inlet temperature to have a stronger impact on the boiling flow. In addition, it was observed that the bubbles sizes at the ONB seemed to be reduced with the flow rate increase.

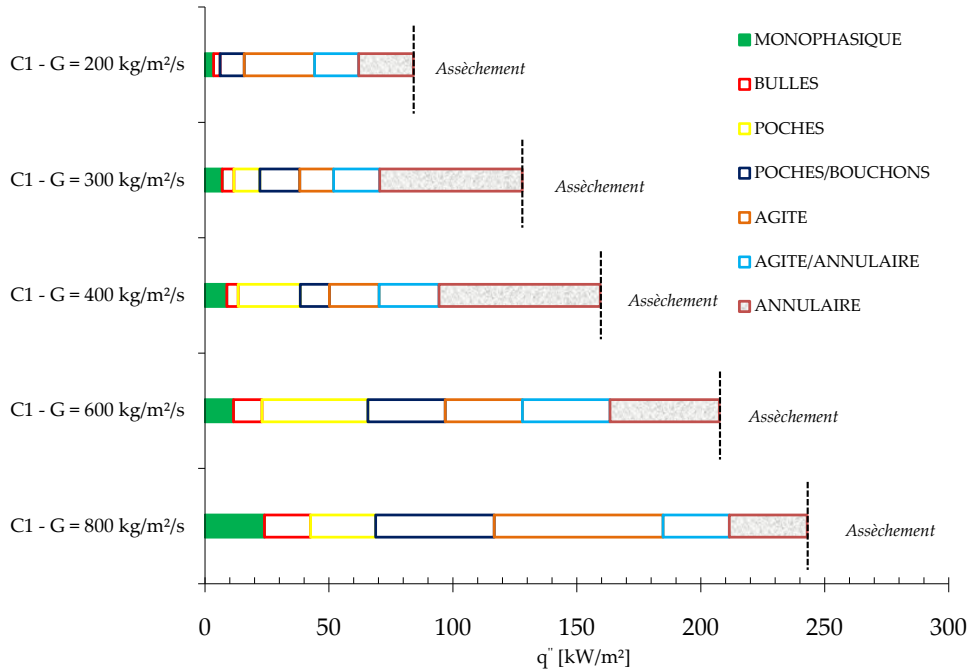


FIGURE 6.15 – Histograms representing the evolution of the transition between the flow regimes in function of the mass velocities for C_1 mini-channel ($a = 2.3 \text{ mm} - b = 1 \text{ mm}$)

✓ C_2 mini-channel ($5.6 \text{ mm} \times 0.816 \text{ mm}$)

The comments that were given in this paragraphs were based on the observation made for the mass velocity of $300 \text{ kg.m}^{-2}.\text{s}^{-1}$, for C_2 mini-channel ($a = 5.6 \text{ mm} - b = 0.816 \text{ mm}$). During these tests, it was noticed that the ONB was seen firstly in the mini-channel corner, whereas the flow centerline was still in single-phase flow conditions. The reader would be able to notice that this behavior was different compare to the one observed for C_1 mini-channel ($a = 2.3 \text{ mm} - b = 1 \text{ mm}$), that has same hydraulic diameter but a different aspect ratio. Indeed, for a same mass velocity, the bubbles remained confined near the walls. These bubbles had a smaller diameter compared to the mini-channel thickness (b) (Figure 6.16a).

In the most cases, ONB took place on the two sides of the C_2 mini-channel ($a = 5.6\text{mm} - b = 0.816\text{mm}$). Regarding the mini-channel width, it was possible to observe the progressive bubbles growth in the width direction when they moved downstream (Figures 6.16a and 6.16b). When the imposed heat flux was increased ($q'' \geq 19 \text{ kW.m}^{-2}$), it was observed that bubbles appeared on the mini-channel bottom plain wall which became active (Figure 6.16b). It can be noticed

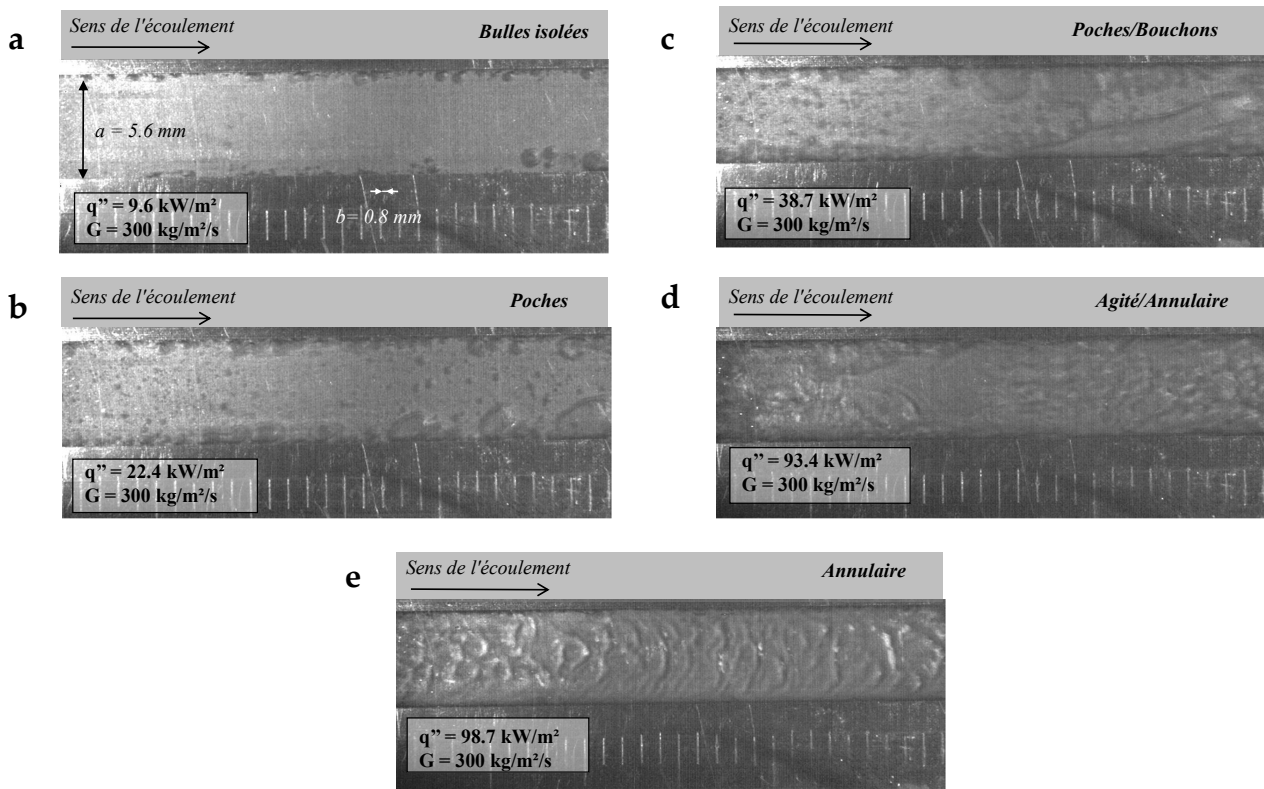


FIGURE 6.16 – Evolution of the flow regimes for a mass velocity of $300 \text{ kg}\cdot\text{m}^{-2}\cdot\text{s}^{-1}$, a working pressure of 0.7 bar and a subcooling of 15°C for the C_2 mini-channel ($a = 5.6 \text{ mm} - b = 0.816 \text{ mm}$)

that the heat flux required to ONB was more important than the one needed for bubbles incipience in the mini-channel corners. For the intermediates heat fluxes ($22 \text{ kW}\cdot\text{m}^{-2} \leq q'' \leq 40 \text{ kW}\cdot\text{m}^{-2}$), the corner bubbles started to coalesce between them (Figure 6.16c). The growth of these bubble was stronger when the heat flux was increased. An asymmetric motion was noticed between the successive plugs growth that were localized on the two sides of this mini-channel. Elongated vapor structures that were located at the mini-channel centerline may occurred and were fed by the bubbles coalescence. For higher heat fluxes ($72 \text{ kW}\cdot\text{m}^{-2} \leq q'' \leq 90 \text{ kW}\cdot\text{m}^{-2}$), the flow alternated between churn and annular regimes (Figure 6.16d). Ripples structures (much more visible compared to the visualizations made with C_1 mini-channel ($a = 2.3 \text{ mm} - b = 1 \text{ mm}$)) were noticed before the wall dryout (Figure 6.16e).

On Figure 6.17 it can be noticed that for mass velocities comprised between $200 \text{ kg}\cdot\text{m}^{-2}\cdot\text{s}^{-1}$ and $300 \text{ kg}\cdot\text{m}^{-2}\cdot\text{s}^{-1}$, the annular regime took place before the liquid dryout close to the wall. The reader may observed that this flow regime was no more observed when the mass velocity was larger than $300 \text{ kg}\cdot\text{m}^{-2}\cdot\text{s}^{-1}$. The flow regime that became dominant in this case was the churn flow regime for this mini-channel. It can be highlighted that the weight of the flow regimes

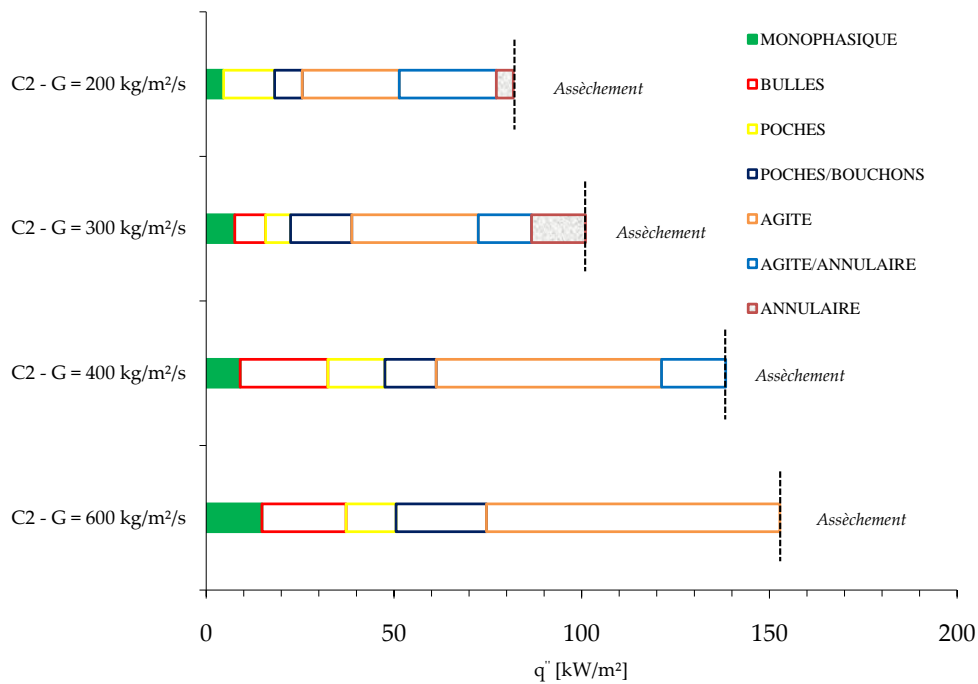


FIGURE 6.17 – Histograms representing the evolution between the transition regimes in function of the mass velocities for C_2 mini-channel ($a = 5.6 \text{ mm} - b = 0.816 \text{ mm}$)

that presented closed interfaces increased significantly with this mass velocity. This was due to the influence of the inlet temperature that became more pronounced and favour the duration of these regimes when the flow rate increased, similarly to the results that were obtained for C_1 mini-channel.

✓ C_3 mini-channel ($8 \text{ mm} \times 0.814 \text{ mm}$)

For the C_3 mini-channel, the impact of mass velocities comprised $100 \text{ kg.m}^{-2}.\text{s}^{-1}$ and $200 \text{ kg.m}^{-2}.\text{s}^{-1}$ were studied only. It should be noticed that on these visualizations, the presence of an internal crack of the visualization window that was generated during the montage of the brass block during an assembly. No liquid leakage due to this crack was noticed for all the experiments that followed this observation.

In a first step, the bubbles were generated in the corners, the flow located at the channel center was subcooled and was still in single-phase conditions (Figure 6.18a). For lower heat fluxes ($5 \text{ kW.m}^{-2} \leq q'' \leq 10 \text{ kW.m}^{-2}$), the subcooling still acted at the mini-channel center and the bubbles that were located in the corner continued to grow to form vapor plugs that remained stuck on these corners (Figure 6.18b). When the heat fluxes were moderated ($10 \text{ kW.m}^{-2} \leq q'' \leq 14 \text{ kW.m}^{-2}$), the bottom wall became active and bubbles of smaller diameters were generated on this wall (Figure 6.18c). At higher heat fluxes ($14 \text{ kW.m}^{-2} \leq q'' \leq 48 \text{ kW.m}^{-2}$), the flow

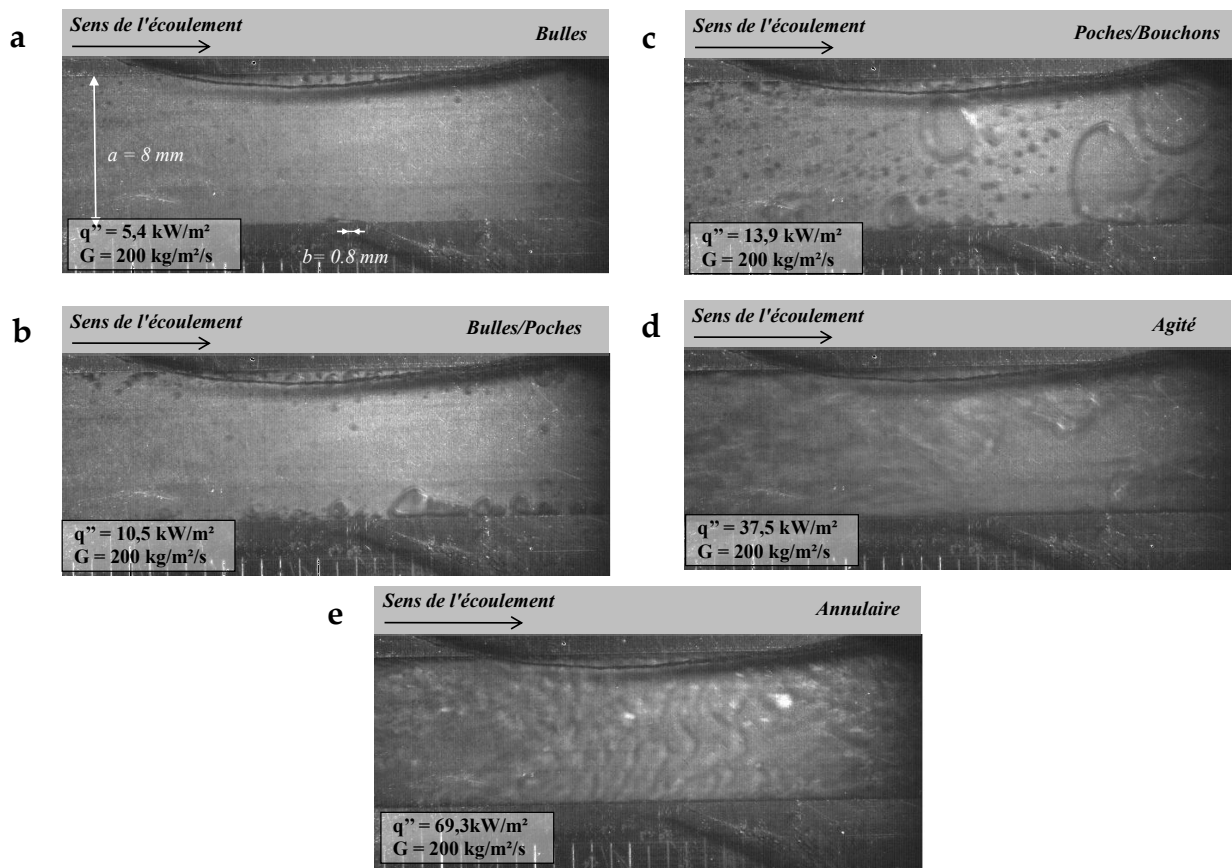


FIGURE 6.18 – Evolution of the flow regimes for a mass velocity of $200 \text{ kg}\cdot\text{m}^{-2}\cdot\text{s}^{-1}$, a working pressure of 0.7 bar and a subcooling of 15°C for the C_3 mini-channel ($a = 8 \text{ mm} - b = 0.814 \text{ mm}$)

became churned (Figure 6.18d) and asymmetric motions of the two-phase flow was also observed similarly to the ones noticed in C_2 mini-channel ($a = 5.6 \text{ mm} - b = 0.816 \text{ mm}$). For the more significant heat fluxes ($q'' \geq 68 \text{ kW}\cdot\text{m}^{-2}$) and when the conditions were closed to the wall dryout, it was observed the occurrence of the annular flow (Figure 6.18e).

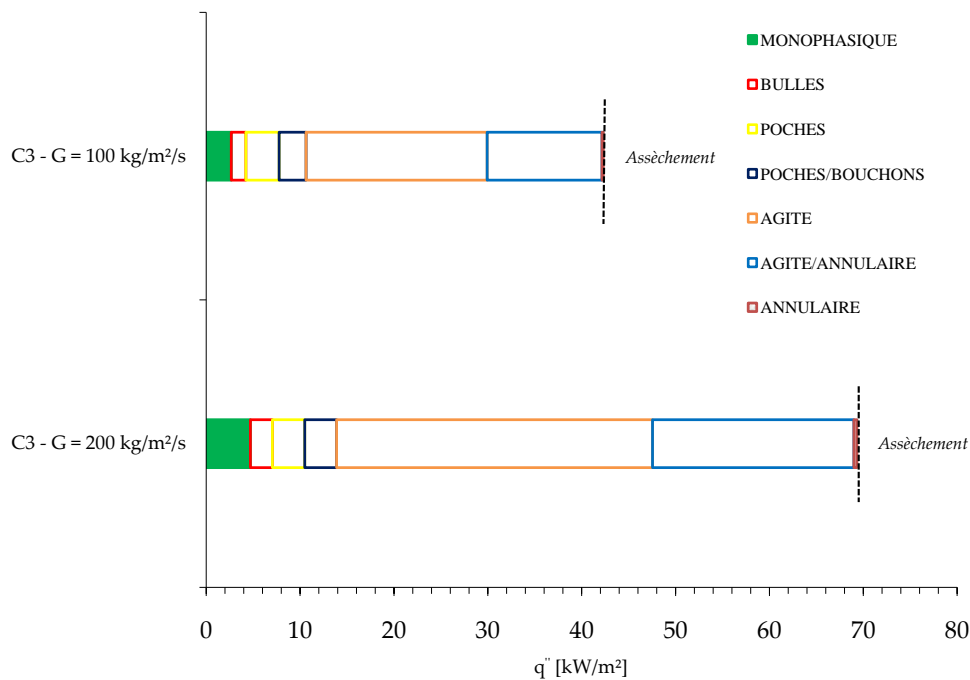


FIGURE 6.19 – Histograms representing the evolution between the regime transitions in function of the mass velocities for C_3 mini-channel ($a = 8 \text{ mm} - b = 0.814 \text{ mm}$)

The results that were given on the histograms of Figure 6.19 showed that when the flow rate was increased, the contribution of the churned flow regime was dominant on a larger range of wall heat flux. It can be noticed that the annular flow regime represent a very small heat flux range compared to the results that have been reported for C_1 mini-channel ($a = 2.3 \text{ mm} - b = 1 \text{ mm}$) and C_2 ($a = 5.6 \text{ mm} - b = 0.816 \text{ mm}$).

✓ C_4 mini-channel ($4 \text{ mm} \times 0.421 \text{ mm}$)

During the visualizations of the boiling flow in C_4 mini-channel ($G = 600 \text{ kg.m}^{-2}.s^{-1}$), it was observed similarly to the other mini-channels, that the corners were first activated and generated bubbles (Figure 6.20a). The flow at the mini-channel center was still subcooled and the bubbles that were generated stayed close the mini-channel corner and may coalesced between them. When the heat flux was increased ($11 \text{ kW.m}^{-2} \leq q'' \leq 30 \text{ kW.m}^{-2}$), larger structures were rapidly formed and filled the flow center (Figure 6.20b). For moderated heat fluxes ($30 \text{ kW.m}^{-2} \leq q'' \leq 41 \text{ kW.m}^{-2}$), the bottom wall of the mini-channel was activated and smaller bubbles may coalesced with the vapor plugs that were located at the center (Figure 6.20c). For the higher heat fluxes ($41 \text{ kW.m}^{-2} \leq q'' \leq 80 \text{ kW.m}^{-2}$), the flow went to churned regime and an asymmetric motion between the bubble that were generated near the corner took place (Figure 6.20d). For the more important heat fluxes ($q'' \geq 80 \text{ kW.m}^{-2}$), an intermittent

Chapitre 6. Boiling flows in mini-channels

behavior between churned and annular regimes (with ripples appearance) has been observed (Figure 6.20e).

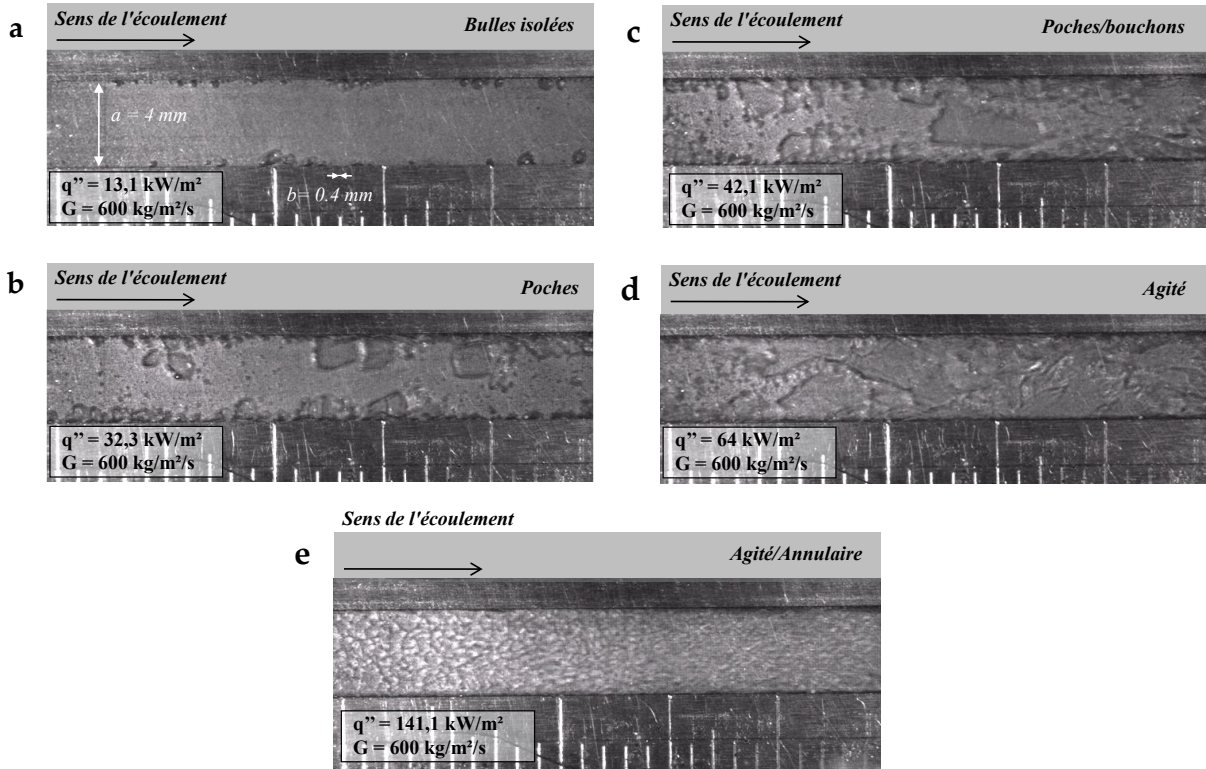


FIGURE 6.20 – Evolution of flow regimes for a mass velocity of $600 \text{ kg.m}^{-2}.\text{s}^{-1}$, a working pressure of 0.7 bar and a subcooling of 15°C for C_4 mini-channel

The data that have been reported on Figure 6.21 showed that the impact of the mass velocity was particularly important for C_4 mini-channel ($a = 4 \text{ mm} - b = 0.421 \text{ mm}$). For a mass velocity of $200 \text{ kg.m}^{-2}.\text{s}^{-1}$, it was observed that the bubbly or plug flow regimes represented a negligible part of the observations because the flow transition were rapid toward the churned regime. This behavior was due to the confinement importance inside this mini-channel compared to the other mini-channels that have been presented. Therefore, as soon as bubbles occurred after ONB, and if the mass velocity was small enough, the bubbles growth may be so rapid that their were quickly confined by the mini-channel thickness, then by the mini-channel width. It was noticed that when the mass velocity was increased, the annular flow regime seemed to vanish similarly than for all other data that were presented formerly. For this mini-channel, it was the transition regime between the churned and the annular regime which became dominant when the mass velocity was increased.

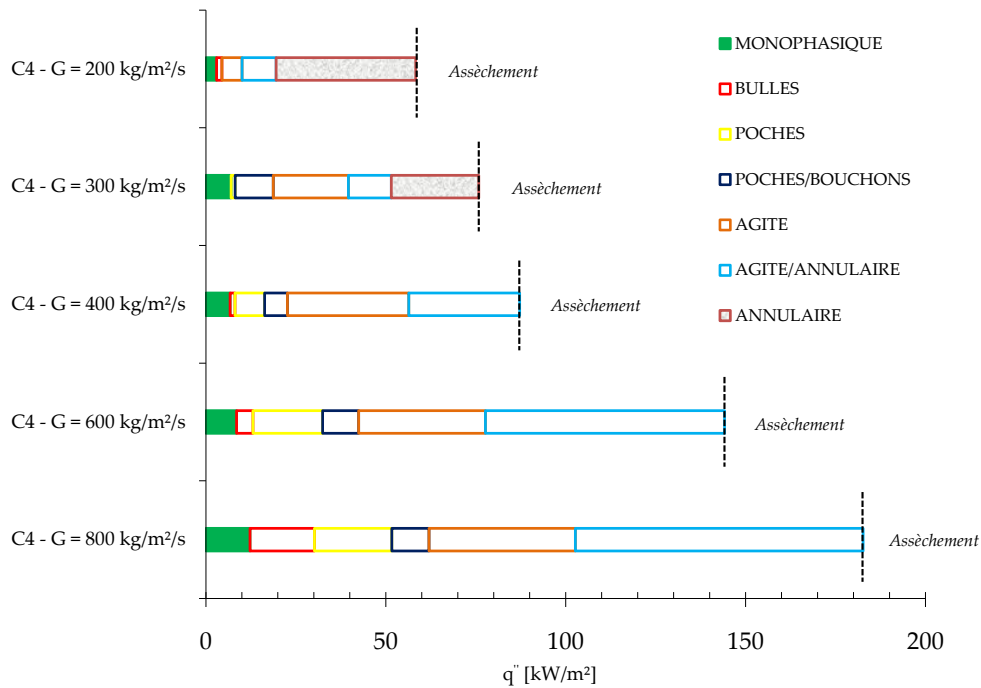


FIGURE 6.21 – Histograms representing the evolution of the transition regimes in function of the mass velocities for C_4 mini-channel ($a = 4 \text{ mm} - b = 0.421 \text{ mm}$)

Impact of the subcooling for the tests made on C_4 mini-channel

In order to complete the preceding information for which the subcooling was of 15°C , additional tests were conducted with a subcooling of 7°C for C_4 mini-channel. The objective for these tests was to establish if the transition between the flow regimes may be affected by this subcooling. It was chosen to not show the flow visualizations for this case in this manuscript, but a summary of these results was reported on Figure 6.22. The results that were obtained showed that the subcooling has a major impact on the flow regime transition that were observed experimentally. Indeed, when its value was reduced (or when the inlet temperature increased), the heat flux that led to ONB was smaller. Moreover, the range of heat flux where closed vapor structure existed was very reduced for the tested mass velocities. In this context, the reduction of the subcooling lead, for the made tests, to favor the occurrence of the annular regime for smaller heat fluxes and for the larger range of heat flux values.

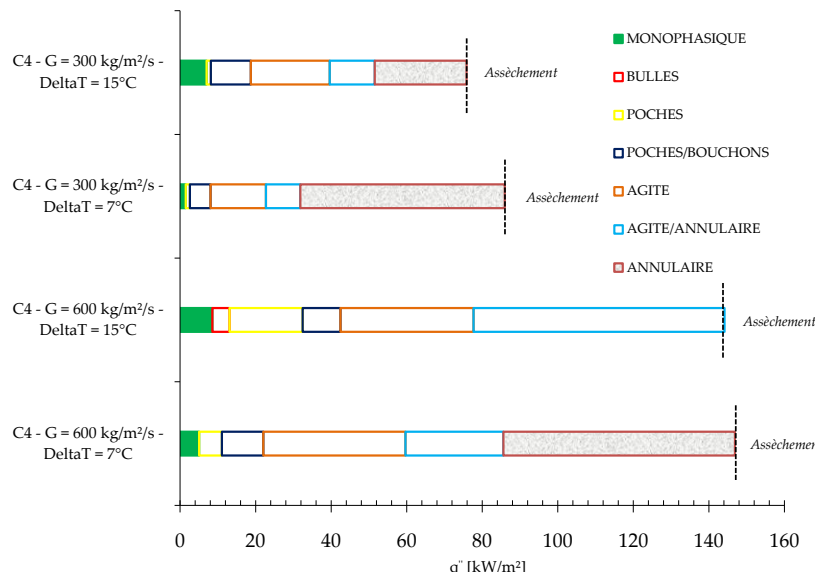


FIGURE 6.22 – Comparison between the flow regimes transition for C_4 mini-channel ($a = 4\text{ mm} - b = 0.421\text{ mm}$) for two different subcooling values of 7°C and 15°C .

Impact of the geometry on the flow regimes transitions

Figure 6.23 showed a summary of the geometry influence on the flow regimes transitions for the mass velocity of $200\text{ kg}\cdot\text{m}^{-2}\cdot\text{s}^{-1}$ (common mass velocity for all the channels).

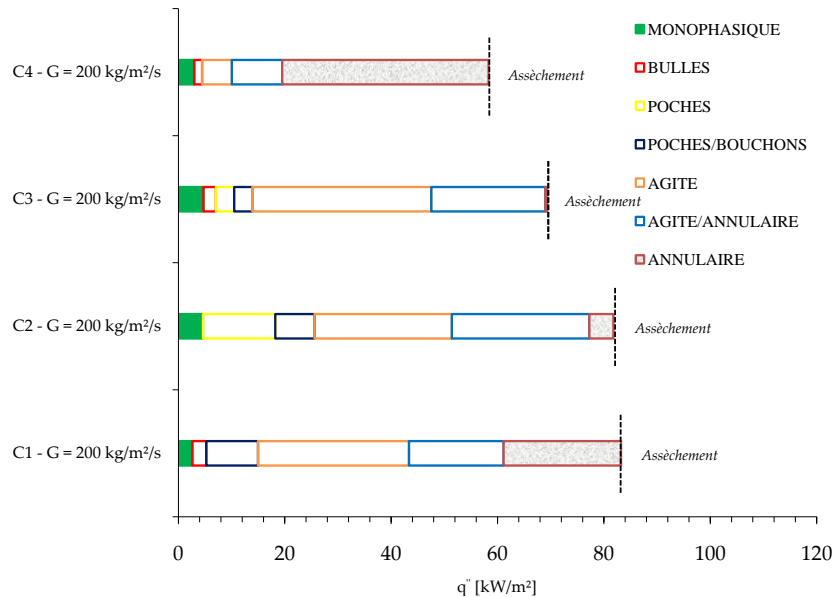


FIGURE 6.23 – Impact of the geometry on the flow regimes transitions

➤ Impact of the mini-channel width

The comparison of the mini-channel width impact (a) was made for the mini-channels $C_2(a = 5.6 \text{ mm} - b = 0.816 \text{ mm})$ and $C_3(a = 8 \text{ mm} - b = 0.814 \text{ mm})$. Here, the importance of having made specific experiments related to ONB may be quantified. Indeed, it can be specified that for the whole set of visualizations, the heat flux step was comprised between 3 kW.m^{-2} and 15 kW.m^{-2} . Therefore, it was decided for the realized comparisons between our mini-channels to justify a difference only when a difference of more than 8 kW.m^{-2} was noticed. As a consequence, this difference corresponded to two stroke lines on the x-axis of Figure 6.23. Starting from this points, the comparison were only made on the flow regimes that followed the vapor plug regime.

Therefore, according to our results, the mini-channel width increase allow for the flow regimes located after the vapor plug regimes to occur at smaller heat fluxes. Indeed, for the C_3 mini-channel, the value of the velocity was slightly smaller on the mini-channel center. In addition, as showed using the data of Figure 6.10, boiling seemed to occur for smaller heat fluxes than those that were applied to C_2 mini-channel. Therefore, bubbles that occurred more rapidly should be less subjected to the mass velocity for this mini-channel at its center and may growth more easily inside this mini-channel, what lead to more rapid transition between the flow regimes.

➤ Impact of the hydraulic diameter

This analysis was made for $C_4(d_h = 0.761 \text{ mm})$ in comparison with the other mini-channels. It was evident that the hydraulic diameter reduction led to the occurrence of the churned flow regime for heat fluxes that were smaller compared to those observed for the other mini-channels. This difference was more pronounced for churned and annular flow regimes. According to our understanding, this phenomena was due to the impact of the higher confinement in this mini-channel. The reader may noticed that the reduction of the diameter allow for the increase of the duration of annular flow regime on a larger heat flux range according to the experiments. Finally, it was noticed that for a same mass velocity, the heat fluxes that led to wall dryout were smaller for this mini-channel $C_4(a = 4 \text{ mm} - b = 0.421 \text{ mm})$.

➤ Impact of the aspect ratio

This comparison was made between $C_1(\gamma_1 = 0.435)$ and $C_2(\gamma = 0.146)$ mini-channels. The impact of the aspect ratio on the flow regime transitions seemed to be obvious according to the data that have been reported on Figure 6.23. Indeed, the transition related to the plug/slug flow regimes took place for smaller heat fluxes for the mini-channel having the higher aspect ratio (b/a). Indeed, the aspect ratio increase led to the flow cross section reduction for a same hydraulic diameter. As a consequence a bubble that grow in C_1 mini-channel would be more rapidly confined than another one that would grow in C_2 mini-channel (for same growing rate). This analysis allow for the justification of the flow regime transition between the plug/slug flow regimes for smaller heat fluxes for this mini-channel.

Summary of the analysis that were made using the images acquisition system

The pictures that were commented and analyzed in this paragraph were essentially made using the images acquisition that came from high speed camera. The obtained results showed that the flow rate impact on the flow regime transitions was significant. Indeed, when it was increased, the required heat flux that allow for the reaching of the same flow regime transition increased. In addition, the flow regime that had closed vapor interfaces (bubbly or slug flow regimes) remained on heat fluxes range that were more extended for larger flow rate. This last result may be explained by the impact of the subcooling that became more pronounced during the flow rate increase in boiling in mini-channel.

During these analysis, the impact of the subcooling on the flow regime transitions was studied also. The observations showed that when the subcooling was reduced, the bubbly or plug flow regimes tend to be reduced in comparison with the whole set of analyzed flow regimes. It was obvious that as the inlet temperature was higher, the bubble growth was more rapid for this case and decreased the time duration toward the churned and annular regimes.

The impact of the mini-channel geometry was analyzed on the flow regimes. The mini-channel width increase seemed to lead to more rapid flow regime transitions. The reduction of the aspect ratio for a same hydraulic diameter led to the increase of the heat flux needed for the flow regime transition. As highlighted in this paragraph, this observation would be due to the mini-channel cross section influence. Finally, according the reported results, the hydraulic diameter was the most important parameter which has an impact on the flow regime transitions in the mini-channels. Indeed, its reduction led to a very rapid transition compared to the other mini-channels toward the flow regimes that did not present clear closed vapor interfaces.

6.4 Evolution of boiling curves with wall heat flux

An important parameter for the convective boiling study was the occurrence of wall dryout (CHF) which led to a rapid reduction of the heat transfer coefficients. Indeed, for correctly sizing a heat exchanger, it was necessary to know the condition that led to this point. It can be highlighted that the pressure drop as well as the heat transfer rate may evolved on the whole range of heat fluxes that were comprised between ONB and CHF. During the state of art review, it was established that one of the relevant tool that allow for the knowledge of the heat fluxes that led to CHF was related to the boiling curves study. Thus, for each of the tested plates, the evolution of the boiling curves up to heat fluxes values that were obtained for reaching CHF were obtained experimentally. Moreover, in order to better understand the

evolution of the pressure drops, of the heat transfer rate, of the conditions that conducted to wall dryout, simultaneous visualizations of the flow in the mini-channels were made. Some of these visualizations have been already presented in § 6.3.

6.4.1 Boiling curves presentation

The boiling curves were studied for three mini-channels ($C_1(a = 2.3 \text{ mm} - b = 1 \text{ mm})$, $C_2(a = 5.6 \text{ mm} - b = 0.816 \text{ mm})$ and $C_4(a = 4 - b = 0.421 \text{ mm})$). It was then made additional tests on C_3 mini-channel ($a = 8 \text{ mm} - b = 0.814 \text{ mm}$), for mass velocities of $100 \text{ kg.m}^{-2}.\text{s}^{-1}$ and $200 \text{ kg.m}^{-2}.\text{s}^{-1}$, for studying the mini-channel geometry impact on the pressure drops and heat transfer coefficients evolutions .

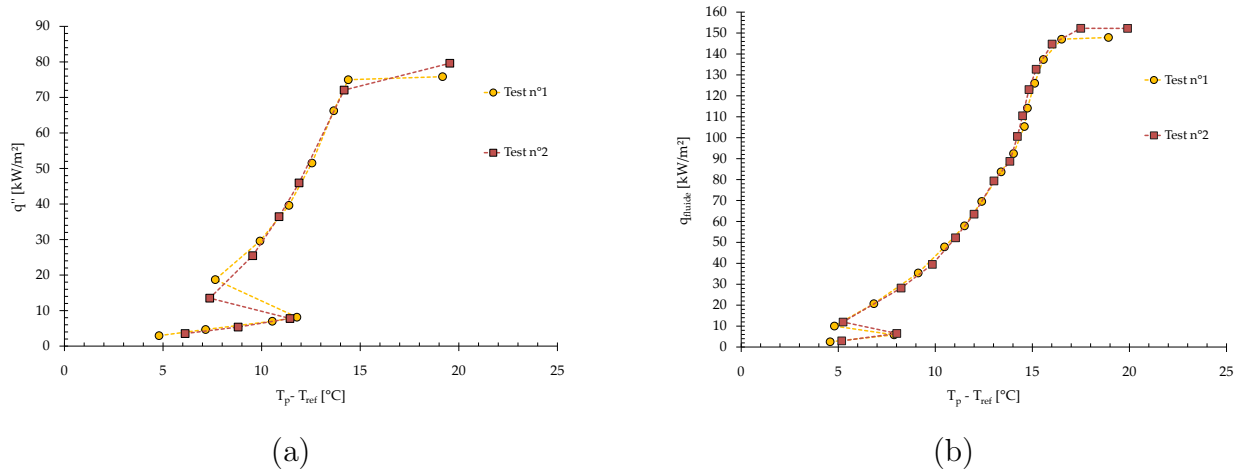


FIGURE 6.24 – Repeatability experiments for $C_4(a = 4 \text{ mm} - b = 0.421 \text{ mm})$: (a) a mass velocity of $300 \text{ kg.m}^{-2}.\text{s}^{-1}$ and a subcooling of 15°C (b) a mass velocity of $600 \text{ kg.m}^{-2}.\text{s}^{-1}$ and a subcooling of 7°C

Similarly to the former experiments, it was first made repeatability tests. These tests have been reported for C_4 mini-channel, for a mass velocity of $300 \text{ kg.m}^{-2}.\text{s}^{-1}$ and a liquid subcooling at the mini-channel entrance of 15°C (Figure 6.24a). Then in a second step and for the evaluation of the subcooling impact, for a mass velocity of $600 \text{ kg.m}^{-2}.\text{s}^{-1}$ and a subcooling of 7°C (Figure 6.24b).

These tests showed good repeatability for the ONB as well as for the heat flux and wall temperatures values that led to dryout. It should be reminded that the wall heat fluxes was controlled according to minimum heat flux steps of about 3 kW.m^{-2} . Therefore, it have to be noticed that the measurements accuracy should have been better if this step was smaller. However for the considered experimental configuration, it was chosen to limit the increment to this value that was estimated as sufficient.

Chapitre 6. Boiling flows in mini-channels

In the following paragraphs, the boiling curves that were obtained for the four selected mini-channels have been given for a subcooling of 15°C and a working pressure of 0.7 bar . For all of these curves, the two parameters of control were the heat flux and the flow rate.

✓ C_1 mini-channel ($2.3\text{ mm} \times 1\text{ mm}$)

The results that have been obtained for C_1 mini-channel are reported in Figure 6.25. The figure inset represent a zoom of the convected heat flux for the smaller heat fluxes.

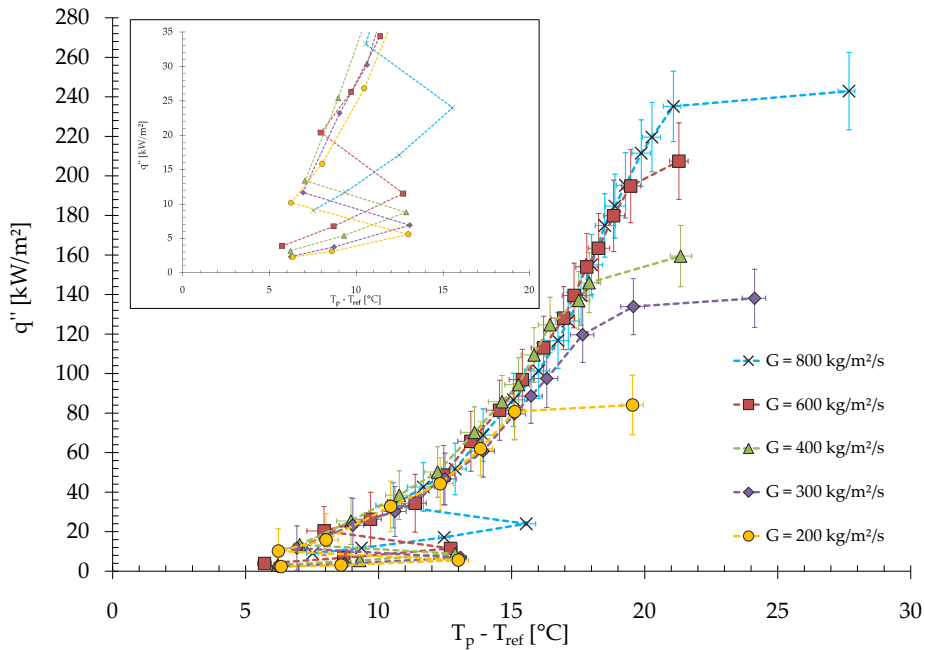


FIGURE 6.25 – Boiling curves for C_1 mini-channel

The text that has been inserted in the below framework summarized a general analysis that applied for all the boiling curves that were given in this manuscript. Therefore, some of the explanations that were discussed here will not be reported later in the manuscript.

Two different evolutions, which depended on the occurrence of saturated boiling, appeared during the boiling curves study. When the flow was in single-phase flow configuration, it was observed that the heat transfer rate increased linearly with the wall superheat. This behavior showed that the heat transfer coefficient (which is equivalent to the ratio between heat transfer and wall superheat) remained constant if the flow rate remain constant also. When the flow rate was increased, it was possible to notice a slight rise of the boiling curve slope which correspond to an improvement of the heat transfer rate for single-phase flow conditions.

When saturation occurred, a wall superheat jump was noticed. Indeed, when boiling developed, the wall temperature was reduced and led to a reduction of the wall superheat that was clearly visible on Figure 6.25. This phenomenon was observed for all the tested mini-channels analyzed in this study, when the subcooling was set to $15^{\circ}C$. It was noticed that this jump became smaller when the subcooling was reduced. After ONB, a slope increase of the boiling curve may occurred for higher heat fluxes. This characteristic slope change was synonym of a improvement of the heat transfer rate.

The results that have been given in Figure 6.25 suggested that ONB was not dependent of the wall superheat for mass velocities that were comprised between 200 and $600 \text{ kg.m}^{-2}.\text{s}^{-1}$. This result did not seem in agreement with the evolutions reported in literature (Liu *et al.* (2005), Harirchian et Garimella (2008)) that showed that this superheat should increased with the mass velocities. This unusual evolution may be due to the heat flux increment that was too high for the experiments. This result suggest that the wall superheat evolution for reaching ONB was the same when the flow rate increase in this range of mass velocities (between 200 and $600 \text{ kg.m}^{-2}.\text{s}^{-1}$). In the other hand, it was observed that the required heat flux for reaching the saturated conditions increased with the flow rate. After ONB, the whole set of boiling curves seemed to follow the same evolution in the fully developed boiling region. Therefore, in this region the heat transfer rate did not seemed to be dependent on mass velocity.

As showed during the flow boiling regime visualization, the wall heat flux that led to dryout increased with the flow rate (Figure 6.25). The dryout was easily noticeable on this curve because it was characterized by a significant increase of the wall temperature that led to the increase of the wall superheat.

✓ C_2 mini-channel ($5.6 \text{ mm} \times 0.816 \text{ mm}$)

Figure 6.26 showed the boiling curve evolution for C_2 mini-channel ($a = 5.6 \text{ mm} - b = 0.816 \text{ mm}$). Similarly to C_1 mini-channel ($a = 2.3 \text{ mm} - b = 1 \text{ mm}$), it was noticed that the heat flux that led to ONB increased with the flow rate. However, the wall superheat evolution for saturated conditions was very different compared to the one observed with C_1 mini-channel.

Chapitre 6. Boiling flows in mini-channels

Indeed, the wall superheat increased significantly with flow rate. It was assumed that this phenomenon was due to the higher difference between the heat flux that led to ONB and the heat flux related to OSV (that characterized the saturated conditions).

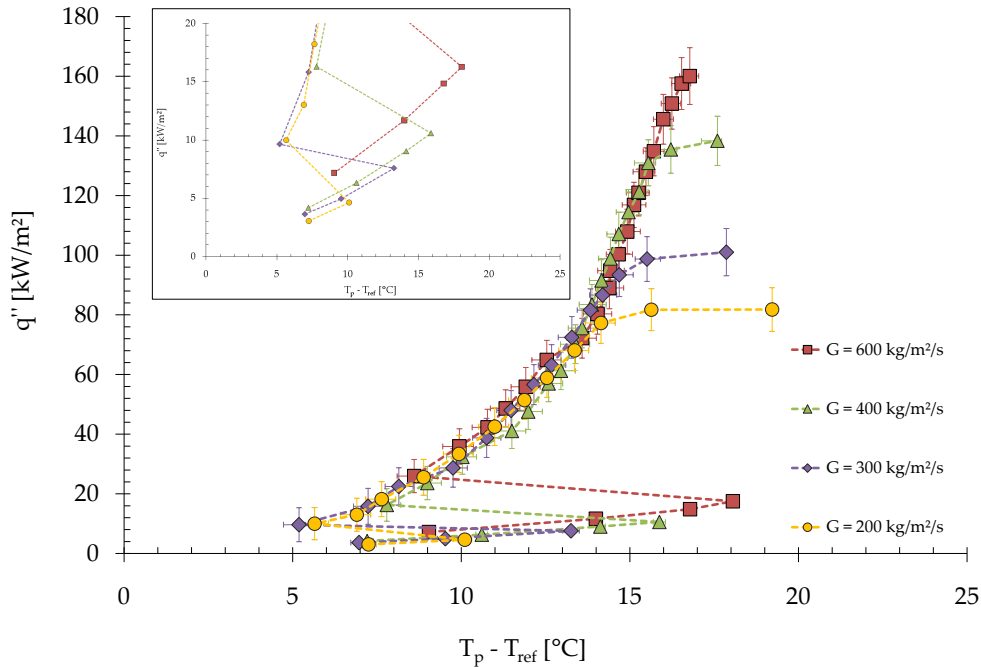
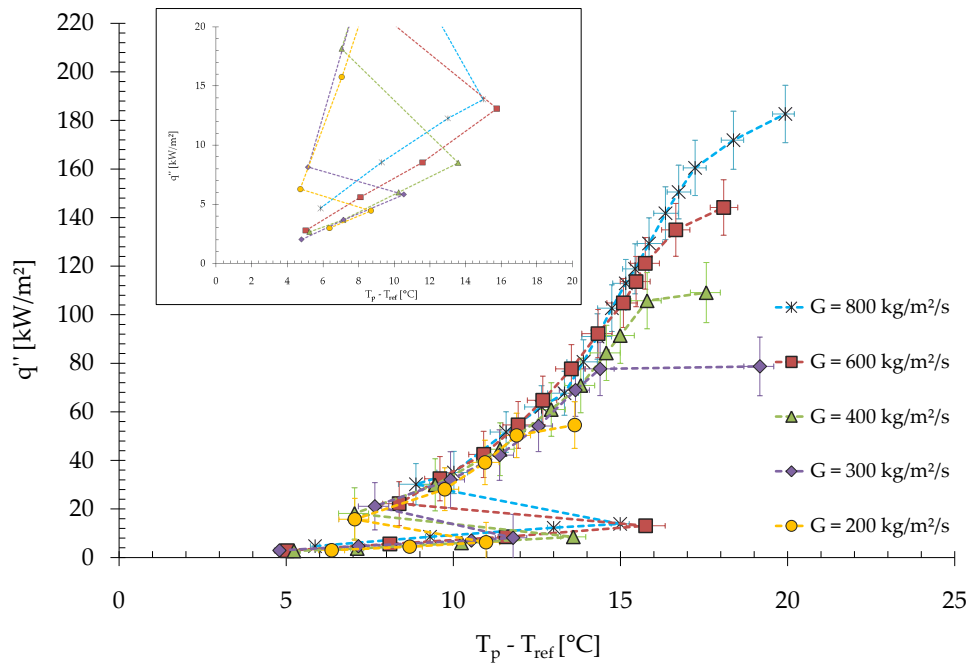


FIGURE 6.26 – Boiling curves for C_2 mini-channel

✓ C_4 mini-channel ($4\text{ mm} \times 0.421\text{ mm}$)

The results that have been obtained for C_4 mini-channel are reported in Figure 6.27. Similarly to preceding cases, the heat flux value that led to occurrence of saturated conditions increased with mass velocity. It was observed that for the most part of the made experiments, the wall superheat increase with mass velocity at ONB.


 FIGURE 6.27 – Boiling curves for C_4 mini-channel

Summary on the boiling curves

The boiling curves study allow for the determination of the conditions that led to wall dryout for the tested mini-channels. It was possible to observe that the minimum heat flux that led to this dryout increased with the mass velocity. Indeed, the flow rate increase led to strengthen the convective transport and increase the cooler liquid amount (that came from entrance) that contributed to the more rapid replacement of the generated vapor on the mini-channel walls (Carey (2008)). The deeper study related to the conditions that led to wall dryout as well as the impact of the geometry on this dryout will be discussed in § 6.4.4. It can be noticed that in parallel to the study related to the determination of these curves, the pressure variations were measured between the mini-channels inlet and outlet also (§ 6.4.2). Finally, the heat transfer coefficients were calculated using these curves in § 6.4.3. The whole set of data, allowed for the definition of the impact of the mini-channel geometry on these conditions.

6.4.2 Pressure drop evolution

Using the data that were obtained during the work on boiling curves, a study related to the impact of the operating conditions on pressure drops and heat transfer coefficients evolutions was made on the selected mini-channels. The experimental results were then compared to the correlations that have been presented in the state of the art review (Chapter 2). To conclude this part, an adapted correlation regarding the selected mini-channels was proposed.

It can be underlined that the pressure drops and heat transfer coefficients evolution may be plotted as the function of vapor thermodynamic quality even if the control parameter was the heat transfer rate between the wall and the fluid. Indeed, for the realized study, it was noticed that the heat transfer coefficient (§ 6.4.3) and the two-phase flow pressure drops evolved very few with the flow rate for a same convected heat flux (when the flow conditions were far from dryout conditions). Therefore, the vapor quality, which represent the vapor concentration and which depended on the convected heat flux, may be chosen in order to represent the evolution of these two parameters in function of the mass velocity for a same mini-channel. It can be expressed according to the following relationship :

$$x = \frac{\frac{\Phi_{conv}}{\dot{m}} + c_{p,l}(T_{amont} - T_{sat})}{h_{lv}} \quad (6.12)$$

where Φ_{conv} is the convected heat flux ; \dot{m} , the mass flow rate ; $c_{p,l}$, the liquid specific heat at constant pressure ; T_{sat} , the saturation temperature and h_{lv} , the liquid latent heat.

Determination of the total two-phase flow pressure drops

When a subcooling is imposed at the channel entrance, a single-phase flow length may exist before boiling. In this configuration, the determination of the pressure drops evolution due to the two-phase flow in the mini-channel was dependent of this single-phase flow length. Indeed, the pressure drops that appeared for the single-phase flow were different to those observed during the saturated boiling. Therefore, it became necessary to estimate the location where the saturated boiling occurred in order to calculate the pressure drops that were only due to two-phase flow.

During the realized experiments, it was observed that as soon as the vapor bubbles started to detach from the channel corner to flow toward the center of the different mini-channels, nucleation sites that were located on the bottom wall were already active and generated several smaller bubbles. Then, when the heat flux became stronger, the single-phase flow length seemed

to vanished very quickly. Theoretically and using an energy balance, this single-phase flow length may be defined using :

$$L_{mono} = \frac{\dot{m}c_{p,l}(T_{sat} - T_{in})}{q''_{moy} \int_0^z \exp\left(f_1(Re)\frac{z}{L} + f_2(Re)\right) dz [2(a+b)]} \quad (6.13)$$

When this location z was smaller to the location where the flow was fully saturated z_{sat} , it was admitted that the pressure drop followed the evolution of the model given by Shah et London (1978) [equation (1.9)]. When $z > z_{sat}$, it was supposed a linear pressure drop from z_{sat} up to the mini-channels outlet.

At the moment where boiling developed in the mini-channel, it was observed that the progression front of this boiling was located very rapidly toward the mini-channel entrance for small heat flux increments above the one leading to ONB. The observed evolution was much more rapid that those predicted using equation (6.13). It was observed that the bubble amount increase due to the heat flux increase, may generate unstable phenomenon that tend to favor the occurrence of boiling toward the mini-channels entrance. Therefore, once the vapor plug regime was reached, this single-phase flow length seemed to vanish. Consequently, it was considered that the length that allow for the calculation of the pressure gradient after this flow regime was the total length of the mini-channels. For these cases, the pressure gradient due to two-phase flow may be calculated using :

$$\left(\frac{dP}{dz}\right)_{diph(tot)} = \frac{P_{aval} - P_{amont} - 1/2\rho_l u^2}{L_{tot}} \quad (6.14)$$

where $1/2\rho_l u^2$ is a term that took into account the fluid acceleration due to the convergent, that generated a reduction of the mini-channels inlet pressure.

☞ *Influence of the mass velocity on the pressure drops*

The evolution of the pressure drops have been represented in function of the convected heat flux (Figure 6.28a) and in function of the thermodynamic vapor quality (Figure 6.28b) for several mass velocities for C_1 mini-channel ($a = 2.3 \text{ mm} - b = 1 \text{ mm}$).

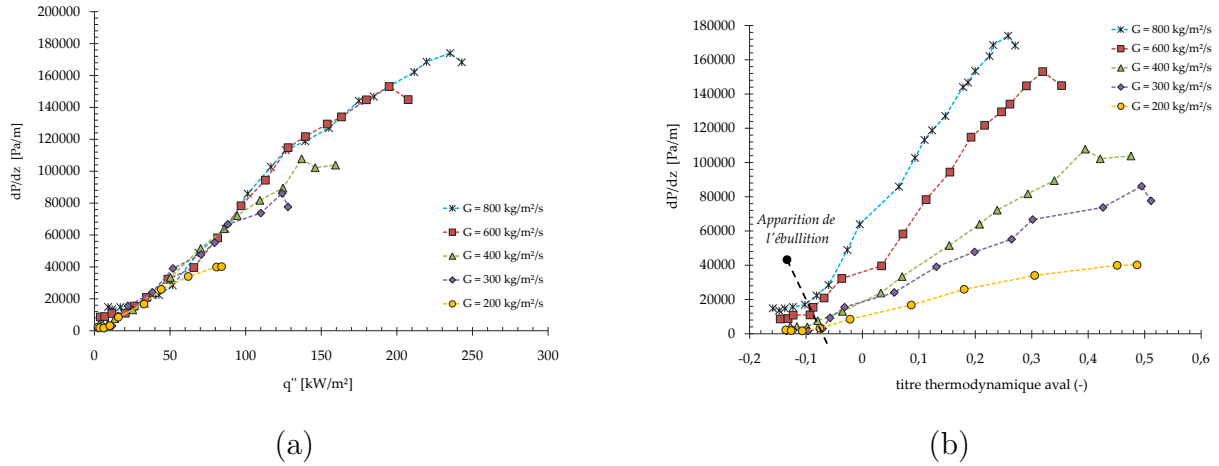


FIGURE 6.28 – (a) Influence of the convected heat flux (b) Impact of the thermodynamic vapor quality on the total pressure drops for C_1 mini-channel ($a = 2.3 \text{ mm} - b = 1 \text{ mm}$) and a subcooling of 15°C

It was observed that during the fully developed boiling regime, the pressure gradient slightly varied for a same convected heat flux. This result showed that the impact of the mass velocity was relatively small when considering the heat transfer rate to the fluid. This observation was made for the other studied mini-channels where a very small variation of the pressure drops were noticed for a same convected heat flux. It was thought that this result may be explained as followed : the mass flow rate impact led to a different evolution of the two terms of pressure drops, that were caused by, on one hand the friction and on the other han by the acceleration between the liquid and vapor phases. These two terms contributed to the total pressure drops (equation 6.15).

$$-\left(\frac{dP}{dz}\right)_{diph(tot)} = -\left(\frac{dP}{dz}\right)_{diph(fr)} + \frac{d}{dz} \left[\frac{G^2 x^2}{\rho_v \alpha} + \frac{G^2 (1-x)^2}{\rho_l (1-\alpha)} \right] \quad (6.15)$$

Indeed, when the mass velocity increased, the thermodynamic vapor quality became smaller for a same heat flux exchanged between the fluid and the wall. Therefore, the contribution of the pressure drops due to the acceleration between the phase was reduced, whereas the pressure drops that were generated by the frictions increased with the mass velocity. Consequently, this reduction would lead to a smaller sensitivity of the pressure drops to the heat flux when the mass velocity varied. The study of these total pressure drops showed that when reasoning at given vapor concentrations, the influence of the mass velocity on the pressure drops was strong (Figure 6.28b) and the increase of the mass velocity led to an increase of the pressure drops. However, in the following sections, the impact of the convected heat flux was considered as the single control parameter.

Impact of the geometry on the pressure drops variations

The charts that have been drawn on Figure 6.29 showed the impact of the mini-channel geometry on the total pressure drops variation in function of the convected heat flux for different mass velocities.

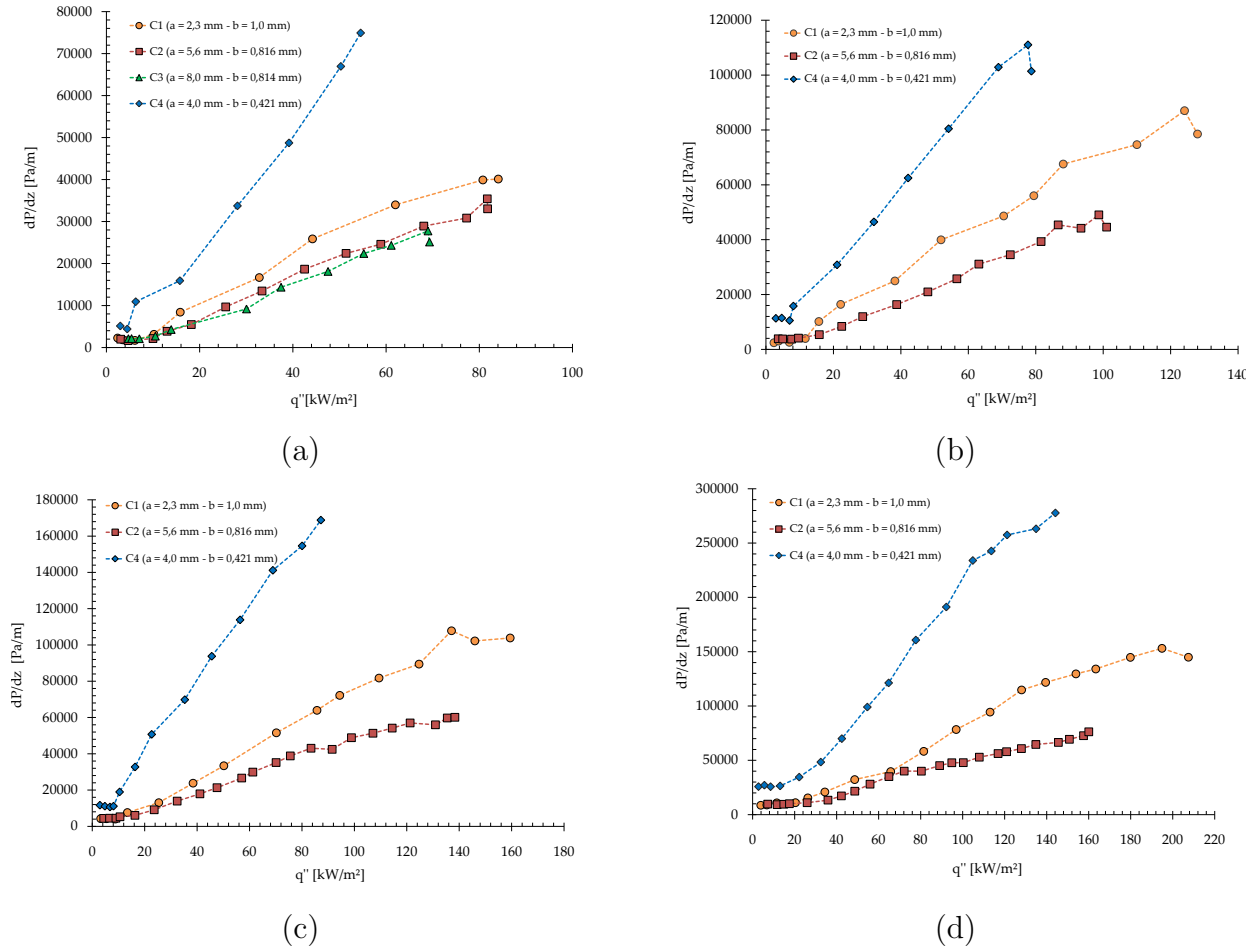


FIGURE 6.29 – Influence of the geometry on the pressure drops variations for the different mini-channels for a mass velocity of : (a) 200 kg·m⁻²·s⁻¹ (b) 300 kg·m⁻²·s⁻¹ (c) 400 kg·m⁻²·s⁻¹ and (d) 600 kg·m⁻²·s⁻¹

During the single-phase flow, the pressure drops evolved slightly for the four tested mini-channels when the convected heat flux increased. It can be noticed that some of the state of the art results (Harirchian et Garimella (2009), Bhide *et al.* (2009)) showed that these pressure drops were reduced due to the liquid viscosity decrease which was due to the temperature increase (case that were observed for 73% of our experiments). For the mini-channels whose hydraulic diameter looked similar [C₁($d_h = 1.39$ mm), C₂($d_h = 1.42$ mm), C₃($d_h = 1.48$ mm)], the pressure drops were very close for the single-phase flow. Once boiling occurred, the pressure drops increased almost linearly with the heat flux. This increased was due to the intensification

of the pressure drops due to the friction as well as those due to the acceleration between the liquid and vapor phases.

The impact of the geometrical parameters on the pressure drops was studied also and the results of this analysis has been given in the following paragraphs.

➤ Hydraulic diameter impact

The data that have been reported in Figure 6.29 showed that the geometrical parameters impacted that total pressure drops. Therefore, when the mini-channel hydraulic diameter was reduced (comparison between $C_4(d_h = 0,762 \text{ mm})$ mini-channels with the other ones), it was observed that for a same convected heat flux, the pressure drop increase significantly. Indeed, this increase was caused by the reduction of the cross section that confined the vapor bubbles that were produced during the boiling. It was observed that the difference between these pressure drops tends to become more important when the mass velocity increased also.

➤ Aspect ratio impact

The aspect ratio (b/a) has a significant impact on the experiments also. This comparison was made for $C_1(\gamma_1 = 0.435)$ and $C_2(\gamma_2 = 0.146)$ mini-channel that have a close hydraulic diameter (1.4 mm). It was noticed that the pressure drops were higher ⁷ for the mini-channel having the larger aspect ratio (C_1), once boiling occurred (Figure 6.29). Indeed, if the hydraulic diameter remained constant, the increase of the aspect ratio induced a reduction of the flow cross section. In this case, when boiling occurred, the bubbles would be more confined in the C_1 mini-channel, what generated a higher pressure drop.

➤ Mini-channel width impact

The mini-channel width seemed to play a role on the pressure drop evolution also. Indeed, when this width was increased, the flow cross section increase and thus the vapor phase confinement was reduced and led to a slight reduction of the pressure drops that were experimentally measured (comparison of $C_2(a = 5.6 \text{ mm} - b = 0.816 \text{ mm})$ and $C_3(a = 8 \text{ mm} - b = 0.814 \text{ mm})$) mini-channels for the mass velocity of $200 \text{ kg.m}^{-2}.\text{s}^{-1}$.

7. Here, the flow rate tend to increase this difference also.

Construction of a confinement number adapted to our study

During the state of the art review, no number was found relevant to allow for the consideration of the boiling flow confinement in the mini-channels. Indeed, the parameter defined by Kew et Cornwell (1997) (equation (2.20)) considered the impact of the hydraulic diameter only. However according to the data that have been obtained, different pressure drops were obtained for boiling conditions as soon as the aspect ratio was modified for a same hydraulic diameter. In an attempt to solve this problem, Agostini (2002) has proposed to consider the smaller dimension of the channel in order to take into account the confinement. However according to these experiments, the pressure drop evolution seemed to be related to the common values regarding the mini-channel width (a) and height (b). Therefore for characterizing the importance of the confinement on the pressure drop evolution in the mini-channel, it may be proposed (according to our experiments this parameter seemed to depend on the flow rate only) to consider the impact of the cross section and of the aspect ratio. This confinement number (Co_{ad-hoc}) was built as followed :

$$Co_{ad-hoc} = \sqrt{\frac{\sigma}{g(\rho_l - \rho_v)}} \left(\frac{1}{a \times b \times \gamma^{0.22}} \right)^{0.5} \quad (6.16)$$

The construction of this number^a was based on the mean differences that have been observed experimentally between $C_1(a = 2.3 \text{ mm} - b = 1 \text{ mm})$, $C_2(a = 5.6 \text{ mm} - b = 0.816 \text{ mm})$ and $C_4(a = 4 \text{ mm} - b = 0.421 \text{ mm})$ mini-channels. This number allow for the establishment, using the geometrical data only, of the importance of the pressure drops inside these mini-channels. The value of this new number for each mini-channels is :

- ▷ $Co_{ad-hoc}(C_1) = 0.729$, for C_1 mini-channel
- ▷ $Co_{ad-hoc}(C_2) = 0.584$, for C_2 mini-channel
- ▷ $Co_{ad-hoc}(C_3) = 0.509$, for C_3 mini-channel
- ▷ $Co_{ad-hoc}(C_4) = 0.996$, for C_4 mini-channel

These evolutions were in very good agreement with the mean differences that have been observed between C_1 , C_2 and C_4 mini-channels. It can be noticed that for the correlation construction, C_1 mini-channel was taken as the reference. The reader may notice that when the aspect ratio equaled 1, the confinement number was strictly equaled to the one defined by Kew et Cornwell (1997) (6.30).

^a. It should be specified that the value of γ cannot have a value higher than 1.

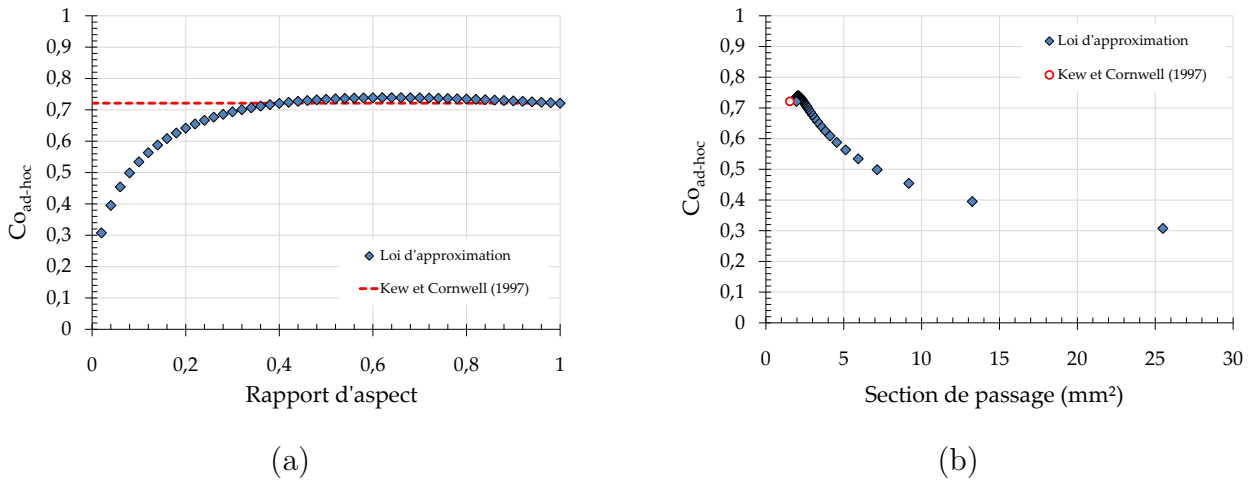


FIGURE 6.30 – Influence of the geometry on the confinement number evolution (equation 6.16) for different mini-channel having the same hydraulic diameter (1.4 mm) in function of the mini-channel : (a) aspect ratio (b) cross section

The evolution of the confinement number (Co_{ad-hoc}) has been represented on Figure 6.30, for the mini-channels having similar hydraulic diameter (1.4 mm) but with different aspect ratios or cross sections. As a reference, the evolution of the confinement number that have been defined by Kew et Cornwell (1997) (equation (2.20)) has been reported on these two charts. The evolution of this number suggest that the flow confinement tend to increase with the aspect ratio when the hydraulic diameter was kept the same. Figure 6.30b showed that this confinement number was reduced when the flow cross section increase.

Comparison of the experiments with the correlations of the state of the art review

In order to evaluate the pressure drops that were obtained, the experiments have been compared to the literature data. The expression of the total pressure drops in two-phase flow for a horizontal flow has been already given (equation (6.15)). Therefore, in order to compare the total pressure drops that have been obtained experimentally to the correlations from the literature, it was necessary to estimate the pressure drop term due to the acceleration between the vapor and liquid phases (second term at the right of equation (6.15)) in order to calculate the total pressure drops. As it was not possible to determine the void fractions during the experiments, it was necessary to make a choice among the correlations that allow for the prediction of this parameter in function of the thermodynamic vapor quality (correlations that were defined in § 2.4). To do so, it was chosen to follow the recommendation made by Thome (2006) by using the Steiner correlation (1993) (equation (2.72)).

➤ Analysis of the data related to $C_1(a = 2.3 \text{ mm} - b = 1 \text{ mm})$ mini-channel

The comparisons that were made with the correlation that allow for the determination of the total pressure drop related to $C_1(a = 2,3 \text{ mm} - b = 1 \text{ mm})$ mini-channel have been reported in Figure 6.31. The whole set of predictive models (homogeneous; Lockhart et Martinelli (1949) (noted L-M), Grönnerud (1972), Chisholm (1973), Friedel (1979); Müller-Steinhagen et Heck (1986) (noted M-S-H)) has been represented at $\pm 25\%$ for evaluating their prediction performances regarding our experiments.

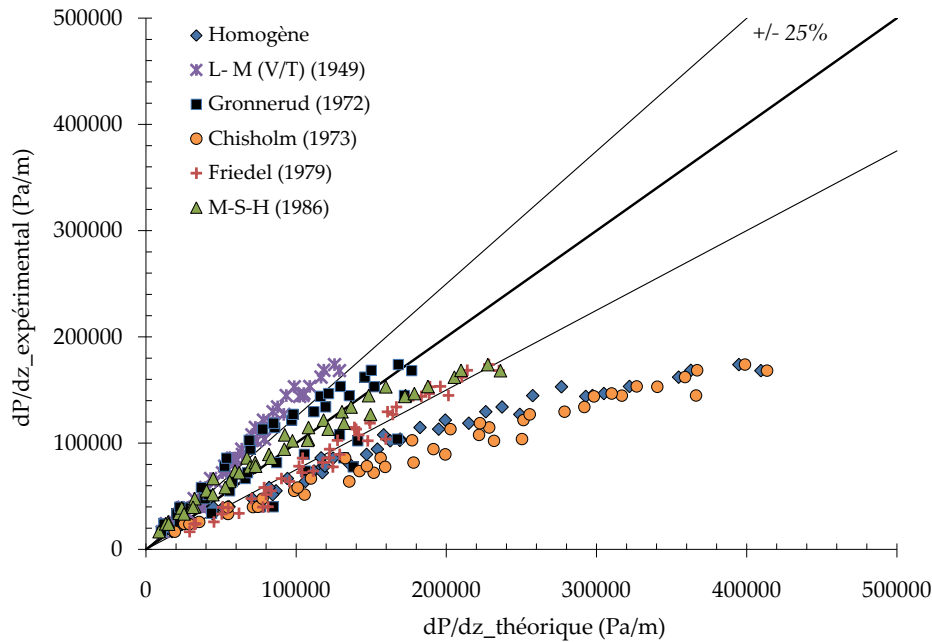


FIGURE 6.31 – Comparison between the total pressure drops that have been obtained experimentally to those predicted by the correlations taken from the literature for $C_1(a = 2.3 \text{ mm} - b = 1 \text{ mm})$ mini-channel

It can be noticed that for the Lockhart et Martinelli (1949) correlation, it was considered that the liquid phase was laminar (or viscous according to Chisholm et Laird (1958)) and that the vapor phase was turbulent. It was observed that the models that took better into account the experimental pressure drops evolutions were those of Müller-Steinhagen et Heck (1986) with 69.6 % of the data point that were predicted at $\pm 25\%$ and Friedel (1979) with 45.6% at $\pm 25\%$. The Grönnerud (1972) model allow for the prediction of almost 50% of the experimental data point but present a very important scattering. It lead us to conclude that the physical phenomena that have been taken into account for the construction of this model were not analogous to the behaviors that have been observed during our experiments. According to these comparisons, the predicted results due to homogeneous model remained very far to those that have been measured experimentally for this mini-channel $C_1(a = 2.3 \text{ mm} - b = 1 \text{ mm})$.

Chapitre 6. Boiling flows in mini-channels

➤ Analysis of the data related to $C_2(a = 5.6 \text{ mm} - b = 0.816 \text{ mm})$ mini-channel

On Figure 6.32, the predictive correlations for the pressure drops were compared to the experiments for $C_2(a = 5.6 - b = 0.816 \text{ mm})$ mini-channel.

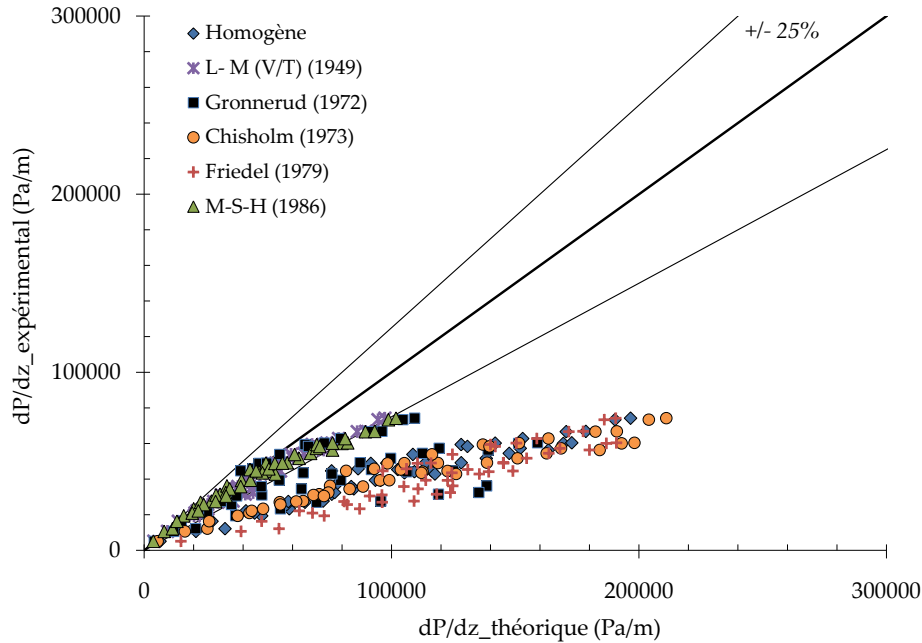


FIGURE 6.32 – Comparison between the total pressure drops that were obtained experimentally to those given by the literature for $C_2(a = 5.6 \text{ mm} - b = 0.816 \text{ mm})$ mini-channel

Differently to the results that have been obtained with $C_1(a = 2.3 \text{ mm} - b = 1 \text{ mm})$ mini-channel, the model that allow for best prediction of the pressure drop for $C_2(a = 5.6 \text{ mm} - b = 0.816 \text{ mm})$ was the one of Lockhart et Martinelli (1949) with 93.6% of the data predicted at $\pm 25\%$ what is a very good agreement. This model is followed by the one of Müller-Steinhagen et Heck (1986) that have predicted 82.9% of the data points at $\pm 25\%$. This last model showed again is very good ability for predicting the data, even when the mini-channel aspect ratio changed for a same hydraulic diameter (comparison made for C_1 and C_2 mini-channels).

It can be observed that the homogeneous model for C_2 mini-channel, was not able to predict the total two-phase flow pressure drops.

➤ Analysis of the data related to $C_3(a = 8 \text{ mm} - b = 0.814 \text{ mm})$ mini-channel

On Figure 6.33 the data related to the tow-phase flow pressure drops have been given for $C_3(a = 8 \text{ mm} - b = 0.814 \text{ mm})$ mini-channel.

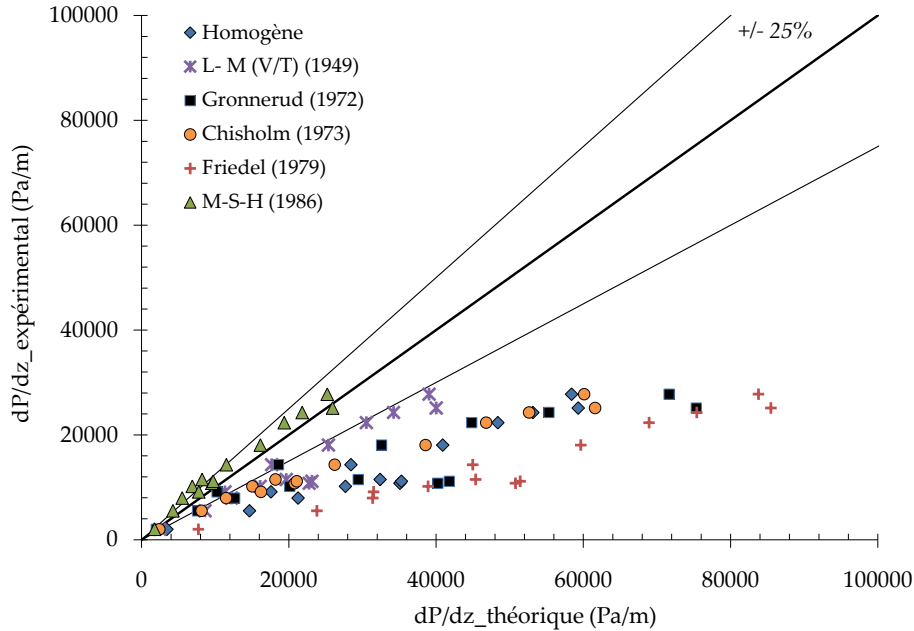


FIGURE 6.33 – Comparison between the total pressure drops that have been obtained experimentally and those given by the literature correlations for $C_3(a = 8 \text{ mm} - b = 0.814 \text{ mm})$ mini-channel

It should be reminded that these results have been obtained for mass velocities of $100 \text{ kg.m}^{-2}.s^{-1}$ and $200 \text{ kg.m}^{-2}.s^{-1}$ what explained the difference in term of data points number compared to those related to the preceding mini-channels. Still here, the model that was able to predict the more important number of experimental data points was the one of Müller-Steinhagen et Heck (1986) with 71.4% of data points that were predicted at $\pm 25\%$. However, regarding the small number of data point for this mini-channel, it was not possible to confirm this trend for the higher pressure drops values.

The reader may notice that the data predicted using the homogeneous model remained far from the experiments for this mini-channel also.

➤ Analysis of the data related to $C_4(a = 4 \text{ mm} - b = 0.421 \text{ mm})$ mini-channel

Finally, the comparisons between our experiments and the correlations given by the literature for $C_4(a = 4 \text{ mm} - b = 0.421 \text{ mm})$ mini-channel have been reported in Figure 6.34.

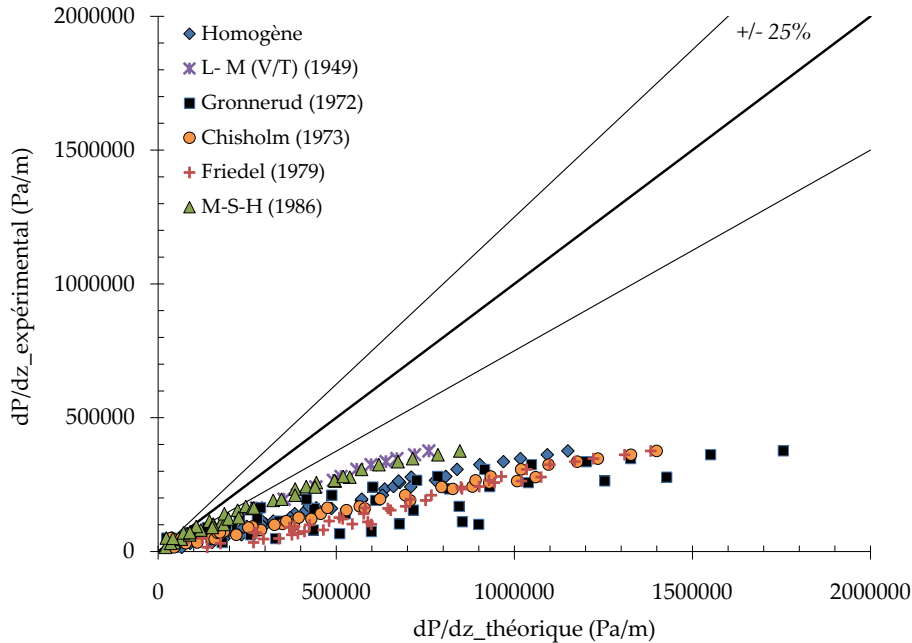


FIGURE 6.34 – Comparison between the total pressure drops that have been obtained experimentally compared to the correlations given by literature for $C_4(a = 4 \text{ mm} - b = 0.421 \text{ mm})$ mini-channel

The data that have been given on Figure 6.34 showed all the importance of the hydraulic diameter impact on the two-phase flow pressure impact. Indeed, for this mini-channel, none of the models reported here were able to correctly predict the experimental data points. However it can be observed that the model that was able to predict better the results was the one of Müller-Steinhagen et Heck (1986) which predicted 24.4% of the experimental data points at $\pm 25\%$, what is poor.

Still here the homogeneous model was unable to be used as a predictive tool for the pressure drop determination, which tended to confirm that as soon as the cross section of the duct differed from circular cross sections, a difference exists regarding the evolutions usually reported in mini-tubes. Indeed, some authors (Saitoh *et al.* (2005), Ribatski *et al.* (2006), among others) supported that the flow cross section reduction of a mini-tube tends to force the two phases (liquid and vapor) to flow to close velocities and thus the pressure drops should get closer to the homogeneous model. According to these experiments, this evolution would be different for these mini-channels.

In the following paragraphs, it was proposed to establish a correlation that would be able to take into account the pressure drops evolutions that were observed in our experiments.

☞ *Proposal of a correlative law adapted to the presented experiments*

After the study of all these data, it was possible to notice that the homogeneous model was far to be able to predict the pressure drops that have been obtained experimentally. Therefore, in order to define a correlative law that allow for the prediction of the experimental data points, the analysis was based on a approach that considered the separated flow model. This very intuitive approach allow for the use of the concept of two-phase multipliers that have been defined by Lockhart et Martinelli (1949). These multipliers may be obtained using :

$$\left(\frac{dP}{dz}\right)_{diph(fr)} = \Phi_l^2 \left(\frac{dP}{dz}\right)_{l(fr)} = \Phi_v^2 \left(\frac{dP}{dz}\right)_{v(fr)} = \Phi_{lo}^2 \left(\frac{dP}{dz}\right)_{lo(fr)} \quad (6.17)$$

The theoretical pressure drop for the liquid phase could be obtained using :

$$\left(\frac{dP}{dz}\right)_{l(fr)} = -\frac{2f_l G^2 (1-x)^2}{\rho_l d_h} \quad (6.18)$$

By considering the two-phase multiplier of the liquid phase we obtained :

$$\Phi_l = \left(1 + \frac{C}{\chi} + \frac{1}{\chi^2}\right)^{1/2} \quad (6.19)$$

where χ is the Lockhart et Martinelli (1949) parameter that can be calculated according to :

$$\chi = \left[\frac{(dP/dz)_l}{(dP/dz)_v}\right]^{1/2} = \left(\frac{\rho_v}{\rho_l}\right)^{1/2} \left(\frac{f_l}{f_v}\right)^{1/2} \left(\frac{1-x}{x}\right) \quad (6.20)$$

Therefore, in order to correlate the experiments to a predictive law, it was necessary to tune the value of the parameter C according to an approach similar to the separated flow model. It can be noticed that the determination of the two-phase multipliers (equation (6.17)) took into account the term due to the two-phase pressure drops due to the friction and not the term due to the total pressure drops.

➤ How to determine C for the experiments ?

On Figure 6.35 the data related to the evolution of the experimental two-phase multipliers in function of the Lockhart et Martinelli (1949) parameter for the whole set of four mini-channels have been reported. It was also given the evolution of the two-phase multipliers given by Lockhart et Martinelli (1949) by considering the liquid and vapor phases as being : laminar/laminar ; laminar/turbulent ; turbulent/turbulent.

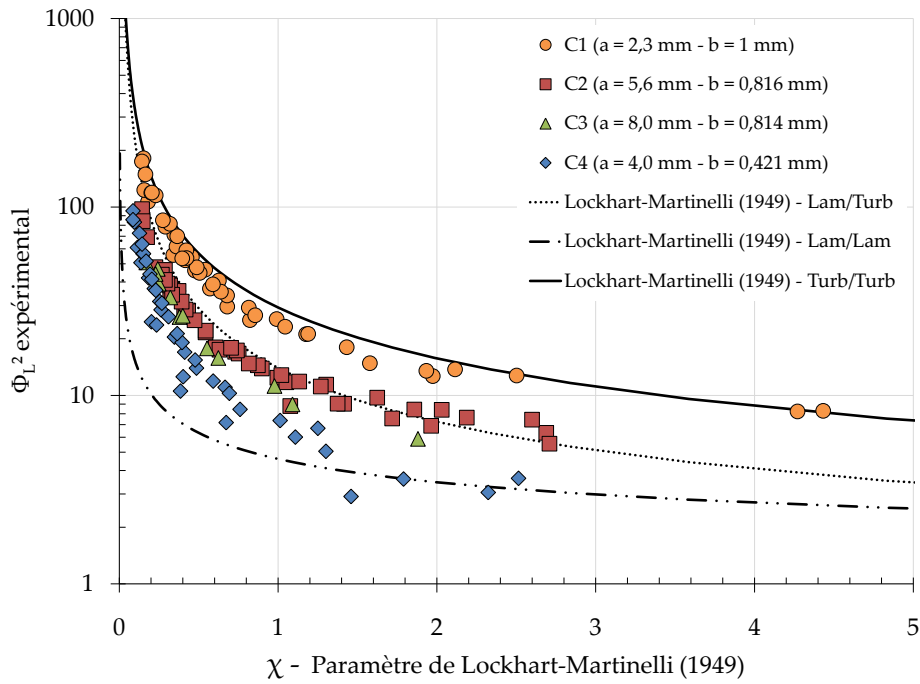


FIGURE 6.35 – Evolution of the experimental two-phase multipliers for the whole set of mini-channels

Once this chart has been given, it was easy to find the equation related to C evolution that allow for the calculation of the experimental two-phase multipliers. Similarly to Lee et Lee (2001b), it was observed that this variable depended on the flow rate and may be written as :

$$C = c_1 Re_{l0}^{c_2} \quad (6.21)$$

Therefore, by adjusting the value of c_1 and c_2 parameters for the whole set of mass velocity range, the constant C that allow for the best approximation of the experimentals pressure drops can be obtained. These pressure drops may be expressed as :

$$\left(\frac{dP}{dz} \right)_{diph(fr)} = \left(1 + \frac{c_1 Re_{l0}^{c_2}}{\chi} + \frac{1}{\chi^2} \right) \left(\frac{dP}{dz} \right)_{l(fr)} \quad (6.22)$$

The data reported in Figure 6.35 showed that the values of this variable C depended on the tested mini-channel. Therefore, the values of the parameter C in function of the tested mini-channels were reported on Table 6.1.

These data showed that it was possible to find a law that predict better the experiments than those defined in the literature for each of the tested mini-channels. Therefore, a summary of the comparisons between the whole set of correlations with our experiments have been given in Figure 6.36.

Section 6.4. Evolution of boiling curves with wall heat flux

Tested mini-channel	C	Prediction at $\pm 25\%$
$C_1(a = 2.3 \text{ mm} - b = 1 \text{ mm})$	$2.23Re_{lo}^{0.31}$	95.6 %
$C_2(a = 5.6 \text{ mm} - b = 0.816 \text{ mm})$	$0.82Re_{lo}^{0.34}$	95.7%
$C_3(a = 8.0 \text{ mm} - b = 0.814 \text{ mm})$	$1.3Re_{lo}^{0.27}$	85.7%
$C_4(a = 4.0 \text{ mm} - b = 0.421 \text{ mm})$	$0.133Re_{lo}^{0.52}$	75%

TABLE 6.1 – Determination of the value of C for the whole set of tested mini-channels

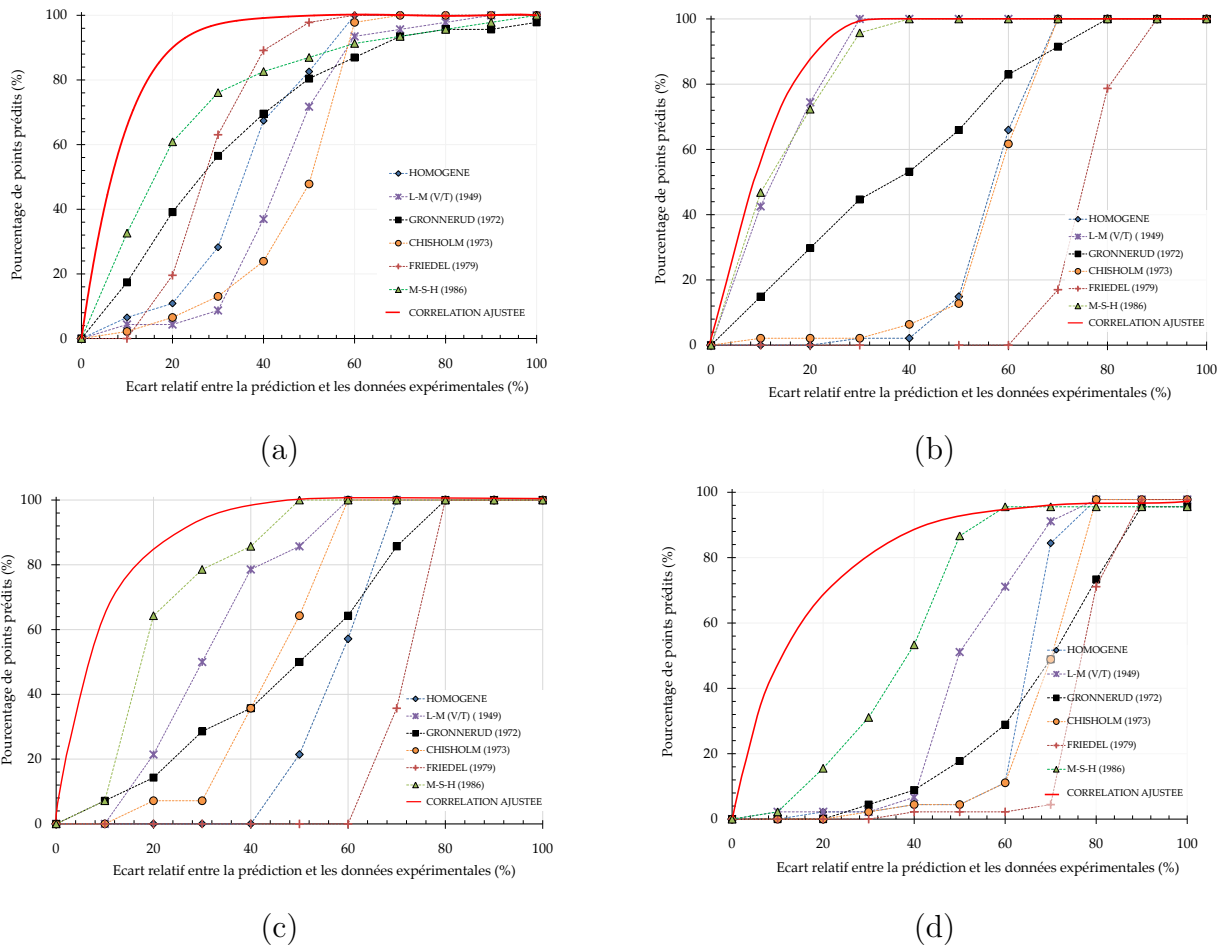


FIGURE 6.36 – Percentage of the predicted experimental data points regarding the relative difference for : (a) $C_1(a = 2.3 \text{ mm} - b = 1 \text{ mm})$ (b) $C_2(a = 5.6 \text{ mm} - b = 0.816 \text{ mm})$ (c) $C_3(a = 8 \text{ mm} - b = 0.814 \text{ mm})$ (d) $C_4(a = 4 \text{ mm} - b = 0.421 \text{ mm})$ mini-channel

Construction of a generalized correlation for estimating the pressure drops

It was shown, in this paragraph, that it was possible to find a specific correlation to each mini-channels that was able to give better results compared to the correlations that have been found in the literature. This new correlation was able to predict at least 75% of the experiments within $\pm 25\%$. Regarding the correlations that were made, it was decided to look for a generalized law that was able to take into account the mini-channel geometry impact on the evolution of the two-phase flow pressure drops due to friction. Therefore, a generalized writing of the Chisholm et Laird (1958) number for the mini-channel may be proposed according to :

$$C_{ad-hoc} = c3 \times \gamma^{c4} (Co_{ad-hoc})^{c5} Re_{lo}^{(c6 \times \gamma^{c7} (Co_{ad-hoc})^{c8})} \quad (6.23)$$

It should be recalled that the expression, as well as the construction, of the confinement number Co_{ad-hoc} has been defined in equation (6.16). By adjusting the parameters $c3, c4, c5, c6$ and $c7$ using an iterative method, the following generalized law was obtained :

$$C_{ad-hoc} = 3.3 \times \gamma^{1.43} (Co_{ad-hoc})^{-2.52} Re_{lo}^{(0.318 \times \gamma^{-0.22} (Co_{ad-hoc})^{0.66})} \quad (6.24)$$

The originality of this correlation came from the fact that all the terms that have been expressed here are non-dimensional and took into account the mini-channel flow confinement. This generalized correlation was based on more than 150 experimental data points and allow for the prediction of 90.1% of the experimental data points within $\pm 25\%$ as showed in Figure 6.37a.

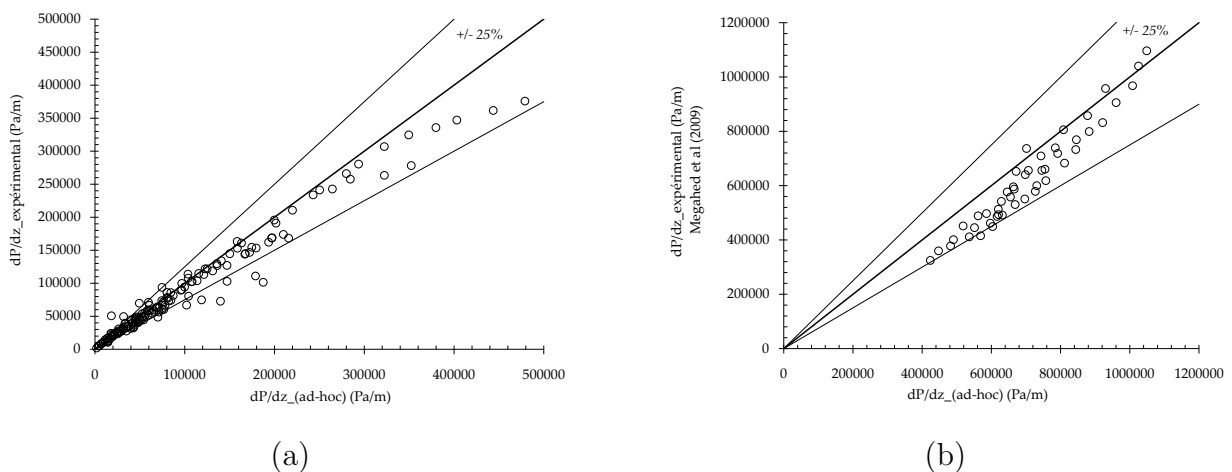


FIGURE 6.37 – Comparison between the predictive correlation and : (a) the current experiments (b) the Megahed et Hassan (2009) experimental results

In order to make sure that the relevance of this correlation was good, the predictive behavior was tested on the Megahed et Hassan (2009) results who proposed to study the pressure drops for a FC-72 flow in boiling conditions for a rectangular channel having $225\ \mu\text{m}$ width and $276\ \mu\text{m}$ height. It was possible to notice that the aspect ratio ($\gamma = 0.81$) that was defined was larger than 0.43 which was the maximal value that allow for the construction of this correlation. However, the comparison of this predictive tool to this experimental work have showed a very good agreement with 95.7% of the experimental data points that were predicted within $\pm 25\%$ as showed in Figure 6.37b. Other comparison with the results the literature should be made to check this correlation validity.

6.4.3 Evolution of the heat transfer coefficients

Similarly than the pressure drops, it was decided to compare the experimental results to the data from the literature for the heat transfer rate in order to formulate an adapted correlation regarding the results that have been obtained. It should be reminded, that the calculation of the thermodynamic vapor quality as well as the heat transfer coefficients were made at the location of the thermocouple $n^{\circ}3$ according to the assumptions that were made in the conclusions of Chapter 5. The thermodynamic vapor quality at the location of this thermocouple could be expressed as :

$$x_{(Tp3)} = \frac{\frac{\Phi_{conv,3}}{\dot{m}} + c_{p,l}(T_{amont} - T_{sat,3})}{h_w} \quad (6.25)$$

where $\Phi_{conv,3}$ was the convected heat flux up to the location of the wall thermocouple $n^{\circ}3$. $T_{sat,3}$ was the saturation temperature on a cross section located at the location where this thermocouple was placed. It should be reminded that this temperature may be obtained using the saturation pressure that has to be determined at the location z of this thermocouple. The determination procedure of the pressure drops during the saturated boiling flow has been already detailed in § 6.4.2. The calculation of the heat transfer coefficients at the location of this thermocouple may be calculated according to :

$$h_{Tp3} = \frac{q''}{T_{p3} - T_{sat,3}} \quad (6.26)$$

After defining these two essential parameters, the impact of the mass velocity as well as the geometry on the heat transfer coefficients have been studied in the next paragraphs.

Impact of the mass velocity on the heat transfer coefficients

Using the data from Figure 6.38, the impact of the convected heat flux and of the thermodynamic vapor quality on the heat transfer coefficient were analyzed. This study was made for different mass velocities for $C_1(a = 2.3 \text{ mm} - b = 1 \text{ mm})$ mini-channel.

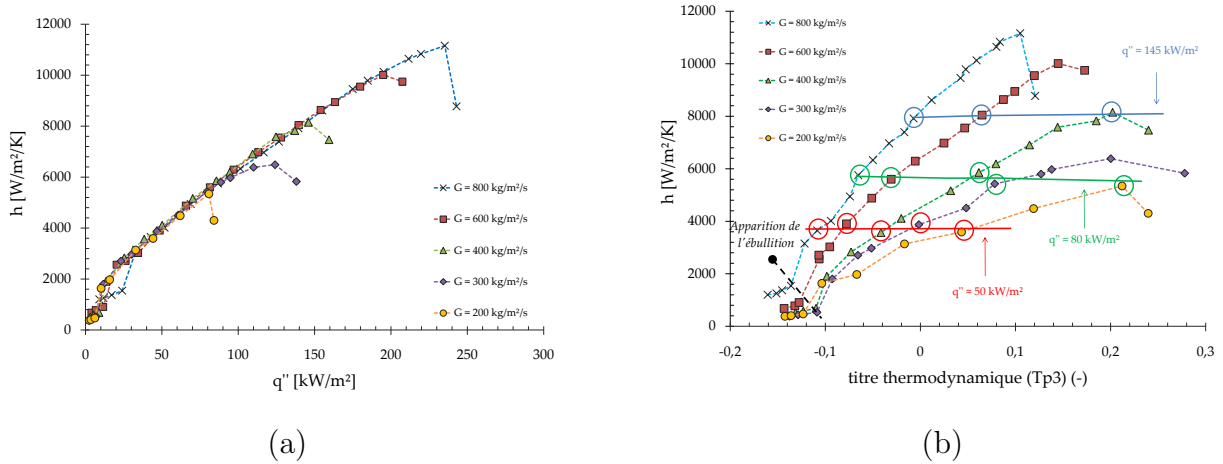


FIGURE 6.38 – (a) Influence of convected heat flux (b) Impact of the thermodynamic vapor quality on the heat transfer coefficients for $C_1(a = 2.3 \text{ mm} - b = 1 \text{ mm})$ mini-channel and a subcooling of 15°C

The data related to this figure showed that when the heat was considered, the evolution of the heat transfer coefficient did not depend on the mass velocity (for fully saturated boiling condition and for conditions that were far from dryout). During the convective boiling, two mechanisms can drive (sometimes simultaneously) the heat transfer rates : nucleated boiling or convective evaporation. For determining which one of these mechanisms was dominant (§ 2.2.4), it is relevant to represent the heat transfer rate evolution in function of the thermodynamic vapor quality. In this case, for evaluating the importance of one of these two mechanisms, it was necessary to keep either the mass velocity or the wall heat flux at a constant value. Indeed, if the heat transfer coefficients evolved with the mass velocity but not with the heat flux, then it is the mechanism of evaporative convection that drive the heat transfer and the correlation that allow for the prediction of these evolution depended on the thermodynamic vapor quality. Otherwise, if these heat transfer coefficients evolved with heat flux, but not with flow rate then it is the nucleated boiling regime that is dominant.

Therefore, according to the experiments, it was observed that the increase of the heat flux (which led to the increase of the thermodynamic vapor quality), for a same mass velocity, lead to an increase of the heat transfer coefficients. This result showed that the mechanism that drove the heat transfer rate should be the nucleate boiling. In order to corroborate this result, the

thermodynamic vapor quality values were drawn for different mass velocities but a same wall heat flux. It was noticeable to observed that the heat transfer coefficients were not dependent of the thermodynamic vapor quality for this configuration. Therefore, these two analyzes may demonstrate that the main mechanism that allow for the characterization of the heat transfer rates was nucleate boiling.

However, it was observed using the image acquisition system that the flow regimes that were more numerous were those that did not presented close interfaces, once the thermodynamic vapor qualities were higher than 0. Generally, this is the evaporative convection that should drive the heat transfer rate for these conditions. How this result could then be explained? According to our understanding, this behavior may be related to the occurrence of instabilities that may lead to a non-dependence of this heat transfer coefficient with the flow rate (or thermodynamic vapor quality) for a same heat flux.

☞ Impact of the geometry on the heat transfer coefficients

The evolution of the heat transfer coefficients with the heat flux for different studied mini-channels and for the different mass velocities has been reported on Figure 6.39.

Chapitre 6. Boiling flows in mini-channels

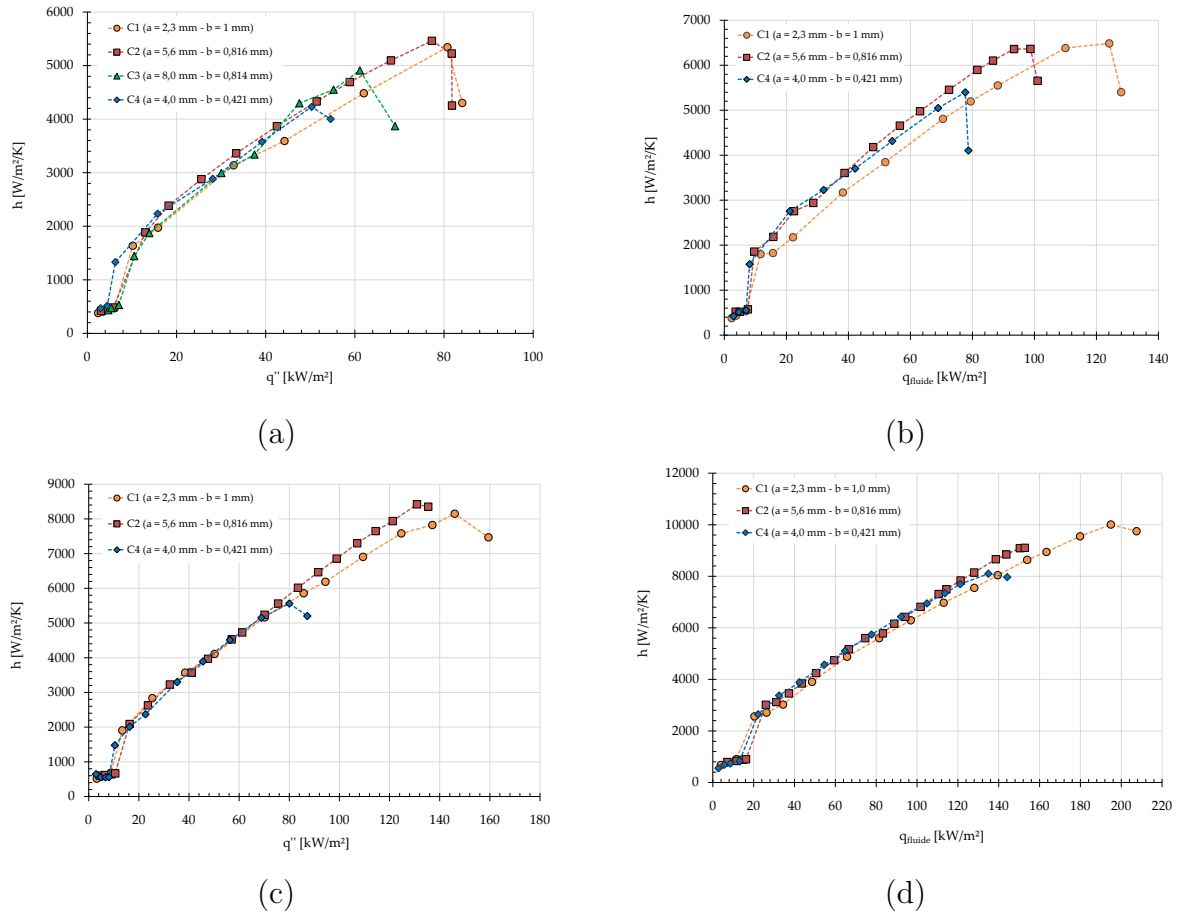


FIGURE 6.39 – Influence of the geometry on the heat transfer coefficients in function of the heat flux for mass velocity of : (a) $200 \text{ kg.m}^{-2}.\text{s}^{-1}$ (b) $300 \text{ kg.m}^{-2}.\text{s}^{-1}$ (c) $400 \text{ kg.m}^{-2}.\text{s}^{-1}$ and (d) $600 \text{ kg.m}^{-2}.\text{s}^{-1}$

The data that have been reported on this figure showed that for a same heat flux between the wall and the fluid, the heat transfer rate was approximately the same, whatever the mini-channel (as a consequence of the geometry) chosen during fully developed boiling.

In order to better show the impact of the confinement on the heat transfer, the variations of the heat transfer coefficient in function of the thermodynamic vapor quality were given on Figure 6.40.

Section 6.4. Evolution of boiling curves with wall heat flux

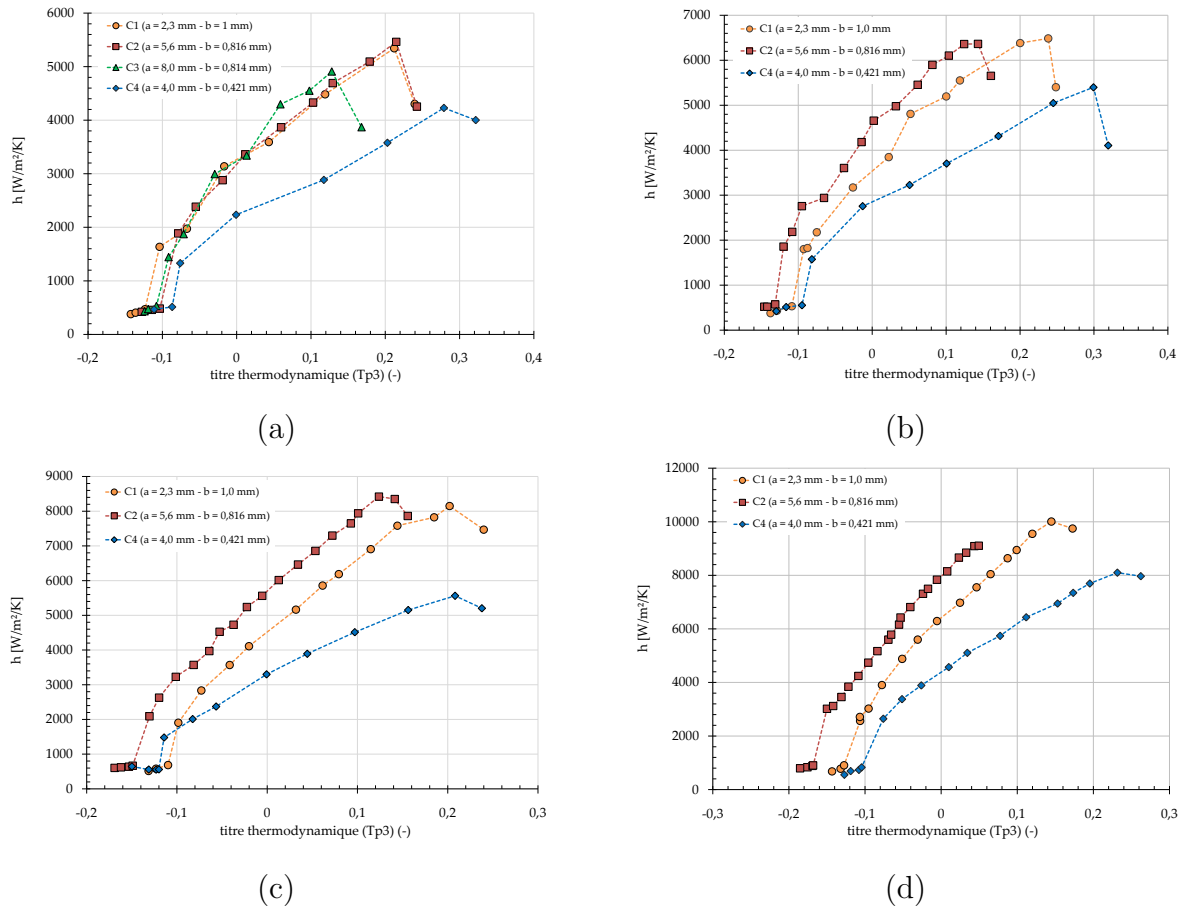


FIGURE 6.40 – Influence of the geometry on the heat transfer coefficient in function of the thermodynamic vapor quality for a mass velocity of : (a) $200 \text{ kg.m}^{-2}.\text{s}^{-1}$ (b) $300 \text{ kg.m}^{-2}.\text{s}^{-1}$ (c) $400 \text{ kg.m}^{-2}.\text{s}^{-1}$ and (d) $600 \text{ kg.m}^{-2}.\text{s}^{-1}$

The data given in this figure showed that the geometry of the different channels may impact the evolution of the heat transfer coefficients for a same thermodynamic vapor quality. Indeed, if the mass velocity was kept constant, the increase of the mini-channel cross section for a same hydraulic diameter led to an increase of the heat transfer coefficients, whereas the reduction of the hydraulic diameter would lead to a decrease of the heat transfer transfer coefficients. This was a result that has been reported by Harirchian et Garimella (2009) also. No clear explanation was found regarding this observation and it was thought that unstabiles phenomenon may lead to the reduction of the heat transfer rate when the cross section was reduced for a same mass velocity.

However, regarding the application, it seemed relevant to compare the geometry impact for a same flow rate. Therefore, the evolution of these heat transfer coefficients in function of the thermodynamic vapor quality for close flow rate for the 4 mini-channels has been given in Figure 6.41.

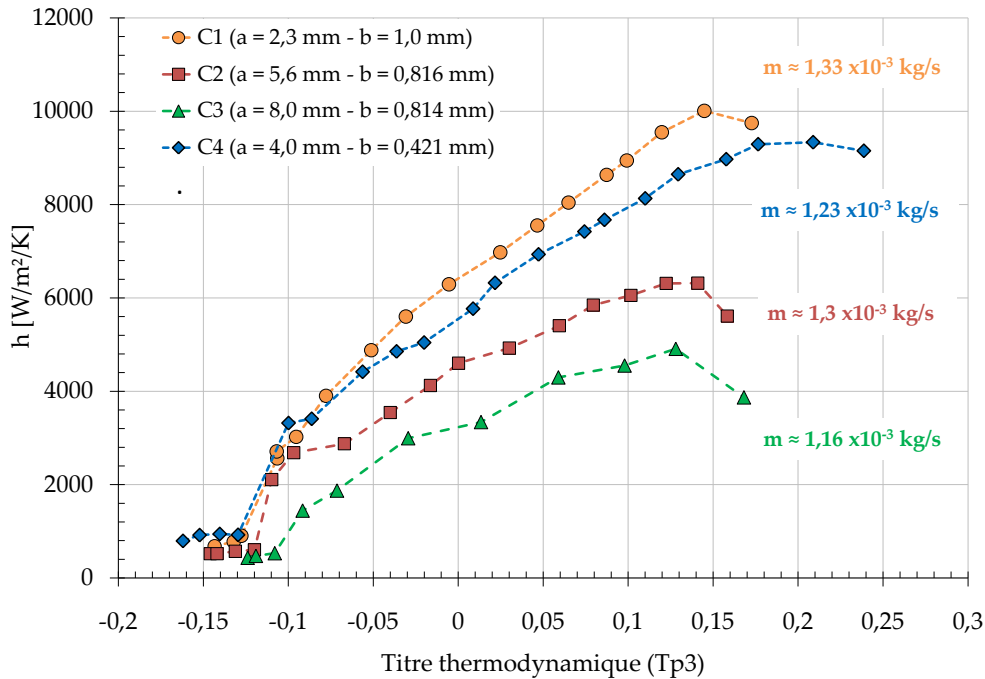


FIGURE 6.41 – Influence of the geometry on the heat transfer coefficient for a same mass flow rate

According to this representation, the geometry impact seemed to be in a better agreement with the confinement evolution in the mini-channels. The influence of the each of these geometrical parameters have been detailed below :

➤ Impact of the mini-channel width and aspect ratio

The impact of the mini-channel width was analyzed for $C_2(a = 5.6mm - b = 0.816mm - \gamma_2 = 0.146)$ and $C_3(a = 8 mm - b = 0.814 mm - \gamma_3 = 0.101)$ mini-channels. It was particularly interesting to notice that the results that were obtained showed that for these cases, the increase of this width led to a reduction of the heat transfer rate for a same vapor concentration. Indeed, the confinement tended to increase with the reduction of the mini-channel width. It was though that the fact to get the lateral wall closer led to an increase of the heat transfers. It is exactly the same phenomenon that would expressed the increase of the heat transfer for $C_1(a = 2.3 mm - b = 1 mm - \gamma_1 = 0.435)$ mini-channel that has an aspect ratio almost three time larger than the one of C_2 mini-channel for a same hydraulic diameter.

➤ Impact of the hydraulic diameter

Therefore, by considering the mini-channels $C_2(\gamma_3 = 0.146)$, $C_3(\gamma_3 = 0.101)$ and $C_4(\gamma_4 = 0.105)$ (which have a close aspect ratio), it was noticed that the cross section increase lead to the reduction of the heat transfer for a same thermodynamic vapor quality. Indeed, the confinement

was reduced with the increase of the cross section and led to heat transfer that was smaller. When comparing the results that were obtained for C_1 mini-channel to those obtained with C_4 mini-channel, it was observed that a competition between hydraulic diameter and aspect ratio reductions existed. Therefore, according to these data, the aspect ratio would have a significant importance and would led to the more important increase of the heat transfer coefficient for a same mass flow ⁸.

In the next paragraphs, the comparisons that were made between the experiments and the predictive methods of the literature for each of the mini-channels have been reported.

☞ Comparison of the experimental data with the correlation reported in the state of the art

➤ Analysis of the data related to $C_1(a = 2.3 \text{ mm} - b = 1 \text{ mm})$ mini-channel

For evaluating the performance of the predictive correlations (Chen (1966), Shah (1976), Gungor et Winterton (1986), Liu et Winterton (1990), Kandlikar et Balasubramanian (2003), Zhang *et al.* (2004)) that have been presented in the state of the art review section (§ 2.5.2), the experiments were compared to these correlations.

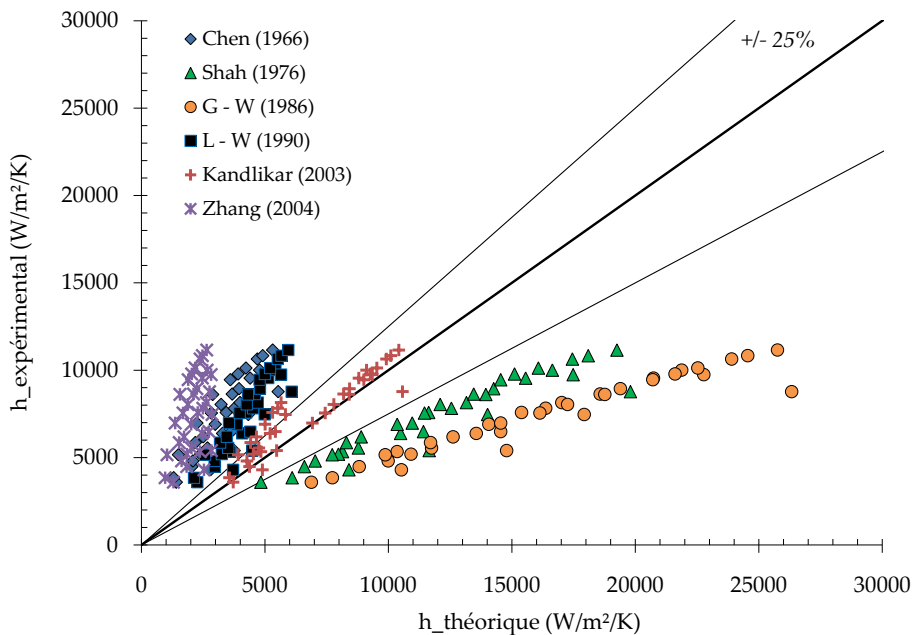


FIGURE 6.42 – heat transfer coefficients and those given by literature for $C_1(a = 2.3 \text{ mm} - b = 1 \text{ mm})$ mini-channel

8. It can be highlighted that for this study, the confinement number that was defined in equation (6.16) was not adapted for justifying the relative importance of the heat transfer rate

Chapitre 6. Boiling flows in mini-channels

The parameter F_l (which has been defined in § 2.5.2) from the Kandlikar et Balasubramanian (2003) correlation is a parameter that depends on the thermophysical properties of the fluid as well as the wettability characteristics. It should be determined experimentally although it has no clear physical signification. Therefore by tuning the value of this parameter with the experiments, it was determined that its value should be equal to 0.8 for forane 365 HX and the whole set of tested mini-channels. The jump that can be seen for the data point that have been predicted using this correlation came from the flow regime change which goes from a transition regime to a turbulent regime. Therefore, in this configuration, the heat transfer coefficients that were predicted using the Kandlikar et Balasubramanian (2003) correlation, which depended on the heat transfer coefficient determination, increased sharply.

The results that were obtained showed that the single correlation that was able to estimate the experiments was the one of Kandlikar et Balasubramanian (2003) with 77.1% of the experiments predicted within $\pm 25\%$.

➤ Analysis of the data reported for $C_2(a = 5.6 \text{ mm} - b = 0.816 \text{ mm})$

On Figure 6.43, the comparison between the experiments and the correlations reported in the state of the art review have been given.

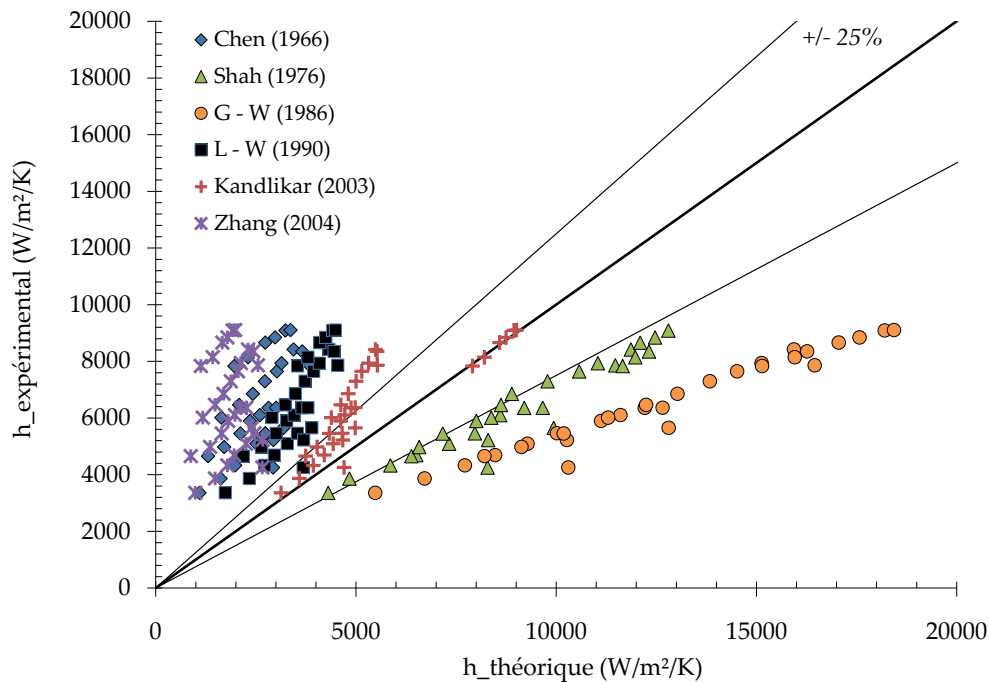


FIGURE 6.43 – Comparison between the experiments and the correlations from the state of the art correlation for $C_2(a = 5.6 \text{ mm} - b = 0.816 \text{ mm})$ mini-channel

Section 6.4. Evolution of boiling curves with wall heat flux

Similarly to the C_1 mini-channel it was noticed that the correlation that better predict the experiments within $\pm 25\%$ was the one of Kandlikar et Balasubramanian (2003) with 55% of the experimental data points predicted.

➤ Analysis for the data reported for $C_3(a = 8 \text{ mm} - b = 0.814 \text{ mm})$ mini-channel

The comparison with the correlations given by the state of the art for determining the heat transfer rate have been reported on Figure 6.44 for $C_3(a = 8 \text{ mm} - b = 0.814 \text{ mm})$ mini-channel. It should be reminded that for this tested mini-channel, the number of experimental data points was smaller due to the fact that the boiling curves were obtained for mass velocities of $100 \text{ kg.m}^{-2}.s^{-1}$ and $200 \text{ kg.m}^{-2}.s^{-1}$ only.

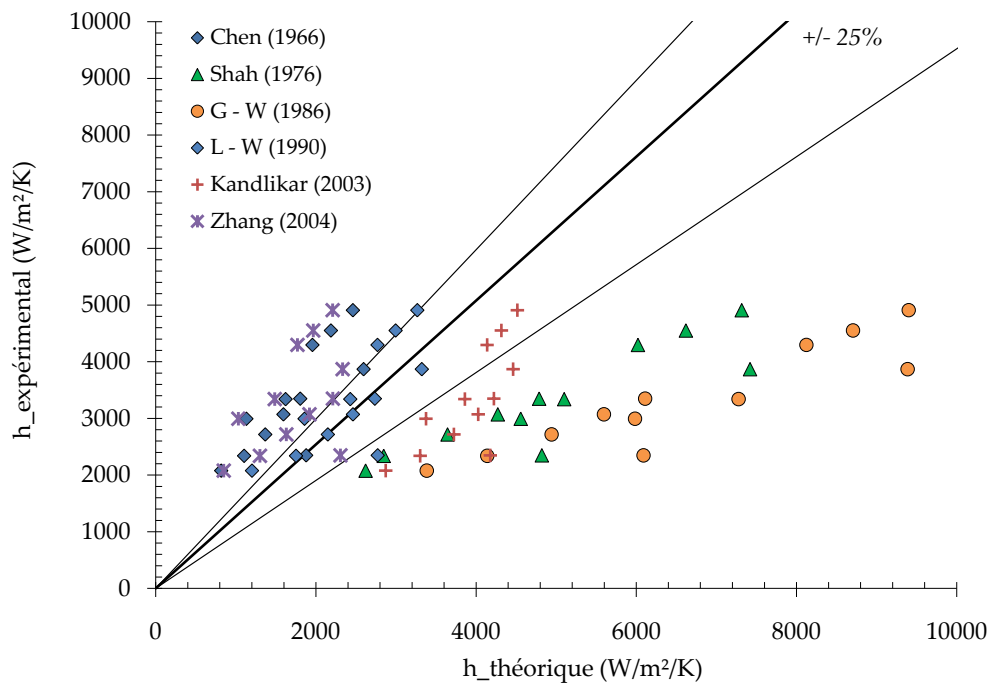


FIGURE 6.44 – Comparison between the experimental heat transfer coefficients and those predicted by the correlations taken from literature for $C_3(a = 8 \text{ mm} - b = 0.814 \text{ mm})$ mini-channel

It was again observed that it was the correlation proposed by Kandlikar et Balasubramanian (2003) which allow for the best predictions with 66.7% of the experimental data points within $\pm 25\%$.

➤ Analysis of the data reported for $C_4(a = 4 \text{ mm} - b = 0.421 \text{ mm})$ mini-channel

Finally, the comparisons that were made for the results obtained for $C_4(a = 4 \text{ mm} - b = 0.421 \text{ mm})$ mini-channel have been reported in Figure 6.44.

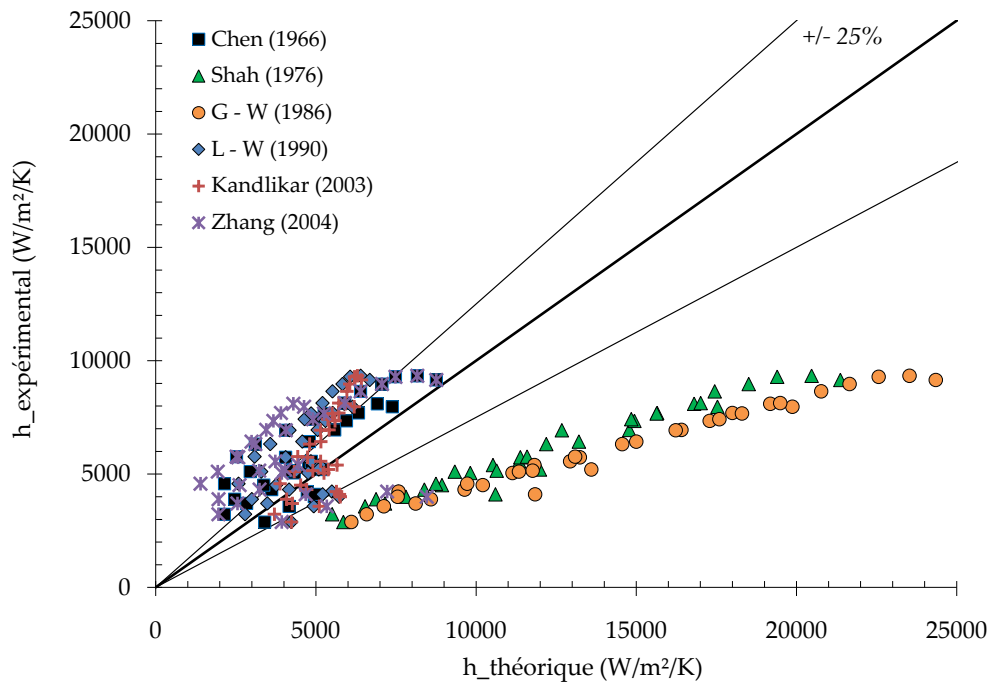


FIGURE 6.45 – Comparison between the experimental heat transfer coefficients and those predicted by the correlation taken from literature for $C_4(a = 4\text{ mm} - b = 0.421\text{ mm})$ mini-channel

The reduction of the hydraulic diameter seemed to impact the evolution of the prediction performance of the correlations taken from the literature. Therefore the model that allow for the best prediction was this time the one proposed by Chen (1966) with 50 % of the experimental data points that were predicted at $\pm 25\%$. The Kandlikar et Balasubramanian (2003) model had a confidence level that was estimated closed to 44%.

✎ Construction of a generalized correlation for estimating heat transfer coefficients

According to the experimental study, the heat transfer coefficients depended on only the heat flux rate that was exchanged between the mini-channel walls and the working fluid. Moreover, it was showed in this paragraph that the heat transfer coefficients did no depended of the geometry for a same heat flux. Therefore, it has been proposed to represent the evolution of the heat transfer coefficient according to the following equation, often encountered for pool boiling conditions :

$$h = c_1 (q'')^{c_2} \tag{6.27}$$

Section 6.4. Evolution of boiling curves with wall heat flux

Therefore by adjusting the constants c_1 and c_2 :

$$h_{ad-hoc} = 2.91 (q'')^{0.6684} \quad (6.28)$$

where h_{ad-hoc} is expressed in $W.m^{-2}.K^{-1}$ and q'' in $W.m^{-2}$. As a consequence, by applying this correlative law to predict the evolution of the heat transfer coefficients that were obtained experimentally, a very good agreement as been found. The performance of this new correlation was compared to the performance of other predictives correlations on Figure 6.46.

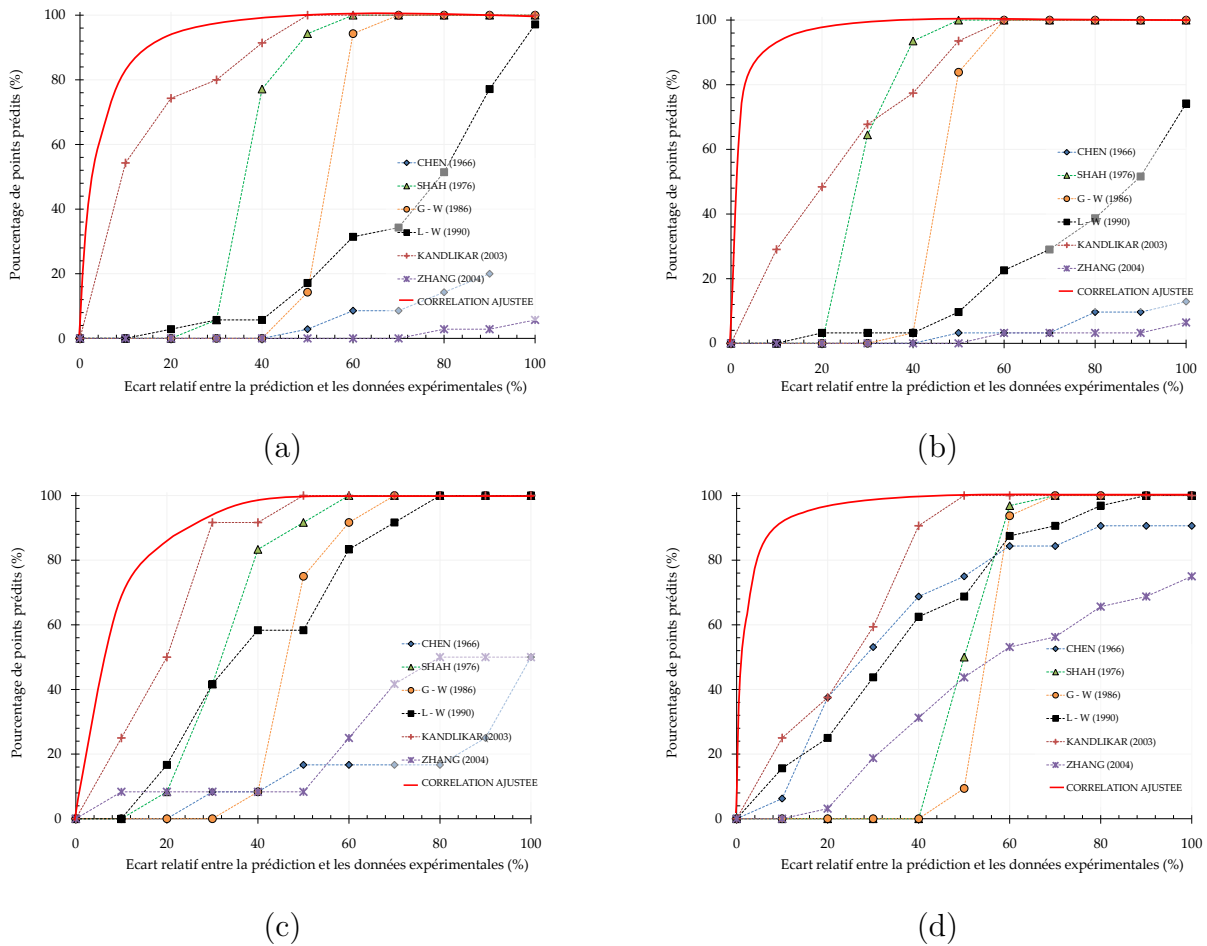


FIGURE 6.46 – Percentage of predicted experimental data point using the correlation defined for heat transfer coefficients determination in function of the relative difference between this new correlation and existing ones for : (a) $C_1(a = 2.3\text{ mm} - b = 1\text{ mm})$ (b) $C_2(a = 5.6\text{ mm} - b = 0.816\text{ mm})$ (c) $C_3(a = 8\text{ mm} - b = 0.814\text{ mm})$ (d) $C_4(a = 4\text{ mm} - b = 0.421\text{ mm})$ mini-channels

The comparisons with the other correlations showed that the proposed correlation gave better results than those of the literature. The performance of this new correlation was very good with 98.3% of the experimental points predicted within $\pm 25\%$ (6.47).

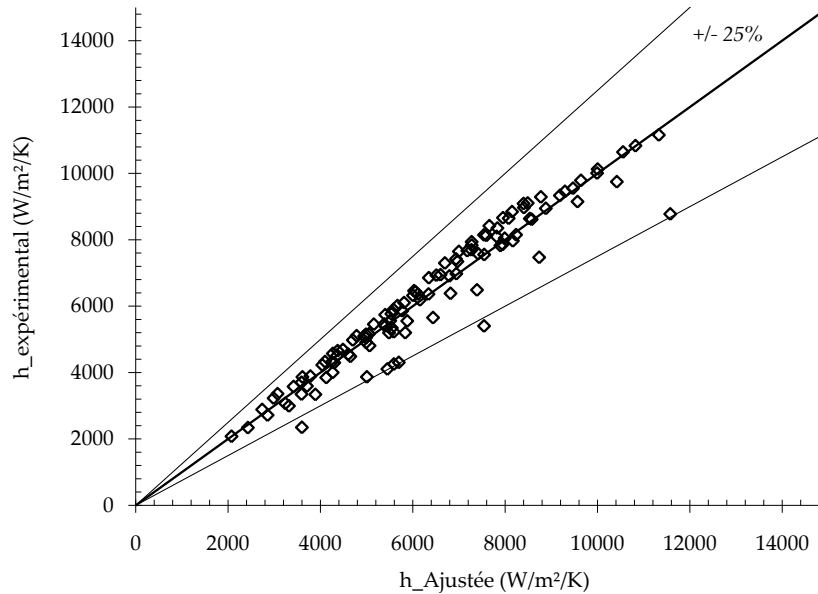


FIGURE 6.47 – Comparison between the experimental data and the correlation h_{ad-hoc} defined in equation (6.28)

6.4.4 Conditions that lead to wall dryout

After analysis the whole set of data, the evolution of the heat that led to wall dryout was studied. This evolution was an important parameter that allow for the characterization of the heat exchanger working in two-phase flow conditions. According to the analysis that has been made using the visualizations, the wall dryout should be partial, for the conditions that were obtained. The images analysis showed that these repetitive dryout phenomena were regularly followed by rewetting of the wall. In addition, for small mass velocities, it was observed that this dryout started on the mini-channel corners then increase up to the center of these channels and may led to an unstability similar to the one that has been observed by Barajas et Paton (1993) (called rivulet - (§ 2.3.2)). Figure 6.48 showed the impact of the $C_4(a = 4\text{ mm} - b = 0.421\text{ mm})$ mini-channel corner in the occurrence of dryout for a mass velocity of $200\text{ kg}\cdot\text{m}^{-2}\cdot\text{s}^{-1}$ and a heat flux of $81.7\text{ kW}\cdot\text{m}^{-2}$.

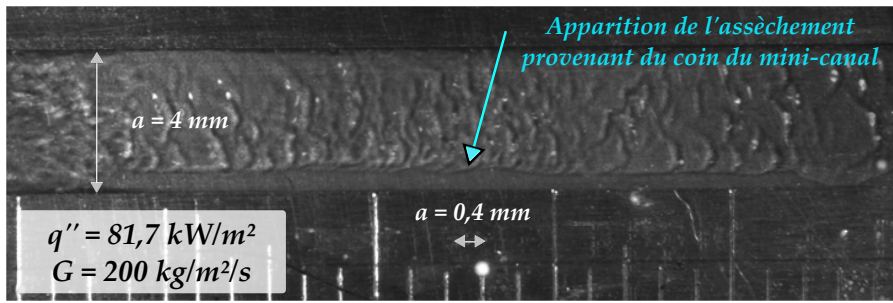


FIGURE 6.48 – Dryout visualization in the $C_4(a = 4\text{ mm} - b = 0.421\text{ mm})$ mini-channel for a mass velocity of $200\text{ kg}\cdot\text{m}^{-2}\cdot\text{s}^{-1}$, a heat flux of $81.7\text{ kW}\cdot\text{m}^{-2}$ and a subcooling of 15°C

Moreover, this phenomenon was observed more clearly (with the occurrence of a liquid rivulet at the center) in $C_1(a = 2.3\text{ mm} - b = 1\text{ mm})$ mini-channel during preliminary tests that were made for a working pressure of 0.35 bar , a mass velocity of $200\text{ kg}\cdot\text{m}^{-2}\cdot\text{s}^{-1}$ and a heat flux of $77.5\text{ kW}\cdot\text{m}^{-2}$. The images that showed the chronology of the evolution of this phenomenon have been reported in Figure 6.49.

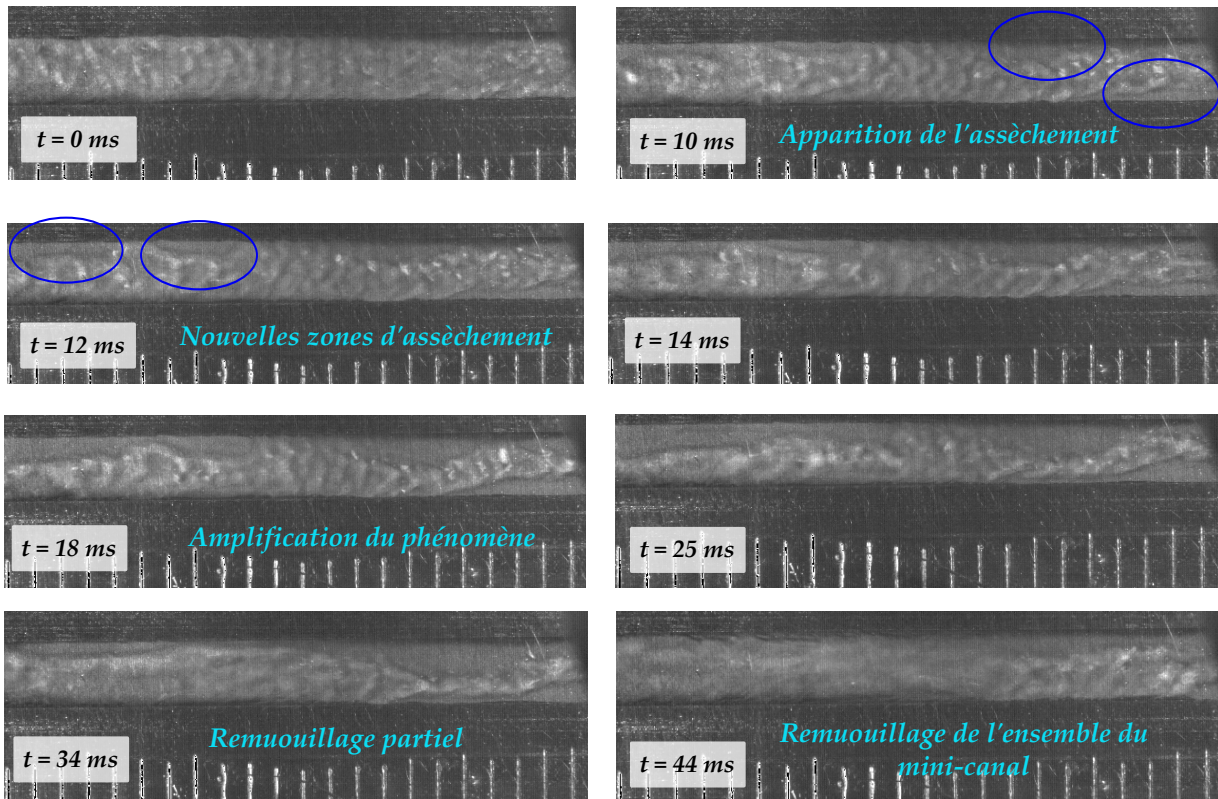


FIGURE 6.49 – Dryout evolution for $C_1(a = 2.3\text{ mm} - b = 1\text{ mm})$ mini-channel for a mass velocity of $200\text{ kg}\cdot\text{m}^{-2}\cdot\text{s}^{-1}$, a heat flux of $77.5\text{ kW}\cdot\text{m}^{-2}$ and a subcooling of 2°C

For larger mass velocities ($G > 300\text{ kg}\cdot\text{m}^{-2}\cdot\text{s}^{-1}$), the corners impact was not so clear as previously.

Chapitre 6. Boiling flows in mini-channels

As specified in preceding paragraphs, the heat flux that led to dryout increased with mass velocity for all the mini-channels. In addition the study of the data reported on the boiling curves suggested that the geometrical parameters seems to modulate the dryout evolution also as showed in Figure 6.50a.

The results that have been given in Figure 6.50b showed that the increase of the mass velocity led to a decrease of the critical thermodynamic vapor quality. Indeed, the vapor velocity became more significant with the increase of the mass velocity. This increase made the interfacial shear stress to be stronger between the vapor core and the liquid film. Therefore the ripples (or waves) generated due to the instabilities of the liquid/vapor interface were broken up in small droplets when the shear stress became very large (generally for high exchanged heat fluxes). In this context, the liquid film that was near the wall shrunk more rapidly with the flow rate increase what may accelerate its vanishing near the wall.

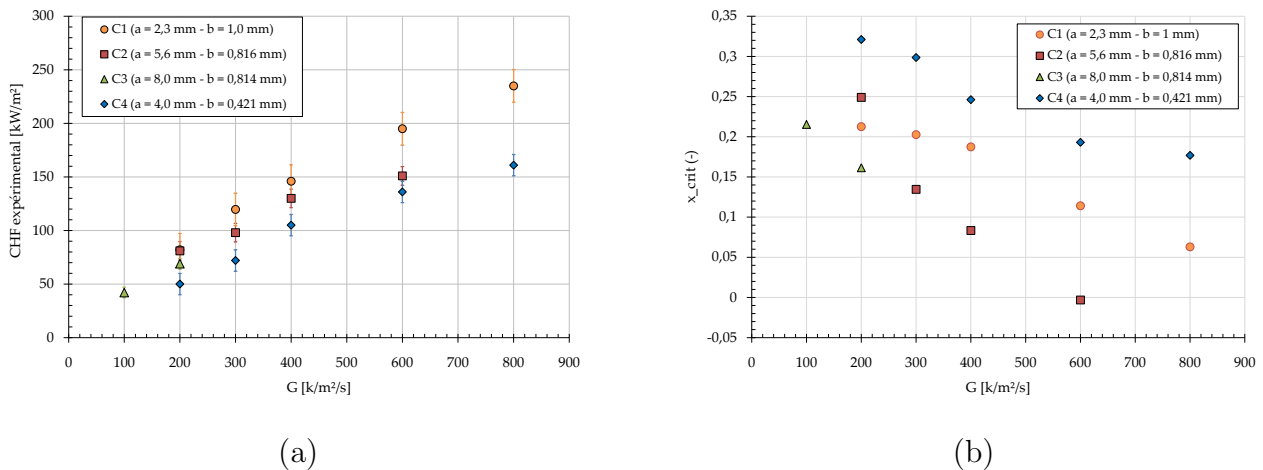


FIGURE 6.50 – Experimental evolution of : (a) critical heat flux (b) critical thermodynamic vapor quality in function of the mass velocity

In the following paragraph it has been proposed some explanations regarding the geometrical impact on the occurrence of the dryout.

➤ Impact of the hydraulic diameter

The comparison of these results were made for C_4 ($d_h = 0.761 \text{ mm}$) mini-channel with other mini-channels. The experiments showed that the hydraulic diameter reduction led to a reduction of the heat flux related to wall dryout for a same mass flux. These data were in good agreement with the experiments of Wojtan *et al.* (2006). This results can be explained by the fact the confinement increase led generally to an intensification of the interfacial and parietal shear stresses that may led to a more rapid breaking up of the liquid film that was located near the mini-channel wall for a same exchanged heat flux.

➤ Aspect ratio impact

The results that were obtained during this study suggested that the aspect ratio increase tended to lead to the augmentation of the needed heat flux related to wall dryout as showed on the data reported in Figure 6.50 (comparison of $C_1(\gamma = 0.435)$ and $C_2(\gamma_2 = 0.146)$ mini-channels). During the images analysis, it was noticed that the dryout may started from the mini-channel corners toward their centerlines. As a consequence, these corners may play a major role in the evolution of the dryout occurrence. Therefore, it was though that the produced vapor of the $C_1(a = 2.3 \text{ mm} - b = 1 \text{ mm})$ mini-channel corners would be more easily renewed for this channel compared to C_2 mini-channel and that this phenomenon allowed the conditions that led to dryout to be delayed.

🔍 Comparison with correlations defined in literature

In order to evaluate the experiments on the dryout heat flux variations, the data were compared to the reference predictive method of Katto et Ohno (1984) and to the Wojtan *et al.* (2006) correlation, which has been defined for refrigerant. The comparisons that were made between the experiments and these correlation have been reported in Figure 6.51 within $\pm 15\%$.

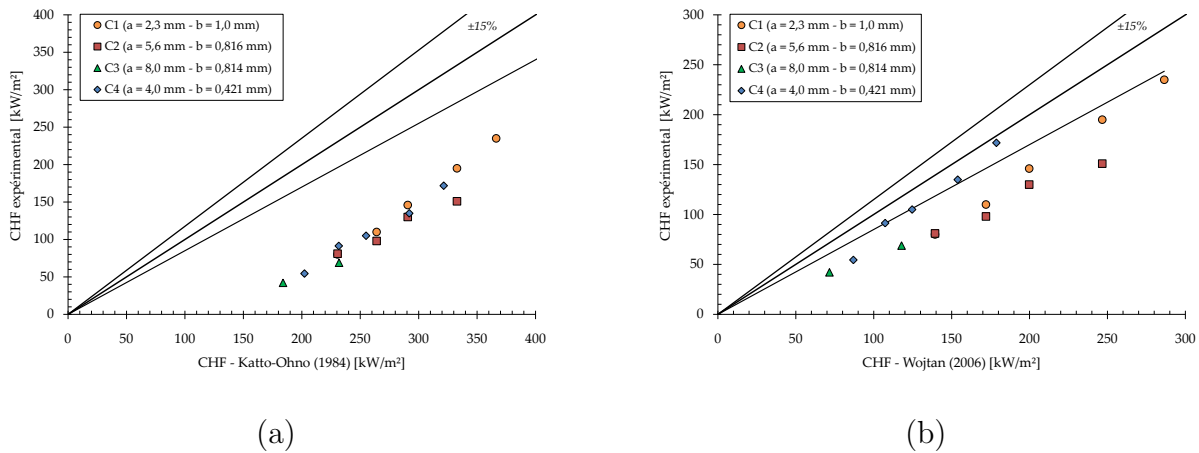


FIGURE 6.51 – (a) Comparison between experiments and predictive methods of : (a) Katto et Ohno (1984) (b) Wojtan *et al.* (2006) in function of the mass velocity evolution

The results of Figure 6.51a showed that none of the experiments were predicted using the Katto et Ohno (1984) correlation. Indeed, this correlation is generally adapted for water as working fluid and it has been defined for vertical flows. In addition, when analyzing the data from the state of the art review, it was observed that the correlations were working-fluid dependent (or to a category of working fluids). The Wojtan *et al.* (2006) correlation, which is an adaptation of the Katto et Ohno (1984) correlation was defined for R134a and R245fa. The data reported in Figure 6.51b showed that this correlation was able to predict only 25% of the experimental data points. It can be concluded that as none of these two correlations was able to predict a sufficient number of the experimental data points, therefore it may be useful to define an adapted correlation related to these current experiments. The methodology that has been employed is given in next paragraphs.

✎ Construction of a predictive correlation for CHF determination

By studying the correlations reported in literature, it was deduced that a generalized formulation that would allow for the prediction of dryout phenomenon for a convective boiling flow should be written as followed :

$$\dot{q}_{CHFad-hoc}'' = c_1 \left(\frac{\rho_v}{\rho_l} \right)^{c_2} We^{c_3} \left(\frac{L}{d_h} \right)^{c_4} Gh_{lv} \quad (6.29)$$

The values of the constants c_1 , c_2 , c_3 et c_4 must be tuned using an iterative method in order to correlate as best as possible the experimental data points.

After, adjusting them to the experiments, the critical heat flux that led to dryout may be correctly represented using :

$$\dot{q}_{CHFad-hoc}'' = 0.6 \left(\frac{\rho_v}{\rho_l} \right)^{0.54} We^{-0.15} \left(\frac{L}{d_h} \right)^{-0.51} Gh_{lv} \quad (6.30)$$

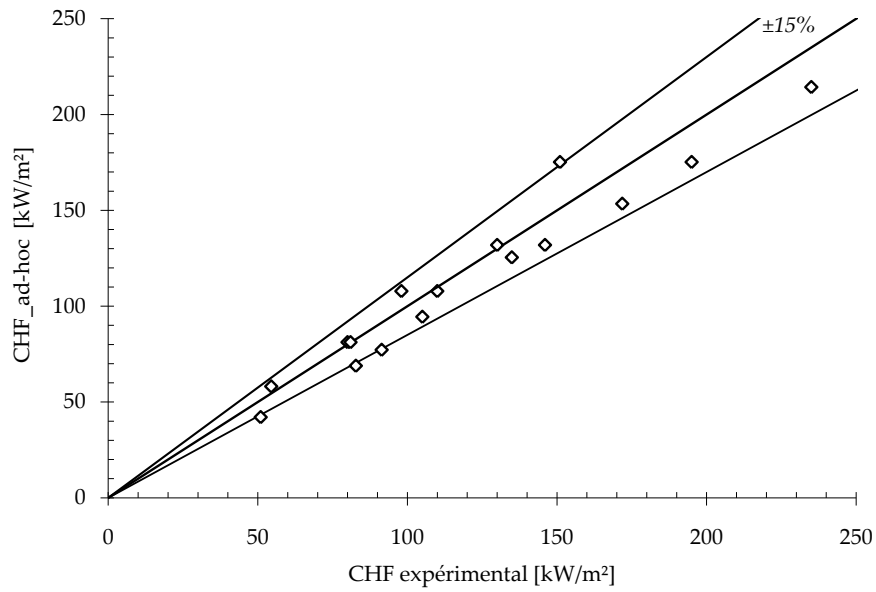


FIGURE 6.52 – Comparison between the experiments and the adapted predicting correlation

Using this correlation, it was possible to predict 81.2% of the experimental data points within $\pm 15\%$ as showed in Figure 6.52. Once the conditions that allow for the occurrence of dryout were known, it was possible to define, the heat flux working range of the heat exchanger.

6.5 Chapter 6 conclusions

Through this chapter, the boiling phenomenon evolution was studied (from ONB to CHF) for a forane 365 HX flow inside different mini-channels.

▷ In a first step, a parametric study has been made for determining the operating conditions that impacted particularly the [onset of nucleated boiling](#). The obtained results suggested that this is the liquid temperature at mini-channel inlet that would have more impact on the incipience of boiling. In addition, it was showed that at high masses velocities, the needed energy for ONB increased with aspect ratio⁹ (for mini-channels of about same hydraulic diameters) but this energy decreases when hydraulic diameter was reduced.

▷ Then, the [pressure drops evolutions](#) were analyzed for boiling conditions. A specific confinement number has been defined that allow for the prediction of the relative importance of the confinement inside the different mini-channels of this study. After comparing the experiments to the literature data, it was deduced that the more adapted correlation was the one of Müller-Steinhagen et Heck (1986). However this correlation may become not relevant when the hydraulic diameter was reduced. Therefore, in order to predict more correctly the whole set of experiments that was done in this study, an original general correlation related to the studied mini-channel, was proposed.

▷ The [heat transfer coefficients](#) were analysed for the different mini-channels. Similarly to Harirchian et Garimella (2009), it was observed that for a same heat flux and a same mass flow velocity, the impact of the geometry was small on heat transfer rates variations. After studying the impact of the thermodynamic vapor quality on the heat transfer coefficients, it was concluded that the heat transfer mechanism that was dominant was nucleate boiling. Regarding this observation, an adapted correlation that was able to better predict the experimental results was proposed also.

▷ Finally, in order to characterize the whole set of working range (in term of exchanged heat fluxes) of the heat exchanger, the [wall dryout](#) was studied. The experimental results have showed that the mini-channel geometry has a very important impact on this parameter. The larger CHF values were obtained for the mini-channel having the larger aspect ratio (when considering mini-channels of about same hydraulic diameters). After studying the data, a correlation that allow for the prediction of the experimental points was proposed.

At the end of this work, it was possible to evaluate and fully predict the heat transfer performances in function of the dimensions of the mini-channels. Therefore we propose to transpose the results that has been given in this chapter, to an idealized case related to the cooling of a proton exchange membrane fuel cell. This part has been discussed in Chapter 7.

9. When the aspect ratio is high the mini-channel cross section is smaller for having same hydraulic diameters

Quatrième partie

TRANSPOSITIONS TO THE APPLICATION

Application to proton exchange membrane fuel cell cooling

7.1	Short presentation of the working principle	249
7.1.1	General system presentation	249
7.1.2	Thermal regulation of a fuel cell	251
7.2	Comparison of the energy efficiency	256
7.3	Sizing of the cooling channels	260
7.4	Chapter 7 conclusions	261

Summary :

THIS chapter aimed at presenting in a synthetic way the working principle of a proton exchange membrane fuel cell as well as its cooling system. In a first step, the different hydraulic loops that served to feed the electrochemical reaction that took place inside the PEMFC have been introduced. Then in a second part the different constitutive elements of this fuel cell have been described and the cooling regulation system also. The results related to the energy balance that have been given for establishing the best conditions during the single-phase flow where compared to boiling flow. The mini-channel geometry effect has been studied on the evolution of these hydraulic and thermal powers. Starting from these results, it was proposed to model a very simplified case of PEMFC cooling.

7.1 Short presentation of the working principle

7.1.1 General system presentation

Figure 7.1 showed the working principle of a fuel cell. The montage is composed of three hydraulic loops. Indeed, as introduced in the Preface, the working of PEMFC needs oxygen (O_2) and hydrogen (H_2) for the two half reaction of oxydo-reduction (equations (1) and (2) - Preface). In this current work, the considered fuel cell was a PEMFC (Proton Exchange Membrane Fuel Cell)¹.

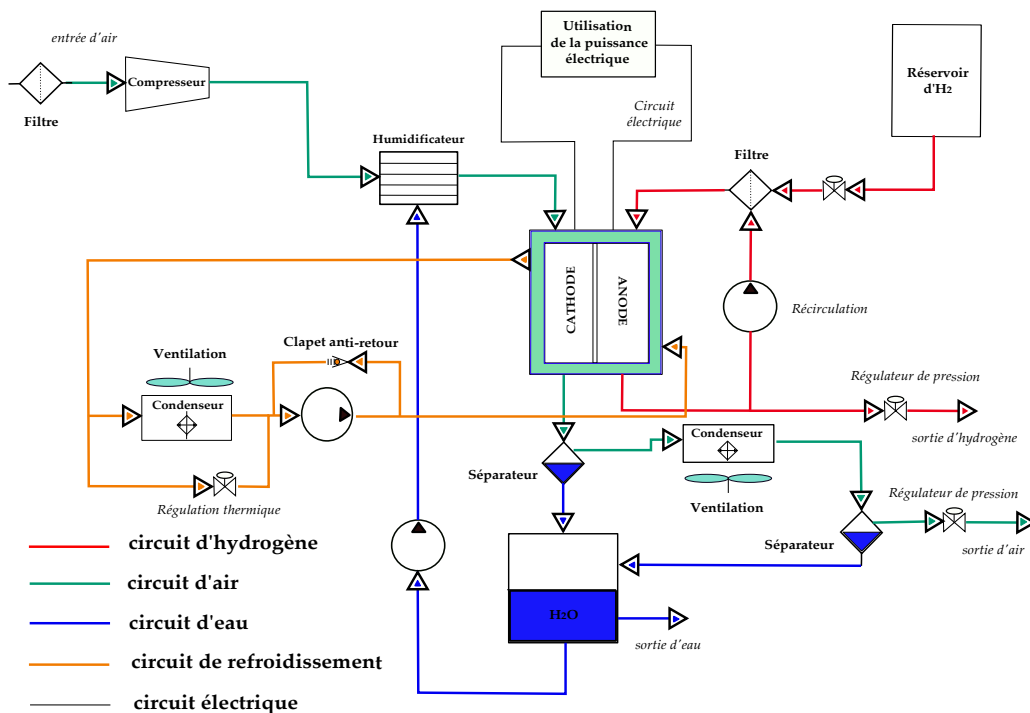


FIGURE 7.1 – System of electricity generation which include a fuel cell

➤ Hydrogen flow

The use of hydrogen, as a combustible of the electrochemical reaction, make appear the problem of compactness. Indeed, the energy power of hydrogen, when used at atmospheric pressure, is relatively small compared to the other sources of available energy². Therefore, in order to increase the hydrogen energy efficiency, it is necessary to pressurize it³. Once stored,

1. Some of the pictures reported in this manuscript related to the fuel cell working, have been based on the data given in Antoni (2006).

2. 1 liter of fuel has approximately the same energy efficiency than 1500 liters of hydrogen at atmospheric pressure.

3. The storage took place in reservoir having a pressure of 700 bars. In this context, 3 liters of hydrogen have approximately the same energy than 1 liter of fuel.

Chapitre 7. Application to proton exchange membrane fuel cell cooling

the pressurized fluid is driven through a specific loop that feed the fuel cell. This flow is realized using a pressure regulation associated with a valve. A pump that is placed in a parallel branch of this loop allow for the recirculation of hydrogen in order to optimize it working inside the fuel cell.

When hydrogen is produced using a reforming process, the limitation (or suppression) of carbon monoxide (CO) production in the fuel cell core must be considered. Indeed, the low working temperature of the PEMFC, make it very sensitive to this gas which degrades rapidly the electrodes performances by poisoning the nucleation sites. These sites are the locations where the electro-chemical reaction is catalyzed (§ 7.1.2).

➤ Air (or oxygen) flow

The air is taken from the atmosphere and is filtered in order to limit the pollutants impact. This air goes through a compressor which allow for the increase of the loop working pressure. The rise of this pressure generally improves the performance of the fuel cell. In order to bring humidity, which is necessary for the working of the electrochemical reaction near the membrane, air is humidified thanks to water that has been stored in a reservoir then it is sent to the core of the fuel cell. Inside this fuel cell, the electrochemical reaction produced water, heat, as well as electrical energy. The mixing between water / air is afterward, released from the fuel cell, on cathode side. A first separation took place at the outlet of the fuel cell and the water is stored inside a reservoir whereas remaining air is sent to a condenser. The additional air is then released outside of the system.

➤ Refrigerant flow circulation

This loop is closed and allow for the thermal regulation of the fuel cell. Indeed, the refrigerant (which has anti gel properties) flowed thank to a pump up to the fuel cell core. The selected fluid must maintain the fuel cell temperature below the condition that would lead to membrane dryout but allowing it for the reaching of its working temperature. This fluid must fulfill the specifications that were defined in Chapter 3. The valve, which is present inside this loop, drove the working pressure and the flow rate regulation. The non return valve that is positioned near the pump, controlled adequately the working pressure by limiting the overpressure in the closed circuit that may damaged the fuel cell.

7.1.2 Thermal regulation of a fuel cell

A fuel cell is made of several elements which are submitted to several thermal solicitations. The most sensitive part regarding these thermal solicitation is the proton exchanging membrane. This membrane should work according to specific thermal conditions for extending its lifetime⁴. The constitutive elements of the fuel cell will be detailed in next paragraphs.

Elements related to a PEM fuel cell

▷ Electrodes

Electrodes are the location where electrochemical reaction took place. There are generally porous for ensuring the efficient contact between the ionic conductor (electrolyte) and the electronic one (electrical circuit). These electrodes are composed of two regions :

① Active region

Electrodes are the activator of the oxidation reaction, on anode side and of reduction reaction on cathode side. The reaction, that took place on these electrode have a kinetic which is generally slow at low temperature. Therefore for accelerating the oxidation and reduction reactions, catalysts are used for PEMFC. The most often used catalyst for these last years was platinum, which is deposited on active coals which have a very important specific area. The main drawback related to the use of this catalyst is currently its very prohibitive cost⁵ regarding the mass production analysis. Moreover, the active nucleation sites located on these electrodes are very sensitive to carbon monoxide. Generally, the whole filtering system is fabricated to limit or suppress the presence of carbon monoxide. For increasing the kinetic of the reaction, other complementary methods exist. Indeed, these electrochemical reactions can be accelerated when the working pressure of the system is increased. The electrical fuel cell production also served to power auxiliaries (compressor, pumps, fans). These auxiliaries units used approximately 20% of the total produced electric energy (Wahdame (2006)). Therefore, for efficiency purposes, the needed power of these auxiliaries, and in particular of the compressor for increasing this working pressure must be limited to acceptable values.

② Diffusion region

This region must ensure three key points : authorize and diffuse the gases on the whole surface of the active region ; ensure the management of the water by humidifying the membrane and at same time remove the additional water generated by the reaction, in order to not hinder

4. Nowadays, the mean lifetime of a membrane is about 4000 hours (Bigot (2005)).

5. The cost of fabrication of the electrode represent the second most important part in the total cost of the fuel cell (Antoni (2006))

Chapitre 7. Application to proton exchange membrane fuel cell cooling

the arrival of fresh gases⁶; ensure the electrons transport from the active region to the bipolar plates.

▷ The membrane (the electrolyte)

This electrolyte is used to ensure at same time the flow of proton species H^+ and the blockage of electrons and gases. For PEM fuel cells, the electrolyte is in solid state (the most often used electrolyte is Nafion[®], that is produced by DuPont de Nemours company). However, important efforts are made in laboratories for finding a membrane that may replace it and would allow for the increase the performances in terms of ionic conduction. These efforts are made on the increase of the working temperature also. Indeed, the increase of this temperature would allow for the acceleration of the electrochemical reaction but would mostly allow for the limitation of the poisoning effect due to carbon monoxide on the nucleation sites.

▷ Bipolar plates

The bipolar plates are reported on the anode and the cathode. They have several functions :

① **Direct the gases that come from outside**

② **Collect the electrical current**

③ **Manage the water**

These plates must have a very good electrical conductivity, and at same time allow for the homogeneous distribution of the gases up to the electrodes. These plates play an important role in the water management that need to be bring or release to the membrane for humidifying purposes. A large part of the weight related to the fuel cell come from these bipolar plates. During the 90, these plates were made in graphite, which was chosen for its very good electrical properties. However, due to the difficulty related to the fabrication of the feeding channels (gases or coolant)⁷, it cost was then a key problem for mass production. Moreover for insuring the leakage proof of the system, the thickness of the plates must be important, what explained the large weight of this fuel cell. Therefore new techniques and new materials have been defined for fabricating these plates. One of the most promising techniques is embossing of aluminum plates for realizing the pattern of channels that can be easily produced. The main advantage of this technique is related to the already known « know-how » in industry. In addition, the bipolar plates thickness can be in this case very reduced and then lead to the reduction of the fuel cell weight. Consequently, its compactness as well as its performances could be increased.

6. At cathode, this diffusion region was generally made with PTFE particles, which are very hydrophobic and allow for the insurance of the water management. Beside, on anode side, these particles were not present; what ensure a good humidifying of the membrane

7. The graphite plate was machined using a tool which was controlled numerically. This technique ensured the leakage proof but made the fabrication cost very high (price ranged between 300-400 € for a single plate of 200 cm^2). However the price target should be around 1 to 2 € for each plate (<http://www.afh2.org>)

Montage AME

The montage of an assembly electrode membrane (AME) was reported in Figure 7.2. On this schematic, the channels related to air, hydrogen and cooling liquid flows having rectangular cross sections have been represented. It is generally the sizing of the channels related to the combustible flows that set the cooling channel cross section. The reader may notice that the rectangular cross section for the cooling channels may be relevant for PEM fuel cells.

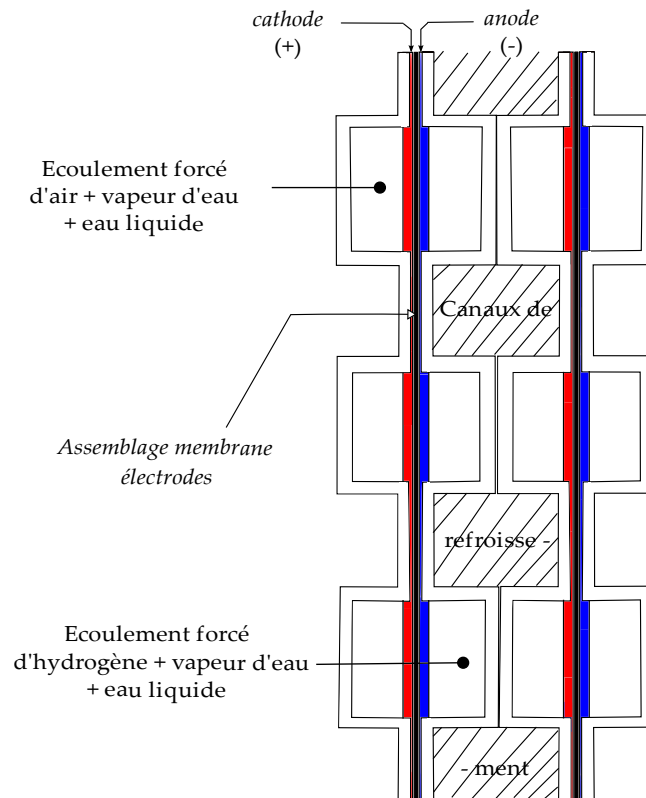


FIGURE 7.2 – Representation of the location of the cooling channels (with hatching)

Thermal management

The balance of the global oxido-reduction reaction is exothermic and release an averaged energy value of 237 kJ.mole^{-1} . This heat generation is produced on cathode side, but regarding the small dimensions of the AME, the temperature increase due to this energy release is global. In addition, beside the system using internal combustion, the thermal power which is generated in the fuel cell core may not be evacuated using a system that released the reactive products. Therefore, 1 kW of produced electricity, generally leads to evacuate 1 kW of thermal energy from the fuel cell core. This heat must be extracted from the fuel cell to protect the membrane. Indeed, when dryout occurred at the membrane level, the ionic conduction drop sharply. But worst situations may occur and this membrane may be destroyed if relative humidity become too low.

When the thermal energy is extracted for the fuel cell core, this heat may be used in a secondary loop (co-generation), or simply rejected from fuel cell core in a loop which has a condenser (Figure 7.1).

Therefore, the sizing of the fuel cell cooling system is of first importance. Indeed, it should take into account the impact of the pressure drops in the cooling channels as well as the thermal homogeneity in order to obtain targeted performances in term of energy. Moreover, the homogenization of the bipolar plate temperature allow for the increase of the lifetime of the system by limiting the thermal gradients. It is in this context that boiling in mini-channel appeared to be an interesting candidate. Indeed, the liquid vapor phase change is made at constant temperature if the working pressure is set. In addition, when the bipolar plate thickness is small, the plate temperature is at same time controlled by fluid temperature at saturation. It may be noticed that the thermal hotspot management is of significant importance and should be considered in parallel with the sizing of the cooling channels.

Section 7.1. Short presentation of the working principle

In the remaining part of this chapter, a fuel cell cooling will be evaluated according to criteria closed to the working conditions. This approach was made for proposing different ways of reflexion related to the sizing of the heat exchanger. Therefore, by considering the experimental results (Chapter 5 and Chapter 6), it was possible to make simple transpositions in function of the working conditions of the mini-channels (in terms of flow rate, wall heat fluxes). This analysis, would allow for the determination of the « relevant » elements for the geometry selection that look more adapted for the cooling of the considered fuel cell. This analysis was made considering realistic order of magnitudes in terms of dissipated heat fluxes. The studied region would be limited to the cooling channels located in the fuel cell core. Therefore the refrigerant feeder and collector will not be considered in this approach. Several assumptions must be defined in the context of this transposition.

Simplifying assumptions for transposing the results

- ▷ The targeted fuel cell have a working temperature that is comprised between $60^{\circ}C$ and $70^{\circ}C$. This temperature was based on the boiling curves that were obtained during this work.
- ▷ The flow rate was set in order that the heat flux was about $7000 W.m^{-2}$. This heat flux will be considered as homogeneous along the mini-channel walls.
- ▷ The fuel cell consisted of 24 cells (whose cooling area dimensions were of : width \times length \times height = $10 cm \times 10 cm \times 10 cm$) and the thermal power to be extracted was of $1.5 kW$.
- ▷ The cooling channels allow for the evacuation of one part of this heat flux (thermal losses to environment relate to convection or radiation exist). The efficiency of the thermal exchanger is set at 65%.
- ▷ The flow was considered to be horizontal, therefore the pressure drops due to gravity were negligible.
- ▷ The impact of hot spots on the heat transfer was not considered.
- ▷ The flow cross section of the cooling was rectangular and the technology considered straight rectangular mini-channels instead of serpentine technology.
- ▷ The flow velocities were considered as uniformed and the interaction between the channels was neglected.
- ▷ Each channel has the same hydraulic behavior than its neighbored channel at same time.

7.2 Comparison of the energy efficiency

Questions about the performance comparison between a single-phase and a boiling flow

In a first step it was chosen to compare the thermal exchanger performance for single-phase condition and then for boiling conditions for forane 365 HX. This very interesting comparison allow for the tradeoff analysis between single-phase and a boiling flow. The evaluation of these performances were made at equivalent heat flux. In this context, the parameter that was compared was the hydraulic power. The theoretical hydraulic powers were obtained using :

$$P_{pompe} = \dot{v} \times \Delta P \tag{7.1}$$

where \dot{v} represent the flow rate and ΔP the pressure drop in the mini-channel.

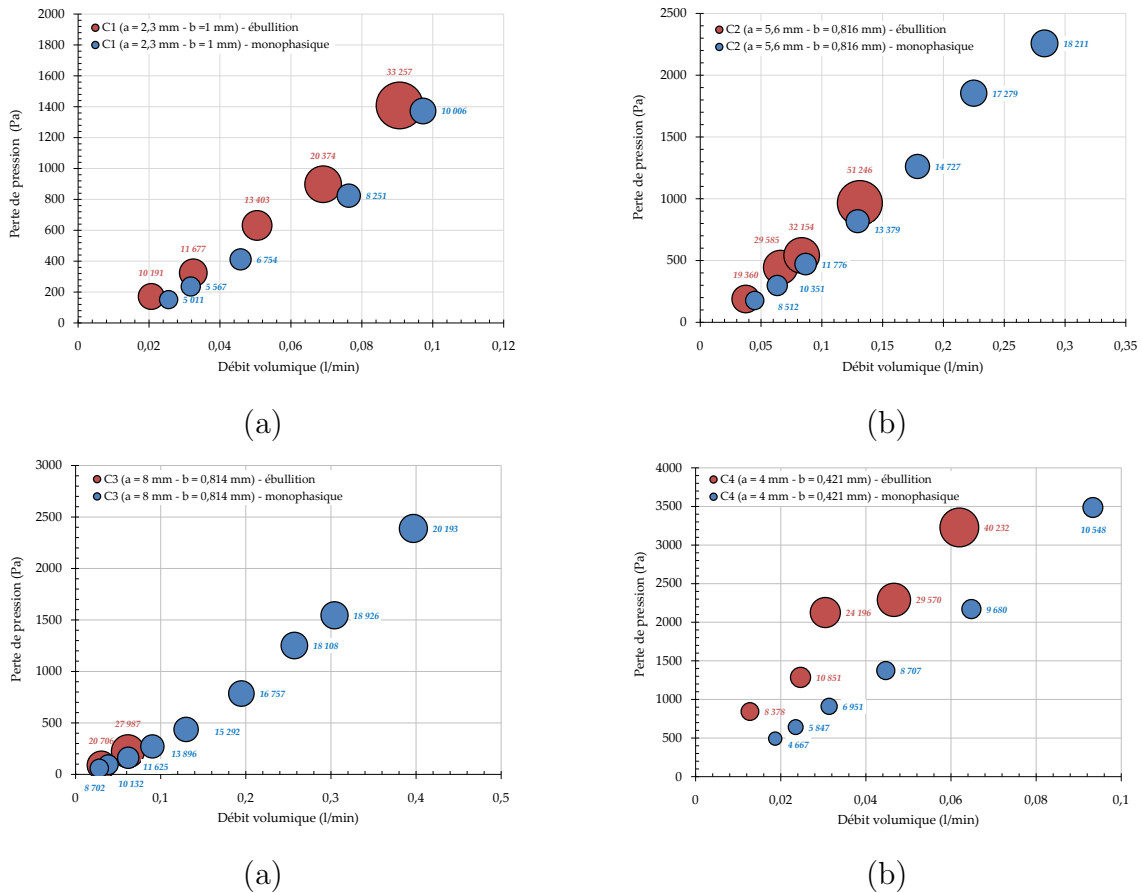


FIGURE 7.3 – Comparison of the energy efficiency between a single-phase and boiling flows for : (a) $C_1(a = 2.3 \text{ mm} - b = 1 \text{ mm})$ (b) $C_2(a = 5.6 \text{ mm} - b = 0.816 \text{ mm})$ (c) $C_3(a = 8 \text{ mm} - b = 0.814 \text{ mm})$ (d) $C_4(a = 4 \text{ mm} - b = 0.421 \text{ mm})$ mini-channels. beside each circles, the heat flux was given in $W.m^{-2}$

The powers that were compared were closed (when possible) to those regarding the cooling

conditions of a PEMFC according to the assumptions made in § 7.1.2. The comparisons have been showed for the four mini-channels in Figure 7.3. The visible circles (and mainly their sizes) on the whole set of series represent the heat flux exchanged between the wall and the fluid. This heat flux was expressed in $W.m^{-2}$.

It was possible to notice that for a selected flow rate, boiling led to a pressure drop slightly higher than the single-phase flow configuration for $C_1(a = 2.3 \text{ mm} - b = 1 \text{ mm})$, $C_2(a = 5.6 \text{ mm} - b = 0.816 \text{ mm})$ and $C_3(a = 8 \text{ mm} - b = 0.814 \text{ mm})$ mini-channels. This increase was more pronounced for $C_4(a = 4 \text{ mm} - b = 0.421 \text{ mm})$ mini-channel, where the confinement phenomena were more important, as already explained in Chapter 6. Generally, it was possible to observe that if the « iso-pressure drop » or « iso-volumetric flow rates » are drawn, the heat flux exchanged was always higher for the boiling conditions.

A more relevant study, should led to think on the thermal power exchanged between the fluid and the wall. Indeed, for the example of $C_1(a = 2.3 \text{ mm} - b = 1 \text{ mm})$ mini-channel, the heat flux that was compared was about 10000 W.m^{-2} , what is close to the one of a fuel cell in terms of heat fluxes exchanged. Therefore, it was observed that for reaching the same heat flux, the required hydraulic powers were very different in function of the flow regime. Therefore, it was summarized that the ratio between the pumping power in single-phase flow and the pumping power in boiling condition for equivalent heat flux in Table 7.1.

Tested mini-channels	\dot{q}''	$P_{pump, single-phase} / P_{pump, boiling}$
$C_1(a = 2.3 \text{ mm} - b = 1 \text{ mm})$	$\approx 10000 \text{ W.m}^{-2}$	38
$C_2(a = 5.6 \text{ mm} - b = 0.816 \text{ mm})$	$\approx 19000 \text{ W.m}^{-2}$	91
$C_3(a = 8.0 \text{ mm} - b = 0.814 \text{ mm})$	$\approx 20000 \text{ W.m}^{-2}$	350
$C_4(a = 4.0 \text{ mm} - b = 0.421 \text{ mm})$	$\approx 8500 \text{ W.m}^{-2}$	10

TABLE 7.1 – Comparison of the theoretical hydraulic power to supply for an equivalent heat flux exchanged between a single-phase and the boiling flows

In the next paragraphs, an analysis allowing for the determination of the impact of the channel geometry on the efficiency of the heat transfer efficiency during convective boiling.

➤ Impact of the mini-channel width

This comparison was made for $C_2(a = 5.6 \text{ mm} - b = 0.816 \text{ mm})$ and $C_3(a = 8.0 \text{ mm} - b = 0.814 \text{ mm})$ mini-channels. The data reported on Table 7.1 showed clearly that this parameter was very (*the most*) important regarding the evolution of the heat exchanger performance. Indeed, the mini-channel width increase allow for the reduction of the pressure drop reduction. Therefore when boiling occurred in the mini-channel, there was a small increase of the pressure drop, but a very important increase of the heat transfer rate. This situation occurred for C_2 mini-channel also, but less sharply.

➤ Aspect ratio impact

This comparison was made for $C_1(\gamma_1 = 0.435)$ and $C_2(\gamma_2 = 0.146)$ mini-channels, that have a different aspect ratio, but a hydraulic diameter very closed to 1.4 mm . Here, it was noticed that the increase of the aspect ratio did not improved the thermal performances of the system. Indeed, as showed in § 6.4.2, the increase of the aspect ratio lead to the increase of the pressure drop for a same heat transfer rate due to the increase of the confinement which was caused by the reduction of the mini-channel cross section. This reduction led to an important increase of the interfacial shear stress which contributed to the increase of the total pressure drops.

➤ Impact of the hydraulic diameter

The reduction of the hydraulic diameter (comparison of $C_4(d_h = 0.762 \text{ mm})$ mini-channel to the other ones) led to a more limited increased of the system thermal efficiency. Indeed, the confinement for this mini-channel was important and led as specified previously to an increase of the pressure drops which limit of the improvement of the performances related to incipience of boiling.

Using this analysis, it was possible to confirm that whatever the tested mini-channels, the thermal performances were better for a boiling flow. In the next paragraph, a comparative study related to the thermal performance of these mini-channel during boiling has been made.

Comparison of the thermal performances between the tested mini-channels (for boiling)

On Figure 7.4, the data allowing for the comparison of the thermal performances of the mini-channels have been reported.

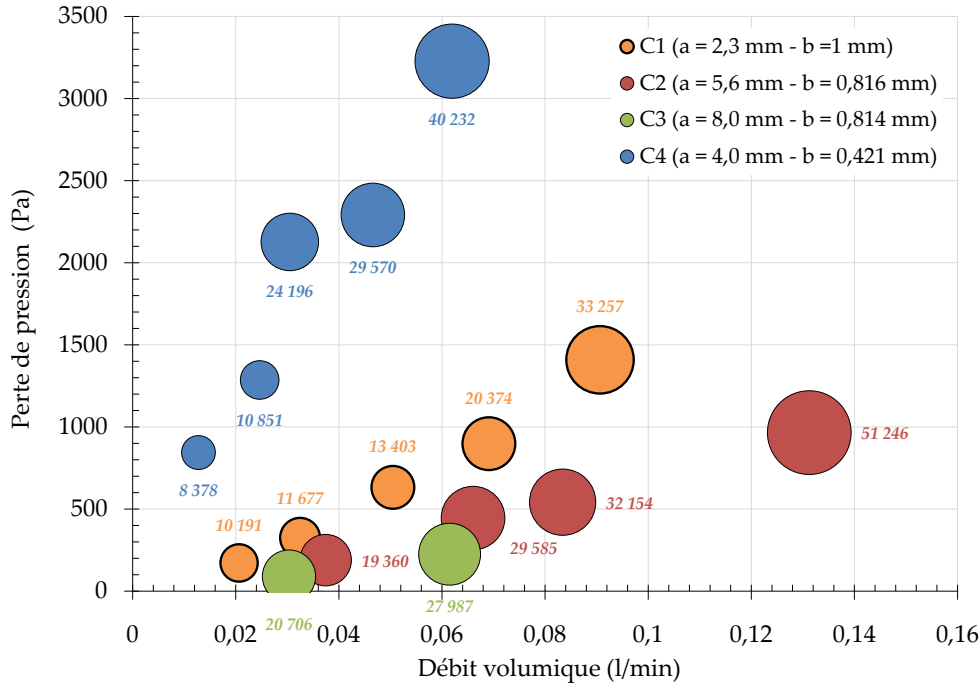


FIGURE 7.4 – Thermal performances in boiling for the whole set of mini-channels

The data given in this figure showed that the best performances were reached (for this experimental configuration) for $C_3(a = 8 \text{ mm} - b = 0.814 \text{ mm})$ mini-channel. In order to realize a comparative analysis with the other mini-channels on a fixed thermal parameter, the ratio of the hydraulic power to a heat flux of the order of 20000 W.m^{-2} regarding C_3 mini-channel has been evaluated. These comparisons have been presented in Table 7.2.

Mini-channel	q''	$P_{pump,C_i}/P_{pump,C_3}$
$C_1(a = 2.3 \text{ mm} - b = 1 \text{ mm})$	$\approx 20373 \text{ W.m}^{-2}$	23
$C_2(a = 5.6 \text{ mm} - b = 0.816 \text{ mm})$	$\approx 19360 \text{ W.m}^{-2}$	3
$C_3(a = 8.0 \text{ mm} - b = 0.814 \text{ mm})$	$\approx 20706 \text{ W.m}^{-2}$	1
$C_4(a = 4.0 \text{ mm} - b = 0.421 \text{ mm})$	$\approx 24196 \text{ W.m}^{-2}$	24

TABLE 7.2 – Comparison of the theoretical hydraulic power to supply for an equivalent heat flux exchanged between the different mini-channels

The data reported on this table confirmed that when the hydraulic diameter and/or the mini-channel cross section were large, the energy efficiency related to the heat transfer rates increased

for a boiling flow in single mini-channel. However, for an in-situ cooling application, the heat flux amplitude that have to be transferred required more complex configurations (serpentine or parallel channels). Here, it was chosen to limit the analysis to the parallel mini-channels.

7.3 Sizing of the cooling channels

In § 7.2, it was demonstrated that the mini-channel that would allow for the best energy efficiency during convective boiling was C_3 mini-channel. This interesting information, should not be considered as definitive when analysis the sizing issues. Indeed, the cooling area of the fuel cell that had been defined (see assumptions section) had the following dimensions : width \times length \times height = $10\text{ cm} \times 10\text{ cm} \times 10\text{ cm}$. In addition, the thermal power that has to be removed is of 1.5 kW for a heat flux of 7000 W.m^{-2} .

It was assumed that the fuel cell was made with 24 cells. Therefore, starting for this point, it was possible to simplify the system by specifying that the heat flux on each pair of cells was of 65.2 W (by considering 23 spacings where the cooling channels could be located). The question to answer is related to the number of channels required for the extraction of the heat knowing that the heat flux is of 7000 W.m^{-2} . This heat flux condition set the flow rate. Without considering the fuel cell feeding channels architecture, it was possible to notice that the cross section of some of the cooling mini-channels cannot allow for the extraction of the total heat (according to the assumptions that have been made). On Table 7.3, the thermal powers that can be extracted have been summarized by considering a heat transfer efficiency of 100% (for comparison) and of 65%.

Mini-channel	max channels number	$P_{extr} (\eta = 100\%)$	$P_{extr} (\eta = 65\%)$
$C_1(a = 2.3\text{ mm} - b = 1\text{ mm})$	22	101.6 W	66 W
$C_2(a = 5.6\text{ mm} - b = 0.816\text{ mm})$	9	79.5 W	51.6 W
$C_3(a = 8.0\text{ mm} - b = 0.814\text{ mm})$	6	77.1 W	50.1 W
$C_4(a = 4.0\text{ mm} - b = 0.421\text{ mm})$	12	77.3 W	50.3 W

TABLE 7.3 – Estimation of the extracted thermal power in function of the heat transfer rate efficiency regarding the different tested mini-channels

The number of channels that was reported in this table was fixed due to each cross section of the thermal exchange area of the fuel cell. The data reported on this table clearly showed that the energy efficiency parameter for a single mini-channel (defined in § 7.2), would not allow for the justification of the selection of a specific geometry for the global cooling of the fuel cell. Indeed, in this configuration only the C_1 mini-channel would allow for the extraction of a sufficient heat. Evidently, this whole analysis, which has been simplified gave some insights related to the confinement inside the fuel cell and on the sizing of the cooling system. Moreover,

the sizing of the gases feeding channels of the fuel cell is very often more important than the one of the cooling mini-channels. Therefore, if this channel C_1 was chosen for the cooling of a fuel cell subjected to a heat flux of 7000 W.m^{-2} , with a subcooling of 15°C (in order to be similar to the experimental data), it would be possible to obtain boiling inside the mini-channels, by setting the flow rate to a value lower than $\dot{v} \leq 0.027 \text{ l/min}$. Therefore, by supposing that this flow rate was set to 0.022 l/min the heat flux value that led to the dryout according to our experiments was about 80 kW.m^{-2} , what is much larger to the heat flux density of 7 kW.m^{-2} . Therefore the selection of this C_1 mini-channel for convective boiling would prevent from the dryout conditions for a constant flow rate in the context of this approach.

It should be specified that the whole sizing approach was based only on the impact of the mini-channel geometry on the energy efficiency. However, regarding the results that have been reported in Chapter 6, the evolution of the inlet temperature has a very important impact on the cooling system efficiency. Therefore, it would be interesting to add to the regulation system a component that would allow for the control of this inlet temperature.

7.4 Chapter 7 conclusions

In this chapter, the working principle of the PEM fuel cell has been given briefly. Energy balances were made and they showed that a boiling flow gave better results in term of energy efficiency than a single-phase flow. The study of the geometry, showed that the use of a single $C_3(a = 8 \text{ mm} - b = 0.814 \text{ mm})$ mini-channel resulted in the better thermal performances. However, in the context of the fuel cell cooling analysis, it was demonstrated that the selection of a mini-channel having a different cross section would allow for the obtaining of a better global thermal management (in a multi-channels cooling approach). To conclude, the geometry is of first importance for the heat exchanger cooling channels sizing and its dimensions must be considered with care.

General Conclusions and Prospects

This work was dedicated to the study of pressure drops and heat transfer for single-phase and convective boiling flows. Four mini-channels of rectangular cross section have been tested. The selected dimensions allow for the characterization of the impact of the aspect ratios, hydraulic diameters as well as the mini-channel widths on the convective boiling.

A working fluid, forane 365 HX, has been selection according to the specifications that were defined for following the constraints related to the fuel cell regarding its cooling. It should be specified that this fluid was never analyzed in convective boiling in mini-channels according to the analyzed literature survey.

Formerly to the boiling tests, the hydrodynamic and thermal behaviors were studied for single-phase flow conditions. A numerical model, made for single-phase flow, allowed for the estimation of the heat flux repartition along the mini-channels walls. It was demonstrated that the heat flux was not homogenous and it was larger at the channel inlet. The working fluid as well as the mini-channel geometry also act on this characteristic. As an example the reduction of the channel width increase the non-homogeneous characteristic of the heat flux. It was demonstrated during the study that the estimation of this repartition was very important before realizing the tests related to boiling in order to calculate correctly the heat flux that was transferred to the fluid in order to make good estimation of the heat transfer coefficients.

The results obtained in boiling conditions showed that the geometry impact on the onset of nucleate boiling (ONB) may be significant. For mini-channels having larger aspect ratio, the needed heat flux for ONB was larger due to a higher distortion of the temperature field (cooler on the corners compared to mini-channel center) for large mass velocity. In addition, the hydraulic diameter reduction led to the more rapid occurrence of the ONB when the mass velocities were larger than $200 \text{ kg.m}^{-2}.\text{s}^{-1}$. For smaller mass velocities, there were no specific parameter that seemed to characterize the influence of the geometry. The range of working conditions for the thermal exchanger, used in boiling conditions is considered as fully characterized when the conditions that led to dryout are known. Therefore, the impact of the evolution of the critical heat flux was studied for the four mini-channels. The reported data showed that the aspect ratio as well as the hydraulic diameter seemed to modify the occurrence of this critical heat flux (CHF) when considering same mass velocities. The CHF increase with mini-channel aspect ratio and decrease with mini-channel hydraulic diameter.

General Conclusions and prospects

It was showed that the mini-channel geometry has a very important impact on the total two-phase pressure drops for same hydraulic diameter :

The data of the literature showed that the hydraulic diameter reduction led to the increase of the total pressure drops for boiling flows, what was observed in the experiments presented in this manuscript also. However, it was noticed that these pressure drops increased with the aspect ratio. According to our understanding, this increase was related to the reduction of the two-phase flow cross section. This reduction led to the increase of the interfacial shear stress between the liquid and vapor phases as well as to the increase of wall frictions. Thanks to the study of the pressure drops evolutions, a confinement number ($C_{Oad-hoc}$) that took into account the aspect ratio influence and allow for the prediction of the relative importance of the pressure drops between the different mini-channels has been proposed. After comparing the experiments with the existing predictive correlations, a generalized correlation which was based on the new confinement number was suggested. For these experimental campaigns, the geometry did not impacted much the evolution of the heat transfer coefficients for a same transferred heat flux. For these thermal exchanges, a correlation that allowed for the prediction of our experiments was defined also. This correlation was based on the assumption of the preponderance of nucleate boiling.

Thanks to this study, it was shown that the selection of the geometrical parameters impacted the evolution of thermal performances of a heat exchanger made using a single mini-channel. The transposition of these results to the cooling of a fuel cell (comprising several mini-channels) should be made with caution. Indeed, the area dimension where the heat fluxes have to be dissipated played an important role because their set the mini-channels number that will be placed on this surface. Therefore a sizing work must be realized in order to optimize the extraction of heat generated by the electrochemical reaction.

There was some element that may led to a better evaluation of the heat transfer. Therefore it was though that an original system that would allow for the measurement of the fluid temperature may help for a better determination of the local heat transfer coefficients. Indeed the knowledge of the fluid temperature variation in boiling conditions may improve to whole analysis. In this context, a measurement methodology without contact may be though using an infrared (IR) measuring system. Therefore, the use of an IR camera would allow for the obtaining a spacial resolution that would allow for the better understanding of the boiling flow nature.

Moreover, the void fraction fraction would be a relevant data for characterizing the total two-phase flow pressure drops. Therefore, a measuring system or the treatment of the acquired

images⁸ that allow for the obtaining of this value with precision for various mass velocities would be very appreciated.

Finally, the acquired images, allowed for the demonstration the mini-channel geometry has an impact on the flow regime transitions. However, these flow regimes differences (observed between the mini-channels) did not impacted the heat transfer evolution for a same heat flux. Therefore, it was though that it would be very interesting to analyze the instabilities occurrence inside the mini-channels that led, according to our understanding, to a non-dependence of the heat fluxes variation with heat flux when the conditions were far from wall dryout conditions.

On short term basis, we though that it would be particularly fruitful to realize new experiments that allow for the characterization of the ONB for mass velocities smaller than those analyzed during this study. Indeed, this study would allow for the better understanding of these evolutions that seemed to be not linear for small mass velocities. Moreover, these tests would supplement the ones given here and should allowed for the formalization of a correlation giving the threshold heat flux in function of the mass velocity. On a longer-term basis, the data that have been obtained in this study should be compared to the results made in multi-channels configurations. The aim of this followed up study would be obviously to made in-situ cooling inside a PEM fuel cell.

8. A very interesting approach has been initiated by Longa (2008) during this work and the methodology for the obtaining of the void fraction has been reported in Appendix F

Bibliography

- AGOSTINI, B. : *Etude expérimentale de l'ébullition de fluide réfrigérant en convection forcée dans des mini-canaux*. Thèse de doctorat, Université Joseph Fourier, 2002.
- AGOSTINI, B., FABBRI, M., PARK, J. E., WOJTAN, L., THOME, J. R. et MICHEL, B. : State of the art of high heat flux cooling technologies. *Heat Transfer Engineering*, 28(4):258–281, 2007.
- AGOSTINI, B., REVELLIN, R. et THOME, J. R. : Elongated bubbles in microchannels. part i : Experimental study and modeling of elongated bubble velocity. *International Journal of Multiphase Flow*, 34(6):590–601, 2008.
- AGOSTINI, F. : *Boiling on a Tube Bundle : Heat Transfer, Pressure Drop and Flow Patterns*. Thèse de doctorat, École Polytechnique Fédérale de Lausanne, 2008.
- ANTONI, L. : Les piles à combustible. *École Énergies et Recherches - 23 mars 2006 (CEA)*, 2006.
- BAKER, O. : Simultaneous flow of oil and gas. *Oil and Gas Journal*, 53:185–195, 1954.
- BARAJAS, A. et PATON, R. : Effet of contact angle on two phase flow in capillary tubes. *International Journal of Multiphase Flow*, 19:337–346, 1993.
- BAROCZY, C. : Correlation of liquid fraction in two-phase flow with application to liquid metals. *Chemical Engineering Progress Symposium series*, 61(57):179–191, 1965.
- BAROCZY, C. : A systematic correlation for two-phase pressure drop. *Chemical Engineering Progress Symposium series*, 62:232–249, 1966.
- BAVIÈRE, R. : *Etude de l'hydrodynamique et des transferts de chaleur dans des microcanaux*. Thèse de doctorat, Université Joseph Fourier, 2005.
- BAVIÈRE, R., FAVRE-MARINET, M. et LE PERSON, S. : Bias effects on heat transfer measurements in microchannel flows. *International Journal of Heat and Mass Transfer*, 49:3325–3337, 2006.
- BERGLES, A., LIENHARD, J., KENDALL, G. et GRIFFITH, P. : Boiling and evaporation in small diameter channels. *Heat Transfer Engineering*, 24(1):18–40, 2003.
- BERGLES, A. et ROHSENOW, W. : The determination of forced-convection surface-boiling heat transfer. *Journal of heat transfer*, 86:365–372, 1964.

Bibliography

- BERTSCH, S., GROLL, E. et GARIMELLA, S. : Effects of heat flux, mass flux, vapor quality, and saturation temperature on flow boiling heat transfer in microchannels. *International Journal of Multiphase Flow*, 35:142–154, 2009.
- BHIDE, R., SINGH, S., SRIDHARAN, A., DUTTAGUPTA, S. et AGRAWAL, A. : Pressure drop and heat transfer characteristics of boiling water in sub-hundred micron channel. *Experimental Thermal and Fluid Science*, 33:963–975, 2009.
- BIGOT, J. : *Etude du refroidissement diphasique d'une pile à combustible de traction automobile*. Thèse de doctorat, Université Joseph Fourier, 2005.
- BLASIUS, H. : Das Ähnlichkeitsgesetz bei Reibungsvorgängen in Flüssigkeiten. *Forsch Arb Ing Wes*, 131, 1913.
- BUTTERWORTH, D. : A comparison of some void-fraction relationships for co-current gas-liquid flow. *International Journal of Multiphase Flow*, 1:845–850, 1975.
- CAREY, V. : *Liquid-Vapor Phase Change Phenomena*. Taylor & Francis, New-York, second édition, 2008.
- CHEN, J. C. : Correlation for boiling heat transfer to saturated fluids in convective flow. *IEC Process Design and Development*, 5(3):322–329, 1966.
- CHEN, P.-H., LEE, Y.-W. et CHANG, T.-L. : Predicting thermal instability in a closed loop pulsating heat pipe system. *Applied Thermal Engineering*, 29:1566–1576, 2009.
- CHENG, P., WU, H.-Y. et HONG, F.-J. : Phase-change heat transfer in microsystems. *Journal of Heat Transfer*, 129:101–108, 2007.
- CHISHOLM, D. : Pressure gradients due to friction during the flow of evaporating two-phase mixtures in smooth tubes and channels. *International Journal of Heat and Mass Transfer*, 16:347–358, 1973.
- CHISHOLM, D. et LAIRD, A. : Two-phase flow in rough tubes. *Transactions of the ASME*, 80:276–286, 1958.
- CHOI, K.-I., PAMITRAN, A., OH, J.-T. et SAITO, K. : Pressure drop and heat transfer during two-phase flow vaporization of propane in horizontal smooth minichannels. *International Journal of Refrigeration*, 32(5):837–845, 2009.
- CICCHITTI, A., LOMBARDI, C., SILVESTRI, M., SOLDAINI, G. et ZAVATTARELLI, R. : Two-phase cooling experimentals - pressure drop, heat transfer and burnout measurements. *Energia Nucleare*, 7(6):407–425, 1960.

- COLEBROOK, C. : Turbulent flow in pipes with particular reference to the transition region between the smooth and rough pipes laws. *Journal of the Institute of Civil Engineers*, 11:133–156, 1939.
- COLIN, C., YOSHIKAWA, H., LEGENDRE, D. et MONTOUT, M. : Hydrodynamics of bubble detachment in convective boiling. *In 7th ECI International conference on boiling heat transfer*, Florianopolis , Brésil., 2009.
- COLLIER, J. et THOME, J. R. : *Convective boiling and condensation*. Oxford University Press, New-York, 1994.
- CONSOLINI, L. : *Convective Boiling Heat Transfer in a Single Micro-Channel*. Thèse de doctorat, École Polytechnique Fédérale de Lausanne, 2008.
- DAVIS, E. et ANDERSON, G. : The incipience of nucleate boiling in forced convection flow. *AIChE Journal*, 12:774–780, 1966.
- DESRATS, C. : *Etude expérimentale de l'ébullition d'hydrocarbures dans les échangeurs à plaques et ailettes. Analyse des écoulements et des transferts de chaleur par une approche locale*. Thèse de doctorat, Université de Provence Aix-Marseille, 2006.
- DIAZ, C. et SCHMIDT, J. : Experimental investigation of transient boiling heat transfer in microchannels. *International Journal of Heat and Fluid Flow*, 28:95–102, 2007.
- DITTUS, P. et BOELTER, L. : Heat transfer in automobile radiators of the tubular type. *Univ. Calif. Publ. Eng.*, 2:443–461, 1930.
- DUPONT, V. et THOME, J. R. : Evaporation in microchannels : influence of the channel diameter on heat transfer. *Microfluid Nanofluid*, 1:119–127, 2005.
- FLUENT 6, I. : *Fluent 6 user's guide*, 2001.
- FORSTER, H. et ZUBER, N. : Dynamics of vapor bubbles and boiling heat transfer. *AIChE Journal*, 1:531–535, 1955.
- FRIEDEL, L. : Improved friction pressure drop correlations for horizontal and vertical two-phase pipe flow. *In European Two-phase Flow Group Meeting Paper E2*, volume 18, pages 485–492, Ispra, 1979.
- FRITZ, W. : Berechnung des maximal Volume von Dampfblasen. *Phys. Z.*, 36:379–388, 1935.
- FROST, W. et DZAKOWIC, G. : An extension of the methods of predicting incipient boiling on commercially finished surfaces. *In ASME, éditeur : National Heat Transfer Conference*, pages Paper 67–HT–61, Seattle, Washington, 1967.

Bibliography

- FU, X., ZHANG, P. et WANG, R. : Visualization of flow boiling of liquid nitrogen in a vertical mini-tube. *International Journal of Multiphase Flow*, 31:333–351, 2007.
- GAMRAT, G. : *Modélisation de l'hydrodynamique et des transferts de chaleur dans des micro-canaux à parois rugueuses*. Thèse de doctorat, INP Grenoble, 2007.
- GAO, P., LE PERSON, S. et FAVRE-MARINET, M. : Scale effects on hydrodynamics and heat transfer in two-dimensional mini and microchannels. *International Journal of Thermal Sciences*, 41:101.–1027, 2002.
- GEISLER, K. et BAR-COHEN, A. : Confinement effects on nucleate boiling and critical heat flux in buoyancy-driven microchannels. *International Journal of Heat and Mass Transfer*, 52:2427–2436, 2009.
- GHIAASIAAN, S. et CHEDESTER, R. : Boiling incipience in microchannels. *International Journal of Heat and Mass Transfer*, 45:4599–4606, 2002.
- GNIELINSKI, V. : New equations for heat and mass transfer in turbulent pipe and channel flow. *International Chemical Engineering*, 16:359–368, 1976.
- GRÖNNERUD, R. : Investigation in liquid holdup, flow resistance and heat transfer in circular type evaporators, part IV : Two-phase resistance in boiling refrigerant. *Bulletin de l'Inst. du Froid*, Annexe 1972-1, 1972.
- GUNGOR, K. E. et WINTERTON, R. H. : A general correlation for flow boiling in tubes and annuli. *International Journal of Heat and Mass Transfer*, 29(3):351–358, 1986.
- HARIRCHIAN, T. et GARIMELLA, S. : The critical role of channel cross-sectional area in microchannel flow boiling heat transfer. *International Journal of Multiphase Flow*, 35:904–913, 2009.
- HARIRCHIAN, T. et GARIMELLA, S. V. : Microchannel size effects on local flow boiling heat transfer to a dielectric fluid. *International Journal of Heat and Mass Transfer*, 51:3724–3735, 2008.
- HASAN, M. I., RAGED, A., YAGHOUBI, M. et HOMAYONI, H. : Influence of channel geometry on the performance of a counter flow microchannel heat exchanger. *International Journal of Thermal Sciences*, 48:1607–1618, 2009.
- HETSRONI, G., MOSYAK, A., POGREBNYAK, E. et SEGAL, Z. : Periodic boiling in parallel micro-channels at low vapor quality. *International Journal of Multiphase Flow*, 32:1141–1159, 2006.

- HRNJAK, P. et TU, X. : Single phase pressure drop in microchannels. *Heat and Fluid Flow*, 28:2–14, 2006.
- HSU, Y. : On the size range range of active nucleation cavities on a heating surface. *Journal of Heat Transfer*, 84:207–213, 1962.
- HUH, C., KIM, J. et KIM, M. H. : Flow pattern transition instability during flow boiling in a single microchannel. *International Journal of Heat and Mass Transfer*, 50:1049–1060, 2007.
- HUO, X., CHEN, L., TIAN, Y. S. et KARAYIANNIS, T. : Flow boiling and flow regimes in small diameter tubes. *Applied Thermal Engineering*, 24:1225–1239, 2004.
- JASSIM, E. et NEWELL, T. : Prediction of two-phase pressure drop and void fraction in microchannels using probabilistic flow regime mapping. *International Journal of Heat and Mass Transfer*, 49:2446–2457, 2006.
- JUDY, J., MAYNES, D. et WEBB, B. : Characterization of frictional pressure drop for liquid flows through microchannels. *International Journal of Heat and Mass Transfer*, 45:3477–3489, 2002.
- KANDLIKAR, S. G. : A general correlation for saturated two-phase flow boiling heat transfer inside horizontal and vertical tubes. *Journal of Heat Transfer*, 112:219–228, 1990.
- KANDLIKAR, S. G. : Fundamental issues related to flow boiling in minichannels and microchannels. *Experimental Thermal and Fluid Science*, 26:389–407, 2002.
- KANDLIKAR, S. G. : Nucleation characteristics and stability considerations during flow boiling in microchannels. *Experimental Thermal and Fluid Science*, 30:441–447, 2006.
- KANDLIKAR, S. G. et BALASUBRAMANIAN, P. : An extension of the flow boiling correlation to transition, laminar, and deep laminar flows in minichannels and microchannels. *Heat Transfer Engineering*, 25:86–93, 2003.
- KANDLIKAR, S. G. et BALASUBRAMANIAN, P. : An experimental study on the effect of gravitational orientation on flow boiling of water in 1054x197 μm parallel minichannels. *Journal of Heat Transfer*, 127:820–829, 2005.
- KATTO, Y. et OHNO, H. : An improved version of the generalized correlation of critical heat flux for forced convective boiling in uniformly heated vertical tube. *International Journal of Heat and Mass Transfer*, 27:1641–1648, 1984.
- KEW, P. et CORNWELL, K. : Correlations for the prediction of boiling heat transfer in small-diameter channels. *Applied Thermal Engineering*, 17:705–715, 1997.

Bibliography

- KLINE, S. et MCCLINTOK, F. : Describing uncertainties in single-sample experiments. *Mechanical Engineering*, 75:3–8, 1953.
- KOHL, M. J., ABDEL-KHALIK, S. I., JETER, S. M. et SADOWSKI, D. L. : An experimental investigation of microchannel flow with internal pressure measurements. *International Journal of Heat and Mass Transfer*, 48(8):1518–1533, 2005.
- KUO, C.-J. et PELES, Y. : Local measurement of flow boiling in structured surface microchannels. *International Journal of Heat and Mass Transfer*, 50:4513–4526, 2007.
- KUTATELADZE, S. : Boiling heat transfer. *International Journal of Heat and Mass Transfer*, 4:31–45, 1961.
- LANCEREAU, Q. : Étude numérique d’une convection forcée en régime laminaire monophasique dans un micro-canal. Rapport technique, ENSE3 - G-INP, 2008.
- LEE, C. Y. et LEE, S. Y. : Influence of surface wettability on transition of two-phase flow pattern in round mini-channels. *International Journal of Multiphase Flow*, 34:706–711, 2008.
- LEE, H. J. et LEE, S. Y. : Heat transfer correlations for two phase flow within horizontal rectangular channels with low aspect ratio. *International Journal of Multiphase Flow*, 27:2043–2062, 2001a.
- LEE, H. et LEE, S. : Pressure drop correlations for two-phase flow within horizontal rectangular channels with small heights. *International Journal of Multiphase Flow*, 27:783–796, 2001b.
- LEE, J. et MUDAWAR, I. : Two-phase flow in high-heat-flux micro-channel heat sink for refrigeration cooling applications : Part I : pressure drop characteristics. *International Journal of Heat and Mass Transfer*, 48:928–940, 2005a.
- LEE, J. et MUDAWAR, I. : Two-phase flow in high-heat-flux micro-channel heat sink for refrigeration cooling applications : Part II : heat transfer characteristics. *International Journal of Heat and Mass Transfer*, 48:941–955, 2005b.
- LEE, J. et MUDAWAR, I. : Fluid flow and heat transfer characteristics of low temperature two-phase micro-channel heat sinks part 2. subcooled boiling pressure drop and heat transfer. *International Journal of Heat and Mass Transfer*, 2008:4327–4341, 2008.
- LEE, P.-S. et GARIMELLA, S. V. : Thermally developing flow and heat transfer in rectangular microchannels of different aspect ratios. *International Journal of Heat and Mass Transfer*, 49:3060–3067, 2006.
- LI, H., TSENG, F. et PAN, C. : Bubble dynamics in microchannels. part ii : two parallel microchannels. *International Journal of Heat and Mass Transfer*, 47:5591–5606, 2004.

- LIU, D., LEE, P.-S. et GARIMELLA, S. : Prediction of the onset of nucleate boiling in micro-channel flow. *International Journal of Heat and Mass Transfer*, 48:5134–5149, 2005.
- LIU, Z. et WINTERTON, R. H. : A general correlation for saturated and subcooled flow boiling in tubes and annuli, based on nucleation pool boiling equation. *International Journal of Heat and Mass Transfer*, 24:51–56, 1990.
- LOCKHART, R. et MARTINELLI, R. : Proposed correlation of data for isothermal two-phase, two-component flow in pipes. *Chemical Engineering Progress*, 45(1):39–48, 1949.
- LONGA, F. : L'étude des effets d'échelle lors d'une ébullition en micro-canal. Rapport technique, Université Joseph Fourier, 2008.
- MANDHANE, J., GREGORY, G. et AZIZ, K. : Flow pattern map for gas-liquid flow in horizontal pipes. *International Journal of Multiphase Flow*, 1:537–553, 1974.
- MARANZANA, G., PERRY, L. et MAILLET, D. : Mini- and micro-channels : influence of axial conduction in the walls. *International Journal of Heat and Mass Transfer*, 47:3993–4004, 2004.
- MARTIN-CALLIZO, C., PALM, B. et OWHAIB, W. : Subcooled flow boiling of R-134a in vertical channels of small diameter. *International Journal of Multiphase Flow*, 33:822–832, 2007.
- MCPHAIL, S. : *Single-Phase Fluid Flow and Heat Transfer*. Thèse de doctorat, Université de Stuttgart, 2007. Ecoulement monophasique.
- MEGAHED, A. et HASSAN, I. : Two-phase pressure drop and flow visualization of FC-72 in a silicon microchannel heat sink. *International Journal of Heat and Fluid Flow*, 30(6):1171–1182, 2009.
- MEHENDALE, S. S. et JACOBI, A. M. : Fluid flow and heat transfer at micro- and meso-scales with application to exchanger design. *Applied Mechanical Engineering*, 53:175–193, 2000.
- MISHIMA, K. et HIBIKI, T. : Some characteristics of air-water two-phase flow in small diameter vertical tubes. *International Journal of Multiphase Flow*, 22:703–712, 1996.
- MÜLLER-STEINHAGEN, H. et HECK, K. : A simple friction pressure drop correlation for two-phase flow in pipes. *Chemical Engineering Processing*, 20:297–308, 1986.
- MOODY, L. : Friction factors for pipe flow. *Transactions of the ASME*, 66:671–684, 1944.
- NIÑO, V. : Characterization of two-phase flow in microchannels. Rapport technique, University of Illinois, 2002.

Bibliography

- NUKIYAMA, S. : Maximum and minimum values of heat transmitted from metal to boiling water under atmospheric pressure. *Journal of the Japanese Society of Mechanical Engineers*, 37(53-54):367–374, 1934.
- ONG, C. et THOME, J. R. : Flow boiling heat transfer of R-134a, R-236fa and R-245fa in a horizontal 1.030 mm circular channel. *Experimental Thermal and Fluid Science*, 33:651–663, 2009.
- PARK, C. Y. et HRNAJK, P. : Flow boiling heat transfer, pressure drop, and flow pattern for CO_2 in a 3.5 mm horizontal smooth tube. *Journal of Heat Transfer*, 131:1501–1512, 2009.
- PETUKHOV, B. et POPOV, V. : Theoretical calculation of heat exchange in turbulent flow in tubes of an incompressible fluid with variable physical properties. *High Temp.*, 1:69–83, 1963.
- PHAN, H., CANEY, N., MARTY, P., COLASSON, S. et GARVILLET, J. : Surface wettability control by nanocoating : The effects on pool boiling heat transfer and nucleation mechanism. *International Journal of Heat and Mass Transfer*, 52:5459–5471, 2009.
- PREMOLI, D., FRANCESCO, A. et PRINA, A. : A dimensional correlation for evaluating two-phase mixture density. *La Termotecnica*, 25:17–26, 1971.
- QU, W. et MUDAWAR, I. : Experimental and numerical study of pressure drop and heat transfer in a single-phase micro-channel heat sink. *Heat and Mass Transfer*, 45:2549–2565, 2001.
- QU, W. et MUDAWAR, I. : Prediction and measurement of incipient boiling heat flux in micro-channel heat sinks. *International Journal of Heat and Mass Transfer*, 45:3933–3945, 2002.
- QU, W. et MUDAWAR, I. : Measurement and prediction of pressure drop in two-phase micro-channel heat sinks. *International Journal of Heat and Mass Transfer*, 46:2737–2753, 2003.
- REFPROP 7, N. : Reference fluid thermodynamic and transport properties, 2002.
- REVELLIN, R., AGOSTINI, B., URSENBACHER, T. et THOME, J. R. : Experimental investigation of velocity and length of elongated bubbles for flow of R-134a in a 0,5 mm microchannel. *Experimental Thermal and Fluid Science*, 32:870–881, 2008.
- REVELLIN, R. et THOME, J. R. : Adiabatic two-phase frictional pressure drops in microchannels. *Experimental Thermal and Fluid Science*, 31:673–685, 2006.
- REVELLIN, R. et THOME, J. R. : A theoretical model for the prediction of the critical heat flux in heated microchannels. *International Journal of Heat and Mass Transfer*, 51(5-6):1216–1225, 2008.

- RIBATSKI, G., WOJTAN, L. et THOME, J. R. : An analysis of experimental data and prediction methods for two-phase frictional pressure drop and flow boiling heat transfer in micro-scale channels. *Experimental Thermal and Fluid Science*, 31:1–19, 2006.
- ROHSENOW, W., HARNETT, J. et CHO, Y. : *Handbook of heat transfer*. McGrawHill, New-York, 1998.
- SAISORN, S. et WONGWISE, S. : The effects of channel diameter on flow pattern, void fraction and pressure drop of two-phase airwater flow in circular micro-channels. *Experimental Thermal and Fluid Science*, 34:454–462, 2010.
- SAITOH, S., DAIGUJI, H. et HIHARA, E. : Effect of tube diameter on boiling heat transfer of R-134a in horizontal small-diameter tubes. *International Journal of Heat and Mass Transfer*, 48:4973–4984, 2005.
- SATO, T. et MATSUMURA, H. : On the conditions of incipient subcooled boiling and forced convection. *Bull. Japan Soc. Mech. Engineers*, 7:392–398, 1964.
- SHAH, M. M. : A new correlation for heat transfer during boiling flow through pipes. *Transactions of the ASHRAE*, 82:66–86, 1976.
- SHAH, R. et LONDON, A. : Laminar flow in forced convection ducts. *Advances in Heat Transfer Suppl. 1 - Academic Press*, 1978.
- SHAH, R. et SÉKULIC, D. : *Fundamentals of heat exchanger design*. John Wiley & Sons, New-Jersey, 2003.
- SHEN, S., XU, J., ZHOU, J. et CHEN, Y. : Flow and heat transfer in microchannels with rough wall surface. *Energy conversion and management*, 47:1311–1325, 2006.
- SOBIERSKA, E., KULENOVIC, R. et MERTZ, R. : Heat transfer mechanism and flow pattern during flow boiling of water in a vertical narrow channel experimental results. *International Journal of Thermal Sciences*, 46:1172–1181, 2007.
- STEINKE, M. E. et KANDLIKAR, S. G. : Control and effect of dissolved air in water during flow boiling in microchannels. *International Journal of Heat and Mass Transfer*, 47:1925–1935, 2004.
- STEINKE, M. E. et KANDLIKAR, S. G. : Single-phase liquid friction factors in microchannels. *International Journal of Thermal Sciences*, 45:1073–1083, 2006.
- STUTZ, B. : La nucléation. *In Le changement de phase liquide-vapeur et ses applications*, Cargèse, France, 2003.

Bibliography

- TAITEL, Y. et DUKLER, A. : A model for predicting flow regime transitions in horizontal and near horizontal gas-liquid flow. *AIChE Journal*, 22:47–55, 1976.
- THOM, J. : Prediction of pressure drop during forced-circulation boiling of water. *International Journal of Heat and Mass Transfer*, 7:709–724, 1964.
- THOME, J. R. : Boiling in microchannels : a review of experiment and theory. *International Journal of Heat and Fluid Flow*, 25:128–139, 2004.
- THOME, J. R. : Engineering data book III, 2006.
- TRAN, T. N., CHYU, M.-C., WAMBSGANSS, M. W. et FRANCE, D. M. : Two-phase pressure drop of refrigerants during flow boiling in small channels : an experimental investigation and correlation development. *International Journal of Multiphase Flow*, 26:1739–1754, 2000.
- TRAN, T. N., WAMBSGANSS, M. W. et FRANCE, D. M. : Small circular and rectangular channel boiling with two refrigerants. *International Journal of Multiphase Flow*, 22:485–498, 1996.
- TRIPLETT, K. A., GHIAASIAAN, S., ABDEL-KHALIK, S. I. et SADOWSKI, D. L. : Gas-liquid two-phase flow in micro-channels part i : two-phase flow patterns. *International Journal of Multiphase Flow*, 25:395–410, 1999.
- TUCKERMANN, D. et PEASE, R. : High performance heat sinking for vlsi. *IEEE EDL-2*, 5, 1981.
- ULLMAN, A. et BRAUNER, N. : The prediction of flow pattern maps in mini-channels. In *4th Japanese-European Two-Phase Flow Group Meeting*, pages 24–28, Kyoto, Japon, 2006.
- VALDENNAIRE : Création d'un programme d'acquisition de données dans le cadre de l'étude des écoulements diphasiques aux petites échelles. Rapport technique, IUT - Mesures Physiques, 2008.
- WAHDAME, B. : *Analyse et optimisation du fonctionnement de piles à combustible par la méthode des plans d'expériences*. Thèse de doctorat, Université de Franche Comté, 2006.
- WALLIS, G. : *One-Dimensional Two-Phase Flow*. John Wiley, New-York, 1965.
- WANG, G., CHENG, P. et WU, H.-Y. : Unstable and stable flow boiling in parallel microchannels and in a single microchannel. *International Journal of Heat and Mass Transfer*, 50(21-22):4297–4310, 2007.
- WANG, R., CONG, L. et KIDO, M. : Evaluation of the wettability of metal surfaces by micro-pure water by means of atomic force microscopy. *Applied Surface Science*, 191:74–84, 2002.

- WEBB, R. L. et GUPTA, N. S. : A critical review of correlations for convection vaporization in tubes and tube banks. *Heat Transfer Engineering*, 13(3):58–81, 1992.
- WOJTAN, L., REVELLIN, R. et THOME, J. R. : Investigation of saturated critical heat flux in a single, uniformly heated microchannel. *Experimental Thermal and Fluid Science*, 30:765–774, 2006.
- WU, H.-Y. et CHENG, P. : Visualization and measurements of periodic boiling in silicon microchannels. *International Journal of Heat and Mass Transfer*, 46:2603–2614, 2003.
- YEN, T., SHOJI, M., TAKEMURA, F., SUZUKI, Y. et KASAGI, N. : Visualization of convective boiling heat transfer in single microchannels with different shaped cross-sections. *International Journal of Heat and Mass Transfer*, 49:3884–3894, 2006.
- YOU, S., SIMON, T., BAR-COHEN, A. et HONG, Y. : Effects of dissolved gas content on pool boiling of a highly wetting fluid. *Journal of Heat Transfer*, 117:687–692, 1995.
- YUN, R., HEO, J. H. et KIM, Y. : Evaporative heat transfer and pressure drop of R-410a in microchannels. *International Journal of Refrigeration*, 29:92–100, 2006.
- ZHANG, W., HIBIKI, T. et MISHIMA, K. : Correlation for flow boiling heat transfer in mini-channels. *International Journal of Heat and Mass Transfer*, 47:5749–5763, 2004.
- ZIVI, S. : Estimation of the steady-state steam void-fraction by means of the principle of minimum entropy production. *Journal of Heat Transfer*, 86:247–252, 1964.
- ZUBER, N. et FINDLAY, J. : Average volumetric concentration in two-phase flow systems. *Journal of Heat Transfer*, 87:453–468, 1965.

Appendices

Forane 365 HX properties

A.1 Forane 365 HX thermophysical properties

On Table A.1, the needed coefficients for the determination of the evolution of the fluid thermophysical properties are given in function of temperature (in degrees Celsius ($^{\circ}C$)). The measurement techniques that have been presented in Chapter 3, allow the determination of the evolutions reported in the table for the liquid specific heat value at constant pressure and of the dynamic liquid viscosity. The other thermophysical properties have been given by the supplier using a model developed under the software ASPEN.

Units	Formula	Coefficients			
		a	b	c	d
$\rho_l \text{ kg.m}^{-3}$	$aT^3 + bT^2 + cT + d$	-1.8×10^{-5}	-0.00471	-1.8	1280
$\rho_v \text{ kg.m}^{-3}$	$aT^3 + bT^2 + cT + d$	1.66×10^{-5}	8.57×10^{-4}	0.057	1.1
$h_{lv} \text{ J.kg}^{-1}$	$aT^2 + bT + c$	-8.3×10^{-4}	-0.343	182	
$c_{p,l} \text{ J.kg}^{-1}.K^{-1}$	$aT + b$	0.00197	1309		
$c_{p,v} \text{ J.kg}^{-1}.K^{-1}$	$aT^3 + bT^2 + cT + d$	3×10^{-7}	-3×10^{-5}	0.0033	0.874
$\mu_l \text{ Pa.s}$	$aT^3 + bT^2 + cT + d$	-1.49×10^{-10}	3.81×10^{-8}	-5.5×10^{-6}	0.000664
$\mu_v \text{ Pa.s}$	$aT^2 + bT + c$	4.17×10^{-11}	3.41×10^{-8}	8×10^{-6}	
$\lambda_l \text{ W.m}^{-1}.K^{-1}$	$aT^2 + bT + c$	6.62×10^{-7}	-3.44×10^{-4}	0.111	
$\lambda_v \text{ W.m}^{-1}.K^{-1}$	$aT^2 + bT + c$	6×10^{-8}	7×10^{-5}	0.0091	
$\sigma \text{ N.m}^{-1}$	$aT + b$	-1.08×10^{-4}	0.0175		

TABLE A.1 – Evolution laws of the forane 365 HX thermophysical properties

A.2 Chemical compatibility tables for forane 365 HX with other materials

On Figures A.1 and A.2 the results of tests that have been made to evaluate the chemical compatibility of forane with some plastics have been given.

Tableau de compatibilité:

ELASTOMERES à 40°C		% prise de poids 5minutes après sortie du bain			
		5 minutes	1 heure	24 heures	100 heures
STYRENE BUTADIENE S 6510		0	0	0	0
ETHYLENE PROPYLENE EP 701		0	0	0	0
NITRILE HYDROGENE 7DT 1566		0	5	25,7	24,7
POLYCHLOROPRENE N 658		0	0	0	-1,1
POLYACRYLATE DA 65		24	24	107,6	131
HYPALON DH 70		0	0	1,5	1,5
FLUOROCARBONE DF 801(VITON)		9,9	33,5	55,4	65,7
NITRILE PB 701		0	4	9,5	14,9
SILICONE SL 1002		4	12,7	12,7	12,7
POLYISOPRENE POLYBUTADIENE C 6514		0	0	3,6	3,6
TEFLON 62945R		0	0	0	0

FIGURE A.1 – Chemical compatibility with some elastomers

Arkéma strongly suggest to users of forane 365 HX to make their own compatibility tests.

PLASTIQUE à 40°C		1: compatible; 2: attaque (à tester)			
		5 minutes	1 heure	24 heures	100 heures
ABS		1	1	1	1
PVC		1	1	1	1
PBT		1	1	1	2
PEHD		1	1	1	1
PEBD		1	1	1	1
PMMA		1	1	2	2
PET		1	1	1	1
PS CHOC		1	1	1	1
PS CRISTAL		1	1	1	1
PS 1160		1	1	1	1
PP		1	1	1	1
PA 11		1	2	2	2
PC		1	1	1	1
PVDF		1	1	1	1
PEBAX		1	1	2	2

FIGURE A.2 – Chemical compatibility with some polymers

ANNEXE B

Visualization window

The drawing of the top block (that comprises the visualization window) and its machining have been made by Joseph Virone and Milé Kusulja, people belonging to the LEGI « pool technique » (Figure B.1). All the test section dimensions can be found in Bavière (2005).

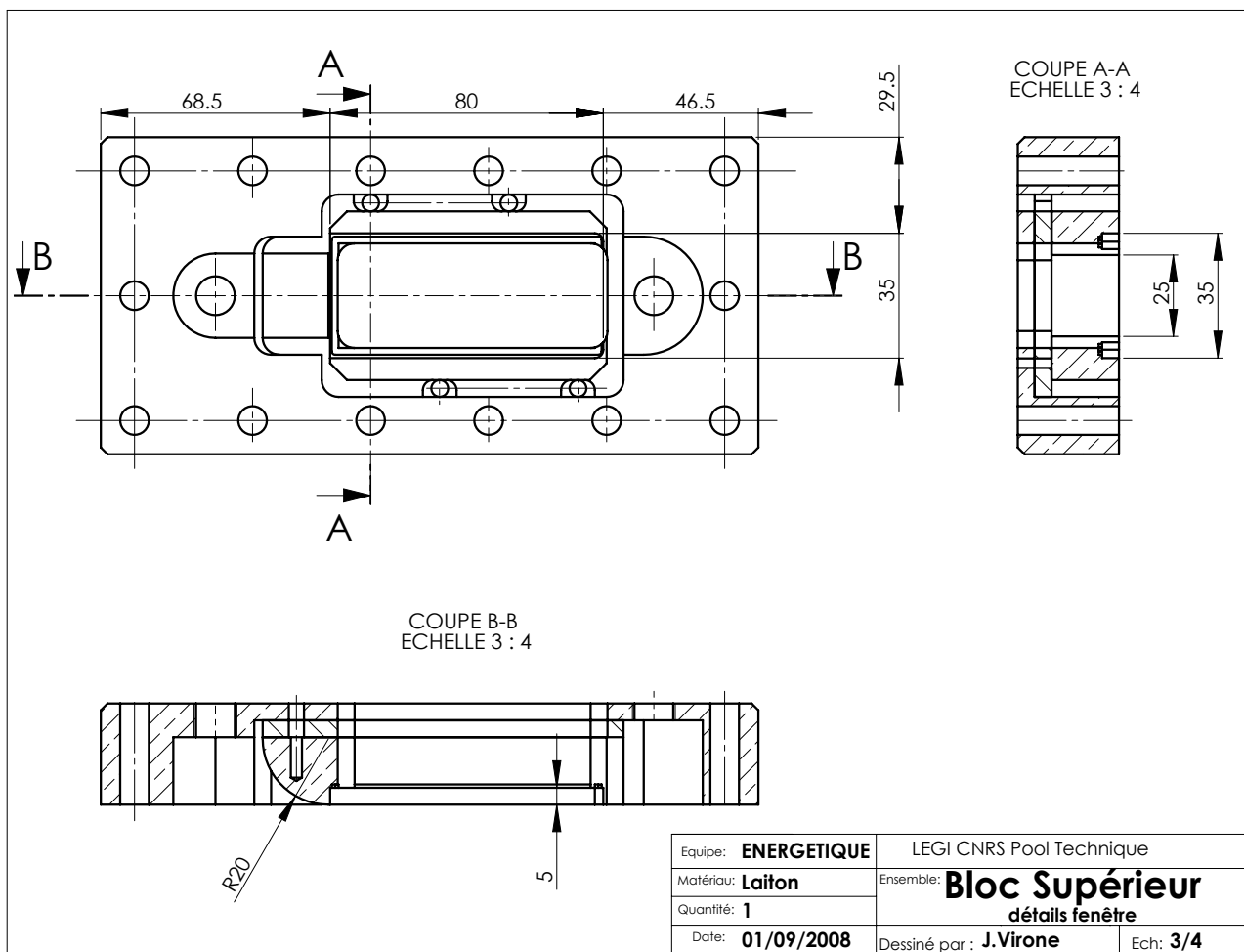


FIGURE B.1 – Test section top block with its visualization window

Appendices

In addition, we give on Table B.1 some characteristic regarding mechanical and thermophysical properties of this window.

Mechanical properties	
Toung modulus	74.5 Gpa
Poisson coefficient	0.28
Hardness	1.6 Gpa
General characteristics	
Chemical purity	99.99%
Mass density	4.08 g.cm^{-3}
crystalline structure	<i>cubique</i>
Electrical resistance	$> 10 \Omega.\text{cm}$
Grain size	$2 \text{ à } 20 \mu\text{m}$
Thermal properties	
Thermal expansion coefficient (at 20°C)	$6.5 \times 10^{-6} .\text{K}^{-1}$
Thermal conductivity (at 20°C)	$27.2 \text{ W.m}^{-1} .\text{K}^{-1}$
Specific heat	$0.53 \text{ J.g}^{-1} .\text{K}^{-1}$

TABLE B.1 – Mechanical and thermophysical properties of the visualization window

How the experiments were made...

The experiments that have been realized during all the analyze were acquired using a Keithley 2700 multimeter that was driven using Labview 7.1[®]¹. Using this software we defined the conditions for reaching steady state conditions for each thermal and hydrodynamic regimes during the tests. All the data, that were saved, came from an average measurement of at least 10 acquisition points (most of the time of 24 acquisition points), regarding the tests, what correspond to a time scale comprised between 1 and 4 minutes. It should be noticed that between each averaging, when a modification of the flow rate was made, it was necessary to wait for a time period comprised between 15 to 30 minutes in order to reach a new steady state regime before making a new averaging measurement (plateau with stable temperature). The whole set of experiments followed an initial procedure (common to all experiments) that will be not repeated for all cases. This common procedure is given for the determination of the friction coefficients (§ C.1).

C.1 How to determine friction coefficients ?

During our measurement we proceed as followed to determine the friction coefficients :

- ① Selection and assembly of the mini-channel,
- ② Opening of the valves and starting of the pump in order to have a flow rate in the range between 0.4 and 0.8 l min^{-1} (during at least 1 min),
- ③ Checking of the fluid level in the tubes connected to the differential pressure sensor and readjustment if needed,
- ④ Stopping of the pump and starting of the data acquisition system using Labview 7.1² when no flow occurred,
- ⑤ Restarting of the pump at a low flow rate value,
- ⑥ Adjustment of the rotation frequency of the pump engine in order to reach the targeted flow rate,

1. More information on all the procedure related to the migration of the data acquisition systems from TestPoint[®] to Labview[®] are in the report of Valdenaire (2008).

2. We wanted to determine the pressure sensor signals values when no flow occurred in the test loop

- ⑦ In steady state regime, acquisition of the mean value of 10 experimental data points³,
- ⑧ Stopping of the pump and closing of the valves,
- ⑨ Copy of the experimental data points and end of the data acquisitions.

C.2 How to determine heat exchange coefficients ?

The way we determined the heat exchanged coefficient can be summarized as follow :

- ⑤ Starting of the pump and adjustment of the flow rate at a high value ($Re > 7000$),
- ⑥ Triggering of the heating system (cartridges) and setting of the required electrical power,
- ⑦ Adjustment of the rotation frequency of the pump engine in order to reach the targeted flow rate,
- ⑧ In steady state regime, saving of an average measurement resulting from 20 experimental data points⁴,
- ⑨ Stopping of the pump and closing of the valves,
- ⑩ Copy of the experimental data points and end of the data acquisitions.

C.3 How to identify the onset of nucleate boiling ?

The experimental protocol to determine the minimal heat flux allowing the occurrence of boiling in mini-channel is the following one :

- ④ Stopping of the pump and starting of the data acquisition system using Labview 7.1,
- ⑤ Starting of the degassing procedure,
- ⑥ Setting of the diaphragm valve in order to set the test loop working pressure,
- ⑦ Adjustment of the rotation frequency of the pump engine to reach the targeting flow rate,
- ⑧ Starting of the pre-heating system in order to control the fluid inlet temperature,
- ⑨ Triggering of the heating system and progressive increase of the heat flux (following step of small increment) up to the occurrence of the onset of nucleate boiling,
- ⑩ Stopping of the pump, closing of the valves, stopping of the data acquisition system and copy of the data.

3. Steps 6 and 7 are repeated for all the range of Reynolds number from 200 to 8000

4. The steps, 6, 7 et 8 are repeated on all the required range of Reynolds number.

C.4 How to obtain the boiling curves ?

How experimental protocol to obtain the boiling curves follow the steps below :

- ④ Stopping of the pump and starting of the data acquisition system using Labview 7.1,
- ⑤ Starting of the degassing procedure,
- ⑥ Setting of the diaphragm valve in order to set the test loop working pressure,
- ⑦ Adjustment of the rotation frequency of the pump engine in order to obtain the wanted flow rate,
- ⑧ Starting of the pre-heating system in order to control the fluid inlet temperature,
- ⑨ Triggering of the heating system and progressive heating of the heat flux (small increments), then saving of the average value of 24 experimental data point when the wall temperatures of the lower block are stable⁵,
- ⑩ Stopping of the pump, closing of the valves, stopping of the data acquisition system and copy of the data.

5. The heat flux is increased by small increments and this increase is followed up to the occurrence of dryout. When the fluid inlet temperature is increased then the pre-heating system temperature is lowered in order to obtain the required fluid inlet temperature in the test section.

Other results coming from this study

D.1 Results for the evolution of the single phase flow data

Evolution of the friction coefficients

The data that are given in Figures D.1 and D.2 showed that the good agreement that was obtained when comparing the results with literature correlations for the mini-channels $C_1(a = 2.3 \text{ mm} - b = 1 \text{ mm})$ and $C_2(a = 5.6 \text{ mm} - b = 0.816 \text{ mm})$ was also observed for mini-channels $C_3(a = 8 \text{ mm} - b = 0.816 \text{ mm})$ and $C_4(a = 4 \text{ mm} - b = 0.421 \text{ mm})$ with the two tested working fluid.

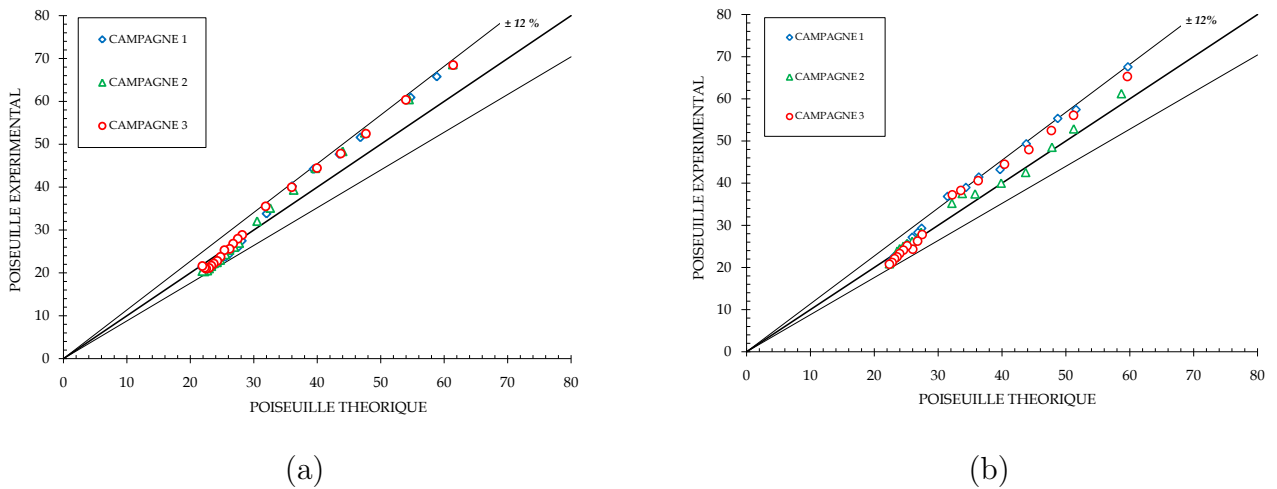
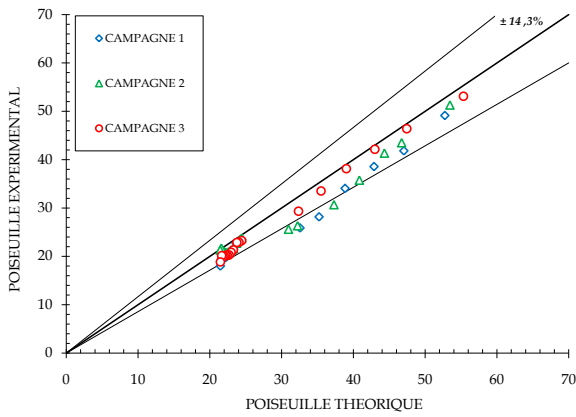
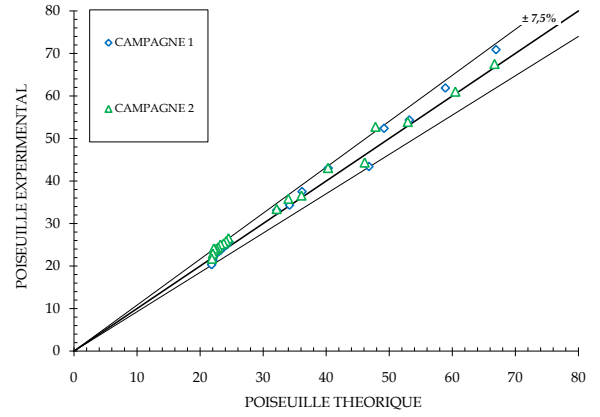


FIGURE D.1 – Comparison between experimental data and correlations for friction coefficient for mini-channel $C_3(a = 8 \text{ mm} - b = 0.816 \text{ mm})$ with : (a) water (b) forane 365 HX

Appendices



(a)

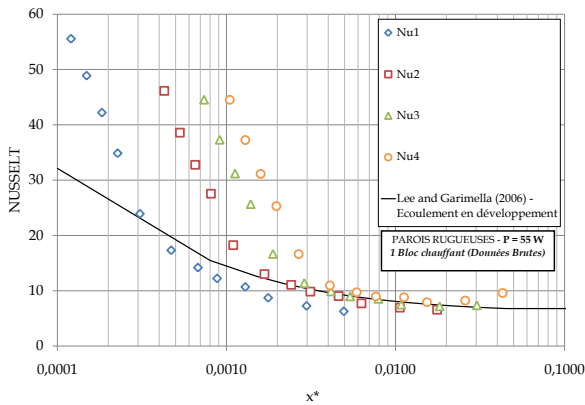


(b)

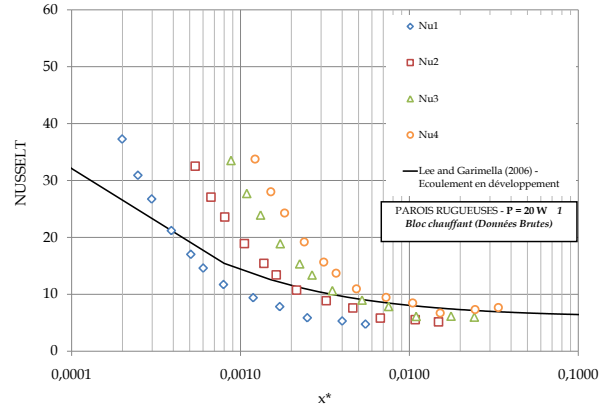
FIGURE D.2 – Comparison between experimental data and correlations for friction coefficient for mini-channel $C_4(a = 4 \text{ mm} - b = 0.421 \text{ mm})$ with : (a) water (b) forane 365 HX

Evolution of heat transfer coefficients

The data from Figures D.3 and D.4 showed the difference between the experiments and the correlation from the state of the Art.



(a)



(b)

FIGURE D.3 – Evolution of the Nusselt number (without the correction due to wall heat flux non-uniformity) in function of the non-dimensional thermal length, z^* . Comparison with the theoretical data from Lee et Garimella (2006) for the mini-channel $C_3(a = 8 \text{ mm} - b = 0.816 \text{ mm})$ with : (a) water (b) forane 365 HX

In addition, the discrepancy that was noticed between the experimental points (for forane 365 HX as working fluid) when the thermal boundary layers were fully developed (for large z^*), lead us to suppose that the heat flux was not homogenous for these two mini-channels.

Consequently, the results would be similar to the ones that have been presented for mini-channels $C_1(a = 2.3 \text{ mm} - b = 1 \text{ mm})$ and $C_2(a = 5.6 \text{ mm} - b = 0.816 \text{ mm})$ in the § 5.2.4.

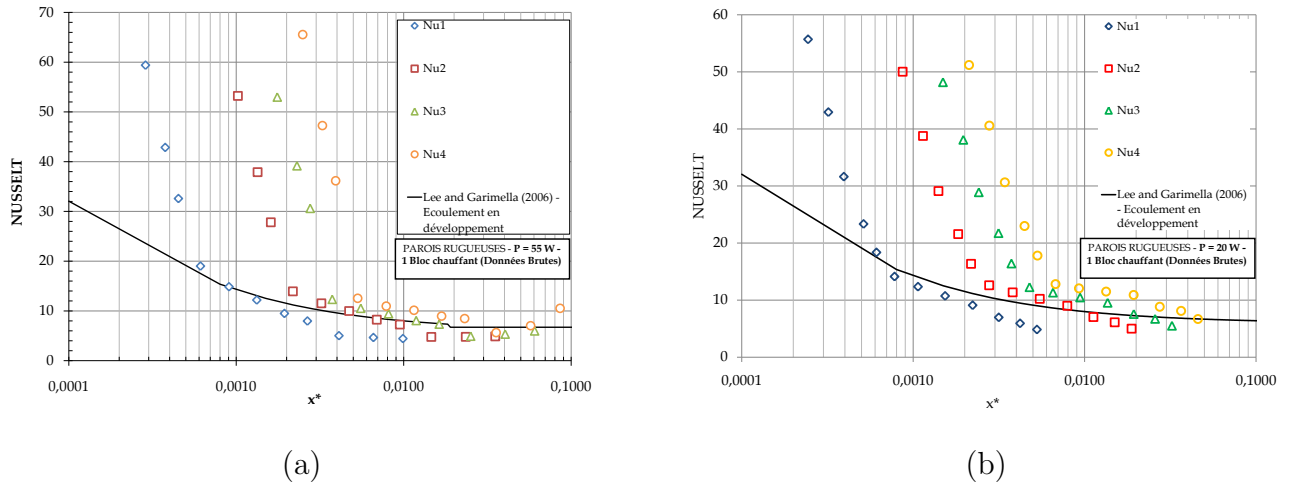


FIGURE D.4 – Evolution of the Nusselt number (without the correction due to wall heat flux non-uniformity) in function of the non-dimensional thermal length, z^* . Comparison with the theoretical data from Lee et Garimella (2006) for the mini-channel $C_4(a = 4 \text{ mm} - b = 0,421 \text{ mm})$ with : (a) water (b) forane 365 HX

D.2 Results for the evolution of boiling data

Impact of the pressure and of the subcooled temperature on ONB

We studied the impact of the working pressure (0.35 - 0.5 et 0.7 bar) for mini-channel C_4 ($d_h = 0.727 \text{ mm}$) on ONB occurrence. However, for this specific case, the inlet temperature was kept constant. We observed that the transferred heat flux before ONB increase with this working pressure (Figure D.5). As demonstrated in § 6.2.2, this would be due to the subcooling more than the working pressure effect.

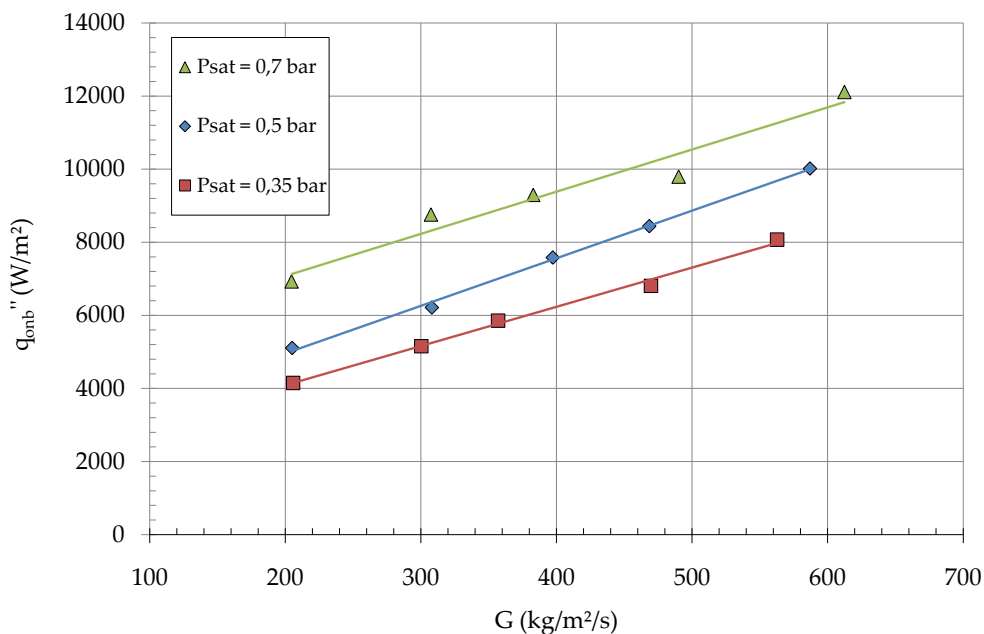


FIGURE D.5 – Impact of the saturation pressure and of the subcooling ($T_{amont} \approx 40^\circ C$ for all the tests) on the heat flux that was transferred from the block walls to the mini-channel C_4 for 0.35 - 0.5 and 0.7 bar

Presentation of the modeling

The test section geometry has been drawn on Gambit 2.2.30 from the technical drawings. The model comprises the top block with its visualization window. We represent only a longitudinal plan of symmetry. On the calculations have been made for a three-dimensional configuration for the whole set of experiments occurring in the four selected mini-channels.

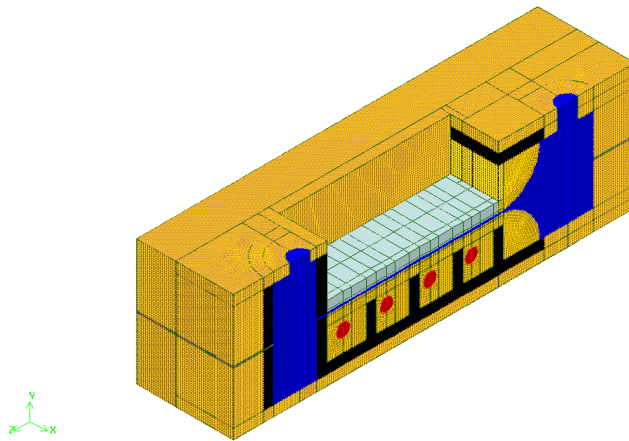


FIGURE E.1 – Representation of the test section using Gambit 2.2.30

The aim of this study was to obtain qualitative results by formulating the minimum hypotheses. In order to « easily » built the geometry, we split the initial test section volume in multiple sub-parts of lower dimensions that had symmetrical faces. This technique allows for the realization of a very fine controlled mesh on the whole volume of the test section. The working fluid volume has been split in a specific way in order to control the mesh density when the flow became in close proximity to the mini-channel inlet (that will be finer). This technique allows the reduction of singular numerical behavior at the mini-channel inlet. Figure E.1 shows the built geometry with a color code associated regarding the different sub-groups of the test sections. The total number of sub-volume was of 471. The mesh zone (represented in yellow) represent the top and lower blocks of the test section, the insulating resin is represented in black, whereas the heating cartridges are in red. The blue volumes are corresponding to the working fluid.

The whole test section has been modeled excepted the drill holes used for the assembly of the top block, the mini-channel and the lower block, the holes for the housing of the thermocouples

Appendices

(in the lower block) and the thermocouples¹. Table E.1 gives the thermophysical properties of the materials that have been used to fabricate the test section.

Materials	ρ ($kg.m^{-3}$)	c_p ($J.kg^{-1}.K^{-1}$)	λ ($W.m^{-1}.K^{-1}$)	Location
Brass	8400	376	121	Top and lower blocks
Epoxy resin	600	795	0.071	Lower block
Stainless steel (301)	7900	460	14.7	Mini-channel
Zinc Sulfide	4080	530	27.2	Top block
Fluids (20°C)	ρ ($kg.m^{-3}$)	c_p ($J.kg^{-1}.K^{-1}$)	λ ($W.m^{-1}.K^{-1}$)	μ ($Pa.s$)
water	998.2	4182	0.6	0.00103
forane 365 HX	1247	1344	0.102	0.000606

TABLE E.1 – Thermophysical properties of the used materials and fluid in the test section

The thermophysical properties were considered to be dependent of the average fluid temperature that flowed inside the test section. A « pressure-inlet » condition (boundary condition defined on Fluent 6 (2001)) was set at the test section inlet. On the outlet, a « pressure-outlet » conditions was set by supposing that the flow was at atmospheric pressure. The heating cartridges were modeled using a homogeneous surface heating source condition. For the whole set of experiments, the external surfaces of the test section were at ambient (room temperature). Consequently, the external surfaces were subjected to natural convection (between 10 and 20 $W.m^{-2}.K^{-1}$ for an external temperature of about 300°K in the model.

The scheme numerical resolution has been made by using the classical conservation relations (mass, momentum, heat balance) that were simplified regarding following hypotheses :

- ① Laminar flow and steady state regime,
- ② Non-compressible flow,
- ③ Heat transfer between solid element considered as purely conductive,
- ④ Constant thermophysical properties for the solids,
- ⑤ Thermophysical properties of the fluid are temperature-dependent.

These equations for the fluid can be reduced as :

$$\nabla \cdot \vec{U} = 0 \quad (E.1a)$$

$$\rho(\vec{U} \nabla \cdot \vec{U}) = -\nabla P + \nabla \cdot \tau \text{ with } \tau = \mu((\nabla \vec{U} + \nabla \vec{U}^T) - \frac{3}{2} \nabla \cdot \vec{U} I) \quad (E.1b)$$

1. It should be noticed that the estimation of the wall temperatures was determined at the exact location where the thermocouples were located.

$$\rho \nabla \cdot (\vec{U} (h + \frac{U^2}{2})) = \nabla \cdot (\lambda \nabla T) \quad (E.1c)$$

and for the solid as :

$$\nabla^2 \cdot T = 0 \quad (E.1d)$$

Mesh sensitivity

For all the geometries, the mesh has been built on Gambit 2.2.30, then the mesh was refined in Fluent 6 (2001) in the different part of the fluid volume. The validation of this mesh was realized by comparing the friction coefficients evolutions and the velocity profiles (for fully developed boundary layers) (see [equations (1.2) and (1.6)]) to the theoretical data for the different mini-channels. For the thermal conditions, the refining of the mesh was stopped when the numerical data showed small variations with the increase of number of meshed elements.

In this paragraph, we discuss the mesh refining impact on the evolution of behavior of the hydrodynamic laws. All the charts that are given in this paragraph were obtained for the mini-channel C_2 ($a = 5.6 \text{ mm} - b = 0.816 \text{ mm}$) with water as the working liquid. A structural meshing was imposed to the whole drawn geometry and also for the working liquid volume, except for the volumes that were near the convergent that need a non-structural mesh. The friction coefficients have been given in Figure E.2 in function of the mesh refinement for the mini-channel C_2 with water as the working fluid.

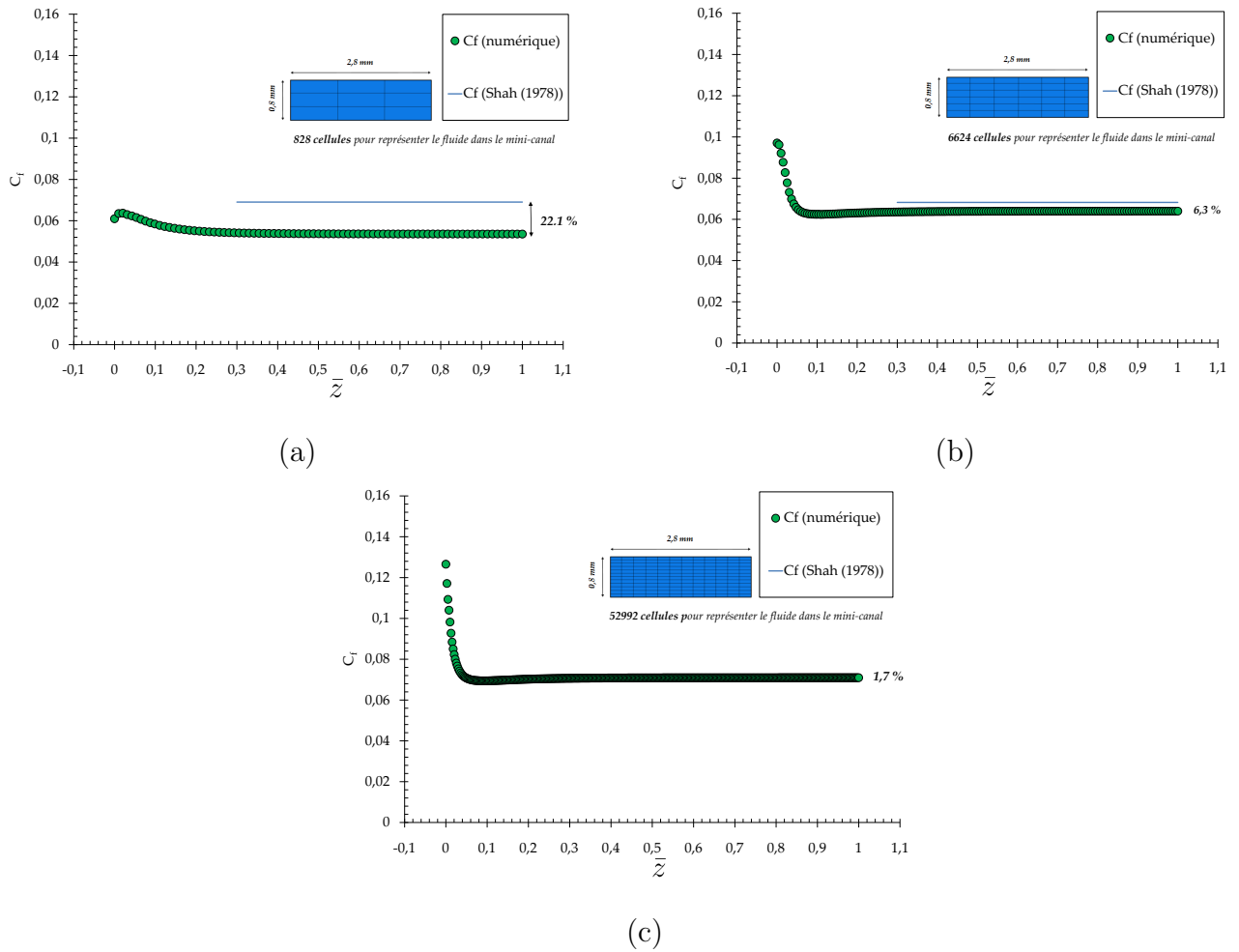


FIGURE E.2 – Evolution of the friction coefficients for $Re = 300$ in function of the non-dimensional length (\bar{z}) for the mini-channel C_2 with water as the working fluid for : (a) 828 cells (b) 6624 cells (c) 52992 cells

The deviations from the friction coefficients given by Shah et London (1978) for the fully developed single phase flow regime have been reported in Table E.2 for mini-channels $C_1(a = 2.3 \text{ mm} - b = 1 \text{ mm})$ and $C_2(a = 5.6 \text{ mm} - b = 0.816 \text{ mm})$ for water and forane 365 HX as working fluids. These results lead us to conclude that the mesh refinement had a strong impact. When the refinement reach a level of 52992 cells, the maximum difference with the approach of Shah et London (1978) was about of 1.7% for water as working fluid. The numerical tests that have been made with forane 365 HX showed a very good agreement with the data of Shah et London (1978) with a maximal difference of 2.3%.

Type	Refin.	Cells numb.	Smaller element	$(C_{f,\text{water}})$	$(C_{f,\text{F365}})$
C_1	0	736 cells	$250\mu m$	49.7 %	45.7%
C_1	1	5888 cells	$125\mu m$	12.1 %	10.9%
C_1	2	47104 cells	$62.5\mu m$	0.9 %	2.3%
C_2	0	828 cells	$266\mu m$	51.8 %	44.1%
C_2	1	6624 cells	$133\mu m$	6.3 %	6.2%
C_2	2	52992 cells	$66\mu m$	1.7 %	1%

TABLE E.2 – Mean Average Error (MAE) between the numerical friction coefficients and the ones defined by Shah et London (1978) for a Reynolds number of ≈ 300

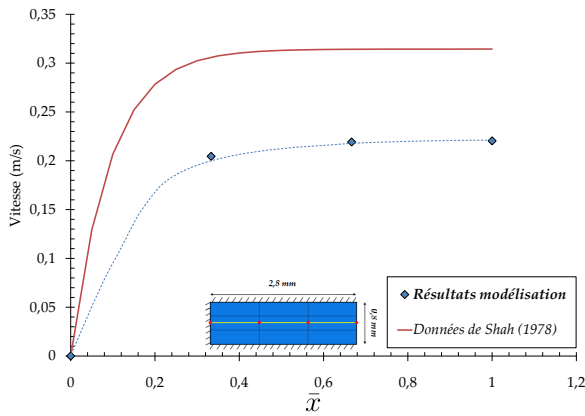
We used another checking procedure (regarding our numerical analysis) and compare the velocity profiles that were obtained for the numerical modeling to the ones defined in equations (1.2). We chose to calculate the velocity profiles on two perpendicular lines that were intersecting at the mini-channel center on a xy plane located at $z = 76\text{ mm}$ from the mini-channel entrance. A summary of these comparison is reported for the two working fluid in Table E.3.

Type	Cells numb.	$U_{\text{water}}(x, y = 0)$	$U_{\text{water}}(x = 0, y)$	$U_{\text{F365}}(x, y = 0)$	$U_{\text{F365}}(x = 0, y)$
C_1	736 cells	27.5%	20%	29.6%	20%
C_1	5888 cells	6.1%	5.4%	6.2%	5.6%
C_1	47104 cells	0.6%	0.15%	0.64%	0.14%
C_2	828 cells	35.4%	21.1%	35.8%	21.2%
C_2	6624 cells	7.1%	6.6%	8.3%	6.7%
C_2	52992 cells	1.7%	1.2%	1.1%	0.7%

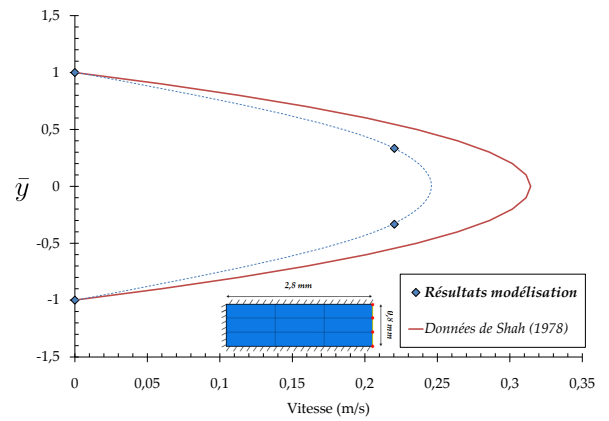
TABLE E.3 – Mean Average Error (MAE) between the numerical velocity profiles and the ones defined by Shah et London (1978) for a Reynolds number of ≈ 300

The profiles that were obtained for our numerical model and the ones defined by Shah et London (1978) are in good agreement when the cells number is of 47104 for the mini-channel $C_1(a = 2.3\text{ mm} - b = 1\text{ mm})$ and of 52992 for the mini-channel $C_2(a = 5.6\text{ mm} - b = 0.816\text{ mm})$ with a deviation that was below 2%. All the comparisons are given on Figure E.3 for C_2 mini-channel with water as working fluid.

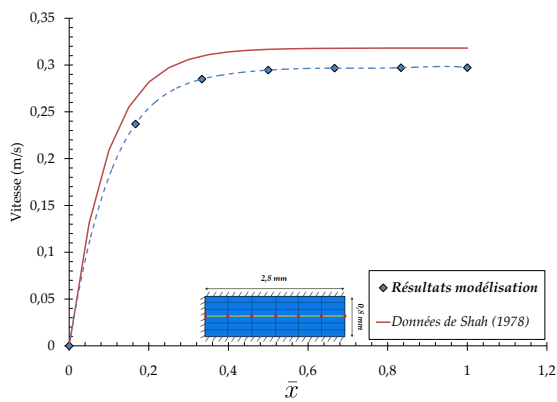
Appendices



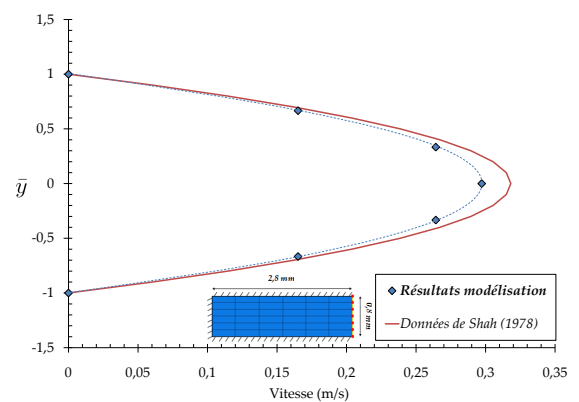
(a)



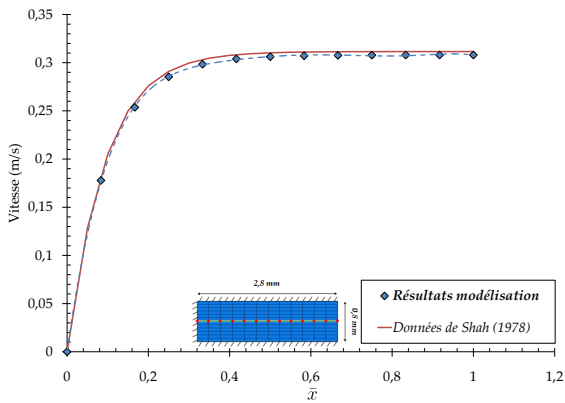
(b)



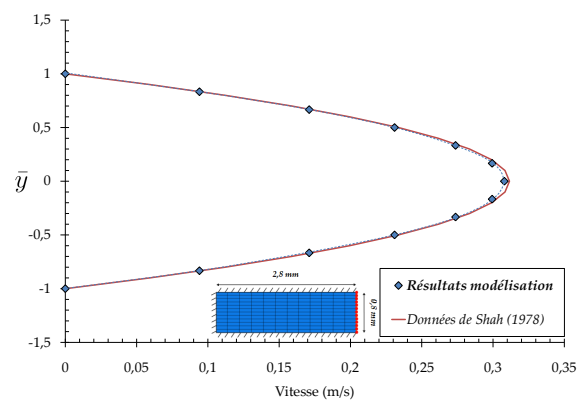
(c)



(d)



(e)



(f)

FIGURE E.3 – Evolution of the velocity profiles for a Reynolds number of 300 in function of the non-dimensional half width (\bar{x}) or of non-dimensional height (\bar{y}) for the mini-channel C_2 with water as working fluid for : (a) 828 cells (b) 6624 cells (c) 52992 cells

The whole set of results that has been presented in § 5.3.1 was obtained with a higher level of refinement.

Void fraction determination via image processing

F.1 Why to go through image processing to analyze the results ?

In order to build the flow map that will allow the determination of the conditions for which the heat transfer coefficients are the best one, it could be relevant to know the repartition of the liquid and vapor phases.

For determining these repartition, the void fraction, α (equation 2.1.1), seems to be a relevant parameter. For our experimental tests, we can obtain under specific conditions, this coefficient using an image processing method. Consequently, we can calculate using the visualizations surface void fraction. For succeeding in the determination of the global void fraction, it is necessary to estimate the global volume of the bubbles that are inside the mini-channel. Sobierska *et al.* (2007) gave a methodology for the determinations of the successive flow regime. Three flow regimes that are similar to the ones presented in this manuscript are given on Figure F.1 :

- a - Bubbly flow regime
- b - Plug flow regime
- c - Slug flow regime

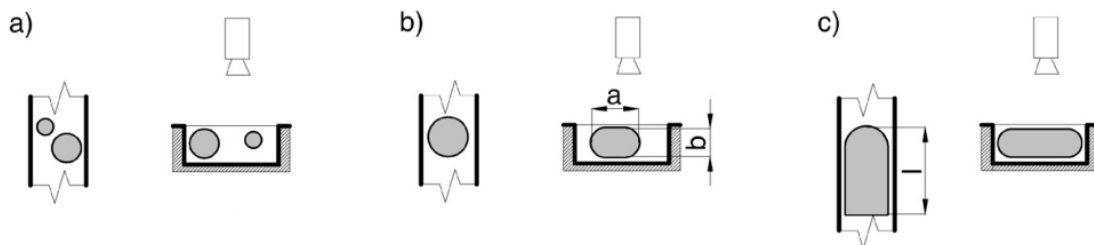


FIGURE F.1 – Flow regime classification according to Sobierska *et al.* (2007)

For reducing the errors on the determination of α , we decided to constraint the study to low mass velocities and low heat flux density $< 150kg/(m^2s)$ and $< 1W/cm^2$ respectively.

F.1.1 Bubbly flow regime

In this flow regime, the bubbles are of small dimensions and are not constricted neither by the width nor by the height of the flow zone. They can be considered as spherical and their volume can be calculated as follows :

$$V_1 = \frac{4}{3}\pi R^3 \quad (\text{F.1})$$

F.1.2 Plug flow regime

The increase in the heat flux density leads to the growth of the bubble size, as a consequence they become constrained regarding the mini-channel height in a first step. Indeed, for all the experimental cases that we observed, the mini-channel width was always larger than the height. Thus, the first geometrical constraint coming from the mini-channel came from this height. We considered for this regime only the bubbles that are a circular shape when looking at them from the top surface of the visualization window. The volume of these bubbles was given by the volume of a bubble of same radius than the visualizing disk (from top surface) whose spherical caps have been subtracted. The calculation formula is given as :

$$V_2 = \frac{4}{3}\pi R^3 - 2 \times \pi H^2 \times (R - H/3) \quad (\text{F.2})$$

where R is the bubble radius and where H is the difference between the cap height (e) and the bubble apex (R) :

$$H = R - e$$

Figure F.2 gives an illustration of these different distances.

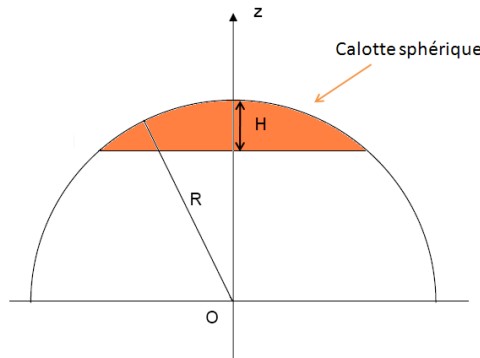


FIGURE F.2 – Removal of the spherical caps

e is the mini-channel height also.

F.1.3 Slug flow regime

The bubbles continue to growth up to be constrained by the mini-channel width. When this situation occurred we enter in the third flow regime configuration. For this specific case, we considered that the bubbles are similar to projected surfaces regarding mini-channel height and their volume can be calculated using :

$$V_3 = \pi R^2 \times e \tag{F.3}$$

with e that is the mini-channel height.

The total void fraction is the sum of these three different volume divided by total fluid volume that is visualized in the mini-channel :

$$\alpha = \frac{V_1 + V_2 + V_3}{V_{total}} \tag{F.4}$$

F.2 Image processing using Matlab

From an image, it is possible to calculate the surface void fraction, then by using the formal procedure to determine the global void fraction on this specific image.

The quality of the image is dependent of various parameters that are not easy to adjust in an optimal and constant way. The impacting parameters are the following ones :

1. The most important parameter is the lighting. This lighting was made using two optical fibers that were connected to a stereo-microscope. When their position was not « perfectly » normal to the mini-channel, some shadow area exist at the front or a the rear of the bubbles. The point was to determine « how to numerically considered these shadow areas? » Our image was obtained in gray-scale. These shadow areas were not neither in the same color of the liquid nor of the bubbles.
2. The second parameter was linked to the quality of the window visualization. Indeed, even small scratches on it can cause the bubbles cut off during the numerical data image processing.
3. The third parameter came from the optical fibers. We observe (during image processing) that the light provided by the system was not perfectly constant (it was pulsating). On the image, the gray scale of the liquid or of the gas that is located in the pulsating zone varied. However, the intensity variation of the gray scale level for each fluid state (liquid, gas) still allowed the difference to be observed.

During this study we look for solution to minimize these issues. During the numerical image data processing, the image is converted in data, this means that from an image we obtained a

Appendices

matrix. If the image has a size of $n \times m$ pixels then the matrix will have n row and m column. As our image was in gray scale, each pixel was associated to a color code that had a value between 0 and 255. This is this gray scale that will be saved in the matrix.

At the end of each series of images acquisition, we captured a last one that will be called « background image ». This image was taken in the same lighting and flow rate conditions that was considered in the experimental but with a single-phase flow condition (liquid). Once the images have been converted in matrix, we subtracted the matrix from the captured images to the matrix of the background one. This procedure allow the removal of all the elements (impurities, scratches of the visualization window, etc...) that were located exactly on same location compared to background image. The resulting matrix contained only the new elements (compared to background image) only bubbles appear. This procedure allow the resolution of the issue related to the visualization window quality. We did not find a satisfactory solution for the first issue relating the lighting, thus during all the experiments we tried to position the optical fiber in order to limit as much as possible the creation of shadows (the more normal to the window visualization). The light pulsation (due to the optical fiber) were treated using the numerical data image processing. These pulses were treated as background noise that was easily corrected inside the code.

After these treatments we obtained images on which we can continue to work. We then go through binarization process by using a threshold analysis. From a threshold value we colored all the pixels that were below this value in white and all the other ones in black. The definition of threshold value was very important because its allow for the identification of the liquid and vapor phases. It cannot be set arbitrarily. This is for this reason that we go through the writing of MATLAB script in order to define the « optimal » threshold value that corresponds to our images analyzes.

In order to better understand the impact of the threshold value on the data image processing, we compared an acquired image to the ones obtained after processing following the situations : too low, too high and optimal threshold. The example that has been given in Figure F.3 was obtained for a flow rate of 0.015 l/min , a mini-channel having a height of 914 microns , a width of 3 mm , and for a heat flux lower to 1 W/cm^2 . 14 bulles were identified on this image and the void fraction was of 0.065.

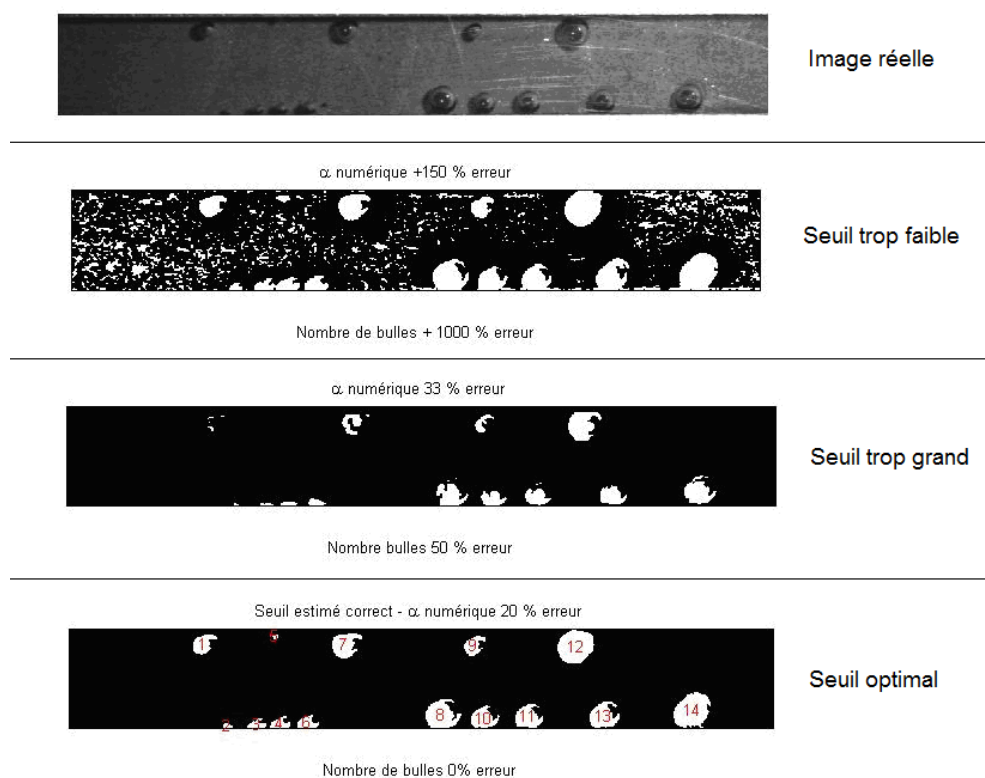


FIGURE F.3 – Threshold impact on a processed image

F.2.1 Block diagram for the threshold program

Figure F.4 show a simplified view of the working of the threshold methodology.

The second part of this code allow for the identification of the thresholds that fit better the values of calculated void fraction (void fraction is first calculated on reference images in the series and these value are compared to the numerical procedure).

Our method is describe in the following :

For our numerical protocol, the increase of the threshold parmeter allow for the reduction of the vapor proportion compared to the liquid one. The small, averaged and large bubbles are then forced to be reduced when this threshold parameter increase if we can to keep a physical meaning. Our first driving parameter for the determination of a relevant range of threshold values concerned the small bubbles. Indeed, the number of small bubbles were decreasing up to the moment for which their number increase due to the splitting or the vapor areas. As a consequence, the minimal values of the small bubble number will constitute a first border for the threshold value range. Then the knowledge of experimental void fraction will allow for the determination of threshold that correspond to the minimal error that can be made of

Appendices

this parameter. The time to experimentally determine the void fraction is long as the time to count the bubbles (in function of their category) and finally to determine their radius may be prohibitive when large number of image are considered. Thus, several comparisons at different moment of the series of images were realized in order to evaluate the impact of the selected threshold parameter on void fraction for the whole set of images.

For a typical series of 500 images, we made three comparisons on a series of 20 images. The time for determining experimentally is long and last about three hours for 60 images. However this calculation showed that the comparison with 3 series of 5 images seemed sufficient for the analysis. In this condition optimal threshold were always determined.

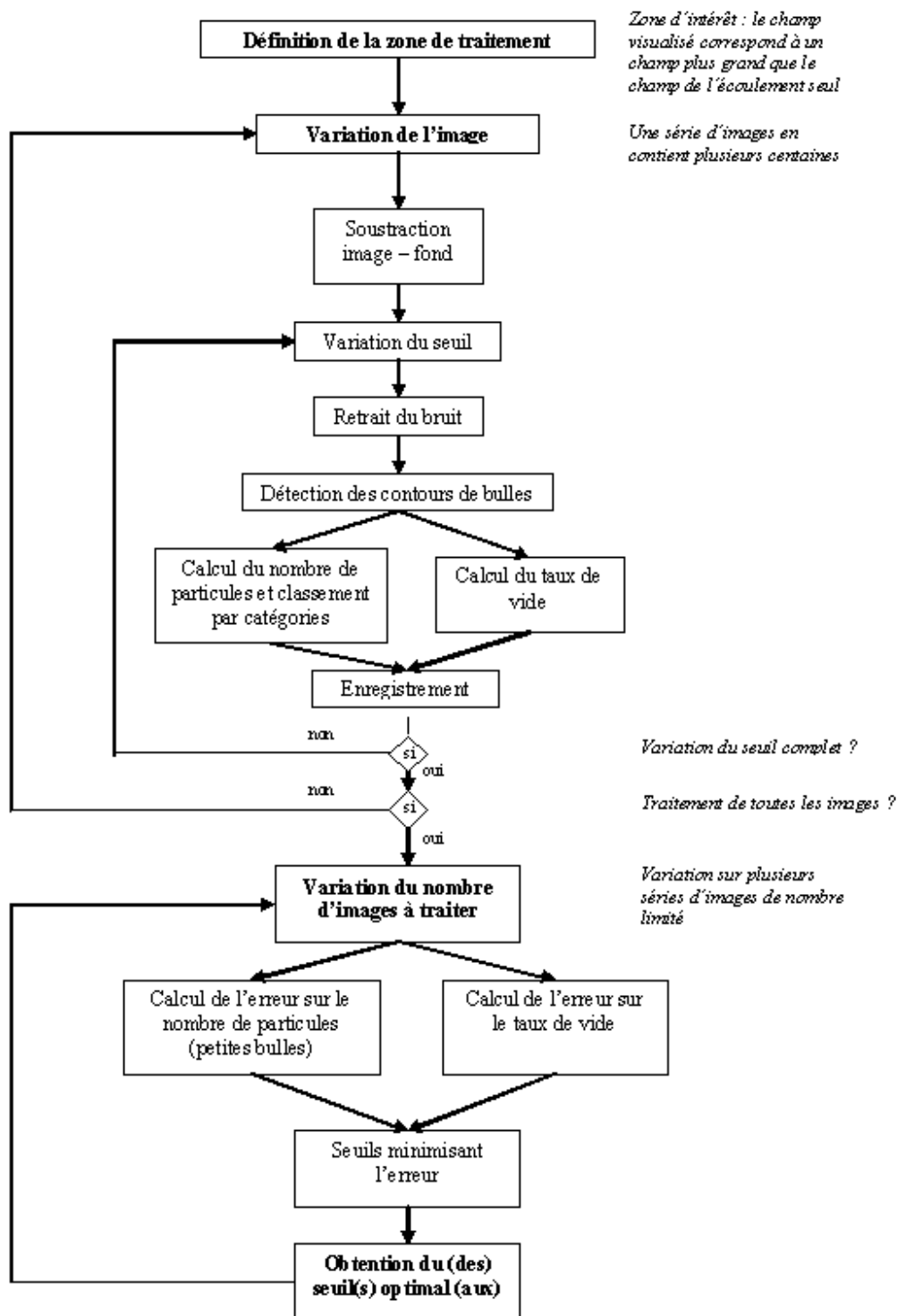


FIGURE F.4 – Block diagram for determining the threshold

RÉSUMÉ :

Cette thèse est consacrée à l'étude des écoulements internes en ébullition dans des canaux de petites dimensions. L'application visée est le refroidissement des piles à combustible de type PEMFC. Le confinement de plus en plus marqué des PEMFC et l'accroissement des densités de flux de chaleur produites au cœur de pile nécessitent une étude approfondie des transferts de chaleur dans les mini-canaux. Pour cette étude, le fluide utilisé a été le forane 365 HX, qui présente des propriétés intéressantes pour l'objectif visé. Comparativement aux écoulements monophasiques, une quantité élevée d'énergie peut être extraite des parois en limitant le gradient thermique pariétal en condition d'ébullition, lorsque le fluide se trouve à saturation. De manière à effectuer un dimensionnement adéquat d'un échangeur thermique, nous avons étudié l'influence de la dimension de la section droite de la mini-conduite sur les performances de l'appareil. Nous avons ainsi étudié quatre mini-canaux de section rectangulaire et de diamètre hydraulique compris entre $0,727\text{ mm}$ et $1,45\text{ mm}$. Nous avons centré notre étude sur l'influence du rapport d'aspect en définissant deux mini-canaux de même diamètre hydraulique et de rapports d'aspect différents. Nous avons constaté que les valeurs de flux thermiques conduisant à l'apparition de l'ébullition (ONB) ou à l'assèchement du liquide en paroi (CHF) dépendent de la géométrie du mini-canal. Les évolutions des pertes de pression en régime diphasique sont aussi influencées par ces données géométriques tandis que les coefficients d'échange évoluent peu avec celles-ci. De plus, des visualisations de l'écoulement ont été effectuées simultanément aux mesures et nous avons montré que les paramètres géométriques avaient un impact direct sur les transitions entre les régimes d'écoulement. Pour la majeure partie des expériences réalisées, la pression de fonctionnement était de 70 kPa (relativement à la pression atmosphérique), les vitesses massiques étaient comprises entre $100\text{ kg}\cdot\text{m}^{-2}\cdot\text{s}^{-1}$ et $800\text{ kg}\cdot\text{m}^{-2}\cdot\text{s}^{-1}$ et les flux thermiques testés ont pu atteindre la valeur maximale de $250\text{ kW}\cdot\text{m}^{-2}$, lors de la détermination du flux de chaleur critique (CHF).

Mots clefs : ébullition, mini-canaux, rapport d'aspect, ONB, CHF, perte de pression, coefficient d'échange de chaleur, configuration d'écoulement, forane

ABSTRACT :

This study is devoted to boiling flows in mini-channels of small dimensions. The objective was the enhancement of the thermal performance of PEM fuel cells. Confinement is nowadays one of the key parameters when considering a fuel cell. Indeed, the amount of heat flux to be removed from the fuel cell increases when its dimensions are decreased. As a consequence, thorough investigations of heat transfer in fuel cells are required. In our study, Forane 365 HX was selected to be used as the working fluid for the purpose of cooling. In comparison with single-phase flows, an important amount of energy can be extracted in forced boiling conditions while keeping a moderate wall temperature gradient. Thus, in order to properly design a heat exchanger in forced boiling conditions, it is important to understand the influence of the dimensions of one single mini-channel on the pressure drop across the channel and the heat transfer coefficients. Consequently, we investigated the flow and associated heat transfer in four rectangular mini-channels of hydraulic diameter ranging from 0.727 mm to 1.45 mm . We especially studied the influence of the aspect ratio by considering two mini-channels of same hydraulic diameter and different aspect ratios. We found that the heat flux necessary to the onset of nucleate boiling or the critical heat flux are dependent on the geometric dimensions of the mini-channel in our experiments. For the saturated boiling flow conditions, the pressure drop is also related to the channel cross-section area whereas the heat transfer coefficients seem to be nearly independent of the mini-channel under study. Simultaneously to these measurements, a high-speed video camera was used for visualizing the boiling flow. We observed that the mini-channel cross-section has a significant influence on the flow pattern transitions. Most of our experiments were performed for a working pressure of 70 kPa (relatively to atmospheric pressure) whereas the mass flow rate was in the range $[100- 800\text{ kg}\cdot\text{m}^{-2}\cdot\text{s}^{-1}]$. The heat flux removed by the boiling flow reached values as large as $250\text{ kW}\cdot\text{m}^{-2}$ for the critical heat flux conditions.

Keywords : boiling, mini-channels, aspect ratio, ONB, CHF, pressure drop, heat transfer coefficient, flow pattern, forane